Ice-ocean interactions in Milne Fiord

by

Andrew Kent Hamilton

B. Sc., University of Alberta, 1996

M. Sc., The University of British Columbia, 2006

A THESIS SUBMITTED IN PARTIAL FULFILLMENT
OF THE REQUIREMENTS FOR THE DEGREE OF

Doctor of Philosophy

in

THE FACULTY OF GRADUATE AND POSTDOCTORAL STUDIES

(Civil Engineering)

The University of British Columbia

(Vancouver)

August 2016

Abstract

Widespread break up of ice shelves, glacier tongues, and the loss of ice-dammed epishelf lakes on the northern coast of Ellesmere Island has motivated a need to understand fjord dynamics, yet the oceanography of fjords here is not well studied. Here, we present ocean profiling and mooring data collected from 2011 to 2015 in Milne Fiord, the last ice shelf-epishelf lake-glacier tongue fjord in the Arctic.

The data reveal that seasonal and interannual variations of fjord water properties and circulation are strongly impacted by the presence of the Milne Ice Shelf. The ice shelf forms a floating dam that traps surface runoff resulting in strong stratification and an elevated fjord heat content. Water exchange below the ice shelf is restricted to a narrow basal channel, prolonging the export of fjord-modified water, including subglacial runoff, by several months. In contrast, intermediate waters that penetrate to the Milne Glacier grounding line are freely exchanged and respond to offshore variations, with implications for submarine melting.

Unexpectedly, the depth of the halocline between the epishelf lake and seawater, often used to infer the thickness of the ice shelf, varied by several meters each year. This variability resulted from rapid inflow of surface runoff during summer followed by slow drainage under the ice shelf over winter, which is well modelled as hydraulically-controlled flow through a channel. A mixing event also abruptly changed the depth of the halocline by 1.5 m in less than 24 hours, indicating caution must be used when inferring ice shelf mass balance from halocline depth.

Submarine melt rates, estimated by two independent approaches, are strongly dependent on the vertical distribution of heat in the fjord. Spatial variation of ice thickness resulted in a heterogeneous distribution of melt. The highest estimated melt rate (4 m a^{-1}) occurred where the glacier was in contact with warm Atlantic Water at the grounding line, and enhanced near-surface melting is driven by the elevated heat content of the upper water column. Estimated melt rates are limited by weak currents ($\sim$1 cm s^{-1}) in the fjord imposed by the presence of the ice shelf.

Preface

This thesis presents the original research of the author, conducted under the supervision of B. Laval and D. Mueller. The thesis is presented as three, self-contained manuscripts (Chapters 2, 3, and 4) for which I designed the research program, performed the data collection and analysis, and wrote the manuscripts under the guidance of my supervisors. The contribution of my co-authors and colleagues to each manuscript are noted below. Members of my supervisory committee, G. Lawrence and H. Melling, provided comments on drafts of Chapters 2, 3, and 4. Chapter 1 provides the overall context for the work and places the manuscripts within that context. Chapter 5 presents the overall conclusions of the thesis and suggests opportunities for future work.

A version of Chapter 2 is being prepared for submission to a peer-reviewed journal as "Modification of ocean properties and circulation by an ice shelf and glacier tongue in Milne Fiord" by A. Hamilton, D. Mueller, B. Laval, A. White, C. Mortimer, and L. Copland. I was the lead investigator for the work presented in this chapter. A. White, C. Mortimer, and L. Copland collected and processed the ice-penetrating radar data from 2008, 2009, and 2011. D. Mueller and N. Wilson assisted with the collection of and processed the ice-penetrating radar acquired in 2012 and 2013. Additional field data was acquired through collaboration with the SwitchYard Project (P.I. M. Steele, University of Washington) and various publicly available remote sensing data products were utilized. I wrote the manuscript and all co-authors provided comments.

A version of Chapter 3 is being prepared for submission to a peer-reviewed journal as "Dynamic response of the last remaining Arctic epishelf lake to seasonal and long-term forcing" by A. Hamilton, B. Laval, D. Mueller and W. Vincent. I was the lead investigator for the work presented in this chapter. W. Vincent collected and contributed conductivity-temperature-depth profiles from 2004 to 2011, and D. Mueller collected profiles in 2009. D. Mueller performed the digitization of aerial and satellite imagery. I wrote the manuscript and all co-authors provided comments.

A version of Chapter 4 is being prepared for submission to a peer-reviewed journal as "Depth-dependent submarine melt rates of a glacier tongue and ice shelf in a High Arctic fjord" by A. Hamilton, D. Mueller, B. Laval, and W. van Wychen. I was the lead investigator for the work presented in this chapter. W. van Wychen provided the ice surface velocity data. I wrote the manuscript and all co-authors provided comments.

Table of Contents

List of Tables

List of Figures

List of Symbols

A_L	Area of the epishelf lake
a_b	Basal ablation rate at ice-ocean interface
a_{sf}	Surface ablation rate at ice-air interface
b	Effective width of the basal channel
C_d	Drag coefficient for ice-ocean interface
C_e	Discharge coefficient for weir equation
c_h	Constant for weir equation
c_i	Specific heat capacity of ice
c_w	Specific heat capacity of seawater
D_{EL}	Depth of epishelf lake
E	Energy
g	Gravitational acceleration
g'	Reduced gravitational acceleration
H	Ice thickness
h	Water column height
L	Distance dimension
L_i	Latent heat of fusion of ice
N^2	Brunt-Vaisala frequency squared
P_b	Pressure at ice-ocean interface
PE	Potential energy
Q_b^T	Latent heat flux at ice-ocean interface
Q_w^T	Sensible heat flux across ice-ocean boundary layer
Q_i^T	Sensible heat flux into ice
Q_w^T	Sensible heat flux across ice-ocean boundary layer
Q_b^S	Salt or ”freshwater” flux at ice-ocean interface
Q_i^S	Salt flux into ice
Q_w^S	Salt flux across ice-ocean boundary layer

Q_{cf}	Glacier calving volumetric flow
Q_{gl}	Glacier grounding line volumetric flow
Q_{fw}	Total freshwater flux
Q_{sg}	Subglacial freshwater flux
Q_{sf}	Surface freshwater flux
Q_b	Submarine melt freshwater flux
U	Velocity of ambient water
U_i	Velocity of ice
u_*	Friction velocity
$\overline{u}$	Depth-averaged glacier velocity
Ri	gradient Richardson number
S_b	Salinity at ice-ocean interface
S_w	Salinity of ambient water
S_i	Salinity of ice
S_1	Salinity of outflowing layer (Knudsen relation)
S_2	Salinity of inflowing layer (Knudsen relation)
T_i	Internal ice shelf temperature
T_b	Ice-ocean boundary temperature
T_w	Ambient water temperature
T_b^f	Freezing temperature at ice-ocean interface
T_w^f	Freezing temperature of ambient water
$T_w - T_w^f$	Thermal driving
V	Fjord volume
Z_{int}	Interpolated depth of glacier bed below sea level
Z_c	Depth of glacier centreline below sea level
Z_m	Depth of glacier margin below sea level
z	Depth
$z(N^2_{max})$	Depth of maximum Brunt-Vaisala frequency squared
ε	Ratio of iceberg width to height
Γ_T	Turbulent transfer coefficient for heat
Γ_S	Turbulent transfer coefficient for salt
$\Gamma_{(TS)}$	Turbulent transfer coefficient for heat and salt
γ_T	Turbulent exchange velocity for heat
γ_S	Turbulent exchange velocity for salt
κ_i	Thermal diffusivity of ice
$\lambda_{1,2,3}$	Empirical constants

Ψ Composite water property

ρ_w Density of ambient water

ρ_i Density of ice

ρ_w Density of seawater

ρ_i Density of ice

ρ_o Reference density

χ_o Conservative water property

Acknowledgments

The work presented in this thesis has been made possible through the support of a number of organizations and numerous individuals. I would first like to thank the funding agencies that allowed me to pursue my studies, including the Natural Sciences and Engineering Research Council of Canada (NSERC), the Association of Canadian Universities for Northern Studies (ACUNS), and The University of British Columbia (UBC).

My Ph.D. co-supervisors, Dr. Bernard Laval and Dr. Derek Mueller, have my gratitude for their valuable guidance and encouragement over the course of this journey. Bernard was extremely generous in allowing me the freedom to forge my own research direction and having confidence in all my endeavours, from AUVs to icebergs. Derek's intellectual curiosity and shared passion for the North inspired the origins of this thesis and for that I will always be grateful.

This thesis has benefited from the knowledge of members of my supervisory committee, Dr. Greg Lawrence and Dr. Humfrey Melling, who both provided helpful insight into various aspects of the research. Humfrey's expertise in polar oceanography and his dedication to scientific rigour were invaluable to the thesis and my growth as a researcher. I must also mention Dr. Eddy Carmack who sent me off on my first journey to the icy seas many years ago, and Dr. Warwick Vincent who was instrumental in inspiring an interest in Ellesmere Island.

In my time at UBC I have enjoyed the intellectual company of many great people, too numerous to name them all. Current and past EFM group members, including Alex Forrest, Mona Rahmani, Anirban Guha, Kelly Graves, and Ted Tedford, to name a few, have made time inside and outside the Rusty Hut enjoyable. Christian Schoof and the Glaciology group welcomed an outsider into their ranks and taught me a few things about ice. The Physical Oceanography group provided stimulating seminars and allowed me to keep one foot in salty water at all times.

The research in this thesis was only possible with the tireless efforts of all my field colleagues. First and foremost, I must thank Dr. Derek Mueller and Dr. Luke Copland for inviting me on the northern Ellesmere Ranger patrol in 2008, an incredible experience that first introduced me to the fascinating fjord that would later become the focus of my Ph.D. Two years later they again welcomed a polar hitch-hiker into their camp at Purple Valley and have been generous with equipment, field experience, enthusiasm, and good nature since that time. Derek was a seemingly tireless and

constantly enjoyable field companion and it was a pleasure to trek across the ice with him. Others who I have had the great fortune to toil and laugh with in the field, and who have assisted in collecting much of the data presented in this thesis, include Adrienne White, Nat Wilson, Jill Rajewicz, Adam Garbo, and Kevin Xu. Field work on Ellesmere Island would not be possible without the logistical support of all the individuals at PCSP in Resolute and the pilots who fly to the edge of the map. Luke Copland, Adrienne White, Colleen Mortimer, Wesley van Wychen, and Warwick Vincent have also been extremely generous with the sharing of hard-won data.

I must extend a special thank you to my family, who have encouraged and supported my academic and life adventures from the beginning. To all the Hamiltons and Finlays, thank you. Of special distinction are my parents Bill and Linda, who have always supported, encouraged, and inspired me, I truly thank you for that.

Finally, to my wife Karran, and my sons Feynman and Sebastian. It has been quite a journey. Thank you for everything.

Chapter 1

Introduction

The widespread break up of ice shelves, glacier tongues, and the loss of ice-dammed fjord lakes (epishelf lakes) along the northern coast of Ellesmere Island, Canada, has motivated a need to understand the dynamics of fjords here. However, an understanding of how these changes may be influenced by, or influence, ocean properties and circulation in fjords along this coast is limited by a scarcity of oceanographic observations. This thesis aims to: 1) describe the physical oceanography and ice-ocean interactions of a northern Ellesmere Island fjord before the collapse of ice; 2) investigate factors influencing the seasonal and interannual dynamics of an epishelf lake; and 3) estimate the magnitude and spatial distribution of submarine melting of an ice shelf and glacier tongue. To address these goals the thesis presents the results of an extensive oceanographic and glaciological field study undertaken between 2011 and 2015 in Milne Fiord, the last ice shelf-epishelf lake-glacier tongue fjord system in the Arctic.

1.1 Background

Since 2000, the northern coast of Ellesmere Island has undergone accelerated loss of ice shelves (Mueller et al., 2003; Mueller et al., 2008; White et al., 2015a) and the floating termini of glaciers (Pope et al., 2012; Copland et al., 2015). Ice shelves along this coast differ from those surrounding Antarctica, which are the seaward extensions of continental ice sheets. Here, ice shelves generally form in situ at the mouths of fjords from accretion of sea ice below and snow accumulation above, with additional mass acquired from tributary glaciers and low-elevation ice caps (Jeffries, 2002). The largely marine origin of ice shelves here also distinguishes them from glacier tongues, the floating extensions of outlet glaciers at the head of fjords (Jeffries, 2002). From 2000 to 2011 five of the six remaining major ice shelves on northern Ellesmere Island broke up or calved completely from the coast, reducing ice shelf area from 1043 km^2 to 546 km^2 (Mueller et al., 2008; White et al., 2015a). Over the same period, there has been a widespread loss of multi-year land-fast sea ice (Pope et al., 2012) and the collapse of glacier tongues (Pope et al., 2012; Copland et al., 2015).

The breakup of ice shelves on northern Ellesmere Island has resulted in the loss of associated ice shelf-dammed lakes. Where an ice shelf spans the mouth of a fjord, it can form a floating dam that can trap surface meltwater runoff inside the fjord down to the draft of the ice shelf, resulting in a perennial layer of freshwater directly overlying seawater. The freshwater layer Surface ice-cover at this high-latitude (>80°N) and low tidal action (www.tides.gc.ca) limits mixing of the fresh surface layer with seawater below and as a result the freshwater layer can last for decades or longer (Veillette et al., 2008), creating what is known as an epishelf lake. The halocline between freshwater and seawater can be incredibly sharp, with observed salinity gradients of >10 g kg^{-1} m^{-1} (Veillette et al., 2008), and its depth is thought to be determined by the draft of the impounding ice shelf (Vincent et al., 2001). The existence of the epishelf lake is entirely dependent on the integrity of the ice shelf dam, and the breakup of ice shelves along this coast has resulted in the loss of several epishelf lakes (Veillette et al., 2008), including the catastrophic drainage of the Disraeli Fiord epishelf lake caused by the fracturing of the Ward Hunt Ice Shelf between 2000 and 2002 (Mueller et al., 2003). The breakup of ice shelves can therefore cause dramatic changes to fjord stratification.

The collapse of coastal ice along northern Ellesmere Island has been linked to recent atmospheric warming (Copland et al., 2007; Copland et al., 2015). Since 2000, annual mean air temperatures in the Canadian Arctic Archipelago (CAA) rose by 1-2°C (Sharp et al., 2011) resulting in a sharp increase in mass loss from the ∼146 x 10^3 km^2 glaciated area in the region (Gardner et al., 2011; Sharp et al., 2011; Lenaerts et al., 2013). The increased meltwater runoff meant the CAA was the single largest contributor to sea level rise outside of Greenland and Antarctica from 2007-2008 (Gardner et al., 2011). This meltwater runoff is funnelled through fjords where it is transformed by fjord processes before being exported to the open ocean.

Growing evidence from other regions suggests that ocean forcing can also be an important factor in the loss of coastal ice. Submarine melting driven by the ocean accounts for three quarters of the mass loss via ablation from Antarctic ice shelves (Rignot et al., 2013). In Greenland, up to 80% of the mass loss of glacier tongues has been attributed to ocean driven melting (Rignot, 1998; Rignot and Steffen, 2008), and submarine melting of outlet glaciers has been identified as a plausible mechanism contributing to the both the retreat and increased flow rate of tidewater glaciers and collapse of glacier tongues (Holland et al., 2008b; Motyka et al., 2011; Joughin et al., 2012; Straneo et al., 2012). A regional rise in air temperatures over the Greenland Ice Sheet has increased surface runoff, much of which enters the ocean at the bed of tidewater glaciers, leading to enhanced convectively driven circulation and melting at the ice-ocean interface (Straneo and Cenedese, 2015). The rate of submarine melt and the release of freshwater, from both surface runoff and submarine discharge, to the coastal ocean is dependent on the dynamics of fjords, which are generally poorly understood even in the few fairly well-studied Greenland fjords (Straneo and Cenedese, 2015). It is very likely that many of the same ocean-driven processes that have influenced changes in Greenlandic fjords,

and below Antarctic ice shelves, could be driving the changes occurring along the northern coast of Ellesmere Island.

Several characteristics set the fjords of northern Ellesmere Island apart from fjords in other regions and justify focused study. First, very little oceanographic data has been collected in fjords along this coast, so further observations are a valuable contribution to the literature. Second, fjord water properties here appear to be strongly linked to the presence of ice, yet the interactions between the ocean and ice are not well understood. How the loss of ice affects fjord properties, or the role of the ocean in driving these changes, is hampered by the lack of observations from systems prior to the loss of ice. Third, the ongoing dramatic loss of ice means the opportunity to study ice-ocean interactions is limited. Fourth, source waters for fjords here come directly from the Arctic Ocean, which may alter fjord processes compared to other ocean basins with different water mass characteristics and circulation. Finally, the geophysical features of the region, particularly the once widespread ice shelves and associated epishelf lakes, are, to the best of the author's knowledge, unique in all the Arctic. This may be the last opportunity to study such a system before its collapse.

This thesis investigates the ocean properties of Milne Fiord (82°35'N; 81°W), the site of the last remaining ice shelf-epishelf lake system in the Arctic (Veillette et al., 2011a). The Milne Ice Shelf (205 km^2) spans the mouth of the fjord and is the last intact ice shelf along the northern coast of Ellesmere Island. The ice shelf dams an epishelf lake that occupied an area of approximately 52.5 km^2 as of 2009 (Mortimer, 2011). At the head of Milne Fiord the Milne Glacier terminates in a 16 km long glacier tongue. Previous work in the fjord has included glaciological studies of the ice shelf and glacier tongue (Jeffries, 1985; Jeffries, 1986b; Narod et al., 1988; Mortimer et al., 2012), remote sensing analysis of the extent of the fresh epishelf lake ice (Mortimer et al., 2012; Veillette et al., 2008), sampling of the freshwater ecosystem of the epishelf lake (Veillette et al., 2011a), and shallow hydrographic profiles focusing on the depth of the epishelf lake (Jeffries, 1985; Veillette et al., 2008; Veillette et al., 2011a). The oceanography of the fjord has not previously been studied.

In the following section relevant literature is reviewed to provide background on the topics addressed in the thesis, and to place the work in the context of the current state of knowledge.

1.2 Review of relevant literature

1.2.1 Northern Ellesmere Island

The coast of northern Ellesmere Island is characterized by numerous fjords (narrow, deep inlets, carved by glaciers, often with a sill at the mouth) that open to the Arctic Ocean (Fig. 1.1). Although the fjords of northern Ellesmere Island vary substantially in geometry (the largest being the Nansen Sound fjord system extending 340 km inland), a typical fjord along the northern coast is 30-50 km long and 4-8 km wide. The bathymetry in this region is in general very poorly constrained, but existing observations suggest fjords here are typically a few hundred meters deep with sill depths

between 50-350 m (Ford and Hattersley-Smith, 1965). Bathymetric soundings collected along the coast show the continental shelf is relatively shallow ($\sim$250 m) and the shelf break lies $\sim$100 km offshore where it slopes steeply to depths over 2000 m (Jakobsson et al., 2012).

Due to its high-latitude, the northern coast of Ellesmere Island receives no solar radiation during the polar night from mid-October through February, and continual solar radiation from April to September. This results in low annual average air temperatures ($\sim$ -18°C at Alert between 1971-2000; www.ec.gc.ca) but with large amplitude seasonal temperature cycle (varying up to 50°C between winter and summer). Surface temperatures over ice masses exceed the freezing point during only two to three months of the year. The Canadian High Arctic receives low amounts of precipitation (<0.5 m w.e. a^{-1}; Braithwaite, 2005), so regional surface mass balance of ice caps and glaciers is largely governed by the high variability in melt production which is strongly correlated with summer surface air temperatures, which in turn, are highly dependent on local synoptic conditions (Gardner et al., 2011 and references therein).

Long-term glacier mass balance records from the Queen Elizabeth Islands (QEI: Ellesmere, Devon, and Axel Hieberg Islands) indicate that prior to the 1980s the ice masses in this region were largely in balance (Sharp et al., 2011; Van Wychen et al., 2014), however since 2005 changing summer atmospheric circulation patterns have led to increased surface melt and longer melt seasons (Gardner et al., 2011; Sharp et al., 2011; Lenaerts et al., 2013). Consequently, surface mass loss has increased sharply in recent years (averaging -7 $\pm$ 18 Gt a^{-1} between 2004 and 2006, and -61 $\pm$ 18 Gt a^{-1} between 2007 and 2009; Gardner et al., 2011). Flow speeds of glaciers in the QEI are relatively slow, with maximum velocities of tidewater glaciers of 30-90 m a^{-1} along their main trunks, rising to <300 m a^{-1} at their termini in 2012 (Van Wychen et al., 2014). Dynamic discharge of glaciers into the ocean was estimated as 2.6 $\pm$ 0.8 Gt a^{-1}, indicating that iceberg calving accounts for a small proportion of total mass loss, with surface melt and runoff responsible for the majority of mass loss of glaciers of the QEI. However, only two marine-terminating glaciers (Trinity and Wykeham glaciers on the east coast of Ellesmere Island) accounted for 62% of the total dynamic discharge for all glaciers of the QEI in winter 2015 (Van Wychen et al., 2016), suggesting that variations in flow of just a few tidewater glaciers could dramatically alter the total dynamic discharge from the QEI. Changes in glacial hydrological forcing, the buttressing effects of sea ice/melange at the glacier terminus, and ocean-driven melt rates, could lead to increased mass loss at tidewater glacier termini, leading to glacier acceleration and increased contribution to sea level rise (Straneo and Cenedese, 2015). The nature and causes of tidewater glacier variability have not been well investigated in the Canadian Arctic.

Where oceanographic surveys have been conducted on northern Ellesmere Island, including of the Nansen Sound fjord system (Ford and Hattersley-Smith, 1965; Hattersley-Smith and Serson, 1966), Tanquary Fjord (Keys and Seibert, 1969), Disraeli Fjord (Keys et al., 1968; Keys, 1977), d'Iberville Fjord (Lake and Walker, 1973) and Taconite Inlet (Ludlam, 1996), they show stratifica-

tion of water masses that reflect those of the adjacent Arctic Ocean, subject to modification from sills, fresh water runoff during the melt period, and interaction with ice shelves and glaciers. Typical stratification consists of three layers distinguished by temperature and salinity characteristics. At the surface is a fresh, well mixed layer, modified by glacial meltwater runoff and local surface processes. Below is relatively fresh (<34.4 PSU), cold (<0°C) Polar Water (PW), extending down to about 200 m depth, derived from river runoff around the margins of the Arctic Ocean and Pacific Ocean inflow through Bering Strait (Aagaard et al., 1981; Steele and Boyd, 1998). PW lies above a layer of warm (0-3°C), saline (>34.7 PSU) modified Atlantic Water (AW). AW originates as an initially warm (>3°C) water mass at the surface of the North Atlantic that is cooled by the atmosphere as it is transported poleward through Fram Strait, and submerges to depth, slowly losing heat as it is transported around the Arctic, to eventually reach the northern coast of Ellesmere Island. Separating PW and AW is the main Arctic halocline, a layer of low temperature (<-1°C) and salinity between $\sim$ 30.4 and 34.4 PSU, and arguably the most important feature of the Arctic Ocean (Carmack, 1990), due to its effect of limiting convective cooling to the surface $\sim$50 m of the water column and preventing upward flux of heat from the underlying warm AW, processes which allow sea ice to form.

The actual characteristics of ocean waters reaching the fjords of northern Ellesmere Island are dependent on pathways and variability of regional ocean circulation, which are not well constrained by observations. High-resolution model simulations (Aksenov et al., 2010; Jackson et al., 2014a), geostropic calculations (Steele et al., 2004), and observations of ice island and sea ice drift (Copland et al., 2007; Pope et al., 2012), indicate surface waters in the Arctic Ocean typically flow westward along the Canadian continental shelf. Hydrographic analyses of water masses in the western Lincoln Sea, to the northeast of Ellesmere Island, indicate that surface waters found there originate from the Canada Basin (Jackson et al., 2014a), are circulated around the Beaufort Gyre and advected by the Transpolar Drift from the Chukchi Sea (Steele et al., 2004). An eastward flowing boundary undercurrent appears to exist along the continental slope from the base of the mixed layer (30 – 75 m) to the bottom (Newton and Sotirin, 1997) likely an extension of the Arctic Circumpolar Current (Rudels et al., 1999; Aksenov et al., 2010). AW in the Lincoln Sea generally shares characteristics with that of the southeastern Canada Basin (i.e. a cold (<0.5°C Atlantic layer below 350 m depth; Steur et al., 2013) further supporting the likelihood of an eastward flowing shelf break current. Model results indicate North Ellesmere shelf currents are weak (<10 cm s^{-1}) and baroclinic (Aksenov et al., 2010).

1.2.2 Ice shelves

One of the most notable features of the northern coast of Ellesmere Island is the presence of ice shelves at the mouths of several fjords. The ice shelves were first observed by a team led by Lieutenant Pelham Aldrich during the 1875-1876 British Arctic Expedition. Aldrich noted a unique

undulating surface of snow and ice extending along much of the coast (Nares, 1878). Three decades later, polar explorer Robert E. Peary described a broad glacial fringe that extended from Cape Hecla westward some 500 km to at least Nansen Sound (Peary, 1907). This floating glacial fringe, unofficially known as the Ellesmere Ice Shelf, was estimated at 8900 km^2 in area (Vincent et al., 2001). The ice shelves are thought to have formed approximately 4000 years ago during a period of climatic cooling (Evans and England, 1992; Antoniades et al., 2011) and remained stable for almost three millenia before undergoing a major fracturing event 1,400 years ago, then reforming 800 years ago (Antoniades et al., 2011). After the early explorations at the turn of the 20th century the area became the focus scientific research in the 1950s when it was discovered that massive ice islands adrift in the Arctic Ocean originated from the northern coast of Ellesmere (Hattersley-Smith, 1957). The ice islands and subsequent surveys along the coast confirmed that much of the Ellesmere Ice Shelf had disintegrated since Pearys expedition.

In the past century more than 90% of the area of the Ellesmere Ice Shelf has been lost. At the turn of the 21st century six major ice shelves remained: the Ayles, Markham, Milne, Petersen, Serson, and Ward Hunt ice shelves, with a total area of $\sim$1043 km^2 (Mueller et al., 2006). From that time several calving events have resulted in significant loss of the remaining ice shelf area (Fig. 1.1), including a 50% reduction in total ice shelf area, to 563 km^2 by 2011 (D. Mueller, pers. comm.). Reductions included the complete loss of the Ayles Ice Shelf in 2005 (Copland et al., 2007), the Markham Ice Shelf in 2008 (Mueller et al., 2008) and the majority of the Serson Ice Shelf in 2011, combined with further breakup and loss from the Ward Hunt and Petersen ice shelves (White et al., 2015a). In examining the calving of the Ayles Ice Shelf and the breakup of the Petersen Ice Shelf, Copland et al. (2007) and White et al. (2015a) suggested that the ice shelves were weakened by thinning due to long-term negative surface mass balance related to an increase in mean annual air temperatures over the past 50+ years (+0.5°C per decade along the northern coast of Ellesmere Island between 1948 and 2012), the development of fractures, and mechanical erosion due to the presence of open water along their fronts. The fracturing and calving of ice shelves along this coast has led to the loss of associated epishelf lakes.

1.2.3 Epishelf lakes

Epishelf lakes form where ice shelves impose a physical barrier preventing surface meltwater runoff from flowing freely into the ocean. The ice shelf dam is floating on the ocean, so epishelf lakes are connected to the sea, and thus are tidally influenced. A schematic of Milne Fiord, including a representation of an epishelf lake and many other key features and processes discussed in this thesis, is presented in Figure 1.2.

Epishelf lakes were first described in Antarctica (Heywood, 1977) and have been divided into two types depending on their connection to the ocean: those that form in depressions on land where the hydraulic connection to the ocean occurs at a land-ice contact under the ice shelf, or through

cracks in the ice sheet; and those where the freshwater layer floats directly on seawater and the thickness of the freshwater layer is thought to be controlled by the thickness of the ice shelf (Gibson and Andersen, 2002). The former are numerous in Antarctica and are distributed around the margins of the continental ice sheet (Heywood, 1977; Gibson and Andersen, 2002; Laybourn-Parry et al., 2006; Smith et al., 2006). The latter, those that float directly on seawater, are not as common in Antarctica (Wand et al., 2011), but were once relatively numerous along the northern coast of Ellesmere Island (Vincent et al., 2001; Veillette et al., 2008), dammed by ice shelves at the mouth of fjords. Perennial ice cover in this region inhibits wind-mixing, and permits the maintenance of a sharp salinity gradient between the freshwater layer and seawater. Epishelf lakes are known to exist for decades, allowing the evolution of unique ecosystem types with freshwater and marine biota contained within the same water column, vertically separated by a sharp salinity and temperature gradient (Van-Hove et al., 2001; Vincent and Laybourn-Parry, 2008; Veillette et al., 2011a).

The best studied of the northern Ellesmere Island epishelf lakes was the Disraeli Fiord epishelf lake, dammed by the Ward Hunt Ice Shelf prior to its complete drainage between 2000 to 2002. When first surveyed in 1954, the water column of Disraeli Fiord consisted of a 63 m deep freshwater layer overlying 300 m of seawater, the freshwater-seawater interface only a few meters thick (Crary, 1956). A number of authors interpreted the depth of the freshwater layer in Disraeli Fiord as being equivalent to the draft of the ice shelf (Hattersley-Smith, 1973; Jeffries and Krouse, 1984; Keys et al., 1968; Vincent et al., 2001), as excess freshwater below the minimum draft of the ice would flow out of the fjord under the base of the ice shelf. Crary (1956) suggested that outflowing brackish water could freeze to the ice shelf base, thereby influencing ice shelf mass balance. Keys (1978)) observed an outflowing current (9 cm s^{-1}) localized at the base of the freshwater-seawater interface during the surface melt season and ice cores from the north-east region of the Ward Hunt Ice Shelf revealed basal accretion of freshwater ice (Jeffries and Krouse, 1984).

Subsequent profiles taken in Disraeli Fiord between 1960 and 1999 revealed the freshwater layer thinned by 33 m during this interval (Mueller et al., 2003) and the steady decrease in thickness of the freshwater layer suggested a general thinning of the Ward Hunt Ice Shelf (WHIS). The surface mass balance of the WHIS was only slightly negative (-1.1 m w.e. from 1967 to 1999; Braun et al., 2004) suggesting most of the thinning was due to basal mass loss. However, Vincent et al. (2001)) also suggested that the freshwater could have been preferentially draining via a localized conduit at the base of the ice shelf, and questioned to what extent changes in the thickness of the dammed freshwater layer are representative of changes in the mean thickness of the entire Ward Hunt Ice Shelf. The basal mass balance of ice shelves in this region have not been quantified, so the role of basal freezing or melting remains unknown.

A sinuous fracture running the full north-south extent of the WHIS formed between 2000 and 2002, resulting in the complete drainage of the freshwater layer (Mueller et al., 2003). Subsequent profiles in Disraeli Fiord have shown a complete absence of the freshwater layer as continued

breakup of the ice shelf allowed freshwater to flow unobstructed to the open ocean (Veillette et al., 2008). Similarly, calving and mass loss from the Petersen Ice Shelf resulted in the drainage of its associated epishelf lake in August 2005 (White et al., 2015b). From remote sensing data, Veillette et al. (2008) identified nine ice-dammed or epishelf lakes along the northern coast of Ellesmere Island in 2008. Field measurements at the time confirmed the presence of five of those lakes, however with the exception of Milne Fiord, all consisted of a freshwater layer $<$5 m deep.

Apart from the decrease in thickness of the Disraeli Fiord epishelf lake prior to its loss in 2002, observations from epishelf lakes have revealed short-term and interannual variation in depth of the freshwater-seawater interface (Keys, 1977; Veillette et al., 2008). Keys (1977) suggested a tidally-driven internal wave influenced the depth of the halocline in Disraeli Fiord in 1967, and Veillette et al. (2008) suggest this may have been the cause of some of the interannual variation observed in other epishelf lakes, although tidal amplitude in this region is generally small ($<$0.2 m in Disraeli Fiord; Fisheries and Oceans Canada; www.tides.gc.ca). Veillette et al. (2008) also suggest that fjord circulation and shear-induced mixing could further alter the depth of the halocline, although these processes have not been studied.

Antarctica retains numerous, and much deeper, epishelf lakes than those in the Arctic. Examples include Beaver Lake, with a freshwater layer estimated to be 170 to 260 m deep overlying seawater to 435 m (Laybourn-Parry et al., 2001), and the epishelf lakes of the southern Bunger Hills, Transkriptsii Gulf, with the deepest having an 85 m deep freshwater layer in 1992 and 2000 (Gibson and Andersen, 2002). Smith et al. (2006) observed interannual changes in the depth and gradient of the freshwater-seawater interface in Moutonnée Lake, which varied from 66.5 m in 1973, to 64 m in 2000, to 68 m in 2001, and suggested this could reflect changes in thickness of the impounding George VI Ice Shelf, but more likely were the result of either changes in the seasonal supply of freshwater, tidal fluctuation, or changes in the hydraulic connection to the open ocean. The authors conclude that further long-term monitoring is required to determine the cause and significance of these changes, and how epishelf lake depth is related to ice shelf thickness. However, apart from a 90-day tidal record from Beaver Lake, Antarctica (Galton-Fenzi et al., 2012), there are no observations of the seasonal variation of an epishelf lake.

1.2.4 Fjord oceanography

The role of the ocean in influencing the cryosphere, including the submarine mass balance of ice shelves and tidewater glaciers, variation in the depth of epishelf lakes, and the export of freshwater to the open ocean, are determined by the dynamics of fjords. An understanding of factors that influence the spatial and temporal variation fjord water properties and circulation is therefore essential to understanding ice-ocean interactions. The general physics of fjords have been summarized in a number of reviews (Farmer and Freeland, 1983, Inall and Gillibrand, 2010, Stigebrandt, 2012), with other reviews focusing on the physical oceanography of Arctic fjords (Cottier et al., 2010), and

the dynamics of Greenland fjords with marine terminating outlet glaciers (Straneo and Cenedese, 2015).

Fjords are typically strongly stratified with distinguishable water masses including a fresh surface layer, intermediary water that has a stratification that mirrors offshore waters, and deep basin water below sill level. Stratification within a fjord is influenced by freshwater input, surface heat fluxes, and density-driven exchange with the open ocean, and tidal action (Inall and Gillibrand, 2010). Turbulent mixing and vertical exchange in a stratified fjord is driven by mixing along boundaries, convective acceleration and hydraulic jumps at constrictions, shear instabilities, internal wave breaking, and convective overturning (Farmer and Freeland, 1983). In the case of high-latitude fjords with perennial ice-cover wind forcing is negligible within the fjord, but can still be important for coastal processes where open water may be present (e.g. coastal upwelling).

Variations in density and sea level along the continental shelf will induce horizontal pressure gradients that can drive exchange of waters above sill depth between the fjord and coastal water outside the mouth, known as intermediary circulation (Straneo and Cenedese, 2015). Intermediary circulation can originate from along-shore winds that drive upwelling or downwelling, or density anomalies advected past the mouth of the fjord (Straneo and Cenedese, 2015). The density contrast between fjord waters and coastal waters can result in horizontal pressure gradients that drive baroclinic flows which can be an order of magnitude larger than estuarine flows (Stigebrandt, 2012). Intermediary circulation has been shown to be important in Greenland's fjords, explaining the rapid renewal of the upper water column (Straneo et al., 2010), and the reversing of strongly sheared velocities every few days (Sutherland and Straneo, 2012; Sutherland et al., 2014). Intermediary flows have also been shown to dominate fjord circulation and variability in non-summer months, including the advection of shelf anomalies into fjords on submonthly timescales (Jackson et al., 2014b). Variations in intermediary circulation may also explain interannual changes observed in some Greenland fjords (Mortensen et al., 2013; Christoffersen et al., 2011).

Replacement of deep water, that is water below sill depth, will occur when outside water at or above sill depth exceeds the density of water within the basin (Farmer and Freeland 1983). The residence time of the deep water depends on the turbulent mixing rate (the density of deep water will steadily decrease as near surface water is mixed downward), intermediary circulation, and the volume of water below sill level (Stigebrandt, 2012). The timescale of renewal can range from tidal periods to many years and studies from Greenland have shown a wide range of deep water renewal periods in fjords, ranging from months (Jackson et al., 2014b) to tens of years (Johnson et al., 2011). Explanations for the mechanisms for deep-water renewal vary from tidal forcing, to intermediary flow, to buoyancy-driven circulation, and may be fjord specific, and are strongly dependent on the rate of mixing in the fjord. Once over the sill, replacement waters enter the deep basin as a turbulent gravity current, descending to the bottom of the fjord or spreading out as an interleaving layer once it reaches a depth at which it is neutrally buoyant (Farmer and Freeland, 1983).

1.2.5 Glacial fjords

Interest in the physics of glacial fjords, those with marine terminating glaciers at the head, has grown in recent years due to the widespread retreat and speedup of Greenland's outlet glaciers, increasing contributions to sea level rise (Straneo and Cenedese, 2015). As well, most of the freshwater runoff from surface melting of ice sheets is discharged at the head of glacial fjords, where it is transformed by fjord processes before being exported to the open ocean. There are several unique features specific to glacial fjords that distinguish processes here from non-glacial fjords. Straneo and Cenedese (2015) reviewed the state of knowledge of the dynamics of Greenland's glacial fjords. This section provides a brief summary of key processes that are applicable to the glacial fjords of northern Ellesmere Island, including Milne Fiord.

In classic estuarine circulation, freshwater released at the surface at the head of a fjord mixes with ambient water, generating an outflowing brackish surface layer and a compensating inflow of deep, denser water (Farmer and Freeland, 1983). However, in glacial fjords the freshwater release can also occur at depth, via subsurface discharge of runoff at the bed of the glacier, and by submarine melting of the submerged portions of the glacier face. The release of freshwater at depth by either mechanism results in an upwelling turbulent plume that entrains ambient water as it rises. Plume theory (Morton et al., 1956; Turner, 1973), dictates that the evolution of the plume is controlled by the plume's buoyancy forcing, which is dependent on the density difference between the plume and ambient water. The buoyancy forcing determines the rate of ascent which regulates the amount of entrainment and mixing of the plume with ambient fjord water. In glacial fjords the freshwater release that contributes the buoyancy forcing can occur at a fixed depth, as in the case of subglacial discharge at the glacier bed, or over some depth range, as in the case of submarine melting along the glacier front. The sediment concentration and particle size distribution within a plume originating from subglacial discharge can alter the density of the plume and fjord stratification and circulation (Salcedo-Castro et al., 2013). In glacial fjords, the former is likely dominant near subglacial discharge channels in summer, while the later likely dominates in winter or distant from subglacial discharge in summer. The depth at which the plume will detach from the glacier and spread horizontally down the fjord is dependent on the buoyancy flux of the plume and the ambient stratification. If the plume is less dense than ambient water at the same depth, it will continue to rise and may reach the free surface. However, where ambient stratification is stronger, or buoyancy flux is low, the plume will not reach the free surface and will form an interflow at some intermediate depth.

The input of freshwater from subglacial discharge at the grounding line provides a source of buoyancy and drives convective motion along the ice-ocean interface. The heat brought into the plume through entrainment of ambient water is an additional driver of melting at the base of tidewater glaciers and ice shelves (Jenkins, 2011). The application of the theory of buoyant plumes has shown that warming ocean waters and increased subglacial discharge both generate increased

melting near the grounding line, with melt rates dependent on the temperature of ambient water, the flux of subglacial discharge, and the slope of the ice-ocean interface (i.e. near-vertical for a calving glacier terminus, and near-horizontal for an ice shelf or glacier tongue; Jenkins, 2011).

Observations in Greenland show glacial fjords in this region are characterized by a strongly stratified water column with intrusions of glacially modified water at mid-depths, often at the interface between PW and AW (Mortensen et al., 2011; Straneo et al., 2011; Sutherland et al., 2014), likely giving rise to a multi-cell circulation pattern. In addition, numerical models have shown the magnitude of subglacial discharge, and geometry of subglacial channels (point source, multiple channels, or line source) are important in determining the nature of buoyancy-driven circulation in glacial fjords (Sciascia et al., 2013; Xu et al., 2012; Xu et al., 2013; Cenedese and Linden, 2014) and consequently the submarine melt rate (Xu et al., 2013; Kimura et al., 2013). An improved understanding the dynamics of subglacial plumes is hampered by the challenge of acquiring observations near the face of calving glaciers or at the base glacier tongues.

Circulation below ice shelves

Knowledge of circulation in the cavities below ice shelves and glacier tongues, come primarily from studies in Antarctica. Thermohaline circulation in the cavities below Antarctic ice shelves can be driven by the pressure dependency of the freezing point of seawater (Lewis and Perkin, 1986). As seawater in contact with the ice shelf at depth melts ice, the ascending buoyant plume becomes supercooled relative to the in situ freezing point, and leads to ice formation in the water column, and accretion at the base of the ice shelf at shallower depth. Conversely, descent of waters, after having been in contact with the ice, will have sensible heat available to melt ice at depth. The overall effect is to remove glacial ice from greater depths and deposit sea ice at a shallower location, with the effect of evolving a floating ice shelf toward uniform thickness, a mechanisms known as an 'ice pump' (Lewis and Perkin, 1986). This process is driven solely by the pressure dependency of the freezing temperature, and is independent of melt driven by the transport and entrainment of warm water to the ice base.

To date, there are only a few studies that have addressed the water properties and circulation in glacier tongue cavities in the Arctic, including at Petermann Gletscher (Rignot and Steffen, 2008; Johnson et al., 2011) and Nioghalvfjerdsbræ (79NG; Wilson and Straneo, 2015). With the exception of a single water column profile through a borehole in the Petermann Gletscher tongue (Rignot and Steffen, 2008), and through a rift in 79NG glacier tongue, work has primarily been limited to observations at the ice front, tens of kilometers from the grounding line.

1.2.6 Submarine melting

Submarine melting is a critical factor in determining the mass balance of ice shelves and glacier tongues and the position of the boundary between grounded and floating ice, known as the grounding

line. The grounding line marks the boundary between ice that has has yet to displace its full weight of water, and thus the potential for glacier contribution to sea level rise. Submarine melting by warm ocean waters was demonstrated to be a trigger of the thinning and breakup of the floating tongue of Jakobshavn Isbræin Greenland, which was followed by rapid acceleration of the grounded glacier (Holland et al., 2008a; Motyka et al., 2011).

The mass balance of an ice shelf or glacier tongue is determined by the balance of ablation and accumulation at the surface and base, input from glacier flow, and losses from calving at the ice front. Under steady state conditions, and assuming constant ice density, the area-averaged conservation of mass for a glacier tongue reduces to an expression of volume continuity as

$$Q_{gf} - Q_{cf} - a_{sf}A_{gt} - a_bA_{gt} = 0 \tag{1.1}$$

where Q_{gf} is the ice volume flow across the grounding line, Q_{cf} is the change in ice volume over time at the terminus due to calving or terminus advance, a_{sf} and a_b are the net area-averaged surface and basal ablation rates, respectively (expressed as meters of solid ice per unit time and positive for melting), and A_{gt} is the surface area of the glacier tongue. With estimates of ice velocity, ice thickness, changes in terminus position, and surface ablation, an estimate of basal ablation can be obtained.

Submarine melt rates in glacial fjords can also, in principle, be estimated from the net heat flux from the ambient water to the ice (Straneo and Cenedese, 2015). However, there are several challenges to getting accurate estimates of heat flux in a glacial fjord, and studies that have tried to do so are based on synoptic surveys that rely on several broad, and perhaps unjustified, assumptions (Rignot et al., 2010; Sutherland and Straneo, 2012; Xu et al., 2013; Inall et al., 2014). The few existing continuous (moored) observations in glacial fjords do not support several of the usual assumptions made (Jackson et al., 2014b), and other fluxes not often accounted for, including sea ice formation and melting as well as iceberg melting could strongly influence the overall heat budget (Straneo and Cenedese, 2015). At present, it remains difficult to quantify submarine melt using the heat flux method.

Ocean thermodynamic models

Another approach to estimate melt rates is to consider the thermodynamics of heat transport at the ice-ocean interface. The basic assumption made in all ocean models of submarine ice melt is that the temperature and salinity at the ice-ocean interface are related by the equation for the freezing point at a given pressure (Holland and Jenkins, 1999). Estimation of the ablation rate then requires calculating the heat and freshwater fluxes at the ice-ocean interface based on changes in the far-field ocean properties from freezing point conditions.

A conceptual schematic of the relevant temperatures, salinities, and heat and salt fluxes between

layers at the ice-ocean interface are shown in Figure 1.3. The water column is divided into two regions, the ice-ocean boundary layer, typically a few meters thick, where turbulent mixing is influenced by the proximity of the ice boundary, and the ambient ocean mixed layer, a few tens of meter thick, where turbulence is unaffected by the boundary and stratification and rotation control mixing (McPhee et al., 2008). The boundary layer itself consists of an outer turbulent layer (a few meters thick), where rates of exchange of heat and salt are influenced by the velocity shear induced by the stationary ice shelf, and a viscous sublayer (a few millimetres thick) at the ice-ocean interface where molecular diffusion regulates exchange. The gradients in temperature and salinity across the boundary layer determine the fluxes of heat and salt between the ocean mixed layer and the ice (Holland and Jenkins, 1999). In addition, the internal temperature gradient within the ice shelf near its base drives the heat flux between the ice-ocean interface and the ice interior. Assuming the ice-ocean interface is in thermodynamic equilibrium, a melt (or freezing) rate can be estimated from the heat balance.

The ocean models are based on three physical constraints: that the ice-ocean interface is at the freezing point, and that heat and salt are conserved at the interface during phase changes (Holland and Jenkins, 1999). Prescribed quantities are the far-field properties of the ocean and the interior properties of the ice shelf, which are then used to determine the characteristics at the interface based on the above constraints. In the next section we present the fundamental equations governing the freezing point of seawater and the conservation of heat and salt at the ice-ocean interface, based largely on the work of Holland and Jenkins (1999).

Fundamental equations

Freezing point

The freezing point of seawater is a linear function of pressure and a non-linear function of salinity (Millero, 1978). To simplify solving equations for conservation of heat and salt at the ice-ocean interface, coupled ice-ocean models often use a linearized version of the freezing point dependency at the ice-ocean interface (Holland and Jenkins, 1999), of the form

$$T_b^f = \lambda_1 S_b + \lambda_2 + \lambda_3 P_b, \tag{1.2}$$

where S_b and P_b are the salinity and pressure, respectively, at the ice-ocean interface, $\lambda_{1,2,3}$ are empirical constants. Coefficients λ_1 and λ_2 are usually chosen to optimize the the fit at typical seawater salinities, however the formula is then only valid over a limited salinity range ($\sim$4-40 psu) and does not apply to freshwater (Holland and Jenkins, 1999).

Heat conservation

At the ice-ocean interface the change in latent heat, Q_b^T, due to melting or freezing must be balanced by the heat flux into the ice, Q_i^T, and the heat flux supplied by the ambient water to the ice Q_w^T:

$$Q_b^T = Q_i^T - Q_w^T \tag{1.3}$$

where the latent heat term is given by

$$Q_b^T = -\rho_w a_b L_i \tag{1.4}$$

where ρ is density, L is the latent heat of fusion, and superscript T refers to heat (to distinguish from the salt flux below), and subscripts b, i, w refer to the ice-ocean interface, ice, and water, respectively. The ablation rate at the ice-ocean boundary, a_b, is a change in thickness of solid ice per unit time (positive for melting).

Salt conservation

During melting at the base of the ice shelf, the 'freshwater' flux is balanced by the salt flux divergence at the ice-ocean interface

$$Q_b^S = Q_i^S - Q_w^S \tag{1.5}$$

where superscript S is salt. The 'freshwater' flux is

$$Q_b^S = \rho_w a_b (S_i - S_b) \tag{1.6}$$

where S_i and S_b are the salinities of the ice and the ice-ocean interface, respectively. As salt cannot diffuse through the solid ice the diffusive flux into the ice shelf, Q_i^S is zero, and the salt balance is determined by the flux through the oceanic boundary layer. S_i is assumed to be zero.

The various models of ablation at the base of an ice shelf differ in the treatment of the turbulent transfer of heat and salt through the ice-ocean boundary layer, and the flux of heat through the ice shelf (salt cannot diffuse through solid ice so it need not be considered with the ice). Similar models have been developed both for sea ice (McPhee et al., 1987; Holland, 1998) and ice shelves (Holland and Jenkins, 1999; Jenkins et al., 2010) these differ primarily in the estimation of heat flux through the ice due to the vast difference in ice thickness between the two, and the resulting importance of surface conditions.

Heat flux into ice

The general estimate of the heat flux into the ice shelf can be made using the form

$$Q_i^T = -\rho_i c_i \kappa \left.\frac{\partial T_i}{\partial z}\right|_b \tag{1.7}$$

where ρ_i is the density of ice, c_i is the specific heat capacity of ice, κ_i is the thermal diffusivity of ice, and T_i is the internal ice temperature. The density, heat capacity, and thermal diffusivity are assumed constant, and the focus is on estimating the temperature gradient at the base of the ice shelf. The heat transport equation in the ice shelf is

$$\frac{\partial T_i}{\partial t} + U_i \cdot \nabla T_i = \kappa_i^T \nabla^2 T_i, \tag{1.8}$$

where U_i is the flow field within the ice shelf (Holland and Jenkins, 1999). Without knowledge of the ice flow field, reduced forms of the equation are considered. The simplest approximation is that there is no diffusion of heat into the ice shelf. The next level is to assume that there is vertical diffusion of heat, but no advection. The steady state solution to the heat transport equation then is a linear temperature profile throughout the thickness of the ice shelf, in which case the gradient can be defined by the temperature at the surface of the ice shelf, the temperature at the base, and the thickness of the ice. Although common in sea ice models, this approximation is not entirely appropriate for ice shelves given the greater thickness and observed non-linear temperature profiles through the ice. The heat flux into the ice can be parameterized following Nøst and Foldvik 1994 and Holland and Jenkins (1999) using a steady-state, one-dimensional advection-diffusion equation. Heat conduction into the ice is therefore approximated by

$$Q_i^T = \rho_i c_i a_b (T_i - T_b^f), \tag{1.9}$$

Oceanic heat fluxes

The most sophisticated models make no prior assumptions about conditions at the ice-ocean interface and solve the freezing point, heat flux, and salt flux equations (Holland and Jenkins, 1999). In this formulation, the fluxes of heat and salt across the boundary layer are expressed as

$$Q_w^T = \rho_w c_w u_* \Gamma_T (T_b^f - T_w), \tag{1.10}$$

and

$$Q_w^S = -\rho_w u_* \Gamma_S (S_b - S_w), \tag{1.11}$$

where Γ_T and Γ_S are the turbulent transfer coefficients for heat and salt, respectively, that take into account the nonlinear profiles of temperature and salinity in the boundary layer resulting from turbulence, c_w is the specific heat capacity of water, and T_w and S_w are the temperature and salinity in the ambient mixed layer, respectively. Note in this formulation the freezing point is determined using the salinity at the ice-ocean interface (S_b) as in Eq. 1.19.

The friction velocity u_* is defined in terms of the shear stress at the ice-ocean interface. It is assumed to be related to the free-stream current beyond the boundary layer U through a quadratic drag law,

$$u_*^2 = C_d U^2, \tag{1.12}$$

where C_d is a dimensionless drag coefficient. This formulation assumes a constant shear stress in the boundary layer and is derived from measurement of flow across a hydraulically smooth surface. The applicability of these assumptions for the base of an ice shelf is largely unknown due to a lack of observations, however this parameterization is widely used in numerical models where results have compared favourably with observations beneath sea ice (McPhee et al., 1999). Determination of the proper drag coefficient and the turbulent transfer coefficients are the main challenges for accurate modelling of ice shelf ablation rates, and these are discussed further below.

Two-equation model

An alternative approach is to simplify the problem by assuming that the mixed layer salinity and the interfacial salinity are equal, implying infinite salt diffusion (Holland and Jenkins, 1999). The melt rate is therefore determined by the transfer of heat through the boundary layer which is parametrized as

$$Q_w^T = \rho_w c_w u_* \Gamma_{TS} (T_w^f - T_w) \tag{1.13}$$

where u_* is the friction velocity, and Γ_{TS} is a turbulent transfer coefficient for heat and salt. In practice, Γ_{TS} is derived directly from observations, and therefore accounts for the rate-limiting process of salt-diffusion across the boundary layer. Here, the freezing point is evaluated using the far-field salinity (S_w) (McPhee, 1992; McPhee et al., 1999) calculated as

$$T_w^f = \lambda_1 S_w + \lambda_2 + \lambda_3 P_b. \tag{1.14}$$

In summary, the two more sophisticated models used to estimate ablation rates at the base of an ice shelf are the three-equation model,

$$\rho_i a_b L_i = \rho_i c_i a_b (T_i - T_b^f) - \rho_w c_w u_* \Gamma_T (T_b^f - T_w) \tag{1.15}$$

$$\rho_i a_b (S_b - S_i) = -\rho_w u_* \Gamma_S (S_b - S_w), \tag{1.16}$$

$$T_b^f = \lambda_1 S_b + \lambda_2 + \lambda_3 P_b, \tag{1.17}$$

or the two equation model,

$$\rho_i a_b L_i = \rho_i c_i a_b (T_i - T_w^f) - \rho_w c_w u_* \Gamma_{(TS)} (T_w^f - T_w) \tag{1.18}$$

$$T_w^f = \lambda_1 S_w + \lambda_2 + \lambda_3 P_b, \tag{1.19}$$

with the friction velocity in both models parameterized as per Eq. 1.12. The parameters that are least well constrained in the above models are the turbulent transfer coefficients Γ_T, Γ_S, and $\Gamma_{(TS)}$, and the drag coefficient C_d. In the turbulent boundary layer, heat and salt diffuse at the same rate, whereas in the viscous sublayer the turbulent eddy size is reduced so the turbulent diffusivity is replaced by molecular diffusivity (Mellor et al., 1986; McPhee et al., 1987; Steele et al., 1989). Therefore, because the transfer coefficients parameterize all transport processes in the boundary layer, Γ_T must be larger than Γ_S due to the differing rates of molecular diffusivity between heat and salt.

The transport of heat and salt through the boundary layer is also dependent on the shear stress at the ice-ocean interface which is parameterized using the friction velocity u_*, which is itself dependent on the selection of the drag coefficient C_d. The above notation follows that of Jenkins et al. (2010) where the turbulent exchange coefficients have a functional dependence on the frictional velocity (Jenkins and Doake, 1991). Exchange velocities have also been expressed by others as

$$\gamma_{(T,S,TS)} = C_d^{\frac{1}{2}} \Gamma_{(T,S,TS)} U, \tag{1.20}$$

From Eq. 1.10 the turbulent transfer coefficient is defined as,

$$\gamma_T = \frac{Q_b^T}{\rho_w c_w u_* [T_b^f - T_w]} \tag{1.21}$$

which is analogous to a thermal Stanton number, a ratio of heat transferred into a fluid to the thermal capacity of the fluid, except for the use of the friction velocity rather than the velocity of the boundary layer. Stanton numbers derived from laboratory studies of boundary layers on hydraulically smooth surfaces have been used in numerical models of the interactions between ice shelves and the ocean (Jenkins and Bombosch, 1995; Holland and Jenkins, 2001). The application of laboratory results to the boundary layer beneath an ice shelf is questionable, however Holland and Jenkins (1999) showed that it yields similar results to coefficients produced by more complex parameterizations that include the effects of the stabilizing buoyancy caused by the release of freshwater at the ice shelf base during melting, and the effects of rotation (McPhee et al., 1987). The insensitivity of the exchange coefficients to processes that effect mixing in the boundary layer is because exchange rates are largely determined by molecular diffusion across the viscous sublayer. The parameteriza-

tion compared favourably with observations beneath sea ice (McPhee et al., 1999).

Jenkins et al. (2010) found that melt rates derived using both the two- and three-equation models matched observations at the base of the Ronne Ice Shelf, Antarctica, within 40%. Adjustment of the drag coefficient, the parameter that is least well constrained by observation, reduced the mismatch below observational error. However, Jenkins et al. (2010) caution that the value of the drag coefficient used assumes that the turbulent transfer coefficients estimated for sea ice are appropriate for the base of an ice shelf, which given the different nature of boundary flow beneath ice shelves, forced by buoyancy and tides rather than wind-drift of sea ice, could violate that assumption. Further discussion of the parameterization of turbulent transfer coefficients can be found in McPhee et al. (1987), Steele et al. (1989), Holland and Jenkins (1999), and Jenkins et al. (2010). Values for turbulent transfer coefficients and drag coefficients have not been validated by measurements below Arctic ice shelves or glacier tongues.

1.3 Thesis objectives

There exist numerous observation gaps that this research aims to address. Recent studies of the oceanography of fjords in the Canadian Arctic are few (Melling et al., 2015). The last comprehensive oceanographic study of an ice shelf dominated fjord occurred over 50 years ago (Keys, 1977). For glacial fjords, where studies do exists in other regions they are often limited to brief summer surveys, and observations are often restricted to the outer region of the fjord several kilometers from the glacier terminus or grounding line (e.g. Straneo et al., 2010; Straneo et al., 2010; Inall et al., 2014). As well, continuous records of the seasonal cycle of changes in water properties in glacial fjord are rare (Cottier et al., 2005; Jackson et al., 2014b; Mortensen et al., 2014). The factors contributing to variations in epishelf lake depth and how these variation may reflect changes in the thickness of the ice shelf are not well understood (Vincent et al., 2001; Smith et al., 2006), due largely to a lack of continual observations in epishelf lakes. Finally, direct estimates of melt rates for ice shelves or marine terminating glaciers have not been conducted in the Canadian Arctic, so the magnitude of melt rates, and factors that effect its spatial or temporal variability are unaddressed.

This thesis aims to describe the oceanography of Milne Fiord, the last ice shelf-epishelf lake system in the Arctic.

The primary objectives of this thesis are:

- To provide the first comprehensive physical oceanographic description of Milne Fiord, including the influence of the Milne Ice Shelf and Milne Glacier on water properties, circulation, and seasonal variation in the fjord.

- To understand the dynamics of the Milne Fiord epishelf lake and factors that influence its seasonal and long-term variability.

- To estimate the magnitude, and spatial and temporal variation, of submarine melt rates in Milne Fiord.

To aid in the interpretation of oceanographic data and allow estimates of submarine melt rates a secondary objective is:

- To produce a digital elevation model of ice topography and bathymetry of Milne Fiord.

1.4 Thesis outline

An outline of the remainder of this thesis is presented below.

Chapter 2 presents observations of the general water properties and circulation of the fjord and how they are influenced by the presence of an ice shelf and glacier tongue. By conducting extensive hydrographic surveys, including through-ice profiles of water column properties that extend the length and width of the fjord, including from the grounding line of the Milne Glacier to the outer edge of the Milne Ice Shelf, the spatial variation in the fjord is described. An ice-tethered mooring deployed through the epishelf lake in the centre of the fjord recorded variation in ocean properties over the full water column spanning a period of 3-years. The observations are placed in context with maps of ice thickness, produced by a ground-based radar survey of ice thickness in combination with remote sensing data, and bathymetric chart, based on spot soundings acquired during water column profiling.

Chapter 3 presents a description of the seasonal and interannual variations in the epishelf lake, and aims to understand what factors influence its depth and how these are related to the state of the ice shelf. All previous water column profiles acquired of the Milne Fiord epishelf lake since the first observation in 1983 were obtained and compiled with new profiles collected during this study to understand long-term changes in the water column. An ice-tethered mooring provided a continuous record of variation of the epishelf lake over a 3-year period. A simple analytical model of hydraulic controlled flow is used to simulate and explain the drainage of the lake each winter.

Chapter 4 estimates of submarine melt rates of the ice shelf and glacier tongue are presented, and factors determining their spatial distribution and temporal variability discussed. Two independent methods are used to estimate annual melt rates from 2011 to 2015: a divergence of ice flux method that utilizes remotely sensed ice surface velocities and the ice thickness model produced in Chapter 2; and an ocean thermodynamic model that uses field measurements of ocean properties and circulation.

Chapter 5 provides a summary of the entire body of work in the thesis and discusses potential areas for future research.

1.5 Figures

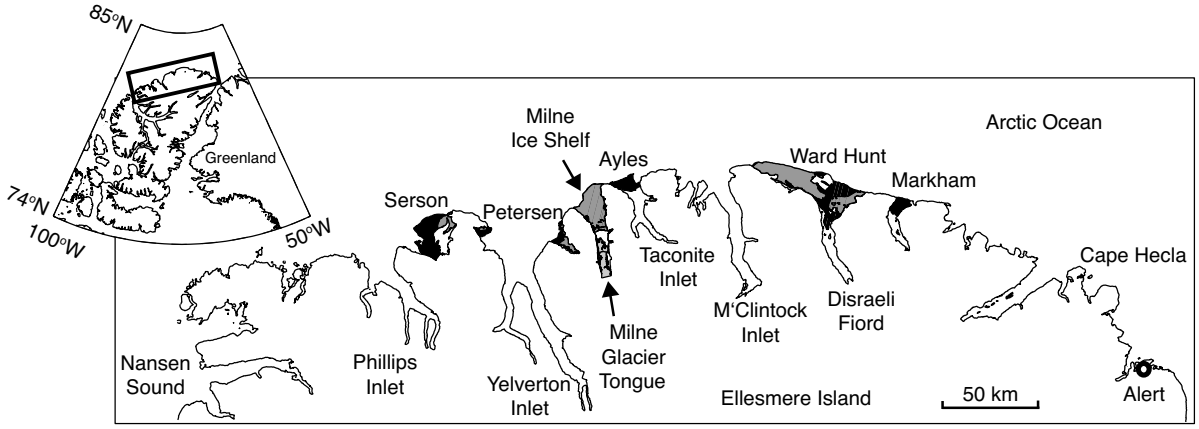

Figure 1.1 Map of the northern coast of Ellesmere Island. Black and grey shading represents the extent of ice shelves in 2003, while the reduced extent as of January 2011 are shown in grey. Over this period the Serson, Ayles, and Markham ice shelves calved completely from the coast, the Petersen and Ward Hunt ice shelves lost large fragments, while the Milne Ice Shelf and Milne Glacier tongue remained largely unchanged during this period. Data courtesy of D. Mueller.

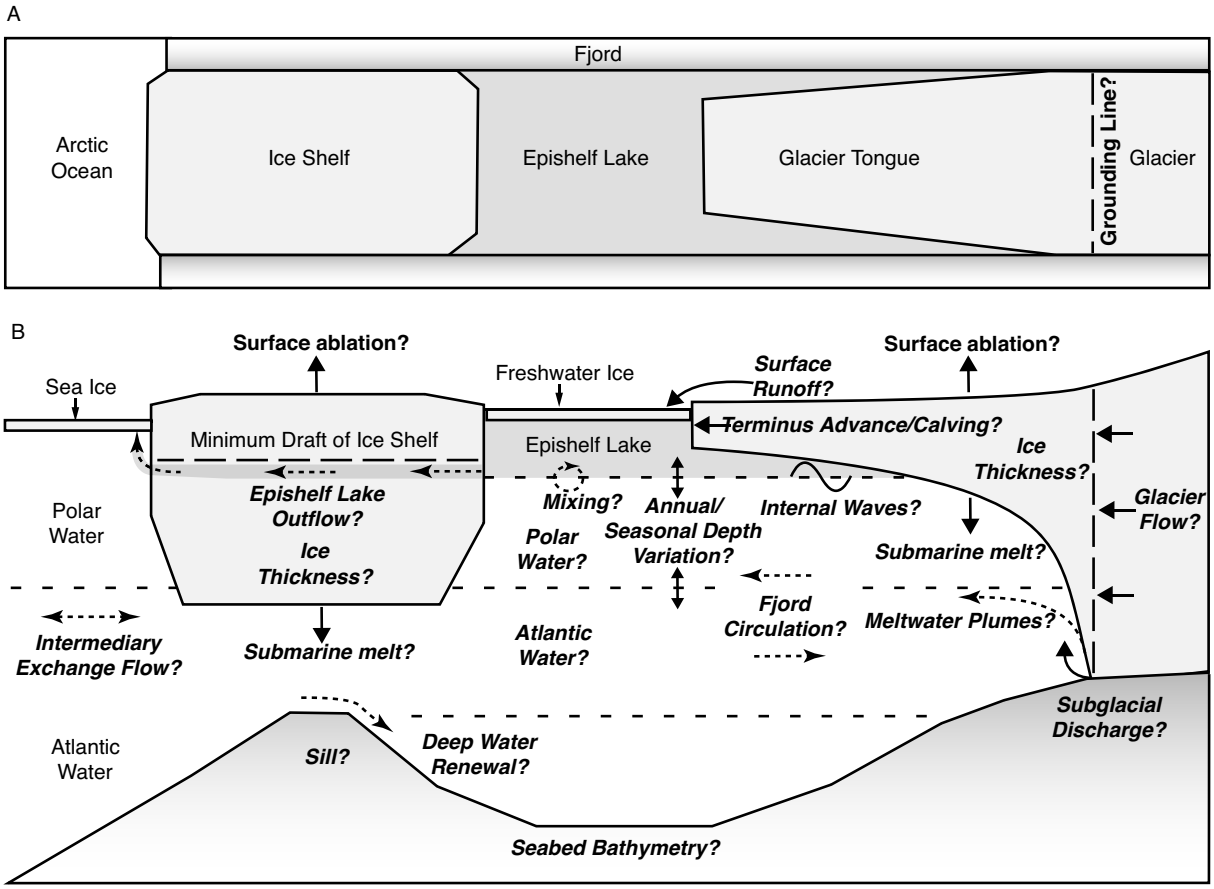

Figure 1.2 Schematic representation of Milne Fiord in A) plan and B) elevation view. Features observed prior to this study are labelled in regular font, while features or processes this study aimed to observe and/or quantify are indicated in bold italic.

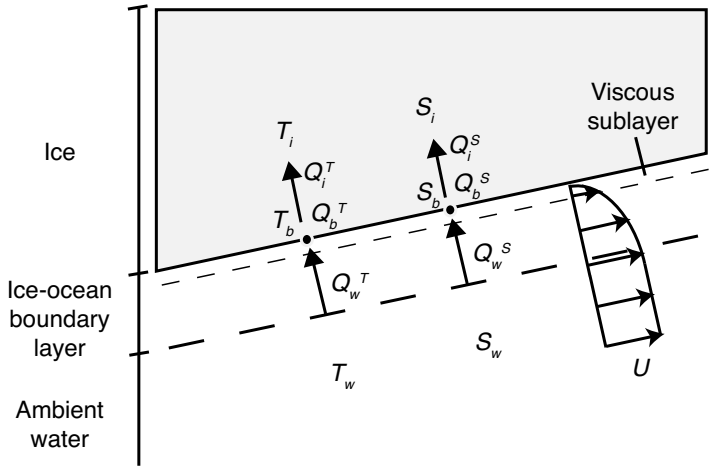

Figure 1.3 Schematic representation of the temperatures, salinities, and the heat and salt balance at the ice-ocean interface at the base of an ice shelf. Modified from Holland and Jenkins (1999) and Straneo and Cenedese (2014).

Chapter 2

Modification of ocean properties and circulation by an ice shelf and glacier tongue in Milne Fiord

2.1 Introduction

Glacial fjords are the critical gateways between the ocean and ice sheets in the Arctic, and understanding their dynamics is important to understanding and predicting changes to ice sheets and their impact on the ocean (Straneo and Cenedese, 2015). Large volumes of freshwater from melting ice sheets are discharged into fjords and modified by fjord processes before being released to the open ocean, with implications for ocean stratification and circulation. Submarine melting of outlet glaciers by warm ocean water has been identified as a plausible mechanism contributing to both the retreat and increased flow rate of tidewater glaciers (Holland et al., 2008b; Motyka et al., 2011; Joughin et al., 2012; Straneo et al., 2012). These processes are all influenced by the properties of the fjord, including its geometry, water mass characteristics, ambient stratification and circulation, so an understanding of glacial fjord oceanography is key to predicting ice sheet dynamics, ocean circulation, and their impact on climate.

The recent loss of coastal ice and and ice-associated features from fjords along the northern coast of Ellesmere Island, Canada, on the Arctic Ocean, is indicative of a shift in climate in this region. Widespread calving of coastal ice shelves (Vincent et al., 2001; Mueller et al., 2003; Copland et al., 2007; Mueller et al., 2008; White et al., 2015a), the almost complete loss of ice-dammed fjord-lakes (Mueller et al., 2003; Veillette et al., 2008), and the collapse of glacier tongues and the loss of multi-year land-fast sea ice (Pope et al., 2012) have been attributed, in part, to regional atmospheric warming. The warming has resulted in an increased freshwater input to the fjords from surrounding glaciers, with mass loss from glaciers of the Canadian Arctic Archipelago being the single largest

contributor to sea level rise outside of Greenland and Antarctica between 2003-2009 (Gardner et al., 2011; Lenaerts et al., 2013). Despite the fact that fjords along the northern coast of Ellesmere Island are impacted by climate change, the last physical oceanographic studies of fjords here occurred over 40 years ago (Ford and Hattersley-Smith, 1965; Lake and Walker, 1973; Keys, 1977), with the exception of one study from a small inlet in 1991-92 (Ludlam, 1996).

There is growing evidence of the importance of fjord dynamics on determining the mass balance of the Greenland Ice Sheet, and its contributions to sea level rise and influence on the ocean and climate, and these processes are likely relevant to the Canadian Arctic. The recent widespread acceleration of outlet glaciers in southeast and southwest Greenland is thought to be linked to enhanced submarine melt due to the migration of warm Atlantic water masses of subtropical origin into deep fjords (Holland et al., 2008b; Straneo et al., 2010; Christoffersen et al., 2011), and the rapid collapse of the 15 km long Jakobshavn Isbrae glacier tongue (Motyka et al., 2011) was linked to a warm water intrusion into the fjord (Holland et al., 2008a). Some estimates suggest that up to 80% of the mass loss of marine-terminating glaciers in Greenland can be attributed to submarine melting (Rignot and Steffen, 2008) although melt rates are largely based on parameterizations that are dependent on a variety of processes that are poorly constrained in glacial fjords. These processes include the ambient stratification and vertical distribution of heat in the fjord (Straneo et al., 2011; Mortensen et al., 2013), and the fjord circulation, which in glacial fjords is influenced by a complex interplay of wind stress and tides (Mortensen et al., 2011), baroclinic response to external forces (Sutherland and Straneo, 2012; Jackson et al., 2014b), convection from ice-ocean interactions, and buoyancy-driven flows from seasonal freshwater runoff (Straneo et al., 2011). In tidewater glacial fjords runoff can enter the fjord at the surface or at depth across the grounding line of the glacier, known as subglacial discharge, with implications for vertical heat distribution, ocean stratification and fjord circulation (Straneo et al., 2011; Xu et al., 2012; Sciascia et al., 2013). However, with a few exceptions (Chauch et al., 2014), observations in glacial fjords are often limited to the outer fjord, several kilometers from the glacier terminus, due to the challenges associated with sampling in the presence of a calving glacier, icebergs, ice mélange, or through thick glacier tongues. While some of the Greenland-derived results are likely relevant to other regions, differences in geography, coastal and climatic conditions, suggest glacial fjords in the Canadian Arctic Archipelago warrant special attention, yet they remain largely unexplored.

We conducted an oceanographic field study of Milne Fiord, on the northern coast of Ellesmere Island, that is fed by the Milne Glacier, an outlet glacier that terminates in a floating glacier tongue at the head of the fjord. A unique feature of Milne Fiord is the presence of the Milne Ice Shelf, distinct from the glacier tongue, that spans the mouth of the fjord. In this paper we distinguish between a 'glacier tongue', defined as the floating extension of an outlet glacier at the head of a fjord, and an 'ice shelf', defined as a floating platform of thick ice at the mouth of a fjord, formed by *in situ* sea ice accretion and snow accumulation, sometimes with additional glacial input from low-

lying coastal ice caps and tributary glaciers (Jeffries, 2002). The Milne Ice Shelf forms an ice-dam that traps runoff within the fjord creating a perennially stratified water column with a freshwater layer floating on seawater, called an epishelf lake. The thin (<1 m) perennial ice cover of the epishelf lake created a stable platform for field work, permitting access to the glacial fjord for oceanographic investigation. To provide context for our study, we first provide a regional overview of the northern Ellesmere climate and oceanographic setting with relation to the source waters that can access Milne Fiord. Next, because fjord dynamics are highly dependent on the geometry of the fjord we present the first bathymetric survey of the fjord, and present a digital elevation map of ice thickness for the entire fjord based on field observations and remote sensing data. From analysis of extensive through-ice hydrographic profiles, including transects that extend along the entire length of the fjord to the glacier grounding line (where the glacier detaches from the bed and is afloat), we describe the vertical and horizontal distribution of water masses, the distribution of submarine meltwater and subglacial discharge, and the modification water properties in relation to bathymetry and ice topography. Using data collected by a full-depth ocean mooring deployed in the fjord we then describe the internally and externally forced temporal variability of ocean temperatures in the fjord over the 3-year study. Finally, we discuss the implications of our observations on how loss of the ice shelf will impact fjord dynamics and the Milne Glacier.

2.2 Methods

2.2.1 Field Site

Milne Fiord (82°35'N; 81°W) lies at the northwest coast of Ellesmere Island on the Arctic Ocean (Fig. 2.1). A combination of low annual average air temperatures ($\sim$ -18°C at Alert between 1971-2000; www.ec.gc.ca), low ocean heat flux (Krishfield, 2005), and ocean circulation (Aksenov et al., 2010) create conditions favourable for the formation and persistence of coastal land-fast ice along this coast. The coast maintains the oldest and thickest multiyear land-fast sea ice in the Arctic (Maslanik et al., 2011; Laxon et al., 2013), the largest concentration of coastal ice shelves in the Arctic (total area of 500 km^2 at end of 2015; Copland and Mueller, *Arctic Ice Shelves and Ice Islands*, Springer-Verlag., In press); and the lowest glacier equilibrium lines in the Northern Hemisphere (Braun et al., 2004), resulting in extensive floating glacier tongues. The coastal ice conditions prevent ship-based measurements and as a result oceanographic studies of the fjords of northern Ellesmere Island are few (Crary, 1956; Ford and Hattersley-Smith, 1965; Lake and Walker, 1973; Keys, 1977; Ludlam, 1996).

Existing observations collected offshore of northern Ellesmere Island reveal a stratified water column consisting of a 30–50 m deep seasonal mixed layer (SML), above comparatively fresh (<34.4 PSU), cold (<0°C) Polar Water (PW) to $\sim$200 m depth (Aksenov et al., 2010 and references therein), overlying warmer (up to 0.5°C), saline (>34.7 PSU) modified Atlantic Water (AW) below

350 m depth (Jackson et al., 2014a; Steur et al., 2013). A schematic of major currents in the Arctic Ocean, including those inferred to exist but not directly observed along northern Ellesmere Island, is shown in Figure 2.1a. Surface waters above 200 m depth originate in the Canada Basin and typically flow westward along the coast Steele et al., 2004; Aksenov et al., 2010). An eastward flowing boundary undercurrent appears to exist along the continental slope from the base of the mixed layer (30 – 75 m) to the bottom (Newton and Sotirin, 1997) likely an extension of the Arctic Circumpolar Current (Rudels et al., 1999; Aksenov et al., 2010). Sparse bathymetric soundings along the coast show the continental shelf shoals to 270 m at the shelf break, separating Milne Fiord, and the 600 m deep basin at its mouth, from the deep ocean (Fig. 2.1b). Published bathymetry for Milne Fiord in the International Bathymetric Chart of the Arctic Ocean (IBCAO v3.0; Jakobsson et al., 2012) was based solely on an interpolation between offshore soundings and the coastline. Soundings inside the fjord prior to this study were limited to two small, shallow (77 m and 80 m deep) inlets on the southwest and northeast shores of the fjord, the bathymetry was otherwise unknown.

The Milne Glacier, a 4–5 km wide, 55 km long outlet glacier that drains $\sim$4% by area of the northern Ellesmere Island icefields (GLIMS and NSIDC, 2005), flows into the head of Milne Fiord (Fig. 2.2a). Previous work suggested that the terminus of the glacier was probably afloat and formed a glacier tongue (Hattersley-Smith, 1969; Narod et al., 1988; Jeffries, 1984), referred to here as the Milne Glacier tongue (MGT). The MGT is actually a composite of three glacier tongues; the central tongue comes from the main valley glacier flowing from the highest elevations of the ice cap and has greater surface relief and thickness, while the southwest and northeast tongues come from tributary glaciers that join the main glacier within 10 km of the present-day grounding line. Van Wychen et al. (2016) found surface velocities of the Milne Glacier on the order of 100 m a^{-1} near the grounding line, and estimated the mean ice discharge to be 0.05 ± 0.02 Gt a^{-1} between 2011 and 2015. The Milne Glacier has been identified as a possible surge-type glacier (Jeffries, 1984; Copland et al., 2003).

At the mouth of the fjord, spanning 18 km between Cape Egerton and Cape Evans, and distinct from the MGT, is the Milne Ice Shelf (MIS; Fig. 2.2a), formed through a combination of sea ice accretion, snow accumulation and input from surrounding tributary glaciers and low-lying coastal ice caps (Jeffries, 1986a). The MIS was mapped using ice-penetrating radar by Mortimer et al. (2012) in 2008/9, and was found to have a mean thickness of 49 m and a maximum thickness of 94 m. The topology of the ice shelf is quite variable owing to its complex origins, and was previously divided into three distinct regions, the Outer, Central and Inner Units, based on surface morphology and ice characteristics (Jeffries, 1986a). The Outer Unit at the seaward edge of the ice shelf, distinguishable by a series of surface ridges and troughs running parallel to the coast, is generally thick (>50 m), but is bisected by two re-healed fractures that have existed since at least 1950 (Hattersley-Smith and Fuzesy, 1969). The Central Unit forms the landward edge of the ice shelf bordering the epishelf lake, and has a more erratic surface morphology and thickness

(Jeffries, 1986a). The Inner Unit, that was thought to have once been contiguous with the MGT, no longer exists, it has been replaced with epishelf lake ice (Mortimer et al., 2012). As of 2009 the epishelf lake consisted of a main basin spanning the width of the fjord between the MIS and MGT, and two arms extending along either side of the MGT, with a total estimated area of 52.5 km^2 (Mortimer, 2011). The epishelf lake was 14.3 m thick as of 2009, its depth presumed to correspond to the minimum draft of the MIS (Veillette et al., 2011b). With the exception of a few shallow hydrographic profiles collected to study the epishelf lake (Jeffries, 1985; Veillette et al., 2008; Veillette et al., 2011a), there was no information on the general oceanography of the main fjord prior to this study.

2.2.2 Bathymetry and ice thickness mapping

Bathymetry and ice topography are critical to understanding fjord circulation and exchange with offshore waters so we produced a digital elevation model (DEM) of Milne Fiord from a combination of field measurements, remote sensing, and available archived data. Between 2011 and 2015, we collected 53 bathymetric soundings by lead line and during CTD profiling through augered ice holes in the epishelf lake, steam-drilled holes in the MIS, and through natural fractures in the MIS and MGT. Soundings extended from 5 km offshore of the MIS to the hinge crack near the Milne Glacier grounding line. NASA's Operation Icebridge 2014 Multichannel Coherent Radar Depth Sounder (MCoRDS; Leuschen et al., 2010) data was used to constrain bed elevation upstream of the grounding line, and the cross-sectional bed profile of the fjord above the grounding line was modelled as a U-shaped valley as in Van Wychen et al. (2014) to model glacier thickness at a flux gate for Milne Glacier. We further constrained fjord bathymetry from analysis of hydrographic data, and ice radar, discussed in detail below. To reconcile the regional IBCAO 3.0 data with our new observations we replaced IBCAO grid points in Milne Fiord with our own data and model bathymetry on a 100 m x 100 m mesh using the Matlab gridfit.m function (J. D'Errico, 2006; www.mathworks.com). Gridfit.m is not an interpolant designed to exactly predict all source data, but rather it is an approximant that produces a smooth surface that represents the behaviour of the source data as closely as possible, allowing for gaps and noise in the data, and allows smooth extrapolation beyond the domain of the source data. Bathymetric soundings are sparse in many areas of the fjord, particularly below regions of the MIS and MGT, so the bathymetric model should be viewed in this context.

To constrain ice thickness in the fjord we utilized a combination of ground and aerial radar measurements. The thickness of the MIS was mapped by Mortimer et al. (2012) using a snowmobile-towed Ice-Penetrating Radar (IPR) system in 2008 & 2009, and we reproduce this data here, but supplement it with new sources. We expanded spatial coverage of the MIS in 2011 and 2013 using a snowmobile-towed Sensors and Software Pulse EKKO Pro 250 MHz IPR system, with data processed as in Mortimer et al. (2012). Ground-based measurements of the MGT were acquired

in 2012 and 2013 using a 50 and 70 MHz Blue System Integration IPR system, as described in Mingo and Flowers (2010)), towed on foot, with data processing as in Wilson et al. (2013). Ice thickness along the centreline of the MGT was further constrained by aerial radar measurements acquired by the Operation Icebridge 2014 MCoRDS (Leuschen et al., 2010). The location of the Milne Glacier grounding line is assumed to correspond to the point of first hydrostatic equilibrium, where the thickness of the ice derived from Airborne Topographic Mapper (ATM) laser altimeter (Krabill, 2010) surface elevation equals that measured by the Multichannel Coherent Radar Depth Sounder (MCoRDS; Leuschen et al., 2010). Error in the ice depth measurements is +- 10 m.

For increased spatial coverage, we estimated ice thickness from surface elevation measurements of the MIS and MGT by assuming that ice downstream of the Milne Glacier grounding line was afloat. Analysis of IPR transects showed very strong bottom reflections, indicative of an ice-water interface, everywhere except a region just south of the confluence of the re-healed fractures in the MIS (2.2c). The ice here was relatively thin (<40 m) and showed intermittent and weak bottom reflections, possibly due to an ice-bedrock interface. These observation, combined with nearby bathymetric soundings through the re-healed fracture that revealed the seabed rose to within 28 m of the surface, suggested the ice shelf may have been partially grounded in this region. Consequently, we exclude an area encompassing the weak bottom reflection IPR transects from the surface elevation to thickness conversion.

Where ice was afloat, or where we have no data to the contrary, ice thickness was estimated from surface elevation by assuming the ice was in hydrostatic equilibrium with a mean ice density of 900 kg m^3 and mean seawater density of 1024 kg m^{-3}. Existing high resolution (13 m x 23 m grid size) digital elevation data from Natural Resources Canada (NRCAN; http://www.geobase.ca) was found to be inaccurate over large regions of the MIS and MGT when compared with field data, so we compiled data from various other sources. Ground-based position and elevation data were recorded using a Topcon HiPerV Dual Frequency Global Navigation Satellite System (GNSS) receiver mounted on the IPR sled sampling at 5-second intervals with precise positioning computed using the online tool available from Natural Resources Canada (http://www.nrcan.gc.ca). Positions are accurate to $\pm$ 10 mm horizontal and $\pm$ 15 mm vertical. We also used the Ice, Cloud, and Land Elevation Satellite (ICESat) laser altimetry data (Zwally et al., 2011) from the GLA06 product (Release-33) acquired between 2003 and 2009. The laser altimeter measures surface topography to a precision of 10 cm with a laser surface-spot diameter of $\sim$70 m every $\sim$170 m. Additional elevation data was utilized from a swath along the MGT collected by the Operation Icebridge 2014 Airborne Topographic Mapper (ATM) laser altimeter (Krabill, 2010). All elevation data were processed by manual removal of outliers and smoothed prior to calculating ice thickness by applying a 1-dimensional 5-point convolution filter. Tides are not accounted for, however nominal tidal range is small, on order of 0.3 m, so we take this as the error in elevation data.

A cross-point error analysis was conducted comparing the measured ice thickness from IPR data

to that estimated from surface elevation data for points within a distance of 35 m (the approximate radius of the ICESat laser footprint). Mean absolute discrepancy was 0.66 m, with a standard deviation of 1.20 m. Given the large ice surface topography variations ($\pm$ $\sim$8 m), tidal height variation, and changes in mass balance over time that would affect the elevation data, as well as the temporal offset of data collection periods, this error was deemed acceptable.

Polygons delineating surface features, including the fjord shoreline, margins of the glacier tongue, epishelf lake, and ice shelf and major fractures were identified using a 21 July 2009 Advanced Spaceborne Thermal Emission and Reflection Radiometer (ASTER) satellite scene and digitized using Matlab (R2012b). Uncertainty in dimensions derived from satellite imagery was estimated to be twice the 15 m image resolution. The thickness of the epishelf lake ice was assumed 1 m everywhere based on numerous field measurements. IPR transects across the re-healed fractures in the MIS revealed a narrow bottom channel at the base of the ice shelf running parallel to the surface expression of the fracture. The ice thickness at the apex of the channel was measured by steam drill at 3 locations and varied between 8–11 m. Using the highest quality IPR transects across the fracture as a reference, we modelled the basal channel as an inverted parabola with uniform cross-sectional thickness along its entire length. The depth below sea level of the channel (Z_{int}) was interpolated as:

$$Z_{int} = \frac{(Z_m - Z_c)}{D_1^2} D_2^2 + Z_c \tag{2.1}$$

where Z_c is the depth at the centerline of the channel (10 m), Z_m is the depth of the ice at the channel margin (40 m), D_1 is half the width of the base of the channel (70 m), and D_2 is the distance from the centerline of the channel to the centre of the interpolated ice column. Ice depth was interpolated at 10 m intervals from the centerline to the margin every 100 m along the length of the channel. All ice thickness data was gridded onto a 100 m X 100 m mesh using the Matlab gridfit.m function (J. D'Errico, 2006) to produce contour maps and raster images of ice thickness for the entire fjord.

2.2.3 Hydrography

Ocean properties were measured over 5 field campaigns in May 2011, May 2012, July 2012, May 2013, July 2013, and July 2014. The 2011 profiles were recorded using a 4 Hz SBE19+ Conductivity-Temperature-Depth (CTD) instrument, all others using a 6 Hz RBR XR-620 CTD. The instruments were lowered at 0.5 m s^{-1} using a manual reel through drilled holes, leads in sea ice and fractures in the ice shelf and glacier tongue. All profiling was completed on foot or by snowmobile, except two $\sim$50 km along-fjord transects which were completed by helicopter in July of 2012 and 2013. During these surveys profiles were collected at up to 12 locations, including through a rift near the grounding line of the Milne Glacier and through leads in the sea ice 5 km beyond the seaward edge of the MIS outside the fjord. Data was processed in Matlab following a procedure that included correction for atmospheric pressure, application of a low-pass filter in time

to the raw pressure, temperature and conductivity, alignment of conductivity and temperature and pressure, a thermal cell mass correction (for the SBE19+ data), and loop editing. Derived variables were calculated using the International Thermodynamic Equation of Seawater 2010 (TEOS-10) Gibbs Seawater Oceanographic Matlab Toolbox (www.TEOS-10.org) and averaged over 0.2 m depth bins. CTDs were calibrated once every 1–2 years. A single turbidity profile near the center of the main basin of the epishelf lake was recorded using a Seapoint Turbidity Sensor at 100x gain in July 2013. Additional offshore hydrographic profiles over the northern Ellesmere Island continental shelf break were obtained from the Arctic SwitchYard Project (PI Mike Steel, University of Washington). Profiles were collected in May of 2012 and 2013 from Twin Otter and helicopter by lowering a SBE19plusv2 Seacat CTD through open leads or drilled holes in the sea ice. Data was downloaded from the Advanced Cooperative Arctic Data and Information System website (www.aoncadis.org) and derived variables calculated as above.

To estimate the amount of meltwater present in the water column we use a simple mixing model described in Jenkins (1999). Conservative properties of a water mixture, χ, are determined by the relative mass input of its individual components, χ_1 and χ_2:

$$Q\chi = Q_1\chi_1 + Q_2\chi_2 \tag{2.2}$$

where $Q = Q_1 + Q_2$ is the total mass of the mixture. On a bivariate property plot, such as a temperature-salinity diagram, measurements of any two conservative properties of a mixture will fall on a straight line between endpoints defined by the properties of the component water masses. For temperature to be used in the mixing model in the case when ice melts in seawater, heat must be conserved. To do so we must account for 1) sensible heat loss from seawater to ice that warms the ice from its internal temperature, Θ_i, to the freezing point of the ambient water, Θ_f, 2) absorption of latent heat during phase change, and 3) sensible heat loss during mixing of the meltwater, at freezing point, with ambient seawater. Ice can then be assigned an effective temperature Θ_i^* that accounts for heat loss during the melting process by:

$$\Theta_i^* = \Theta_f - \frac{L}{c_p} - \frac{c_i}{c_p}(\Theta_f - \Theta_i) \tag{2.3}$$

that allows temperature to be used as a conservative property in (2.2) (Gade, 1979). In Eq. (2.3) L is the latent heat of fusion, and c_i and c_p are the specific heat capacities of ice and seawater, respectively, at constant pressure.

If the ambient water properties are not homogenous, but are a mixture of two water masses, then the meltwater mixture will fall within the triangle bounded by the meltwater lines of each water mass endpoint. In Milne Fiord the ambient water is a stratified mixture of Polar Water (PW) and modified Atlantic Water (AW) and melting may occur over various depths in the halocline. A

composite property Ψ can be defined as in Jenkins (1999):

$$\Psi^{2,1} = (\chi^2 - \chi^2_{w0}) - (\chi^1 - \chi^1_{w0}) \left(\frac{\partial \chi^2}{\partial \chi^1} \right) \tag{2.4}$$

where superscript ^{i} represents temperature or salinity and subscript $_0$ indicates defined endpoint water mass characteristics (PW with -1.7 °C and 31.2 g kg^{-1}, and AW with -0.8 °C and 34.25 g kg^{-1}). The last term in brackets on the right is the gradient of the ambient water line. Values of the composite property can be related to meltwater fraction by:

$$\Psi = \frac{\Psi^{2,1}_{mix}}{\Psi^{2,1}_{melt}} \tag{2.5}$$

where the numerator is the sampled composite property of the mixture, and the denominator is the composite property of ice (in fact, pure meltwater with zero salinity and an effective temperature (Θ^*_i) as above) (Eq 6; Jenkins, 1999). The calculation of meltwater concentration assumes direct mixing between uniform endpoint water masses, but in practice, the transition between PW and AW is non-linear on a temperature-salinity plot, indicative that other processes influence the interface. The non-linear PW-AW interface is consistent with the cold halocline observed on the northern Ellesmere Island continental shelf (Jackson et al., 2014a), that forms in eastern Nansen Basin from heat loss to the atmosphere, lateral mixing between two types of Atlantic water, and the admixture of cold, fresh continental shelf water (Steele and Boyd, 1998; Alkire et al., 2010; Rudels, 2013). The curvature of the profiles away from the mixing line produces an offset in calculated meltwater fractions, so we calculate the meltwater concentration anomaly by subtracting the depth-averaged meltwater concentration offshore. Other studies have used a similar thermodynamic melt model but where ice was assumed to melt into a mixture of homogenous seawater (usually AW) and subglacial freshwater discharge (Mortensen et al., 2013). However, the grounding line depth in Milne Fiord occurs within the interface between PW and AW, not deep within the AW layer as in the other studies, indicating melting may be driven by any mixture of PW and AW, which suggests the use of the Jenkins (1999) heterogeneous water column approach is more appropriate for deriving meltwater fractions in Milne Fiord.

The depth at which the meltwater plume will reach a level of neutral buoyancy can be determined by estimating the salinity (and density) of the rising plume from the concentration of meltwater. Assuming that the plume is a mixture of ambient seawater at the depth of the grounding line and meltwater originating from in situ submarine melting of the glacier with zero salinity and negligible suspended sediment load, the minimum salinity of the plume is $S_a(1 - \Psi_{max})$, where S_a is the ambient salinity at the grounding line depth and Ψ_{max} is the maximum meltwater fraction. If we assume the rising meltwater plume entrains no ambient seawater it will rise to the level of its isohaline and then separate from the base of the ice shelf or glacier and spread out laterally along

the fjord. The meltwater fraction can be bounded at the lower limit to zero, while the theoretical maximum concentration is limited by the heat available in the ambient water to melt ice, so an upper limit on meltwater fraction is found by:

$$\frac{Q_i}{Q} \leq \left[1 + \frac{L + c_i(\Theta_f - \Theta_i)}{c_p(\Theta_w - \Theta_f)}\right]^{-1} \tag{2.6}$$

where Q_i is the mass of ice (meltwater), and Q is the total mass of the mixture (Eq 7; Jenkins, 1999). In polar waters the meltwater fraction is limited to about 1% per °C of temperature above freezing ($\Theta_w - \Theta_f$).

To measure changes in ocean properties over time a mooring was deployed in the centre of the epishelf lake from May 2011 to July 2014. The mooring initially consisted of 20 RBR TR1050/60 thermistors spaced vertically from 0.5 m to 350 m depth, as well as an RBR XR-620 CTD at 355 m depth. The mooring was ice-anchored at the surface and suspended down the water column with the CTD initially just above the bottom. However, the pressure sensor on the CTD indicated it settled onto the seabed after a week, likely from a combination of the surface anchor melting into the ice and mooring line stretch. Sediment fouling of the conductivity sensor on the CTD corrupted the salinity data so only temperature is reported. The mooring was recovered and reconfigured in May 2012, then serviced in July 2012, July 2013, and July 2014, at which times instruments were repositioned as availability required.

2.2.4 Circulation

Water level was recorded using the bottom anchored XR620 CTD at 355 m depth at the mooring site from May 2011 to May 2012. A 3 hr low pass-filter and a linear detrend was applied to the raw data. The dominant tidal constituents were determined by harmonic analysis with nodal corrections using the T_Tide Matlab toolbox (Pawlowicz et al., 2002). Results were compared with predictions over the same time period at the same location from a two constituent (M2 & K1) barotropic inverse model of the Arctic Ocean that predicts tidal range and depth-averaged tidal currents on a 5-km horizontal grid (Padman and Erofeeva, 2004).

Water velocity was recorded over durations of 4, 6, and 10 days in May 2011, July 2012, and July 2013, respectively, using an ice-anchored downward looking 300 kHz RDI Workhorse ADCP located at the mooring site (Fig. 2.2a). The ADCP was secured to a rigid mast 1 m below the epishelf lake ice. In 2013 an additional downward-looking 300 kHz RDI Sentinel ADCP was moored at 50 m depth. Due to the unreliable magnetic field at this latitude the ADCP was deployed on a bifilar (two line) mooring to fix its orientation relative to a known bearing. The ADCPs sampled at 5 min intervals, with 150 pings per ensemble, 2 m depth bins, and had an accuracy of 0.5% water velocity $\pm$ 0.5 cm s^{-1}. The low level of acoustic backscatterers in the water column limited the range of the instruments to less than nominal. Noisy data near the practical range limit of the instruments,

defined as falling below a beam correlation threshold of 60, was removed in post-processing in Matlab. Velocities are reported in along- (positive v is flow out of the fjord) and cross-fjord (positive u is flow toward the northeast shore) components (see Fig. 2.2b).

Air temperature, shortwave solar radiation, wind velocity, relative humidity, and barometric pressure were recorded by a HOBO automated weather station located at 10 m elevation on the shore on Milne Fiord (Fig. 2.2a). Air temperature is correlated with surface meltwater production (Hock, 2003), the number of cumulative of positive-degree days (PDDs) were used as a proxy for the volume of surface meltwater runoff flowing into the fiord each year.

2.3 Results

2.3.1 Mapping

The bathymetry of Milne Fiord (326 km^2), defined as extending 43 km from the Milne Glacier grounding line to the seaward edge of the MIS, is shown in Figure 2.2b. Off the seaward edge of the MIS the bed is over 600 m deep and connected to a deep basin that extends out of neighbouring Yelverton Bay, west of Cape Evans. Soundings through the re-healed fracture show the bed shoals upward from the coast under the Outer Unit of the MIS, rising to within 28 m of the surface near the confluence of the fractures. Weak bottom reflections from surrounding IPR transects, perhaps indicating an ice-bedrock interface, suggest a seabed ridge rises to within 5 m of the surface and extends about 2 km south of the fracture. Comparison of hydrographic profiles collected off the seaward edge of the ice shelf and through fractures in the Central Unit, indicate the ridge does not extend completely across the width of the fjord (i.e. is not a sill) as water properties are the same down to the seabed at 360 m both to the north and south of the ridge. However, a similar hydrographic analysis (discussed below) reveals a $\sim$ 260 m deep bathymetric sill, extending across the width of the fjord, exists below the Central Unit of the MIS, near the northern margin of the epishelf lake. Landward of the sill, a deep basin with a maximum known depth of 436 m exists below the main body of the epishelf lake. Below the terminus of the MGT the seabed slopes upward toward the head of the fjord, rising to a depth of 150 m near the grounding line. The estimated location of the grounding line of the main branch of the Milne Glacier (82.455°N, 80.32°W) is supported by the presence of hinge cracks at this location. The bed topography indicates the glacier is presently grounded on a reverse-sloping bed, and the bed deepens to a maximum of 205 m below sea level 2 km upstream, and remains below sea level for at least 24 km upstream.

The combination of ground, aerial, and satellite radar sources for measurements of ice thickness, and interpolations of ice thickness from surface elevation, provide decent spatial coverage (Fig. 2.2c) for production of the ice draft DEM (Fig. 2.2d). Ice thickness at the Milne Glacier grounding line was estimated to be 168 m, slightly thicker than the previous estimate of 152 m by Van Wychen et al. (2014). The 16 km long MGT thins quickly in the first few kilometers downstream of the

grounding line and then more gradually until the terminus where it is <10 m thick. The mean thickness of the MGT is 44 m ± 36 m, with ice of the central branch thicker than the southwest and northeast branches owing to the different origins of the ice streams that flow into the tongue. The 66 km^2 MGT covers approximately 20% by area of the fjord and has an estimated total volume of 2.6 km^3 w.e.

The updated thickness data for the MIS shows a maximum ice thickness of 94 m and mean ice thickness and standard deviation of 50 m ± 21 m. The MIS covered an area of 206 km^2, approximately 65% by area of the fjord, with an estimated total volume of 9.7 km^3 w.e., within the error of that previously estimated (9.8 ± 0.35 km^3 w.e.) by Mortimer et al. (2012). Our expanded ice thickness coverage generally confirms the model presented by Mortimer et al. (2012), although we find the southern and eastern portions of the Central Unit generally thinner, the difference owing to their lack of data coverage in these regions. Additional IPR transects confirm an area of relatively thin (<40 m), possibly grounded, ice exists south of the re-healed fracture. For relative scale, the ice keels of the MGT and MIS combined, occupy an estimated 16% of the total volume of Milne Fiord (to mean sea level).

The hypsometry of the MIS is such that it must significantly impede water flow into and out of the fjord from the surface down to approximately 50 m depth. Export of buoyant freshwater from the fjord would be preferentially routed along the thinnest ice which coincides with the re-healed fractures in the Outer Unit. IPR transects across the re-healed fractures revealed that narrow basal channels exists at the base of the ice shelf that mirror the surface expression of the fractures. Cross-sectional profiles of the channel indicate it has a width of 50-150 m at its base where the ice is 40–60 m thick, but narrows to less than 10 m at the crest where the ice is ∼10 m thick.

Thin (<1 m) freshwater ice covers the 52.5 km^2 MEL, roughly 15% of the total fjord area. The main body of the MEL is 5.8 km wide, with long narrow arms running 16 km alongside the MGT to the grounding line, and extending into the three small bays off the main fjord. The volume of freshwater in the lake, using a depth of 10 m (from CTD profiles) and assuming vertical shores is 0.525 km^3. SAR imagery shows isolated pockets of lake ice that occupy small fractures in the MGT and the Central Unit of the MIS, suggesting freshwater ponding occurs extensively throughout the fjord. CTD profiling revealed that the depth of the freshwater layer in most, but not all, of these fractures is identical to the main body of the epishelf lake, indicating that a network of basal channels connects these fractures with the main lake. The area and volume of the lake is therefore likely somewhat larger than reported here.

2.3.2 Hydrography

Hydrographic profiles show the vertical stratification of water masses in Milne Fiord (Fig. 2.3 and 2.4). The epishelf lake is evident as a relatively warm (>1°C) layer of freshwater at the surface in all profiles collected within the fjord. The epishelf lake is not present seaward of the MIS (dashed

lines in Fig. 2.3), although some surface freshening from sea ice melt is evident in summer profiles offshore. The thickness of the epishelf lake varied over the study, thinning from ∼13 m in May 2011 to ∼7 m in July 2013 (top salinity inset Fig. 2.3). At the bottom of the epishelf lake salinity rises sharply from <3 g kg^{-1} to over 20 g kg^{-1} in 2 m and this strong halocline is associated with the stratification maximum (Fig. 2.3c). The depth of the stratification maximum is associated with the minimum draft of the MIS, water above this depth cannot exit the fjord and is trapped behind the ice shelf. Below the base of the MEL to a depth of 50 m is seawater that is substantially warmer (up to 1°C) and fresher (20 g kg^{-1} to 34 g kg^{-1}) than that found at equivalent depths offshore, we term this layer fjord-modified water (FMW). FMW is also associated with a secondary halocline between 20–40 m depth (Fig. 2.3c). Below the FMW is a transition from cold, relatively fresh PW (50 to 200 m) to warm, saline AW (below ∼200 m), signifying the main Arctic Ocean halocline. Water properties within the fjord over these intermediate depths are generally similar to those offshore, indicating there is free exchange below the MIS. There is, however, evidence of cooling and temperature interleaving at depths between 50 – 150 m in profiles collected near the head of the fjord, indicative of modification of fjord waters by submarine melting of ice. Below a depth of 260 m, deep water (DW) properties landward of the MIS are nearly homogenous in temperature, salinity and density, ranging by only 0.044°C, 0.028 g kg^{-1}, and 0.03 kg m^{-3}, respectively, over the bottom 180 m of the fjord. The properties of the weakly stratified deep water are distinct from those at equivalent depths offshore (visible in the temperature profile in Fig 2.3a), indicating a topographic sill lies beneath the MIS that limits offshore exchange at these depths.

Thermistors moored at 355 m depth in the fjord recorded an abrupt temperature decrease of 0.05°C between 29–30 January 2012, which indicates a deepwater renewal event occurred (Fig. 2.5). A thermistor moored at sill depth (260 m) from May 2011 to May 2012 showed the deepwater was initially thermally stratified, but became isothermal to sill depth at the time of the renewal, while thermistors moored above sill depth remained thermally stratified throughout the record (not shown). The change in deepwater properties was confirmed by CTD profiles collected before (May 2011) and after (July 2012) the renewal (Fig. 2.5). The deep water was colder, more saline, and denser after the renewal.

The nearly homogenous deep water indicates that the fjord was filled to sill depth by inflowing waters from a narrow depth range offshore. The level of the source waters can be estimated by finding the level where seawater density offshore of the sill is equal to the density of fjord bottom water, known as the effective sill depth. A pair of profiles acquired approximately 3 km apart through the inner edge of the MIS in July 2012 show distinct deep water properties, indicating the sill lies between the two profile locations. Water with the same density as bottom water (1027.825 kg m^{-3}) in the fjord was found at ∼260 m depth outside the sill, indicating this is the effective sill depth. The actual sill depth could be slightly shallower than the effective sill depth as there are internal hydraulic mechanisms such as coastal trapped waves or internal tides that could lift dense

water from greater depths up and over the sill during deep water renewal (Farmer and Freeland, 1983).

The thermistors recorded a steady increase of deep water temperatures in the fjord of approximately 0.037°C per year before and after the renewal event. CTD profiles showed that deepwater salinity increased by 0.015 g kg^{-1} per year after the renewal event, with an associated density increase of 0.01 kg m^{-3} per year. Water properties measured at 260 m depth by annual CTD profiles offshore revealed similar changes of temperature, salinity, and density from May 2012 to May 2015. These observations suggest that offshore changes in stratification and circulation altered the source water properties at sill depth, leading to the observed changes in the deep water. The temperature increase is steady over time, suggesting that small volumes of dense offshore water steadily flow over the sill and continually fill the basin from the bottom. The 355 m temperature record shows a distinct fortnightly spring-neap period (readily visible from October 2011 until the renewal event; Fig. 2.5) suggesting overflow could be tidally driven. This idea is supported by the persistence of a slight vertical density gradient in deepwaters below sill depth (i.e. the deepwaters are not completely homogenous), suggesting small volumes of dense water are continually flowing over the sill and filling the fjord from the bottom up, displacing lighter water upward. In contrast, the January 2012 renewal event appeared to be a major event that completely filled the deep basin to sill depth. Dissolved oxygen concentrations from bottle samples collected at 320 m depth in July 2012 provide further evidence of renewal, as deep water oxygen concentrations ($\sim$9 mg L^{-1}) were only slightly depleted in comparison to measurements at equivalent depths offshore ($\sim$9.5 mg L^{-1}) collected by the SwitchYard project in May 2012. The January 2012 renewal event occurred during a neap tide, when tidal energy and flows are low. Deep water renewal has been associated with neap tides in other fjord systems, including the Strait of Georgia (Masson, 2002), Saanich Inlet (Manning et al., 2010), and Puget Sound (Geyer and Cannon, 1982). In these systems reduced turbulent mixing over the sill generated by weaker tidal flow over the allows stratification to reach a maximum, enhancing dense water overflow into the fjord. A similar process could be occurring in the constriction over the sill in Milne Fiord and under the Milne Ice Shelf, although as only one complete renewal was observed, further investigation of this process is needed.

Observations of submarine melt and subglacial runoff near the Milne Glacier grounding line are shown in the temperature-salinity plots of profiles collected in July 2012 and July 2013 (Fig. 2.6). The mixing line connects the ambient endpoint waters masses, PW and AW, any mixture of which could be in contact with ice and drive melting. Any ambient water with a temperature above the surface freezing point (blackline) has the potential to melt ice. The melt line, with a slope of 2.7°C $(g\ kg^{-1})^{-1}$, was calculated using the ambient water properties at the depth of the grounding line (150 m); internal ice temperature , -15°C, water temperature, -0.8°C, and salinity, 34.25 g kg^{-1}. If submarine melting is occurring, then the mixture of melted glacier and ambient water observed in CTD profiles, called the submarine meltwater mixture, will fall on or close to the melt line (with a

minimum temperature limited to the freezing temperature). Note that the meltwater mixing model is only valid within the triangle defined by the endpoint waters masses (i.e. between PW at 35 m depth and AW at 150 m depth). Profiles collected through hinge cracks at the grounding line (dark blue) exhibit a substantial temperature decrease and fall close to the melt line, indicating submarine melting is occurring. Profiles collected within a few kilometers of the grounding line (light blue), through fractures in the MGT or through the epishelf lake ice along the margins of the MGT, also show a submarine melt signature, but to a lesser degree. At increasing distances from the grounding line the meltwater signature diminishes; offshore profiles show little or no evidence of meltwater. The grounding line profiles also show horizontal excursions away from the melt line toward lower salinity, most apparent at 120 m depth in July 2013, but evident in both years near the grounding line. These horizontal excursions are indicative of fresh subglacial discharge entering the fjord at depth (Straneo et al., 2011; Chauch et al., 2014). A single turbidity profile collected near the mooring site in July 2013 shows a turbidity peak at a salinity corresponding to the depth of the apparent subglacial discharge inflection (2.6b), further evidence that subglacial runoff exits the grounding line at this depth. Turbidity reaches a minimum at 35 m depth, but is elevated above this level. The source of the turbidity in the MEL (not shown) is likely due to terrestrial surface runoff, while elevated turbidity in the FMW layer could be settling of sediment from the MEL, or spreading of a turbid subglacial discharge plume.

Spatial variation in fjord water properties are shown in hydrographic sections from July 2012 (Fig. 2.7) and July 2013 (Fig. 2.8). The overall spatial patterns were similar between years. Water properties are contoured through the ice (i.e. shown above the maximum ice depth) due to the pronounced cross-fjord variability in ice thickness that allows some exchange of water above this depth to the surface. Along-fjord transects show the water column properties offshore of the ice shelf are typical of the Arctic Ocean, including a SML above PW and AW. The warmest AW at 350 m depth extends up the fjord to the location of the inferred topographic sill, below the southern edge of the MIS. The deep waters in the basin inside the inferred sill are nearly homogenous in temperature and salinity, although slightly thermally stratified in 2012. The epishelf lake is apparent as a uniform freshwater layer extending from the Outer Unit of the MIS to the head of the fjord. Water temperatures are generally lower near the head of the fjord, suggestive of cooling by contact with ice near the grounding line. The highest meltwater concentrations are observed at the head of the fjord, with a maximum just above the bed of the glacier. The meltwater fraction is smaller with increasing distance from the grounding line, suggesting the highest melt rates, and the source of meltwater observed in the fjord is from the glacier. The meltwater appears to form several distinct plumes distributed vertically in the water column that spread out horizontally throughout the fjord, and appear to be exported out of the fjord at depth. Some meltwater is observed near the base of the MIS, although the source of the melt, whether produced *in situ* or advected from up-fjord, cannot be determined. This pattern is indicative of an estuarine-type flow, with outflowing meltwater mixing

with seawater inflowing at the same or greater depths.

Cross-fjord hydrographic sections extend from the northeast shore to the southwest through the mooring site at the centre of the epishelf lake. The epishelf lake extends completely across the fjord at a constant depth and there is minimal cross-fjord tilting of isotherms and isohalines. However, temperature inversions and interleaving layers are visible in the upper water column above 150 m and there is some cross-fjord patchiness in melt water fraction. There is very little change between 2012 and 2013, with the exception of a shoaling of isotherms below sill depth in 2013.

The layering of water masses in the fjord is consistent over all field campaigns, however there are changes over time in the properties of each layer. The epishelf lake showed evidence of seasonal and interannual variation, deepening by a few meters from May through July 2012, yet showed very little change in the depth in 2013. The evidence suggests that the lake depth is linked to the volume of inflow due to surface melt water production, although a complete discussion of the dynamics of the epishelf lake is presented in Chapter 3.

Similarly we find evidence that subglacial outflow is linked to seasonal and interannual variations in surface meltwater production (Fig. 2.9). Warm air temperatures facilitate melting of snow and ice in the glacier catchment, which flows down through crevasses and discharges at depth into the fjord across the grounding line at the bed of the glacier. The subglacial discharge (near 0°C and 0 g kg^{-1}) can rise as a turbulent buoyant plume, entraining ambient seawater, until it reaches a depth of neutral buoyancy. Profiles collected over a 10-day period in July 2012 show a decrease of salinity by up to 4 g kg^{-1} between 30 and 55 m depth. Above and below these depths there is little change in salinity over time, indicating the freshening is due to a lateral, not vertical, transport process. Temperature interleaving at these depths is also indicative of advection of water, suggesting a subglacial outflow plume. The temperature (<-1°C) and salinity (31 g kg^{-1}) of the plume indicate it is mainly composed of seawater, and may have been cooled by contact with the base of the glacier tongue. The field campaign in 2012 corresponded to a period of warm atmospheric temperatures (almost 100 PDDs had accumulated by the end of profiling), intense surface melt, and presumably, substantial subglacial discharge. Conversely, the summer of 2013 was cool, with less surface melt water production (<40 PDDs accumulated by the end of profiling) and no apparent evidence of a subglacial discharge plume in salinity or temperature profiles.

2.3.3 Circulation

The tidal range estimated from water level record in Milne Fiord was 0.34 m. Harmonic analysis of 59 tidal constituents showed amplitudes of the M2 (12.42 h), K1 (23.93 h), S2 (12 hr), and O1 (25.82 hr) constituents were 0.056 m, 0.042 m, 0.023 m, and 0.023 m, respectively. A ratio of these constituents given by $(K1+O1)/(M2+S2)$, gives 0.82, indicating a mixed, predominately semidiurnal tide (Thomson, 1981). Tides accounted for 63.7% of the variance of the original water level data over the 245 day record.

Time-averaged velocities in the upper water column at the mooring location for May 2011, July 2012 and July 2013 are shown in Figure 2.10. All years show generally weak ($<$2 cm s^{-1}) baroclinic flow in the upper water column, with cross-fjord currents being of equal or greater magnitude to along-fjord currents. There is little or no flow at the surface in the epishelf lake. The record from May 2011 is a useful baseline, as air temperatures are well below zero and no surface or subglacial runoff is expected. We find a slight outflow peak below the epishelf lake, and a larger outflow at 40 m depth. Velocity profiles in 2012 and 2013 extend further down the water column and show flow reversals. A relatively strong 6 cm^{-1} mean flow to the northeast shore at 60 m depth was recorded in July 2012. Summer of 2012 was a strong melt year and this may be related to the export of subglacial water. Alternatively the current could be associated with exchange below the MIS, which is less obstructed at this depth compared to the restricted flow higher in the water column. The velocity data reveal that circulation in Milne Fiord is fundamentally 3-dimensional and time varying. The depth-averaged internal Rossby radius within Milne Fiord above the depth of the sill is $>$8 km, which is larger than the width of the fjord landward of the MIS so the effects of rotational dynamics on circulation are minimal. Although the stratification of the fjord changes over time, particularly in relation to seasonal freshwater runoff, our data indicate the internal Rossby radius remains larger than the fjord width. The 3-dimensional nature of the circulation is more likely due to the complex ice geometry and bathymetry of the fjord.

2.3.4 Mooring timeseries

Meteorological conditions recorded by the automated weather station and ocean temperature at the mooring site from May 2011 to July 2014 are shown in Figure 2.11. Average air temperature during the mooring deployment was -17.6°C, with extreme hourly temperatures of +20.2°C in July 2012 and -51.8°C in February 2013. Solar radiation varied from near zero during the polar night (mid-October through February), to a summer daily maximum of 650 W m^{-2} in late June during the period of 24 hour sunlight from April to September each year. Cumulative PDDs, a proxy for summer melt conditions, varied substantially among years, with 278, 255, and 92 PDDs in 2011, 2012, and 2013, respectively. Variations in melt water inflow to the fjord were manifested in changes in ocean temperatures in the upper water column in the fjord, while temperature fluctuations in deeper waters are not directly coupled to surface conditions. The highlighted isotherms approximate the interface between water masses: 0°C isotherm around 10 m depth signifies the epishelf lake/FMW interface; -1.5°C isotherm the FMW/PW interface; -0.5°C the PW/AW interface; with nearly homogenous DW below 260 m. The warming and thickening of the MEL and FMW are strongly correlated with the onset and strength of the surface melt season. During the warm summers of 2011 and 2012, when we expect high surface meltwater production and runoff, the MEL and the FMW layer warm and deepen to a much greater degree than during the cool summer of 2013. The changes in the FMW layer are consistent with the subsurface freshening and warming attributed to

subglacial discharge plumes (Fig. 2.9), while the deepening of the MEL is consistent with runoff entering the fjord at the surface. The thinning of the MEL and FMW after the surface melt season ends is much more gradual than the rate of thickening during the melt season, suggesting a slow advection of heat (and freshwater) out of the fjord under the MIS over the remainder of the year. The PW and AW layers show some seasonal variation as well as pronounced high frequency fluctuations above sill depth. The interface between PW and AW in Milne Fiord tends to deepen in winter and shoal in summer, varying by almost 50 m over the year, with excursions of 25 m at periods on the order of days to weeks. These high frequency fluctuations can be more readily seen in Figure 2.12. At 125 m, temperatures seasonally reach a maximum in summer and decrease to a minimum in mid-winter, varying by 0.6°C over the duration of the record, but there are large amplitude (up to 0.5°C), high frequency fluctuations, on timescales of days to weeks at all times during the record. Spectral analysis of temperature fluctuations at 125 m depth (not shown) reveal small peaks at 7–12 days, with stronger peaks at 18 days, 35 days, and 59 days, present throughout the timeseries, including during winter. Temperatures at 25 m and 50 m show smaller amplitude (generally $<0.1^{\circ}$C) high frequency fluctuations, and appear more influenced by summer runoff. The long-term temperature decrease at 25 m from summer is associated with the shoaling of isotherms related to the thinning of the FMW layer. Overall, these observations suggest that waters above 50 m depth are primarily influenced by the import and export of runoff (both surface and subglacial) from the fjord catchment, while waters below 50 m depth are strongly influenced by external forcing, particularly offshore variations in the depth of the PW-AW interface that translate into the fjord.

The heat content of the upper water column of the fjord, from 5 m to 125 m depth, spanning the depths containing most of the ice in the fjord, increases rapidly during warm summers with high meltwater inflow (2011 and 2012), with a smaller increase during cool summers (2013) (Fig. 2.13).

2.4 Discussion

2.4.1 Geophysical setting

We present the first comprehensive bathymetry of Milne Fiord, which reveal a flooded glacial valley with a maximum known depth of 436 m. Hydrographic evidence indicates the presence of a 260 m deep bathymetric sill under the landward edge of the MIS, which could be an ancient terminal moraine from a previous advance of the Milne Glacier. The bathymetric sill is significantly deeper than the thickest ice in the fjord (at the Milne Glacier grounding line) so we expect it has little direct influence on the properties of water that can come in contact with ice and drive melting, though it is fundamental in determining the deep water properties of the fjord. Shallower bathymetric features however, such as the newly discovered ridge that rises to within 28 m of the surface under the MIS, could influence water properties in contact with ice by enhancing mixing, diverting currents, and further reducing the cross-sectional area at the mouth of the fjord for exchange flow under the ice

shelf.

The full spatial extent of the ridge is unknown, although the weak bottom reflections in IPR data suggest it could extend up to 2 km south of the re-healed fracture if the ice is grounded in this region. In an 1981 aerial radar survey, Narod et al. (1988) found a similar band of low bottom reflectivity, extending 4 km south of the re-healed fracture, and stretching across the width of the fjord. However, Narod et al. (1988) interpreted the low-reflectivity as signal attenuation due to brine soaked or brackish ice freezing onto the bottom of the ice shelf. It is not possible with available data to determine which explanation is correct, so we have chosen not to include data from IPR into our bathymetric model. Further investigation is required to verify cause of the weak bottom reflections, and if the ice is indeed grounded, to map the spatial extent and topography of the ridge.

Although the full extent of the grounded ice is undetermined, our limited bathymetric soundings and ice thickness data indicate the ice is almost certainly grounded near the confluence of the re-healed fractures as the ice shelf increases to $>$60 m thick within 200 m of the 28 m deep bathymetric sounding. This finding could explain the origin of the fractures in the MIS (which have existed since the first aerial photographs were acquired in 1959 (Hattersley-Smith and Fuzesy, 1969) as stress fractures (or hinge cracks) between grounded and floating ice. The partial grounding of the MIS would also resist forces acting to detach the MIS from the coast, and help explain why the MIS has been relatively stable in contrast to the full or partial collapse of all surrounding ice shelves along northern Ellesmere Island (Mueller et al., 2008; Veillette et al., 2011a)).

Our revised DEM of ice thickness in Milne Fiord expands on that constructed by Mortimer et al. (2012) for the MIS by improving spatial coverage of regions of the MIS, and providing partial coverage of the MGT. Comparison to Mortimer et al.'s 2012 DEM of the MIS reveals that while the total ice volume is not significantly different, there are some spatial differences in ice thickness. Although most of the difference is due to differences in data coverage, there are likely some differences due to methodology in production of the DEM. In particular, the automated gridding function that we used may underestimate ice thickness by smoothing over sub-grid scale features, such as the re-healed fractures, producing wider and thinner channels than that manually contoured by Mortimer et al. (2012). Despite these minor differences, our DEM represents the source data well and provides the critical context for understanding water properties and circulation in the fjord.

The thickness of the MGT is highly variable across its width, owing to its composite origins from three different ice streams. Based on the grounding line locations estimated by Hattersley-Smith and Fuzesy (1969) from surface features in aerial photographs, the grounding lines of the southwest and northeast ice streams have remained relatively stationary since 1959, while the grounding line of the central ice stream appears to have retreated by 2–3 km. These observations suggests the three ice streams have different grounding line depths, which could be associated with subglacial discharge channels that enter the fjord at different levels. Although there is some supporting evidence for freshwater discharge at different depths in the CTD profiles collected through the hinge crack,

further work is needed to confirm this hypothesis.

Continued retreat of the Milne Glacier grounding line will push it into deeper water. This could lead to breakup of the glacier tongue, and acceleration of the Milne Glacier, as observed at the Jakobshavn Isbrae glacier tongue in Greenland (Motyka et al., 2011; Joughin et al., 2012). The appearance of new crevasses and expanded rifts at the hinge line in 2013 suggest the breakup of the MGT may already be underway. As the Milne Glacier is grounded below sea level 24 km upstream of its present-day grounding line, there is potential for the grounding line to retreat a significant distance, with important ramifications for Milne Glacier dynamics and its contribution to sea level rise. We note that the present-day grounding depth of the Milne Glacier is relatively shallow, and indicates understanding factors that affect the properties of the upper water column in Milne Fiord are critical to future understanding of how the glacier will respond to ocean forcing.

2.4.2 Freshwater inflow and outflow

The dominant influence on the properties of the upper water column in Milne Fiord is the inflow and outflow of freshwater. Freshwater enters the fjord from three main pathways: 1) surface runoff; 2) subglacial discharge; and 3) submarine ice melt. The amount of freshwater runoff entering the fjord, both at the surface and subglacially, is highly dependent on the strength of the melt season. At the surface, freshwater enters the fjord via proglacial streams from surrounding tributary glaciers, and flows directly off the Milne Glacier as supraglacial streams. These surface inflows contribute to an increase in volume and depth of the epishelf lake during summer, but the strong stratification and inhibition of wind-mixing by the perennial ice cover means the influence of surface inflow is largely confined to the epishelf lake.

The largest subsurface source of freshwater to the fjord in summer is subglacial discharge. The subglacial discharge plume, which entrains ambient water during its ascent, appears to reach a level of neutral buoyancy below the epishelf lake halocline during years of high meltwater production (e.g. 2012). Observation of current velocities over the same period show flow at this level is directed out of the fjord, suggesting the subglacial plume spreads out horizontally and is exported from the fjord at depth. In July 2013, surface meltwater production was low, and we expect the volume flux of subglacial discharge was equally small. There was no apparent change in salinity or temperature below the epishelf lake associated with a subglacial discharge plume in 2013, yet the small turbidity peak at 112 m is suggestive of a deeper subglacial plume. The equilibrium depth of the plume will be dependent, in part, on the freshwater volume flux across the grounding line. The relatively small volume of subglacial discharge in 2013, inferred from cumulative PDDs, means the plume mixture's density may have equilibrated to ambient waters after ascending just meters or a few tens of meters. In contrast, a relatively high volume of subglacial discharge occurred in 2012, imparting to the plume sufficient buoyancy to rise much higher in the water column, its ascent ultimately limited by the strong stratification near the base of the epishelf lake.

The export of surface and subglacial freshwater from Milne Fiord is constrained by the thickness of the MIS. The MIS acts as a dam across the mouth of the fjord, restricting water exchange between the fjord and offshore to a depth of approximately 50 m. Flow above this depth is likely routed through a narrow basal channel that runs along a re-healed fracture transversing the ice shelf from east to west. All surface runoff that enters the fjord landward of the ice shelf must flow through this geometric constriction. Thus, to a depth of 50 m the ice shelf is a slowly leaking dam, allowing the fjord to store freshwater and heat (supplied by the runoff water and warm water entrained from depth in the subglacial plume) over longer periods, gradually releasing it out of the fjord through the channel. The hydraulics of the drainage through the channel are discussed in detail in Chapter 3, specifically with regards to the epishelf lake, but similar principles likely apply to drainage of FMW. Substantial volumes of freshwater are exported at depth, and the timing of the export is de-coupled from the timing of the surface melt season due to the flow restriction imposed by the MIS. Although this scenario is likely unique to Milne Fiord at present, it may have been more common when ice shelves along northern Ellesmere Island were numerous. The widespread subsurface export of freshwater for weeks or months after the melt season would have implications for the stratification and circulation of waters along the northern Ellesmere continental shelf.

2.4.3 Submarine melt

A source for freshwater in the fjord is submarine melting. The highest glacial meltwater concentrations were observed near the grounding line of the Milne Glacier. A possible source of bias of observations collected in the narrow hinge crack is that the water here could be isolated, and not representative of the ambient waters near the grounding line. However, the general water column properties in the hinge cracks are consistent with other profiles collected throughout the fiord, showing the same depth of the epishelf lake and the structure of the PW-AW interface. At the surface the cracks are up to 50 m wide, extend most of the distance across the fjord and are visibly connected with other fractures that could permit water exchange. These observations strongly suggest that the water within the hinge crack is not isolated, and the high meltwater concentrations observed are representative of conditions near the grounding line. Melting near the grounding line could be driven directly by contact with warm ambient waters at depth, or further enhanced by convection-driven melt from subglacial discharge.

The submarine meltwater mixture, a mixture of ambient ocean water and freshwater from melting of the glacier, is buoyant and will rise along a vertical ice wall (such as those of the hinge fracture) or along the sloped base of an ice shelf (such as the MGT). Assuming the buoyant plume entrains no additional ambient water during its ascent, the density of the meltwater mixture, and thus its level of neutral buoyancy, is determined by the concentration of fresh meltwater in the plume, which is limited by the amount of heat available to melt ice. The theoretical maximum meltwater concentration at the grounding line is $\sim$2% (from Eq. (2.6) where $\Theta_w - \Theta_f = 2^\circ$C), which would

lower the density of the meltwater mixture enough for the meltwater plume to rise ∼50 m vertically given the ambient stratification. The maximum observed meltwater concentration was 0.7%, representing a reduction in buoyancy that would only permit a ∼25 m vertical displacement of the meltwater plume. In practice, however, a turbulent meltwater plume will entrain ambient seawater, increasing its density, and further reducing the maximum vertical displacement. As a result, a meltwater plume produced solely by submarine melting (no freshwater input from subglacial discharge) will rise at most a few 10s of meters in Milne Fiord before separating from the ice face and spreading out laterally at depth. Indeed, our hydrographic observations show meltwater plumes extending along the fjord at multiple depths, apparently close to their depth of origin, given that they extend horizontally from the grounding line (Fig. **??**). Interleaving meltwater layers have been previously observed adjacent to ice melting in a stratified water column, both in laboratory experiments (Huppert and Turner, 1980) and near floating glacier tongues (Jacobs et al., 1981). The export of submarine meltwater at multiple depths is likely associated with compensating inflow at other depths, suggesting the submarine melt-driven circulation in Milne Fiord is complex.

Subglacial discharge-induced buoyancy-driven circulation has been identified as a key factor in enhancing melt rates of tidewater glaciers in Greenland during summer (Straneo and Cenedese, 2015), and is likely partially responsible for observations of high melt rates near the grounding line in Milne Fiord. This process however, may be quite localized across the fjord, dependent on the location and geometry of the subglacial channels. An even more important factor controlling submarine melt rates is the fjord-scale circulation that the localized buoyancy-driven circulation could drive. Recent observations of horizontal re-circulating cells associated with subglacial plumes in Greenland (Stevens et al., 2015), indicate simple two-layer models of estuarine-like overturning circulation driven by subglacial discharge, are inappropriate (Straneo and Cenedese, 2015). The mooring timeseries does show a pronounced shoaling of isotherms at the depth of the grounding line coinciding with the surface melt season each year that could be related to enhanced circulation driven by subglacial discharge, although we lack sufficient data to conclusively link these processes. Regardless of the processes involved, the shoaling of isotherms means warmer water can access the grounding line and would lead to an increase in submarine melt. While these processes are likely very important to summer submarine melt rates, which may be a large portion of the annual mass balance, the effects are confined to the very brief surface melt season, which lasts $<$2 months at this high latitude. For the remaining 10 months each year, submarine melting at the grounding line is dominated by changes in ambient waters, which are largely influenced by processes external to the fjord.

2.4.4 External forces

The rate of melt and the vertical range over which it will occur in Milne Fiord is dependent, in part, on the ambient source water properties in the Arctic Ocean. Johnson et al. (2011) suggested the

depth of the near-freezing SML, which varies between 25 to 60 m (Jackson et al., 2014a), might be an important factor in limiting the extent of basal melt on the ice tongue of the Petermann Glacier. In Milne Fiord, a narrow band at the base of the SML (50–60 m depth) does appear to penetrate under the MIS to the grounding line. The SML will limit melting over these depths, however, surface properties in the fjord above 50 m are significantly different than those offshore due to the impoundment of runoff by the MIS. The impact of the SML is therefore largely confined to limiting melt on the Outer Unit of the MIS.

The highest submarine meltwater concentrations were observed at the Milne Glacier grounding line, and the main external influence here is the depth of the interface between PW and AW. We observed both seasonal and high frequency temperature fluctuations over the PW-AW interface in Milne Fiord that are likely associated with offshore processes. Thermistors deployed at 160 m depth on the North Ellesmere shelf in the western Lincoln Sea during the Switchyard Project from 2008 to 2009, showed similar temperature fluctuations as observed at 125 m depth in Milne Fiord, with variations up to 0.5°C per day that occurred several times per month throughout the year (Jackson et al., 2014a). Jackson et al. (2014a) explained temperature fluctuations with periodicities of 12 h and 14 days by semidiurnal tides and the spring-neap tide cycle, while they suggested fluctuations with periods of $\sim$ 10 days could be explained by synoptic events, including storms. Jackson et al. (2014b) linked fluctuations in water properties in two Greenland fjords on timescales of 3–10 days to density fluctuations on the continental shelf driven by along-shore down-welling favourable winds inducing velocity pulses into the fjord. Jackson et al. (2014b) also speculate that other phenomenon such as coastal trapped waves and eddies could generate the pressure gradients across the continental shelf and fjord required to generate pulses in the absence of wind forcing. In Milne Fiord, temperature fluctuations that we associate with depth variation of the PW-AW interface, occur at several time scales, from semidiurnal tidal periods, to seasonal variation. Spectral analysis of temperature fluctuations at 125 m depth (not shown) reveals small peaks at 7–12 days, likely associated with the synoptic offshore wind variation, while stronger intraseasonal peaks at 18 days, 35 days, and 59 days, are present throughout the timeseries, including during winter. We speculate these intraseasonal temperature variations are related to the passage of offshore coastal trapped waves. Although not specifically addressed over the 3-year duration of this study, we suspect long-term interannual variation due to shifts in regional circulation patterns may be important in determining water properties in Milne Fiord. Along the northern coast of Ellesmere Island, waters above 100 m depth are usually characteristic of the Canada Basin, and show relatively little variability (Jackson et al., 2014a). However, waters below 100 m can originate in either the Canada Basin or Eurasian Basin, which have very different water column properties, resulting in significant interannual variation in temperature and AW depth depending on regional circulation patterns (Newton and Sotirin, 1997; Jackson et al., 2014a), which could have a profound influence on the ambient properties in Milne Fiord.

Renewal of the deep water below sill-depth in Milne Fiord can also be driven by changes in offshore density stratification. The isopycnals at sill depth were 20 m shallower after the renewal event than prior to it (Fig. 2.5), indicating that shoaling of the halocline offshore allowed denser water to flow over the sill and replace the deep water in the fjord. As only one deep water renewal occurred over the 3-year study, it suggests an interval of at least 1–2 years between events. The cause of the renewal is uncertain; analysis of ice drift patterns and sea ice cover offshore of Milne Fiord in the weeks leading up to the event showed no clear evidence of conditions that might have initiated upwelling over the continental shelf (i.e. surface ice drift toward the southwest). However, the observed changes in Milne Fiord do indicate that deep water properties are linked to regional changes in the depth of the PW-AW interface in the Arctic Ocean.

An along-fjord temperature section from 2012 extended over the continental shelf using profiles collected as part of the SwitchYard Project is shown in Figure 2.14. Beyond the continental break, the AW layer has a temperature maximum near 1°C at 370 m, almost 3°C above the *in situ* freezing point. This warm water is prevented from entering Milne Fiord by the shallow continental shelf and the sill under the MIS. Although this is important from the perspective of general fjord dynamics, including deep water renewal, the core of the offshore AW layer is substantially deeper than the thickest ice in the fjord, so it will not have a direct contact with the ice. Rather, it is the properties of the upper ocean, above 150 m depth, including the SML, PW, and the depth of the PW-AW interface, that will directly influence ice-ocean interactions in Milne Fiord.

The characteristics of AW vary on multidecadal time scales of 50-80 years, likely connected to large-scale atmospheric circulation (Polyakov et al., 2004). The upper boundary of AW shoaled by about 75 m in the late 1980s-90s in the Makarov Basin (Polyakov et al., 2004), and about 40 m in the Amundsen Basin (Steele and Boyd, 1998). If AW along the northern Ellesmere Island continental shelf break responds similarly, this would suggest the properties of water that could propagate into Milne Fiord could vary over the long-term as well. The steady warming of deep water in Milne Fiord, consistent with warming at sill depth offshore, could in fact indicate a regional shoaling of the upper boundary of AW, although our records are much too short to make any definitive link. Long-term variation of the upper boundary of AW in Milne Fiord could significantly alter the heat content of water in contact with ice and have repercussions for submarine melt rates and the mass balance of ice shelves and tidewater glaciers. The recent widespread retreat of tidewater glaciers in Greenland was linked to propagation of a warm AW anomaly around the coast, indicating link between glacier dynamics and mass balance and regional ocean circulation (Holland et al., 2008a; Straneo et al., 2012). Investigation of a similar link between large-scale atmospheric and ocean conditions in the Arctic Ocean and long-term variations in submarine melt rates along northern Ellesmere Island could prove an interesting area of future research and provide greater insight into the long-term stability of ice along this coast.

2.4.5 Outlook

The ice shelves and glacier tongues of Ellesmere Island are in a state of decline, with little chance of regeneration in the present and projected climate. The Canadian Arctic Archipelago was the largest single contributor to eustatic sea level rise outside of Greenland and Antarctica between 2003–2009 (Gardner et al., 2011; Lenaerts et al., 2013), which emphasizes its importance on a global scale. Despite widespread collapse of ice shelves and glacier tongues in surrounding fjords (Mueller et al., 2003; Copland et al., 2007; Mueller et al., 2008; White et al., 2015a; Copland et al., 2015), the MIS and MGT have remained comparatively stable (Mortimer et al., 2012). The presence of the MIS in particular has had a profound impact on the water properties of Milne Fiord, and has likely influenced the stability of the MGT.

However, a network of new fractures extending across the inner portion of the MIS was observed in May 2013. The potential collapse of the ice shelf would result in a much more rapid export of freshwater (with its elevated heat content) out of the fjord, shortening the submarine melt season of the upper water column to roughly coincide with the length of the surface melt season. The loss of the perennial freshwater surface layer would reduce the stratification of the upper water column, potentially allowing subglacial runoff to reach the surface and alter the depth of freshwater export. As well, the loss of the epishelf lake may increase potential of seasonally ice-free conditions, with enhanced calving activity, as has been seen in Disraeli Fiord since the drainage of the epishelf lake (W. Vincent, pers. comm.). This is particularly important for the Milne Glacier, as the collapse of glacier tongues have been linked to the acceleration of glacier flows, with repercussion for sea level rise.

2.5 Conclusion

Relative to the Arctic Ocean, the water properties and heat content within Milne Fiord are strongly modified by the presence of a coastal ice shelf, a tidewater outlet glacier, and a bathymetric sill. The modification is primarily due to three factors: 1) the impoundment of freshwater runoff (both surface and subglacial) behind the ice shelf at the mouth of the fjord; 2) submarine melting at the glacier grounding line where ice is in contact with warm AW; and 3) the presence of a bathymetric sill under the MIS that prevents the warmest AW from entering the fjord. This work is the first comprehensive oceanographic study of Milne Fiord and our findings emphasize the importance of mapping ice topography and bathymetry to provide context for interpretation of ocean observations.

Exchange under the ice shelf, above 50 m depth, is likely restricted to a narrow basal channel extending along a re-healed fracture in the ice shelf. The sub-surface export of freshwater runoff from the fjord is slowed due to the flow constriction imposed by the basal channel in the MIS, partially de-coupling the export of freshwater from the timing of the summer melt season, a unique process warrants further investigation. Although the presence and impact of a largely intact coastal

ice shelf is presently unique to Milne Fiord, we expect many of our results to be applicable to other tidewater glacial fjords in the northern Canadian Arctic Archipelago. Tidewater glaciers drain an estimated 47% of the total glaciated area of northern Arctic Canada (i.e. Ellesmere Is., Axel Heiberg Is., and Devon Is.; Lenaerts et al., 2013), underscoring the need to understand ocean-ice interactions in this region, and how it may differ from other regions.

The MIS is a critical feature that modifies water properties in Milne Fiord and its inevitable breakup in the warming climate will fundamentally alter the oceanography of the fjord, with repercussions for the stability of the MGT and dynamics of the Milne Glacier. A small number of glaciers dominate discharge to the ocean from the CAA (Van Wychen et al., 2014), and as a consequence overall ice discharge may be highly sensitive to changes in the dynamics of only a few marine terminating glaciers. Our findings suggest that long-term monitoring of ocean properties near tidewater glacier termini, along with improved bathymetry and ice topography, will be required to understand glacier-ocean interactions and better predict the influence of these changes in the Canadian Arctic.

2.6 Figures

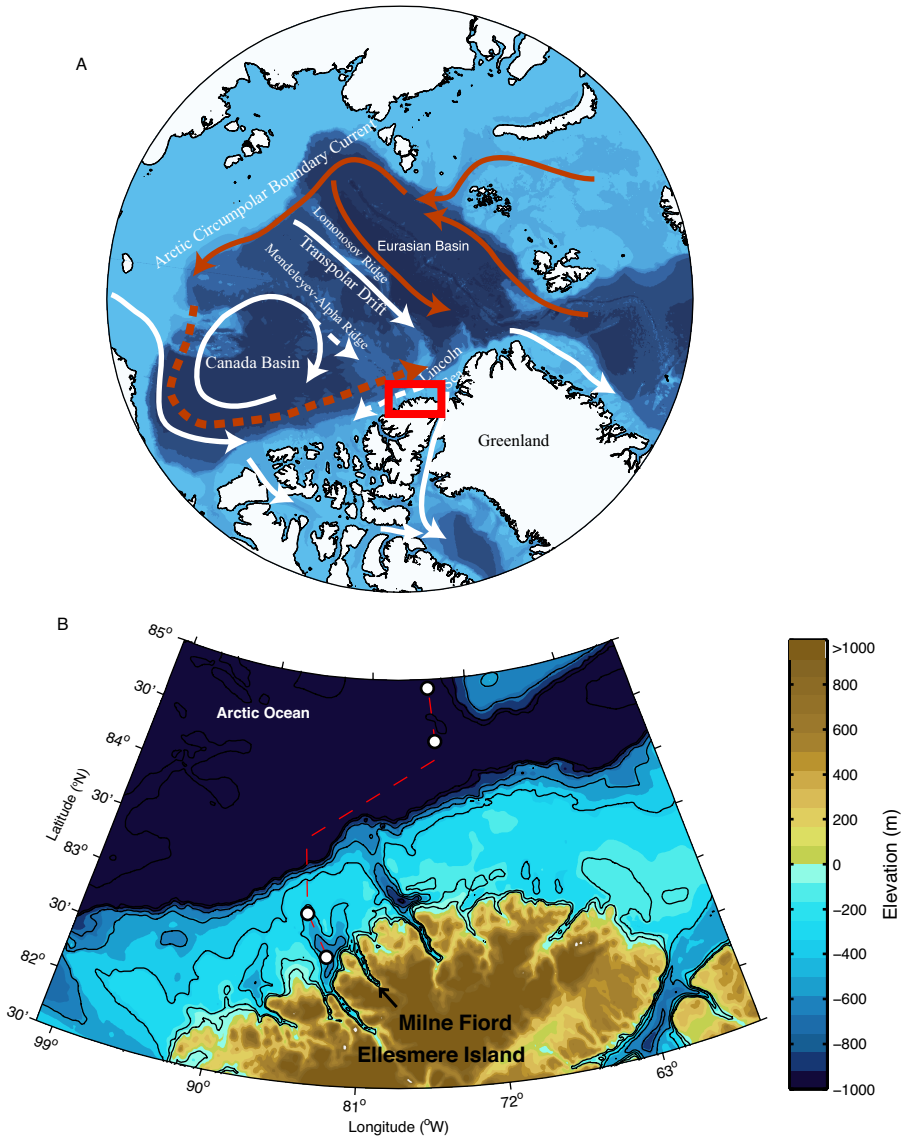

Figure 2.1 Map showing regional setting of Milne Fiord. A) Arctic Ocean bathymetry with major currents overlain showing the path of Atlantic Water (red) and Polar Water (white). Dashed line indicates currents not directly observed (after Aksenov et al. 2013). B) Bathymetry and topography of northern Ellesmere Island, the region defined by the red box in (A). The white circles mark the University of Washington SwitchYard Project 2012 CTD transect shown in Fig. 2.14. Regional bathymetric data from IBCAO v.3 was combined with Milne Fiord soundings collected during this study and re-gridded onto a 2.5 km grid. Contour lines are shown every 200 m to a maximum of depth of 1000 m.

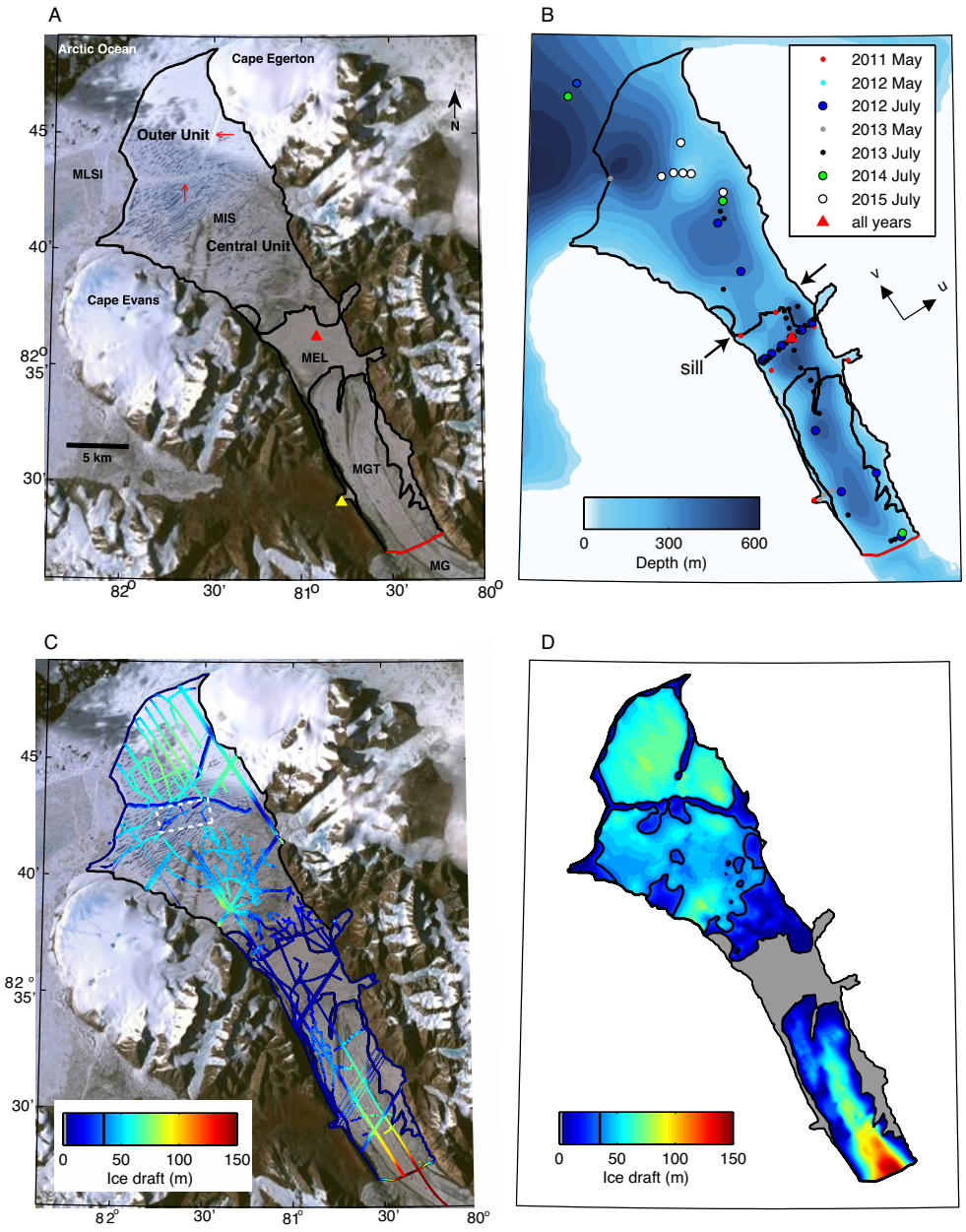

Figure 2.2 Map of Milne Fiord. A) ASTER image mosaic captured 21 July 2009. The Milne Ice Shelf (MIS), Milne epishelf lake (MEL), and Milne Glacier tongue (MGT) are outlined in black. Also indicated are the grounding line of the Milne Glacier (red line), the automated weather station (yellow triangle), the location of the mooring (red triangle), the re-healed fractures in the Milne Ice Shelf (red arrows), and multi-year land-fast sea ice (MLSI) along the coast. B) Modelled bathymetry of Milne Fiord with locations of depth soundings/CTD profiles are indicated. CTD profiles were collected at the mooring location during all field campaigns. The reference axis for ADCP current velocities ($+u$ flow to the northeast, $+v$ flow out of the fjord) measured at the mooring site are shown. C) Ice draft measurements derived from ground-based IPR and surface elevation, aerial 2014 NASA Icebridge radar and altimetry measurements, and ICESat altimetry data, overlaid on 21 July 2009 ASTER image mosaic. The dashed rectangle indicates a region of possibly partially grounded ice. D) Digital ice draft model extending from the Milne Glacier grounding line to the outer edge of the MIS.

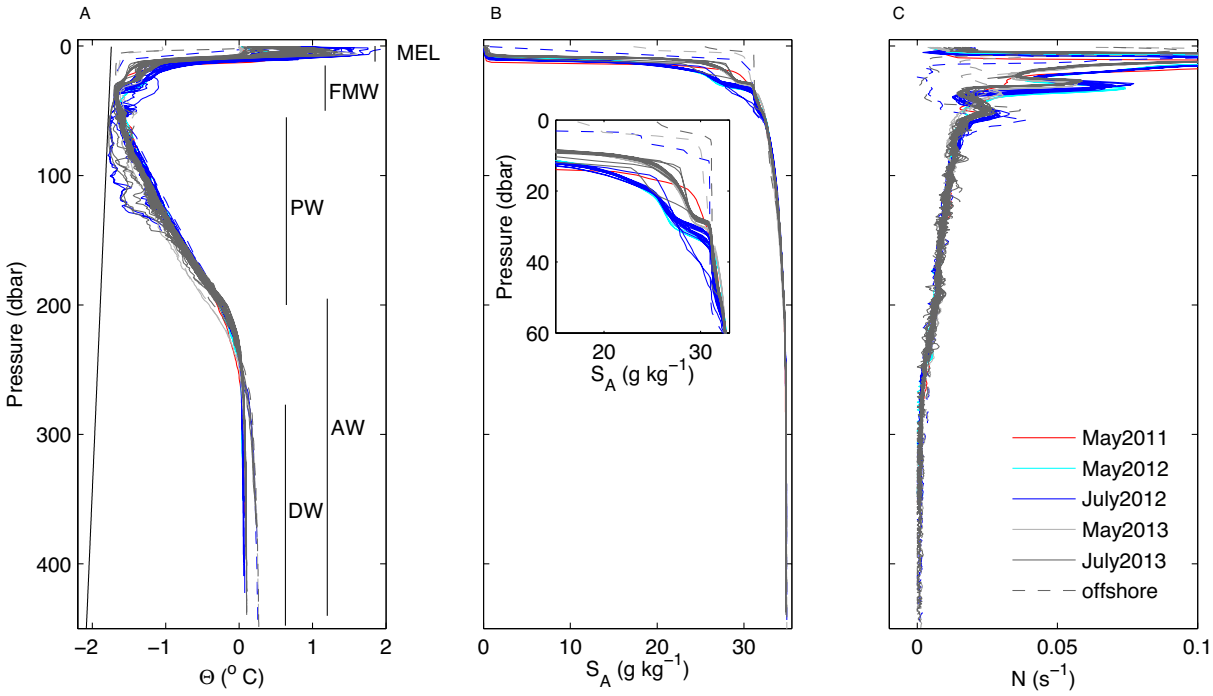

Figure 2.3 Through-ice hydrographic profiles of A) conservative temperature (Θ), B) absolute salinity (S_A), C) buoyancy frequency (N) in Milne Fiord from all field campaigns. Different water masses are indicated: Milne Fiord epishelf lake (MEL); fiord-modified water (FMW); Polar Water (PW); Atlantic Water (AW); and deep water (DW). The freezing point of seawater with salinity of 32 g kg^{-1}, which is representative of the fjord, is shown (grey line in panel (A)). Dashed lines indicate profiles collected offshore of the Milne Ice Shelf.

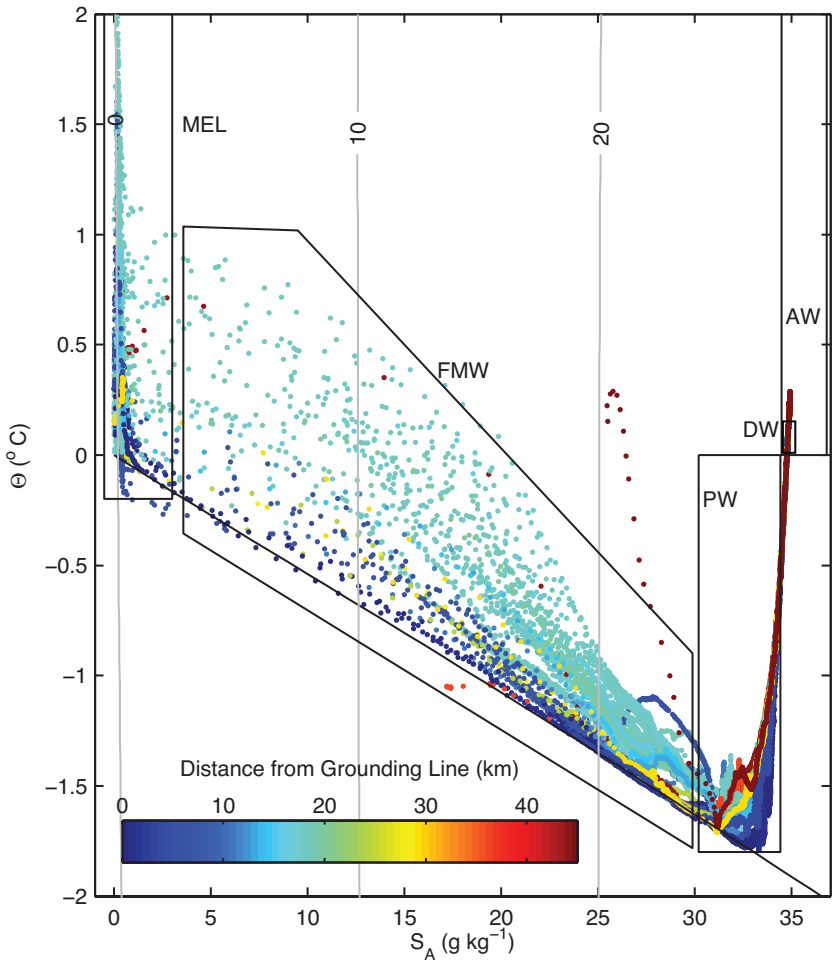

Figure 2.4 Bivariate property plots of conservative temperature and absolute salinity in Milne Fiord showing all profiles collected in July 2012 and July 2013. $\Theta - S_A$ profiles are coloured by distance along the fjord from the Milne Glacier grounding line (KM 0; dark blue) to offshore of the Milne Ice Shelf edge (>KM 45; red). Water masses are labeled (MEL - Milne Fiord epishelf lake; FMW - fjord-modified water; PW - Polar Water; DW - deep water; AW - Atlantic Water). Isopycnals (σ^0 kg m^{-3}; grey lines) and the surface freezing point (solid black line) are shown.

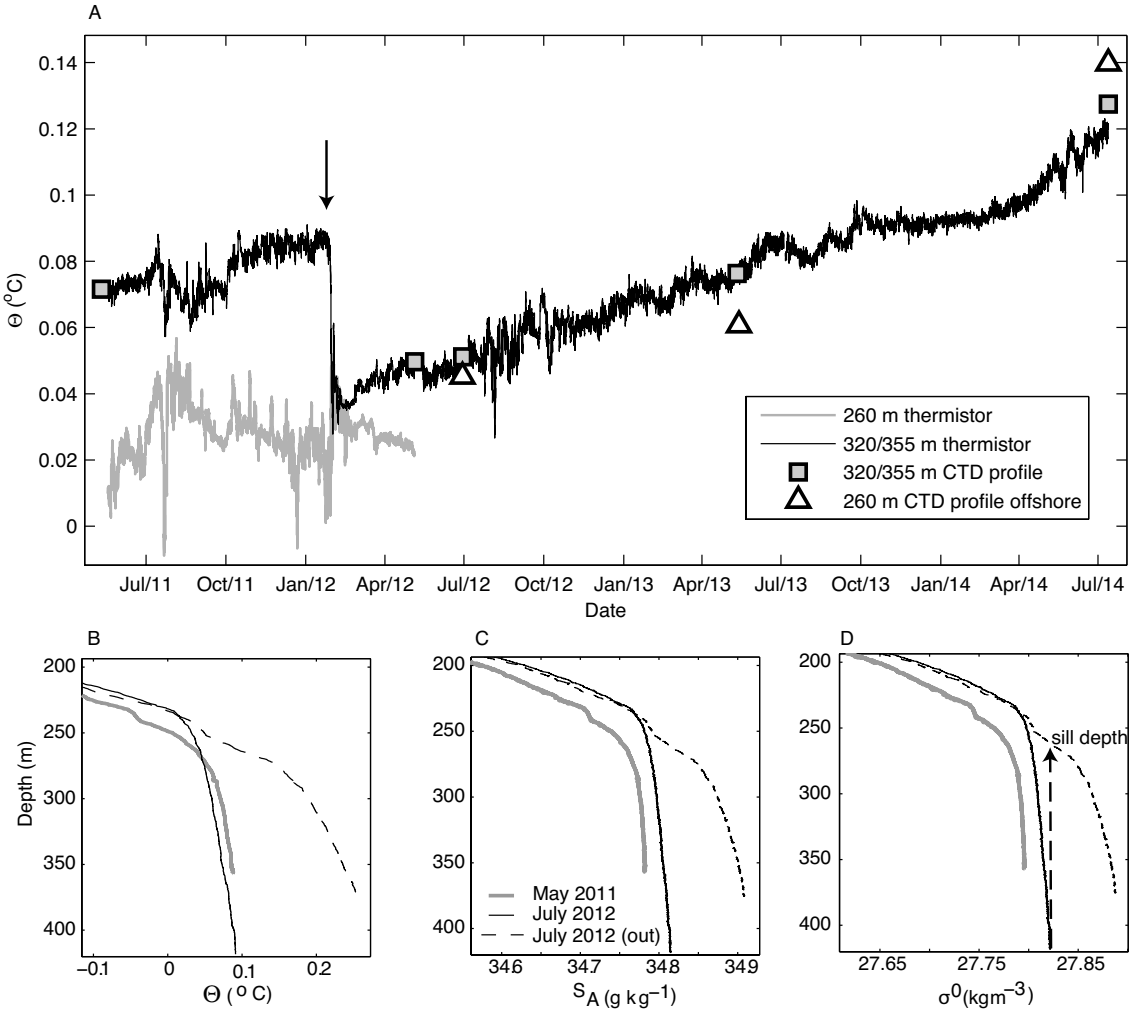

Figure 2.5 A) Timeseries of bottom-water temperature in Milne Fiord from May 2011 to July 2014 showing a deep water renewal, evident by the rapid 0.05°C temperature decrease at 355 m depth on 29–30 January 2012 (arrow). Black lines is hourly data from a thermistors moored at 355 m depth until May 2012, then redeployed at 320 m depth for the remainder of the study (the repositioning was associated with a minor (<0.0025°C) temperature discontinuity). Gray line is data from a thermistor moored at 260 m until May 2012. Squares indicate temperature measured during CTD profiles at the equivalent depth at the mooring location. Triangles indicate temperature measured during CTD profiles at 260 m depth offshore. Profiles of B) conservative temperature, C) absolute salinity, and D) potential density before (May 2011; grey line) and after (July 2012; black line) the deep water renewal. Also shown is a profile collected in July 2012 just outside the sill (dashed line). Effective sill depth is estimated as the level at which density outside the sill corresponds to bottom water density in the fjord in July 2012.

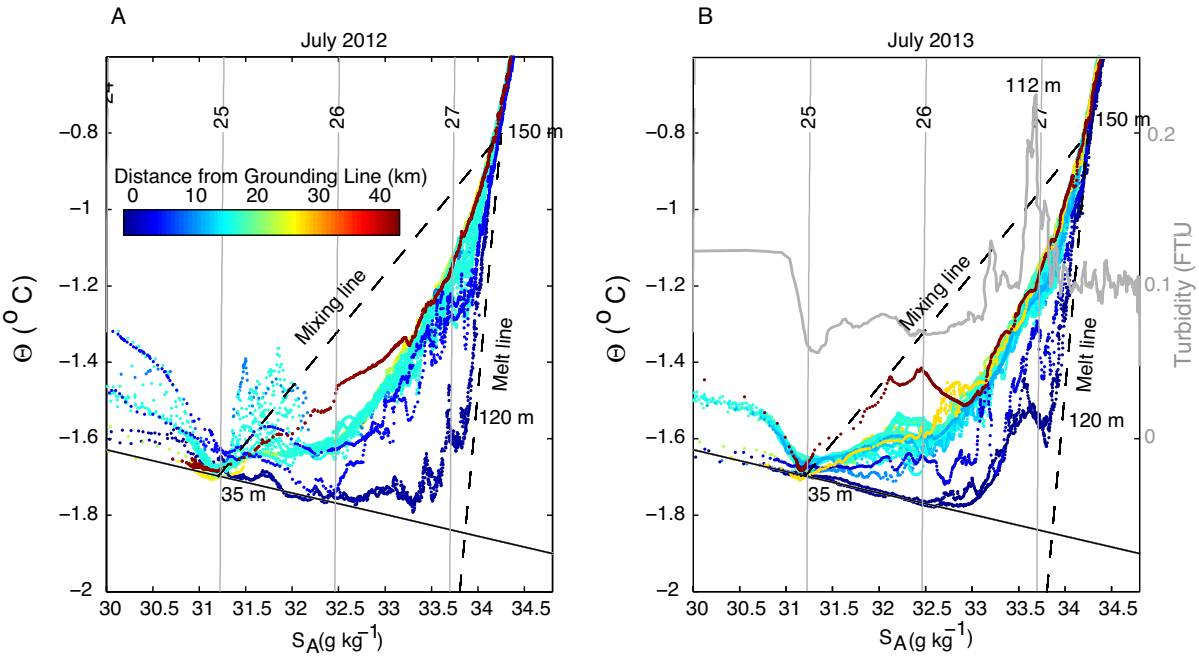

Figure 2.6 Bivariate property plots of conservative temperature and absolute salinity in Milne Fiord from A) July 2012, and B) July 2013. $\Theta - S_A$ profiles are coloured by distance along the fjord from the Milne Glacier grounding line (KM 0; dark blue) to offshore of the Milne Ice Shelf edge (>KM 45; red). In (B) the turbidity vs salinity profile shown was collected near the mooring location. The peak in turbidity corresponds to a depth of 112 m. In (A) and (B) the approximate depths of the Milne Glacier grounding line (150 m), a subglacial runoff outlet (120 m), and the base of the seasonal mixed layer (35 m), and mixing and melt lines (dashed black line) are shown. Isopycnals (σ^0 kg m^{-3}; grey lines) and the surface freezing point (solid black line) are shown. See Section 2.3.2 for the methodology related to the melt and mixing lines.

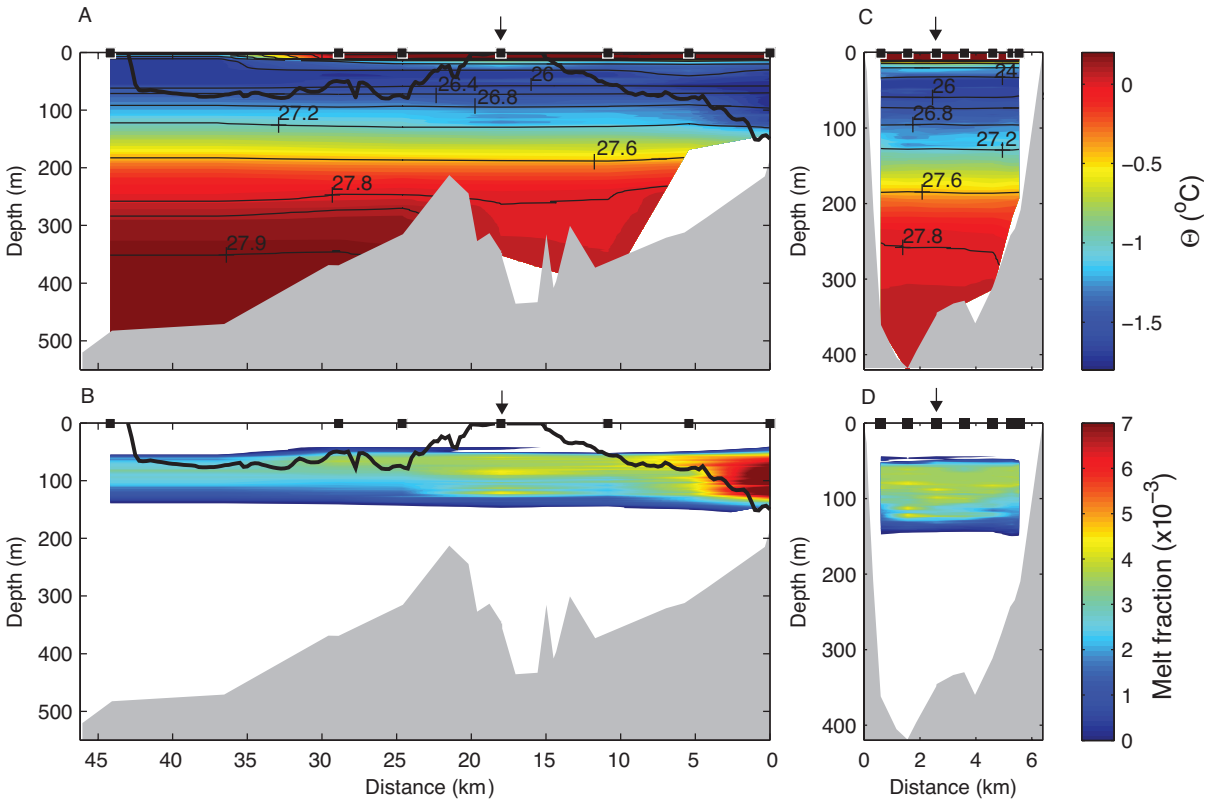

Figure 2.7 Along- (left panels) and cross-fjord (right panels) hydrographic sections from July 2012 of A) and C) conservative temperature with isopycnals overlain, and B) and D) melt water fraction. Along-fjord sections extend from the Milne Glacier grounding line (KM 0) to offshore of the Milne Ice Shelf (KM 45). The cross-fjord maximum ice draft of the MGT (KM 0 to KM 16) and the MIS (KM 20 to KM 43) (black lines) and bathymetry along the centre of the fjord (gray) are shown. CTD casts (black squares) were collected through natural fractures in the ice or through drilled holes in the epishelf lake ice by helicopter over 24 hrs. Hydrographic data is shown above the maximum draft of the ice because cross-fjord variability in ice thickness allows water exchange at all depths within the fjord (inward of the epishelf lake ice shelf dam). The ice dam for the epishelf lake is assumed to be within the Outer Unit of the Milne Ice Shelf, so properties beyond KM 37 are fixed constant to the offshore profile. Cross-fjord hydrographic sections extend from the northeast shore (KM 0) to the southwest shore (KM 5.5) of the epishelf lake, looking toward the glacier grounding line. Bathymetry (gray) is shown. CTD casts (black squares) were collected through drilled holes in the epishelf lake ice on foot over 16 hrs. The epishelf lake ice (not shown) is approximate 0.6 m thick. White areas indicate data gaps. Note that the meltwater fraction is only valid between the chosen PW and AW endpoint water masses at approximately 35 m depth and 150 m depth. The arrow in each panel indicates the mooring site and the intersections of the along- and cross-fjord transects.

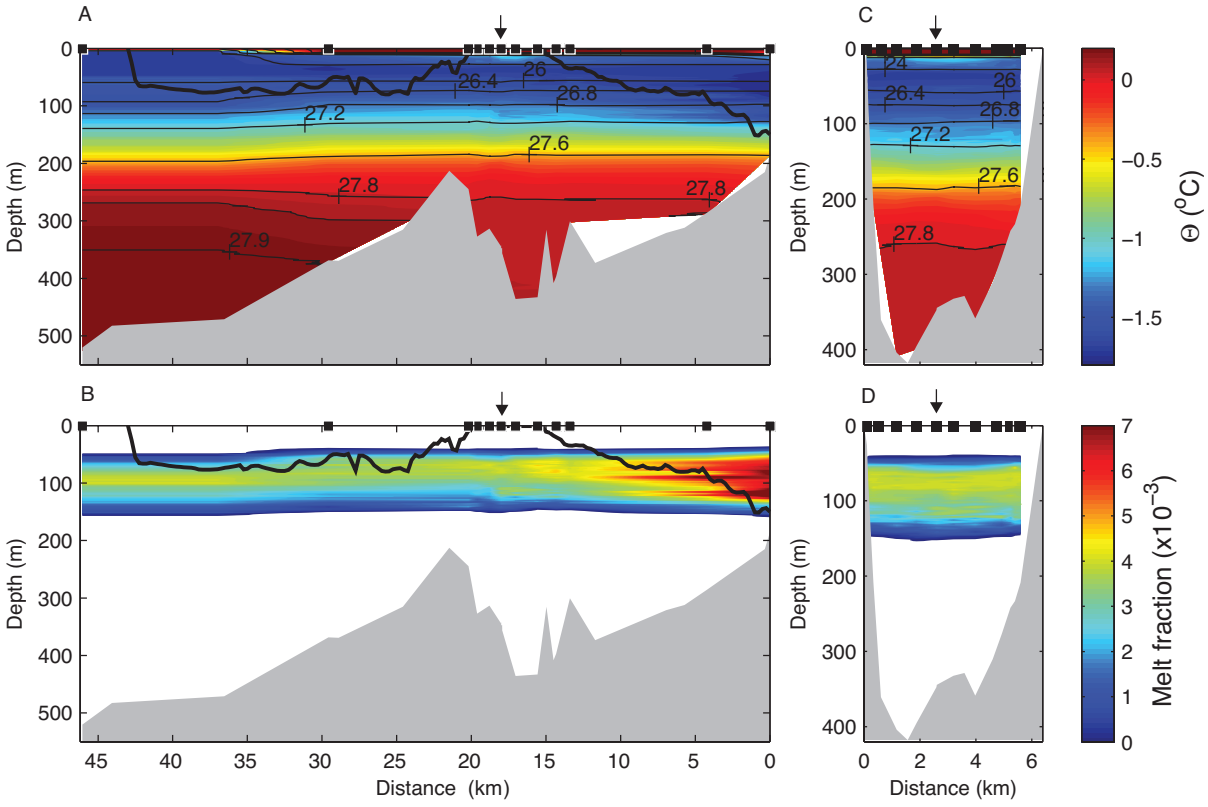

Figure 2.8 Along- (left panels) and cross-fjord (right panels) hydrographic sections, as in Fig. 2.7, but from July 2013. Along-fjord CTD profiles were collected by helicopter and foot over 72 hrs, the cross-fjord profiles by foot over 16 hrs.

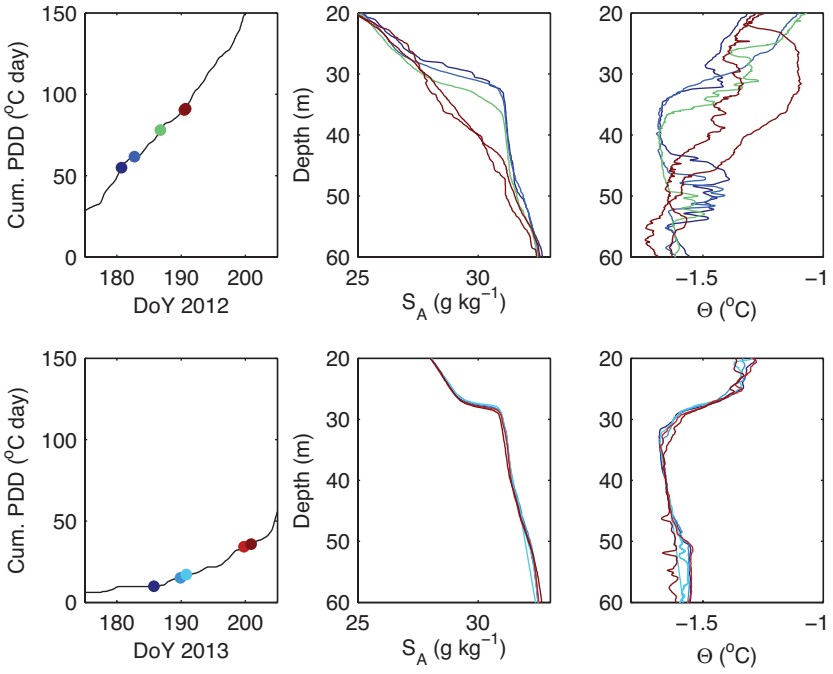

Figure 2.9 Comparison of subglacial runoff in 2012 and 2013. Plotted are the cumulative positive degree-days (PDDs), a proxy for surface melt production, and changes in water column salinity and temperature properties over 2-weeks in July 2012 (top panels) and July 2013 (bottom panels). Profiles are coloured by elapsed time from initial profile each year and the time of profiling is marked on the PDD panel.

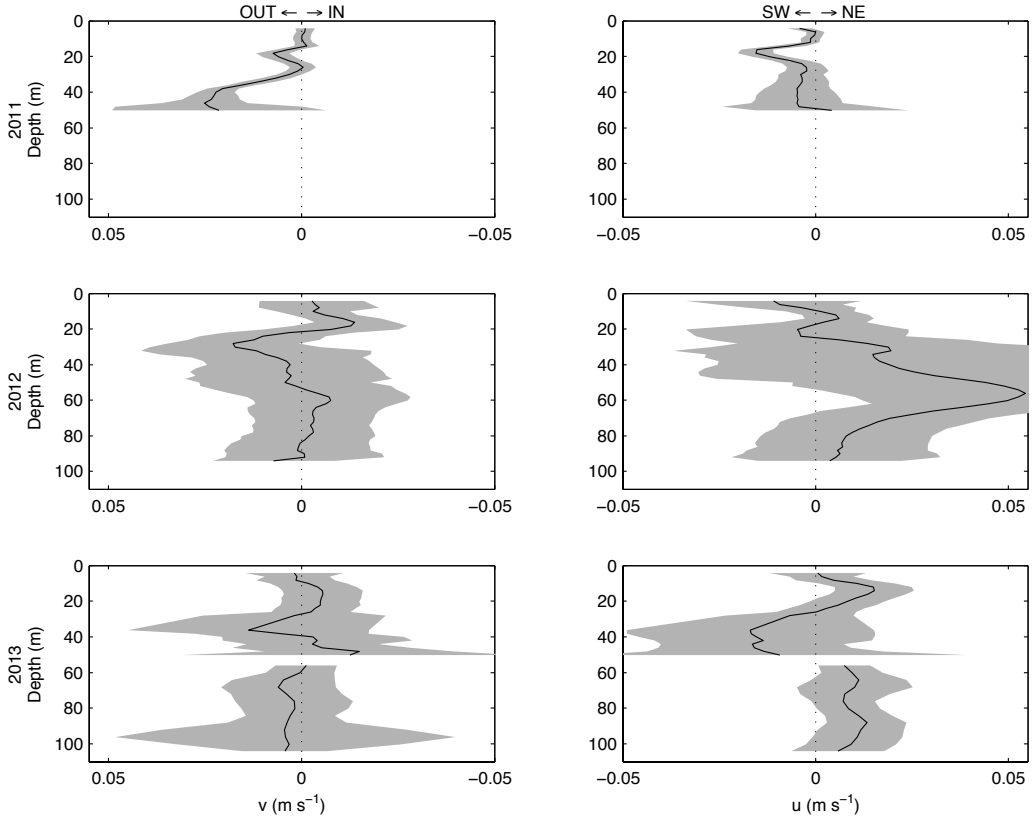

Figure 2.10 Mean along- (v) and cross-fjord (u) current velocities at the mooring location in May 2011, July 2012, and July 2013. Duration over which ADCP measurements were averaged varied among years from 4 days in May 2011, to 6 days in July 2012, to 10 days in July 2013. Grey area indicates one standard deviation from the mean.

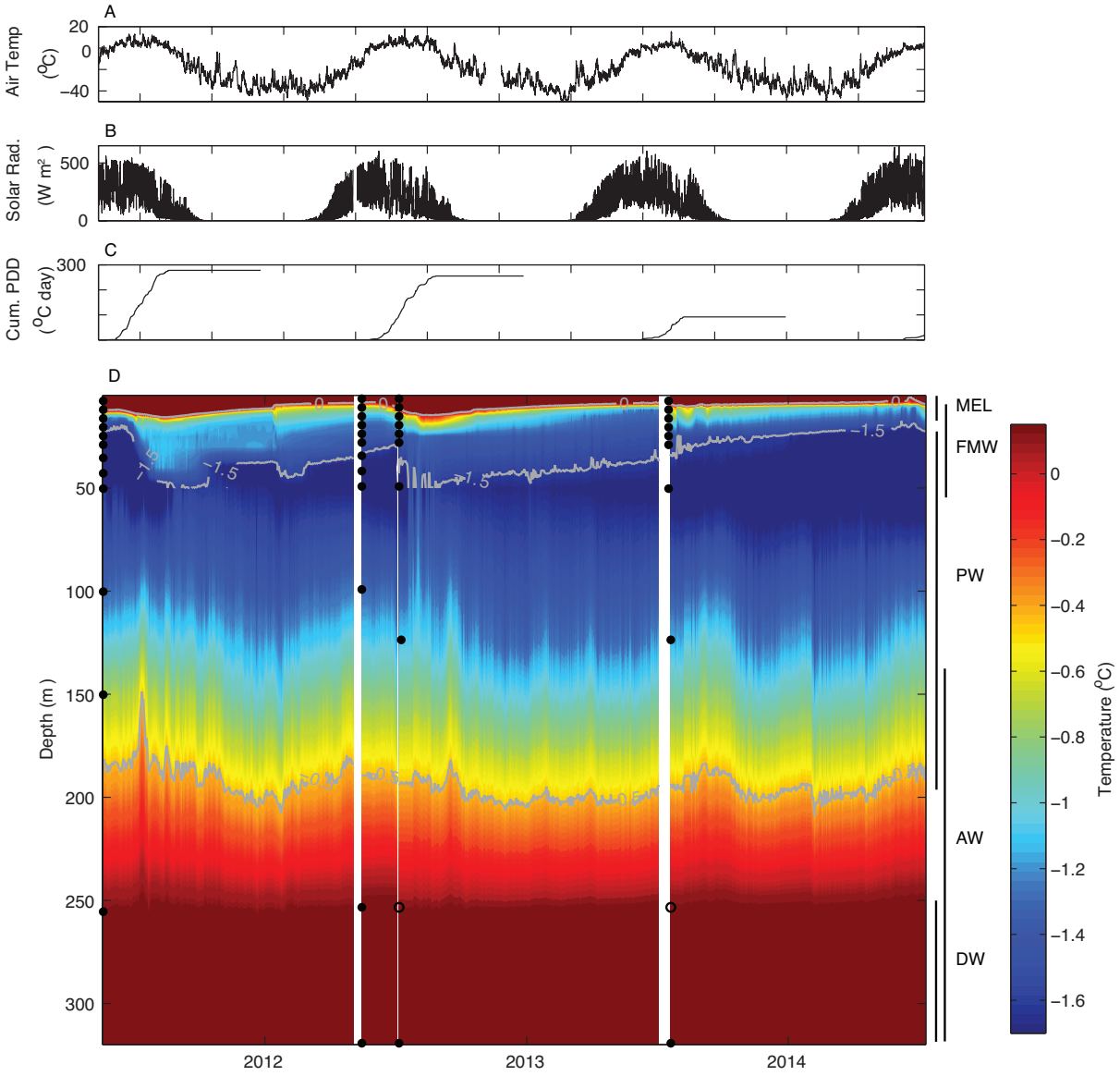

Figure 2.11 Timeseries of A) air temperature, B) shortwave solar radiation, C) cumulative positive degree days (PDDs), and D) ocean temperature at the mooring site from May 2011 to July 2014. In (D) the highlighted isotherms approximate the interface between the epishelf lake (MEL), fjord-modified water (FMW), Polar Water (PW), Atlantic Water (AW), and deep water (DW). Filled black circles indicate thermistor depths at each mooring redeployment. Unfilled circles indicate the sill depth where temperature was interpolated by assuming it was equivalent to temperatures at 320 m depth. White regions indicate data gaps during mooring servicing.

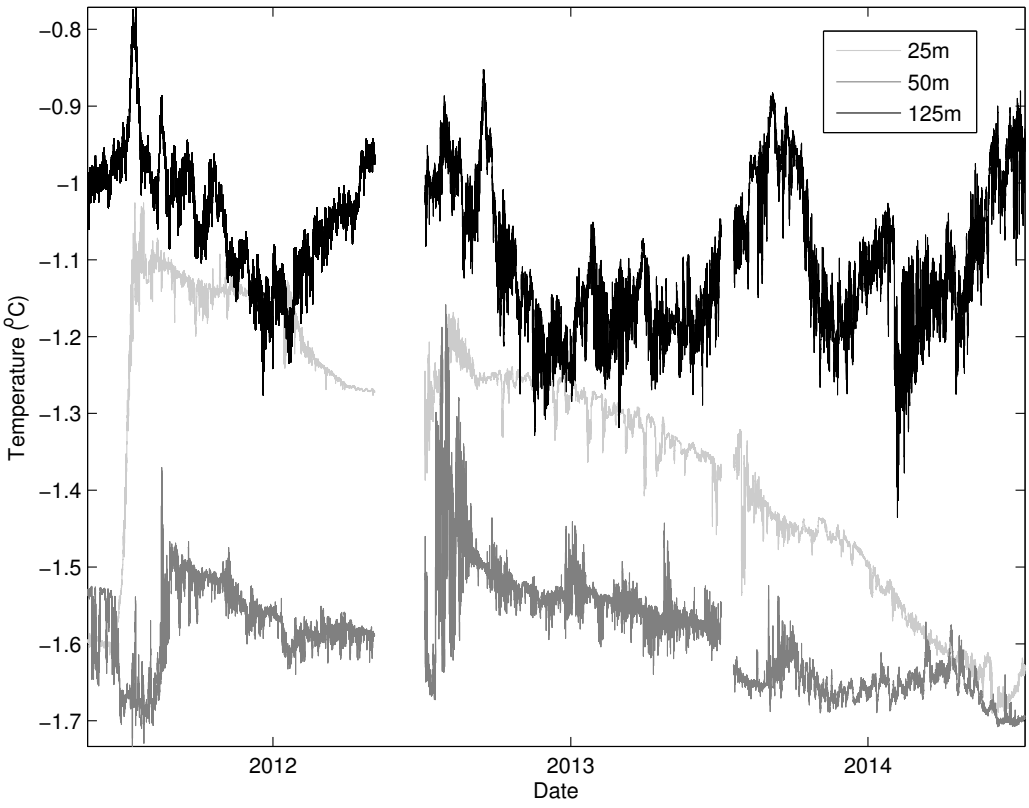

Figure 2.12 Variation in ocean temperature in Milne Fiord at 25 m, 50 m, and 125 m depths from May 2011 to July 2014.

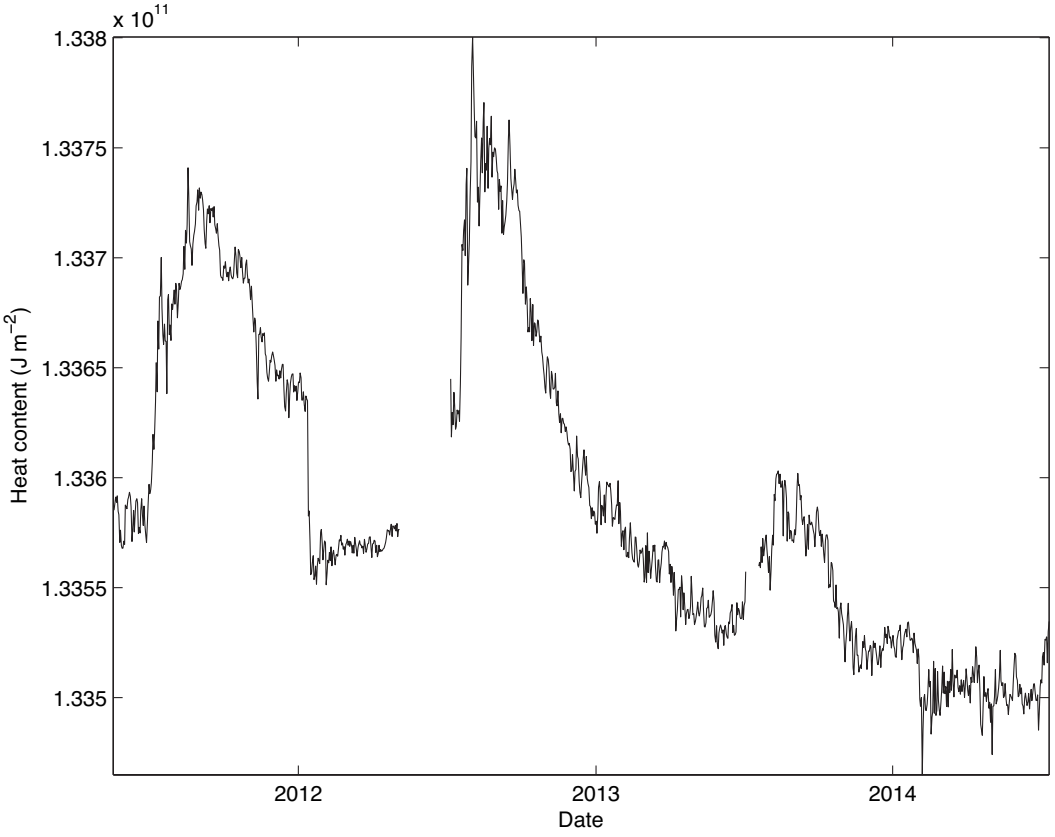

Figure 2.13 Variation in ocean heat content of Milne Fiord between 5 m and 125 m depth from May 2011 to July 2014.

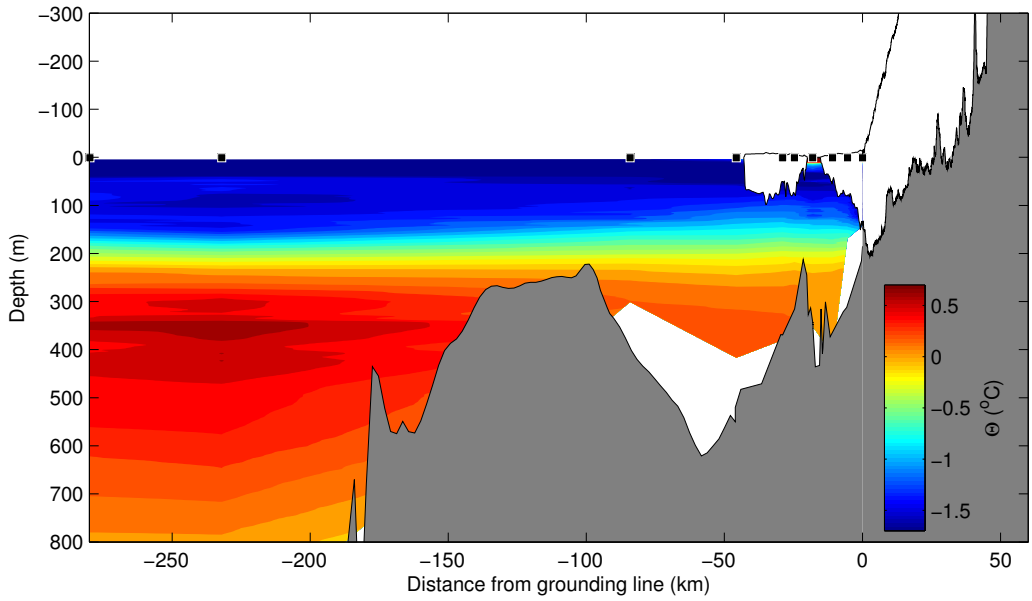

Figure 2.14 Hydrographic section of conservative temperature extending from the Milne Glacier grounding line across the continental shelf. Profiles offshore of the MIS were collected during the University of Washingtons SwitchYard Project (PI Mike Steele) in May 2012 (see Fig. 2.1b for locations), while profiles within Milne Fiord were collected in July 2012 during this study. An ice thickness profile along the centreline of the Milne Glacier from the grounding line to the summit is shown. Offshore bathymetry is from IBCAO v3, while bed topography and ice thickness upstream of the grounding line are from IceBridge 2014 data.

Chapter 3

Dynamic response of the last remaining Arctic epishelf lake to seasonal and long-term forcing

3.1 Introduction

In bays at high latitudes, thick floating ice can create a physical barrier, or dam, behind which meltwater runoff from the surrounding glacial catchment accumulates. Where the dam is formed by an ice shelf (a floating sheet of ice attached to the coast) the impounded freshwater is known as an epishelf lake. Epishelf lakes are freshwater bodies but are tidally influenced and can be divided into two types depending on their connection to the ocean: those that form on land but have hydraulic connection to the ocean below the ice shelf at the land-ice interface; and those where the freshwater layer floats directly on seawater. The former are numerous in Antarctica and are distributed around the margins of the continental ice sheet (Heywood, 1977; Gibson and Andersen, 2002; Laybourn-Parry et al., 2006; Smith et al., 2006), while the latter, those that float directly on seawater, are not as common in Antarctica (Wand et al., 2011), but were once relatively numerous in the Arctic, specifically along the northern coast of Ellesmere Island, Canada. Here, remnants of a once expansive coastal ice shelf (Vincent et al., 2001) blocked the mouths of fjords creating several epishelf lakes (Veillette et al., 2008), the deepest of which was the Disraeli Fiord epishelf lake dammed by the Ward Hunt Ice Shelf which had a maximum depth of 63 m (Crary, 1956).

Over the last two decades, several of the Ellesmere ice shelves have experienced thinning, fracturing, and collapse (Mueller et al., 2003; Copland et al., 2007; England et al., 2008; Vincent et al., 2009; White et al., 2015a) and this has resulted in the loss of all but one epishelf lake along this coast (Mueller et al., 2003; Veillette et al., 2008). The collapse of the ice shelves has been largely attributed to climate forcing, as this region has warmed at twice the global average (IPCC, 2013).

The existence and evolution of epishelf lakes is dependent on the interaction between atmospheric, oceanographic, and cyrospheric conditions, and thus epishelf lakes have been identified as sensitive indicators of climate change (Veillette et al., 2008). They are also a unique type of aquatic ecosystem, containing fresh, brackish and sea water biota within a single water column, with strong vertical gradients in biological as well as chemical properties (Laybourn-Parry et al., 2006; Veillette et al., 2011a).

Studies of Ellesmere epishelf lakes have shown that the transition from freshwater to seawater occurs over only a few meters depth, and the strong halocline can persist for decades (Keys et al., 1968; Vincent et al., 2001), with perennial ice cover and low tidal action limiting vertical mixing. The depth of the halocline has been interpreted as equivalent to the minimum draft of the impounding ice shelf (Hattersley-Smith, 1973; Jeffries and Krouse, 1984; Gibson and Andersen, 2002), and interannual depth changes have been used to infer long-term changes in thickness of the ice shelf (Vincent et al., 2001; Mueller et al., 2003; Veillette et al., 2008). Questions remain however, as to what extent changes in the thickness of the dammed freshwater layer are representative of changes in the mean thickness of an ice shelf (Vincent et al., 2001; Smith et al., 2006).

Prior to its complete drainage between 1999 and 2002 due to fracturing of the Ward Hunt Ice Shelf, the Disraeli Fiord epishelf lake had been thinning since 1954, at a rate roughly corresponding to overall mass loss from the Ward Hunt Ice Shelf (Veillette et al., 2008). Other epishelf and ice-dammed lakes in the region have shown similar long-term thinning, however, with interannual variability on the order of a meter (Veillette et al., 2008). This variability has been suggested to be related to tidal cycles, internal waves, and fjord circulation (Veillette et al., 2008). However, the one study that addressed some of these factors found that internal waves excited by tidal flow were very small in amplitude ($<$20 cm; Keys et al., 1968). Despite lingering questions over the dynamics of epishelf lakes, observations have largely been limited to single water column profiles collected on an opportunistic basis every few years. A targeted study of epishelf lake physical limnology has not been conducted since a campaign to study the Disraeli Fiord epishelf lake in the 1960s (Keys et al., 1968; Keys, 1978), prior to the recent phase of widespread decline and loss of epishelf lakes along this coast.

The objectives of this study were to evaluate the physical structure and temporal dynamics of the Milne Fiord epishelf lake, the last known epishelf lake in the Arctic. We investigated interannual changes in epishelf lake depth, area, and volume over 10 years from analysis of water column profiles and remote sensing imagery. To better understand how the lake changes on sub-seasonal timescales we conducted a targeted 3-year field study that involved periods of intensive water column profiling, collection of tide heights and current velocities, and the collection of a continuous multi-year mooring time series of epishelf lake temperature and salinity, as well as meteorological data. We measured the evolution of the thermal and salt stratification of the lake and its spatial and temporal variation, with the aim to understand the controlling factors for lake depth and the

implication of recent changes for the future of this ecosystem.

3.2 Methods

3.2.1 Study site

The 436 m deep Milne Fiord (82°35N, 80°35W) lies on the northern coast of Ellesmere Island adjacent to the Arctic Ocean (Fig. 3.1). The Milne Glacier flows into the head of the fjord and forms the tapered 16 km long Milne Glacier tongue (MGT), varying from 150 m thickness at the grounding line to 10 m at the terminus (Chapter 2). Spanning the mouth of the fjord, but separate from the MGT, is the Milne Ice Shelf (MIS), which varies in thickness from $<$10 m to 100 m. The MIS originated from a combination of tributary glacier input, in situ snow accumulation and marine ice accretion, and is readily distinguished from other ice types by the undulating surface marked by a series of parallel troughs and ridges.

The MIS forms a floating dam across the mouth of the fjord, trapping surface runoff within the fjord. The first water column samples in the fjord were collected in 1983 through 3.19 m of ice, and revealed an $\sim$17.5 m deep freshwater layer separated from seawater by a sharp halocline only a few meters thick (Jeffries, 1985). Although water profiles are lacking prior to this time, based on aerial photographs and aerial radar measurements of thin ($<$9.7 m thick) ice in the inner fjord in 1981 (Narod et al., 1988), suggests the epishelf lake was present prior to 1983. The next sampling conducted in 2004 showed the freshwater layer had deepened to 18.3 m, but then thinned to 14.3 m by 2009 (Veillette et al., 2011b).

In examining changes in the area of the MIS, Mortimer et al. (2012) suggested that prior to 1959 the MIS and MGT were connected, and over the next few decades the epishelf lake developed from small ice-marginal lakes along the side of the fjord to eventually replace the Inner Unit of the MIS by 2009, severing the connection between the MIS and MGT. Mortimer (2011) estimated the area of the epishelf lake based on identification of lake ice in satellite imagery as 52.5 km^2 in 2009, although the actual extent of the lake had not been confirmed with field observations. The lake appeared to consist of a 6 km wide main basin between the inner edge of the MIS and the terminus of the MGT, and two narrow arms extending 16 km along the sides of the MGT to the grounding line (Fig. 3.1d). The otherwise steep walls of the fjord are punctuated by three shallow bays with inflowing streams at their heads. The lake is fed by snow and glacial runoff from the $\sim$1500 km^2 catchment of the Milne Glacier and its tributaries (GLIMS and NSIDC, 2005). Ice thickness mapping of the MIS (Mortimer et al., 2012; Chapter 2) indicates the only ice thin enough to provide an outlet to the lake is along the re-healed fractures in the MIS, however, the drainage pathway of the lake has not been confirmed by observations.

3.2.2 Area and volume

Changes in the area of the MEL from 1959 to 1988 were estimated from optical imagery acquired by aerial and satellite platforms, and from 1992 onward from Synthetic Aperature Radar (SAR) imagery. The 1 m thick epishelf lake ice was discriminated from other surrounding ice types, including ice shelf, glacier ice and marine ice, in optical imagery by its lack of surface topography, and in SAR imagery by its high backscatter signal (>-6 dB), produced by its lack of surface topography and the freshwater underneath perennial lake ice (regions underlain by salt water have a darker return; Veillette et al., 2008; White et al., 2015a). The epishelf lake included non-contiguous regions of lake ice in fractures in the MIS and between calved pieces of the MIS and MGT. The epishelf lake was digitized in ArcGIS 10.2.2 at an image scale of ∼1:20,000, with a pixel size of 6.5 m.

Lake volume was estimated from area and depth, assuming a spatially uniform depth (see Section 3.3.8) and vertical shores. The volume estimated included the volume of surface ice. The depth was taken from the hydrographic profiles collected the May following image acquisition (usually in Feb or March) when available, otherwise from the profile collected closest to the date of image acquisition.

3.2.3 Hydrography

Near-annual sampling of water properties in Milne Fiord commenced in 2004, with a directed and intensive sampling program from 2011 to 2014. Water properties were measured through drilled holes or natural leads in the ice, including fractures through the ice shelf and glacier tongue, accessed by foot, snowmobile, or helicopter. Where possible, lake ice thickness was measured and varied from a maximum of 3.19 m in 1983 (Jeffries, 1985) to a minimum of 0.65 m in July 2010. Profiles of temperature and salinity were collected using a conductivity-temperature-depth (CTD) profiler lowered at ∼0.5 m s^{-1} using a manual reel, with the exception of the May 1983 profile collected by Jeffries (1985) that was measured using reversing thermometers, a 1 L Knudsen bottle and a Radiometer CDM80 Conductivity Meter. Opportunistic profiles were collected in August 2004, June 2006, and July 2007 using a 1 Hz RBR XR-420 CTD. Subsequent profiles were collected in May & July of 2009, July 2010, May & July 2011, 2012, and 2013, and July 2014 with a 6 Hz RBR XR-620 CTD. Profiles from May 2011 were collected using a 4 Hz Seabird SBE19+ CTD, and in July 2011 using a 1 Hz Hydrolab HLX. CTDs were calibrated once every 2 years after 2011, prior to this the CTDs were not regularly calibrated so we interpret data prior to 2011 with this caveat on its absolute accuracy. Profiles collected between 2004 and 2009 were previously published in Veillette et al. (2011b), although we have reprocessed all these data from raw conductivity and temperature (where available) for consistency. Prior to 2011, profiles were collected in either Purple Valley Bay or Neige Bay (unofficial names), two small inlets on the west and east sides of the fjord, respectively, with water depths of ∼80 m. Hydrographic data suggests Neige Bay has a topographic sill at ∼30 m depth so water properties below this level in the bay are not representative of the fjord.

An exception is the 2004 profile, which was located approximately 2 km southwest of Neige Bay near the MGT terminus.

From 2011 onward multiple profiles were collected during each field campaign throughout the main fjord. Full depth profiles were usually collected to the bottom of the fjord, however here we focus on the upper 25 m of the water column. CTD data were processed in Matlab following a procedure that included: correction for atmospheric pressure, application of a 3 point low-pass filter in time to the raw pressure, temperature, and conductivity; alignment of conductivity and temperature with respect to pressure; a thermal cell mass correction (for the SBE19+ CTD data only); and loop editing (removal of pressure reversals), and bin averaged to 0.2 m intervals. Derived variables were calculated using the International Thermodynamic Equation of Seawater 2010 (TEOS-10) Gibbs Seawater Oceanographic Matlab Toolbox (www.TEOS-10.org). Temperature and salinity are reported here as Conservative Temperature (Θ) and Absolute Salinity (S_A), with the exception of the 1983 data, which are presented as originally published as practical salinity (ppt) and in situ temperature.

For freshwater lakes, the calculation of salinity from temperature, conductivity, and pressure is dependent on the chemical composition of the water, data which we lack. If the chemical composition of the lake varies substantially from seawater, the error in calculated salinity could be as much as 30% for salinities <3 g kg^{-1} (Pawlowicz, 2008). The source of the epishelf lake water is primarily snow and meteoric glacial ice melt, with low ionic concentrations (and conductivity). The measured conductivity of two proglacial meltwater streams entering the fjord in 2012 and 2013 were <0.06 mS cm^{-1}, while the conductivity of the lake was generally >0.15 mS cm^{-1}. The obvious source of salt required to increase the conductivity of the lake water is entrainment of underlying seawater, meaning the bulk chemistry of the lake should reflect that of diluted seawater. The error in calculated salinity is therefore likely $<<30\%$.

In order to compare changes in the thickness of the freshwater layer over time it was necessary to define the bottom of the epishelf lake, which was actually a continuum from freshwater to seawater. Previous studies delineated the bottom of an epishelf lake using the depth of the 3 ppt isohaline (Mueller et al., 2003; Veillette et al., 2008), or the depth of the halocline (which the authors qualitatively define as the zone of abrupt salinity change between freshwater and sea water; Veillette et al., 2011b). We formalized the definition of Veillette et al. (2011b) by defining the bottom of the lake (D_{EL}) as the depth of the stratification maximum as defined by the Brunt Vaisala frequency:

$$D_{EL} = z(N^2_{max}), \tag{3.1}$$

where z is depth (positive downward) and N^2 is the Brunt Vaisala frequency:

$$N^2 = \frac{g}{\rho}\frac{\partial \rho}{\partial z}, \tag{3.2}$$

where g is gravitational acceleration, and ρ is density of the water. Profiles of N^2 were averaged using a 12-point depth window before calculating the maximum. Water density is dominated by salinity at these low temperatures, so D_{EL} represents the maximum salinity gradient. The advantage of this method is that the epishelf lake depth calculation is clearly defined, quantitative, and applicable to other epishelf systems (regardless of the absolute salt content of the epishelf lake, which would affect the 3 ppt method). Due to the bottle sampling method used by Jeffries (1985) we could not calculate N^2 for that profile, so we defined the bottom of the lake as the depth of the sample collected nearest the apparent stratification maximum. The depth of the primary halocline varied by $\pm$ 0.15 m in a series of 18 profiles collected at a single location over a 24 hr period in May 2009, so this was considered to be the error in the depth of the epishelf lake as determined by the CTD profiling method.

3.2.4 Current velocities

Water velocities of the upper water column were measured using an ice-anchored, downward-looking 300 kHz RDI acoustic Doppler current profiler (ADCP) at the mooring site over 4 days in May 2011, 7 days in July 2012 and 10 days in July 2013. The ADCP sampled at 2 min intervals and data were processed in Matlab.

3.2.5 Tidal height

A bottom anchored RBR XR-620 CTD was deployed at 355 m depth from May 2011 to July 2012 sampling at 2 minute intervals to measure changes in water level (accuracy is $\pm$ 0.37 dbar, drift 0.74 dbar a^{-1}). A 3 hr low pass-filter and a linear detrend was applied to the raw pressure data. The dominant tidal constituents were determined by harmonic analysis with nodal corrections using the T_Tide Matlab toolbox (Pawlowicz et al., 2002).

3.2.6 Meteorological time series

Meteorological conditions were measured by a HOBO automated weather station (AWS) located at 10 m elevation on the shore of Milne Fiord (Fig. 3.1 a). Only air temperature (at 1 m and 2 m above ground) and shortwave solar radiation are reported here. Cumulative positive-degree days (PDDs), the daily integrated air temperatures above 0°C, were calculated to provide a direct proxy for summer melting, which has been directly linked to air temperature (Hock, 2003). Prior to the AWS installation in 2009, we estimated summer air temperatures in Milne Fiord from records from Eureka, Nunavut (www.ec.gc.ca). Linear regression showed that air temperature in Milne Fiord T_{Milne}, was related to air temperature in Eureka by $T_{Milne} = 0.47 * T_{Eureka} + 0.48$. T_{Milne}. The predicted temperatures were then used to calculate PDDs prior to 2009. The interpolation was only valid for $T_{Eureka} \geq$0°C, and had a root-mean-squared error of 1.98°C.

3.2.7 Mooring time series

Milne Fiord water properties were measured from May 2011 to July 2014 by a mooring deployed in the centre of the epishelf lake. The mooring was anchored to the epishelf lake ice and suspended in the water column. The mooring consisted of 20 RBR TR1050/60 , 2 RBR XR420-freshwater CTs, 2 Seabird SBE37 CTs, and 1 RBR XR620 CTD from May 2011 to July 2012, then was reduced to 7 TR1060s, 1 XR420 CT, and 1 XR620 CTD for the remainder of the study. Calibrated instrument accuracy is ± 0.002°C, $\pm$ 0.003 mS cm^{-1}, and $\pm$ 0.37 dbar, and nominal drift is ± 0.002°C a^{-1}, $\pm$ 0.012 mS cm^{-1}a^{-1}, and $\pm$ 0.7 dbar a^{-1}. Some time series records were truncated for various reasons, including salinity going beyond the maximum calibrated range (3 PSU) of the freshwater instruments (XR420s), or instrument malfunction. The mooring was serviced once or twice per year and instruments were repositioned to track the halocline. Initially, the instruments were spaced every meter from the surface to 20 m depth, with increasing depth intervals below 25 m. Although the mooring instruments extended to the full depth of the fjord, in this paper we focus on the top 25 m of the water column. Instruments sampled at 30 to 120 second intervals and were calibrated before and after deployment. CTD profiles collected during deployment and recovery were used to correct for instrument drift, which was within manufacturer specifications.

Seasonal changes in the depth of the epishelf lake were estimated from an inferred vertical displacement of the halocline from the mooring time series, where salinity changes at a fixed depth over time are projected onto the initial vertical salinity profile. The accuracy of this method is greatest where dS/dz is highest (i.e. in the halocline), while the error increases substantially where the salinity gradient is weaker (i.e. above or below the halocline). This constraint on the method is acceptable as the lake bottom is defined above as the level of the stratification maximum, so only the instrument initially positioned within the halocline (instrument at 13 m depth from May 2011 to May 2012) is included in the analysis. The method assumes a constant salinity gradient that is displaced downward by inflow (surface runoff) and displaced upward by outflow (drainage under the MIS); it neglects the effects of horizontal advection of freshwater (from subglacial runoff) and vertical mixing processes that alter the salinity gradient.

We also estimated epishelf lake depth using temperature data from the temperature recorders, which were much more closely spaced in depth. Lake depth was estimated from the depth of the isotherm corresponding to the average temperature at the depth of the N^2_{max} measured by the CTD profile at the beginning and end of the mooring deployment. The process was repeated each time the mooring was serviced and CTD profiles were collected. This method assumed isotherm displacement was due to displacement of the halocline, however we acknowledge other processes could have altered the depth of the isotherms that were not related to a depth change of the halocline, such as in situ heating due to solar radiation, horizontal advection of heat, and vertical heat flux across the halocline. However, the results of the isotherm proxy showed good agreement with the salinity proxy and the CTD estimates of epishelf lake depth, providing confidence in the method.

3.3 Results

3.3.1 Area

The area of the lake increased substantially since the first aerial imagery in 1959, reaching 71.2 km^2 as of 27 March 2015 (Fig. 3.1; Table 3.1). The largest change in area occurred sometime between 1959 and 1988, as the epishelf lake replaced the Inner Unit of the MIS. Since 1988 the lake existed in close to its present form, with a main fjord-wide basin and two arms extending along the sides of the MGT. Increases in lake area after 1992 were due the retreat of the southern margin of the MIS, including calving of the MIS into the fjord, the creation of small satellite lakes in fractures of the MIS, and wastage along the margins of the MGT. Where available, the satellite lakes show water column structure that is nearly identical to that of the main basin of the MEL (see Section 3.3.8), suggesting the satellite lakes are connected to the main basin by a network of small fractures or basal crevasses that allow water exchange, so we included them in the area estimates. Some gains in area were partially offset by losses due to the advance of the terminus of the MGT, which ranged from 56.4 m a^{-1} to 173.2 m a^{-1} between 1950 and 2009 (Mortimer 2011).

3.3.2 Stratification

The most striking feature of all water column profiles collected in Milne Fiord was the presence of a several meter thick freshwater (defined here as salinities $<$0.5 g kg^{-1}) layer at the surface, the epishelf lake, which was never present offshore of the MIS. The epishelf lake was a conspicuous feature of the first profile obtained in the fjord in 1983 (Jeffries, 1985), but it has clearly thinned through time. Despite changes in the depth of the lake, several distinct layers in the epishelf lake and upper water column could be identified based on salinity and temperature characteristics. In summer, a 1-2 m thick stratified layer with salinity approaching zero and temperature approaching the freshwater freezing point (0°C) was present just below the ice-water interface. We termed this the surface melt layer. Below the thin surface melt layer was a layer of nearly constant salinity (approximately 0.2 g kg^{-1}), the mixed layer, extending from the base of the surface melt layer to the top of the halocline. The mixed layer was up to 8 m thick, however it was not present in all years, and usually only evident in summer, at other times the lake was weakly salinity stratified.

The salinity gradient below the mixed layer could be divided into an upper halocline and a lower halocline. The upper halocline is the transition from the base of the mixed layer to the bottom of the lake (i.e. the N^2_{max}), while the lower halocline is defined as extending below the N^2_{max} to the level at which properties within the fjord are equivalent to those at the same depth offshore (between 25 - 50 m). A subsurface temperature maximum (up to 3°C) was usually associated with the upper halocline. In some profiles the mixed layer was not present, and the upper halocline extended to the base of the surface ice melt layer (if present) or to the ice-water interface. The gradient and thickness

of the upper halocline varied among years, with a thicker and more gradual salinity gradient apparent prior to 2009 (e.g. in 2004 the upper halocline was 15 m thick and extended almost to the surface), while after 2009 the salinity gradient was thin and sharp (e.g. in June 2012 the upper halocline was $<$3 m thick). Temperatures in the lower halocline decreased rapidly with depth toward the freezing point of seawater (-1.8°C). The gradient and properties of the lower halocline were dependent on local fjord processes, including interactions with ice and advection of subsurface glacial meltwater runoff, so the lower halocline was also referred to as fjord-modified water (Chapter 2).

The stratification at the base of the epishelf lake is very strong, in all years the N^2_{max} is $>$0.1 s^{-2} (or 10^3 cycles per hour). For comparison, typical buoyancy frequencies in the open ocean are generally $<$20 cycles per hour, so the stratification in the epishelf lake halocline is one to two orders of magnitude stronger by this measure. Density in the halocline is determined primarily by salinity, changes in temperature are only important in determining stratification in the isohaline mixed layer. For example, for water at 0.2 g kg^{-1} and 2°C, to change the density by 0.1 g kg^{-1} requires a 4°C change in temperature, but only a 0.15 g kg^{-1} change in salinity. As a result, density profiles (not shown) are nearly identical to the salinity profile. It is important to note that temperatures in the epishelf lake are everywhere below the temperature of maximum density, so a temperature increase results in a density increase.

3.3.3 Current velocities

ADCP deployments revealed a quiescent system with currents $<$2 cm s^{-1} in the upper 25 m of the water column (not shown). The currents were weakly baroclinic, with velocities near zero in the epishelf lake above the level of the halocline, increasing to 1-2 cm s^{-1} just below the halocline. The results support the view that the MIS forms a barrier to flow above the halocline, and acts as a dam preventing offshore exchange at the surface. The potential for velocity shear stress to generate vertical mixing in the water column can be determined by calculating the gradient Richardson Number, a ratio of stratification to velocity shear:

$$Ri = \frac{N^2}{\left(\frac{\partial u}{\partial z}\right)^2} \tag{3.3}$$

where u is horizontal velocity (m s^{-1}) and z is depth (m; positive z down). During all three periods of observation $Ri >> 1$ across the halocline, indicating that stabilizing buoyancy forces dominate and turbulent mixing is not expected. This finding helps explain the persistence of strong stratification in the fjord, as the transfer of heat and mass across the pycnocline is likely limited to molecular diffusion. In the mixed layer of the epishelf lake, however, stratification is much weaker and $Ri < 1$, indicating shear induced turbulent mixing is possible in this layer.

3.3.4 Lake depth: interannual variation

The salinity profiles show a clear long-term thinning of the epishelf lake, from a maximum depth of 18.3 m in 2004 to a minimum of 8.0 m depth in 2013 (Fig. 3.2); Table 3.1). There was little change in the depth of the epishelf lake between 1983 and 2004, however it is unknown how much variation occurred in the intervening 20 years. Between 2004 and 2014 the epishelf lake thinned at an average rate of 1.08 m a^{-1}, however, the rate and direction of change was not constant. An abrupt thinning occurred between 2011 and 2012, when the lake depth decreased by almost 4 m, quadruple the decadal average thinning rate. Conversely, the lake appeared to increase in depth between some years (e.g. between 2006-2007, 2009-2010, and 2013-2014), with a maximum increase of 1.3 m between 2013 and 2014. However, we argue below that the apparent increase in lake depth on an interannual basis is an artifact due to differences in the timing of profiling relative to the melt season.

3.3.5 Lake depth: seasonal variation

CTD profiles collected in Milne Fiord within the same year reveal a pronounced seasonal increase in the depth of the lake (Fig. 3.3). In 2012, the halocline deepened over the summer by 1.9 m, with a 0.7 m increase between May 5th and June 28th, then a further 1.2 m progressive increase over the following 11 days until July 9th. In 2013, however, the lake depth changed very little between May 10th and July 5th, with a small (<0.5 m) depth increase apparent over the subsequent 2-weeks of profiling in July. Changes in depth of the epishelf lake are significantly correlated with the cumulative PDDs (n = 226, R^2 = 92%, p = 0.005), with a ratio of 1.7 cm $^{\circ}C^{-1}$ day^{-1} (Fig. 3.4), which are a proxy for the volume of surface meltwater production from the glacier catchment. The summer of 2012 was very warm, 50 PDDs were accumulated between May and June, and increased to a total of 93 PDDs by the time the final profile was collected that year. The summer of 2013, however, was quite cool, only 10 PDDs had accumulated between May and July, and a total of only 38 PDDs accumulated by the time the final profile was collected that year (despite the final 2013 profile being collected almost 2 weeks later in the year than the final profile of 2012). Neither field campaign spanned the duration of the entire summer melt season. For example, in 2012, profiling ended July 9th when 92 PDDs had accumulated, yet a seasonal total of 253 PDDs accumulated by August 15, so the lake likely deepened substantially more by the end of the melt season which was not captured in the profiles (see Section 3.3.12).

3.3.6 Tides

Harmonic analysis of the water level record reveals the tide in Milne Fiord is mixed, predominately semidiurnal, with a range of 0.31 m. Amplitudes of the dominant M2 (12.42 h) and K1 (23.93 h) tidal constituents are 0.056 m and 0.040 m, respectively, which together account for 86.7% of the variance of the original water level data. The low tidal energy available for mixing in Milne Fiord

was likely to be a factor in the long-term persistence of the epishelf lake halocline.

3.3.7 Lake depth: internal waves

In June 2011, during the 2-weeks prior to the onset of the melt season, the salinity at 13 m depth showed $\sim$2 g kg^{-1} fluctuations in salinity (Fig. 3.6), equivalent to a vertical displacement of the halocline of $\sim$15 cm, that we associate with the passage of internal waves. This suggests that most of the error in synoptic CTD depth estimates is due to vertical displacement of the halocline by the passage of internal waves.

Spectral analysis of the salinity time series (not shown) reveals energy peaks at diurnal and semi-diurnal tidal periods in the halocline, with a strong non-tidal peak at 48 min, and secondary peaks at 70 min and 5.7 hrs. Based on the ratios of the amplitude of the basin-scale wave ($\sim$15 cm) to the thickness of the epishelf lake ($\sim$10 m) and the depth ratio of the epishelf lake to the full depth of the fjord ($\sim$400 m), the epishelf lake falls within a regime where only linear waves are expected (Horn et al., 2001). Application of linear wave theory allows calculation of the nth mode internal seiche period for a two-layer fluid as:

$$T = \frac{2L}{n\sqrt{\frac{g'h_1h_2}{(h_1+h_2)}}}, \tag{3.4}$$

where n is the wave mode, L is the average width of the basin (m) at the depth of the halocline h_1 (13 m), overlying a layer of depth h_2 (440 m), and g' is reduced gravity:

$$g' = g\frac{\rho_2 - \rho_1}{\rho} \tag{3.5}$$

where ρ_1 is the density of the upper layer (1000 kg m^{-3}), ρ_2 the density of the lower layer (1025 kg m^{-3}), and ρ the average density of the two layers. A range of values could be chosen for L given the complex geometry of the lake, although the width of the main basin, 5.8 km, is an obvious starting point. Taking this distance as the length scale L gives a first mode internal seiche period of 129 min and a second mode period of $\sim$54 min, which is very similar to the 48 min periodicity of the strongest non-tidal salinity signal. Alternatively, using the long axis of the epishelf lake, $\sim$20 km from the grounding line to the inner edge of the MIS, results in a first mode internal seiche period up to $\sim$8 hrs, suggesting a range of internal seiche periods are plausible.

These observations are similar to measurements in Disraeli Fiord, where small 17 cm amplitude internal waves propagating along the sharp epishelf lake halocline, with periods ranging from $\sim$6 min to $\sim$6 hrs (Keys, 1977). The driving force for internal waves in epishelf lakes is almost certainly the tidal current, although other possible sources are kinetic energy from inflowing meltwater streams (both surface and subglacial), atmospheric pressure changes, and offshore baroclinic fluctuations propagating into the fjord. The relatively low energy of the background internal wave

field in Milne Fiord, suggests their role is limited to inducing a small amount of mixing across the halocline at the lake boundaries, and for our purposes, they are largely of concern for the error they impart to lake depth estimates derived from CTD profiles.

Temperature fluctuations also occurred above the halocline, confined to the freshwater layer of epishelf lake, and were indicative of long-period internal waves, perhaps excited by the spring-neap tidal processes. An in-depth analysis of these waves, however, is reserved for a separate publication because the focus here is on changes to the depth of the halocline, and how this may influence the interpretation of lake depth based on synoptic CTD measurements.

3.3.8 Spatial extent

Synoptic CTD profiles collected at distant locations over a short time period (i.e. the same colour in Fig. 3.3) show the MEL is spatially uniform in depth (the level of the halocline varies $<$20 cm between profiles $>$20 km apart) and extends throughout the fjord. For example, the depth of the N^2_{max} along a 5.8 km transect across the width of the fjord, from 6 profiles collected in a single 24 hr period in July 2012 (green lines, Fig. 3.3a), varied by only $\pm$ 5 cm, well within instrument error. While the depth of the N^2_{max} varied by only $\pm$ 10 cm along a 23 km transect extending down the length of the fjord, from near the grounding line of the Milne Glacier to a fracture in the Central Unit of the MIS, collected by helicopter on 29 June 2012 (dark blue lines, Fig. 3.3a). That the epishelf lake was present even in fractures in the MGT and MIS suggests a network of basal channels permit exchange of surface waters throughout much of the fjord. Each of the profiling locations where the epishelf lake was present mapped onto regions identified as epishelf lake in SAR imagery, providing verification of the remote sensing method used to map the area of the lake. However, remote sensing cannot determine how far under the MIS the lake extends, nor be used to determine the location of the ice dam. To address these questions, field observations are required.

Our CTD profiling indicates that the ice dam must be located somewhere in the Outer Unit of the MIS, as the epishelf lake was observed in all profiles collected through fractures in the Central Unit of the MIS, but was not present in any profile collected offshore of the seaward edge of the MIS (as expected). Ice thickness maps of the MIS (Mortimer et al., 2012; Chapter 2) indicate the only ice of the Outer Unit of the MIS thin enough to allow drainage of the epishelf lake lies along the two re-healed fractures (Fig. 3.5). Several attempts in 2012, 2013, and 2014 to profile through the re-healed fractures, to constrain the location of the ice dam and confirm the drainage pathway of the MEL, were unsuccessful. Investigation into the location of the ice dam and the drainage pathway of the MEL is ongoing.

3.3.9 Lake volume

The observed spatial uniformity of the depth of the lake (at a moment in time) provides an easy means to estimate the volume of the lake when both area and depth are known (Table 3.1). The

earliest reliable estimate of the lake volume is 1.04 km^3 in 2006, after which the volume decreased substantially, reaching a minimum of 0.54 km^3 in 2013. The decrease in volume is largely due to the decrease in thickness of the lake; the area of the lake varied by only 10% between 2006 and 2014, while the depth varied by over 50% during this period. This observation is evidence that interannual depth changes of the lake are related to changes in the thickness of the ice dam, rather than area changes. We note that the surface ice thickness decreased from a maximum of 3.19 m in 1983 (Jeffries, 1985) to a minimum of 0.65 m in July 2010, varying annually by $\sim$1 m thereafter, however, changes in surface ice thickness do not affect estimated volumes as the surface ice is in hydrostatic equilibrium.

3.3.10 Meteorological time series

The meteorological data recorded by the automated weather station in Purple Valley for the duration of the mooring deployment are shown in Figure 3.6. Average air temperature during the mooring deployment (May 2011 to July 2014) was -17.6°C, with extreme hourly temperatures of +20.2°C in July 2012 and -51.8°C in February 2013. Solar radiation varies from zero during the polar night (mid-October through February) to a summer daily maximum of $\sim$650 W m^{-2} in late June. The site receives 24 hrs of sunlight from April to September. Summer melt conditions varied substantially among years, with cumulative positive degree days of 278, 253, 92 and 110 in 2011, 2012, 2013, 2014, respectively (note that for display purposes the meteorological record is truncated to match the mooring record in Fig. 3.6, but we collected meteorological data through to the end of 2014). The melt season occurs between early-June and mid-August, although the onset and duration vary by up to 2-weeks among years.

3.3.11 Salinity time series

The most striking feature of the salinity time series (Fig. 3.6d) is the seasonal change in salinity of instruments deployed in the halocline (instruments at 13 m and 15 m in 2011-2012, and 10 m in 2012-2013; no instruments were positioned in the halocline in 2013-2014). The substantial freshening at these depths is consistent with a deepening of the halocline from mid-June to mid-August due to surface meltwater inflow to the epishelf lake. The rebound of salinities commencing in mid-August of each year suggests the halocline shoals again after meltwater inflows cease. Focusing on the instrument with the longest continual record (13 m depth), shows the instrument was initially deployed in the strong halocline (at 8 g kg^{-1} in May 2011). Salinity was relatively stable before a suddenly decrease that coincided with the commencement of the melt season. By the end of the melt season, salinity at 13 m depth had decreased to 0.3 g kg^{-1}, suggesting the instrument was then in the mixed layer of the epishelf lake (salinity at 8 m, 11 m, and 13 m overlap, indicating an unstratified water column). After the melt season ceased, salinity increased to $>$22 g kg^{-1} by January 2012, overlapping with the salinity of the lower halocline, consistent with thinning of the

epishelf lake. The sudden drop in salinity in January 2012 is a unique feature, and is examined in more detail in Section 3.3.13. Instruments spaced 2 m apart vertically showed a temporal offset in the seasonal evolution of salinity with depth (on the order of 5-weeks), which is further evidence that the halocline progressively deepened over summer, then gradually shoaled over winter. In the mixed layer, salinity increased over time, the instrument moored at 5 m depth showed an increase of 0.2 g kg^{-1} from August 2012 to July 2014, and the 7 m instrument showed an increase of 0.1 g kg^{-1} from 2013 to 2014.

3.3.12 Temperature time series

The temperature time series (Fig. 3.6e) provides a comprehensive view of the thermal evolution of the epishelf lake over the 3-year deployment period. The most readily apparent features of the time series are that the temperature of the epishelf lake and the depth of the thermocline vary substantially on seasonal and interannual timescales. The lake warms from mid-June to mid-August each year, although the magnitude varies between years, reaching a subsurface maximum of 2.5°C, 4.0°C, and 2.5°C, in 2011, 2012 and 2013, respectively. The strongest warming was observed in summer of 2012 when water temperatures between 5 m and 10 m depth were almost isothermal above 3°C. After peaking in mid-August, the temperatures of the epishelf lake gradually decreased until the following summer, although temperatures remained significantly above freezing all year despite the extreme low air temperatures in mid-winter. The strong thermocline at the base of the epishelf lake, which corresponds to the epishelf lake halocline, varies by several meters each year. The deepening of the epishelf lake commenced between 2-14 June of each year, corresponding to the when air temperatures increased above freezing, and thus the commencement of surface meltwater inflow. The maximum depth of the thermocline occurred at the end of the melt season each year. The thermocline deepened by 3.0 m, 3.3 m, and 1.0 m in summer of 2011, 2012, 2013, respectively.

After the melt season ended the lake gradually thinned each winter, reaching a minimum in early June the following year, just prior to the commencement of the subsequent melt season. On an interannual basis, the depth of the thermocline, measured on June 1st each year, shoaled by 4.1 m between 2011-2012, 1.5 m between 2012-2013, and 1 m between 2013-2014. This interannual thinning of the lake, despite increases in lake thickness of the same magnitude in summer, suggests the MIS is in a state of negative mass balance, and the ice dam is thinning. However, the rate of lake thickness change over time is not constant, as apparent by an abrupt shoaling of the thermocline that occurred in January of 2012, which is examined in more detail in Section 3.3.13.

3.3.13 January 2012 event

A sudden change in temperature and salinity at the bottom of the epishelf lake occurred on 11 January 2012 06:00 UTC (Fig. 3.7). Over a duration of 18 hrs the salinity at 13 m depth dropped from 22 to 12 g kg^{-1}, and remained below 15 g kg^{-1} for the remainder of the winter. At the same

time, the heat content of the upper 25 m of the water column was relatively steady (apart from some fluctuations during the actual event), the slow rate of heat loss was not substantially different from the long-term average over winter. During the event the upper portion of the thermocline (above 11 m depth) was displaced upwards 1.5 m, while isotherms in the lower portion of the thermocline (below 11 m depth) spread apart vertically. The event was associated with rapid vertical fluctuations of isotherms of much larger amplitude then those observed in the days prior to the event. Isotherm fluctuation associated with the event were recorded from the uppermost thermistor (at 2 m depth) down to at least 50 m depth (not shown), and possibly deeper. Profiles collected during the field campaigns months before and after the event show a marked change in the depth of the epishelf lake and the gradient of the lower halocline/thermocline (Fig. 3.7 c & d). These observations indicate that a sudden mixing event occurred at the bottom of the epishelf lake that entrained warm, relatively fresh water from the lake downward, and cool, salty water upward. The result was an abrupt, irreversible, thinning of the lake by 1.5 m and a change in the gradient of the lower halocline. The negligible change in the heat content of the upper water column implies a conservation of heat, indicating the observations show either a) an in situ vertical mixing event, presumably uniform throughout the lake, or b) the advection of a water masses with the same overall heat content, or c) some combination of the two. The latter could probably only be achieved if the advected water mass originated within the fjord where the water column properties were similar (e.g. if vertical mixing occurred in the, presumably spatially uniform, lake at some distance from the mooring site and the resulting mixed water mass, with the same overall heat content, was advected past the mooring location).

3.3.14 Long-term lake depth

The long-term record of lake depth over the past decade is shown in Fig. 3.8. Plotted is the depth of the lake measured by synoptic CTD profiling, as well as that inferred from the continuous mooring records of temperature and salinitiy between 2011 and 2014. Also plotted are the PDD-corrected lake depths, which reveal that during the period 2004 to 2011 the lake thinned at an average rate of 0.51 m a^{-1}. The PDD-corrected depths also show that the lake steadily thinned almost every year during this period, contrary to the apparent deepening in some years as indicated by the uncorrected depths. The steady rate of thinning was interrupted in 2011-2012, when the lake thinned by 4.1 m, in part due to the mixing event in January 2012. From 2012 to 2014 the lake thinned at a rate 0.34 m a^{-1}, although the latter rate is based on only 3 years of CTD profiles, too short a record to conclude the rate has changed from the period prior to 2011.

Continuous observations from 2011 to 2014 reveal that the depth of the lake fluctuated by several meters over a year. Such seasonal changes in the depth of an epishelf lake have not previously been reported, and highlights the importance of continuous records to understand the timescale of variation in a system, so as not to alias long-term trends from annual sampling programs. The

sudden decrease in the thickness of the epishelf lake in January 2012 highlights the importance of episodic events to lake dynamics.

3.4 Discussion

Our compilation of historical data along with new observations shows that the Milne Fiord epishelf lake is a longstanding feature of the northern coast of Ellesmere Island, but with large changes in its area and depth over the last three decades. The lake has thinned over the long-term, at a rate that is likely indicative of thinning of the Milne Ice Shelf. At shorter time intervals, our observations show the lake is seasonally dynamic, increasing and decreasing in depth by several meters a year. We have also shown lake is subject to abrupt mixing events that can dramatically shift the halocline over very short time periods.

3.4.1 Area expansion

The Milne Fiord epishelf lake was first observed in 1983, although it is likely that the lake existed below the Inner Unit (which was 9.7 m thick in 1981) prior to this time (Mortimer et al., 2012). Although the timing of the origin of the lake is unknown, it appears to have expanded in the decades after 1959 as the Inner Unit of the MIS transitioned to lake ice. Since 1988 changes in the area of the lake have been due to a balance between expansion processes, including mechanical breakup and melting of the ice margins, and contraction processes, primarily the advance of the terminus of the MGT. The terminus of the MGT advanced $\sim$2 km between 1988 and 2014, associated with a reduction in lake area, however, this was offset by gains due to erosion of the ice margins of the MIS and MGT. An example of expansion processes was observed in the summer of 2012. In August 2012, satellite imagery revealed that the lake ice in the northwest region of the epishelf lake partially broke up, and fragments of the MIS calved into the fjord. Summer of 2012 was very warm, air temperatures reached an hourly maximum of +20.2°C in July, and lake temperatures peaked at over 3°C, the highest recorded during the 3-year mooring deployment. This strong thermal forcing would have induced substantial surface and submarine melting, which was apparent in the 0.7 m thickness of the surface lake ice, the second thinnest recorded during this study. This event is likely indicative of the future of Milne Fiord under a warming climate, with enhanced thermal erosion weakening the ice cover, leading to further break up of the MIS and MGT, and expansion of the MEL.

3.4.2 Depth changes

Annual CTD profiling in Milne Fiord has shown that the epishelf lake thinned approximately 9 m from 2004 and 2014. The overall decrease in thickness of the lake strongly indicates the ice dam is thinning over time, roughly on the order of 0.5 m a^{-1}. Increases in depth of the lake were

significantly correlated with the number of cumulative PDDs, strongly indicating that meltwater inflow from the surrounding glacial catchment was responsible for the observed depth increase. The gradual thinning of the lake after the cessation of meltwater inflow, suggests the outflow of freshwater from the fjord was restricted by the geometry of the MIS.

The depth of the lake at any given time is is determined by the balance of the volumetric inflow and outflow rates. If drainage of the lake is continuous and hydraulically controlled under the ice shelf, rapid inflow during an intense surface melt season will generate a deeper lake than slow inflow, for the same volume of water added.

3.4.3 Observational error

Seasonal fluctuations in lake depth indicate that timing of observations is critical to prevent aliasing the long-term, interannual record of epishelf lake depth. This is especially important if epishelf lake depth is to be used as a climate indicator, as suggested by Veillette et al. (2011b). Our results have shown that in the absence of continuous records, the best long-term estimate for the lake depth is obtained from CTD profiling each year just prior to the initiation of the melt season (i.e. approximately June 1st). Observations at this time capture the annual minimum depth of the epishelf lake prior to inflow. Although the lake depth may not have reached equilibrium by June 1st, the depth measured at this time is arguably the most reliable indicator of the long-term state of the lake, and the closest indicator of the actual depth of the ice dam. Profiles collected at other times of the year must account for the variations in summer meltwater inflow and drainage hydraulics under the ice shelf.

For Milne Fiord, we have found that depths measured at other times of year can be corrected using the number of PDDs accumulated that season up to the date of profiling. We demonstrate the importance of this timing by examining the apparent increase in lake depth during the periods 2006-2007, 2009-2010, and 2013-2014. Without knowledge of the seasonal deepening of the lake, these observations could be interpreted as periodic thickening of the ice dam, suggesting a fluctuating ice shelf mass balance. However, once the number of cumulative PDDs at the timing of profiling are accounted for, the corrected lake depths reveal thinning of the lake, and by proxy the ice dam, every year between 2004 and 2011, indicating mass loss from the ice shelf occurred at a nearly constant rate during this period. This example clearly demonstrates that to establish a long-term trend, synoptic observations must be placed in the context of the temporal variation of the underlying phenomenon. Ultimately, however, the interpretation of synoptic observations is limited without continuous observations due to the possibility of episodic events, such as the mixing event recorded in January 2012.

3.4.4 January 2012 mixing event

The January 2012 event was associated with the vertical mixing of a stable water column, consisting of warm freshwater above cold seawater. The mixing event appears to have been widespread throughout the lake, as all profiles collected after the event show a consistent change in the gradient of the lower halocline and the depth of the epishelf lake. To induce such a widespread mixing would have required a substantial input of energy. We can estimate the amount of energy required to mixing the stable water column from the change in gravitational potential energy of the water column before and after the event. The closest profiles in time were collected 6 months prior to (July 2011), and 4 months after (May 2012) the event. These profiles are not completely representative of the water column at the time of the event because of changes in the density profile due to seasonal meltwater input and epishelf lake drainage under the ice shelf during the intervening months.

Instead, we estimate the change in potential energy by assuming the water column was an idealized 2-layer system, with freshwater above and seawater below, and the two layers completely mixed, resulting in a homogenous column. The change in potential energy (ΔPE) of a water column per unit area due to mixing is

$$\Delta PE = \frac{1}{2} h_1 h_2 (\rho_2 - \rho_1) g \tag{3.6}$$

where h_1 is the thickness of the upper layer involved in mixing, h_2 is the thickness of the lower layer involved in mixing, ρ_1 is the density of the upper layer (1000 kg m^{-3}), ρ_2 is the density of the lower layer (1025 kg m^{-3}), and g is gravitational acceleration (9.81 m s^{-2}). From the mooring temperature record we choose a range of values for h_1 (0.5 m and 1.5 m) and h_2 (2 m and 7 m), which results in a change in potential energy per unit area of order 10^1 to 10^3 J m^{-2}. This estimate assumes complete mixing into a homogenous water column over the height $h_1 + h_2$. The water column was not fully isothermal after the event, so the calculated change in potential energy is considered the upper limit of that required to induce the observed mixing. Assuming the mixing was uniform across the full area of the lake (64.4 km^2), then the total energy required for mixing was of the order 10^8 to 10^{10} J. What are the possible sources of energy for mixing?

Tidal motion is an obvious source of kinetic energy in Milne Fiord, and the interaction of tidally driven oscillations with bathymetry or ice keels could induce mixing. However, tidal oscillation is continuous and provides no explanation for the episodic nature of this event. In addition, the bottom pressure sensor recorded no water level anomalies prior to or during the onset of the mixing event, meaning tides are unlikely the source. By the same reasoning, any flow associated with barotropic changes in water level, such as tsunamis, are unlikely to have occurred. A sufficient magnitude earthquake could release enough energy to the water column, however there were no substantial earthquakes recorded at this time (http://earthquaketrack.com/r/ellesmere-island-nunavut-canada/recent), and an earthquake would be expected to induce some degree of seiching or mixing

over the full depth of the water column, which is not apparent in the temperature records (the temperature signal associated with this event appears to be limited to depths above ∼50 m).

Another possible source of energy to mix the upper water column in a glacial fjord, is the capsize or calving of an iceberg. In a laboratory study, Burton et al. (2012) found that most (approximately 84%) of the total energy released during an iceberg capsizing event was transferred to the water column via hydrodynamic coupling, viscous drag, and turbulence (with an additional ∼15% to kinetic energy, and ∼1% to radiated surface wave energy). The authors suggest that iceberg capsizing is a potentially important source of mixing in the stratified ocean proximal to marine ice margins. The energy release from a capsizing event (E_{cap}) of a free-floating iceberg with an idealized cuboid geometry can be estimated as

$$E_{cap} = \frac{1}{2}\rho_i g L_i H_i^3 \varepsilon (1-\varepsilon)\left(1-\frac{\rho_i}{\rho_w}\right), \tag{3.7}$$

where L_i is the length of the iceberg parallel to the axis of rotation, W_i is the width, H_i is the pre-capsize height of the iceberg, and $\varepsilon = W_i/H_i$ (Burton et al., 2012). For a large iceberg in Milne Fiord, we estimate L_i is 100 m, H_i is 150 m, W_i is 50 m, and set ρ_i to 900 kg m^{-3}, ρ_w to 1025 kg m^{-3}, resulting in an energy release of 4 x 10^{10} J. If 80% of this total energy liberated from capsize was dissipated through turbulent mixing of the water column, that would have been of sufficient magnitude to induced the mixing observed in Milne Fiord. However, the mixing event appeared to be limited to the upper 50 m of the water column, suggesting perhaps the capsize of a smaller iceberg. Even for a much smaller iceberg, where L_i is 25 m, H_i is 50 m, W_i is 25 m, the energy released is $>10^8$ J, which is still of the correct order of magnitude to induce the observed mixing throughout the lake.

Breakup and calving of the MGT and inner margin of the MIS have increased over the past decade, resulting in dozens of icebergs in Milne Fiord with large enough dimensions that their capsize could have released sufficient energy for mixing. Icebergs are typically frozen into fast-ice year-round, which may reduce the frequency of capsizing and help explain the episodic nature of this event (only one major mixing event recorded in 3 years). Iceberg capsizing and capsize might be expected to be more frequent during the summer melt season, however, preferential melting of the iceberg keels by warm water, with negligible mass from the surface in winter, suggests winter capsize is possible. Although we lack sufficient evidence to exclude other possible mechanisms for the mixing event, such as a landslide, or the propagation of an offshore anomaly into the fjord below the ice shelf, the iceberg capsizing mechanisms appears to be a plausible explanation that can account for the observations.

The abrupt depth reduction of the epishelf lake in Milne Fiord might be considered a drainage event, similar to that recorded in Disraeli Fiord in 2001, caused by the fracturing of the Ward Hunt Ice Shelf (Mueller et al., 2003). However, the observations suggest this is not the case, and a few

simple calculations provide evidence to support this argument. If, for example, we assume the 1.5 m depth change was due to a rapid drainage of epishelf lake water under the MIS, precipitated by a fracturing of the ice shelf, then the total volume change across the $\sim$64.4 km^2 lake was 9.8x10^7 m^3. For all of this water to drain out of the fjord over the observed 18 hr duration of the event, would require a volume flux of 5.4 x 10^6 m^3 hr^{-1}, requiring outflow velocities of $>$100 m s^{-1}, through the $\sim$10 m wide basal channel in the MIS. This result is clearly not realistic, and given the outflow rate is likely hydraulically controlled (see Section 3.4.6), we consider it unlikely that the January 2012 event was related to a rapid drainage event.

3.4.5 Freshwater budget

The volume and residence time of the epishelf lake are determined by the balance between inflows and outflows, and changes in area of the epishelf lake. Mass inputs to the epishelf lake come from surface runoff and basal melting of the MIS and MGT. Although the melting of floating ice around the lake margins contributes a volume of freshwater equivalent to the volume of ice melted (adjusting for density differences), and will affect the residence time of the lake, it will not alter the depth of the lake. Changes to the depth of the lake are primarily determined by the balance between inflow from the fjord catchment and outflow under the MIS.

If we assume the magnitude of deepening of the halocline is equal to the volume of water per unit area that enters the lake from surface runoff each summer, then the volume of the lake that would have been replaced each summer ranges between 13% and 35%. Thus the residence time of the lake is between 3-8 years. However, this estimate is conservative in that it assumes there is no outflow during the deepening of the halocline. If outflow occurs during summer inflow, as we would expect, then the volume entering the lake is potentially much larger, and the residence time will be reduced. As the lake thins over time it appears more likely the residence time will be further reduced.

We compare our findings with published glacier mass balance rates for the northern Canadian Arctic as an independent measure of the volume of freshwater entering Milne Fiord. Gardner et al. (2013) estimated an average glacier mass budget of -310 $\pm$ 40 kg m^{-2} a^{-1} from 2003-2009 for the northern Canadian Arctic, including Ellesmere, Axel Heiberg, and Devon Islands. The Milne Glacier catchment has a glaciated area of 1108 km^2, so the estimated annual mass budget for the Milne Glacier is -0.343 Gt a^{-1}. We can convert this into a volume of freshwater entering Milne Fiord by assuming that all mass is lost as meltwater runoff that enters Milne Fiord at the surface. It must be noted however, the Gardner et al. (2013)estimate does not overlap in time with our data, and is a net glacier mass loss, meaning it does not account for additional runoff from snow melt. Acknowledging this, the volume of freshwater input from glacier melt is equivalent to $\sim$5 m a^{-1} increase in the depth of the lake (assuming an average lake area of $\sim$65 km^2). This is roughly 50% larger than the maximum depth increase recorded by the mooring between 2011 and 2014,

suggesting there is ample meltwater entering the fjord to replenish the epishelf lake at estimated rates.

We have determined that there is sufficient surface runoff entering the fjord in summer to account for the increase in lake depth during the melt season. Once inflow ceases, however, the lake begins to thin, and continues to thin until the following summer. The rate of thinning is linked to the hydraulics of drainage through the basal channel under the MIS.

3.4.6 Outflow hydraulics

The mooring data showed that the lake thinned each year from the time the summer melt season ended, through winter, until meltwater inflow commenced again the following spring. The outflow rate was non-linear and appeared to be dependent on the relative depth difference between the lake and the ice dam, suggesting hydraulically controlled flow.

An idealized schematic of epishelf lake outflow through a basal channel in the ice shelf is shown in Figure 3.9, represented as a simple two-layer system, with freshwater overlying seawater ($\Delta\rho$ = 25 g kg^{-1}). Under steady state conditions the ice dam acts as a hydraulic control, limiting two-way transport below the ice shelf. If the depth of the seawater layer is much greater than the depth of the freshwater layer, then the situation is analogous to single layer flow through an inverted weir, but here the horizontal pressure gradient is supplied by the density difference between freshwater and seawater. If we assume a rectangular channel geometry, the volumetric outflow discharge (Q_d; m^3 s^{-1}) can be estimated using a modified form of the Kindsvater-Carter rectangular weir equation (Kindsvater and Carter, 1959):

$$Q_d = \frac{2}{3}\sqrt{2g'}C_e b h^{\frac{3}{2}} \tag{3.8}$$

where g' is reduced gravity ($g' = g(\Delta\rho/\rho)$), C_e is an empirically derived discharge coefficient, b is the effective width of the outlet channel (m), and h is the effective depth of the lake below the ice dam (m). b and h account for the effects of viscosity and wall friction and will be therefore somewhat larger than the actual physical dimensions.

Assuming vertical sidewalls, the change in volume of the epishelf lake over time (dV/dt) is:

$$\frac{dV}{dt} = A_L \frac{dh}{dt} \tag{3.9}$$

where dh/dt is the change in thickness of the lake over time, and A_L is the area of the epishelf lake. During winter, inflow is negligible, so the change in volume is equal to the volumetric outflow (i.e. $dV/dt = Q_d$). Equating Eq 3.8and Eq. 3.9, solving for dh/dt, and integrating gives:

$$h(t) = \left(\frac{1}{2}at + \frac{1}{\sqrt{h_0}}\right)^{-2} \tag{3.10}$$

where

$$a = \frac{\frac{2}{3}\sqrt{2g'}C_e b}{A_L}, \tag{3.11}$$

and h_0 is the initial depth of the lake below the ice dam at t = 0.

From Eq. 3.10 we modelled the change in depth of the epishelf lake over each winter of the three year mooring record, from approximately September to May of 2011-2012, 2012-2013, and 2013-2014. We assume changes to the draft of the ice dam occurred during the surface summer melt season (which we did not model), so the draft of the ice dam remained constant each winter. The start time ($t = 0$) for each run was chosen as the date when air temperatures fell below zero for the winter, assumed to be when meltwater inflow ceased, and the initial depth of the lake at that time ($z(t = 0)$) was estimated from the mooring temperature record. The model was run for 275 days over each of the three winters. In the model freshwater drains under the ice dam at a rate proportional to h, until the lake depth $z(t)$ shoals to the level of the ice dam z_i (i.e. when $z(t) - z_i = h = 0$). The mooring records show the lake depth was still shoaling when meltwater input commenced the following spring, so we could not directly estimate z_i, nor could we directly calculate the initial depth of the lake below the ice dam (h_0). Instead, we estimated h_0 as the sum of the difference between the initial lake depth and the depth when t = 240 elapsed days (the maximum duration of the shortest mooring record), plus some unknown offset c_h (i.e. $h_0 = z(t = 0) - z(t = 240days) + c_h$). We run the model to find values for parameters c_h and $C_e b$ that gave the best fit to the observed depth changes each year, keeping the parameters constant for all years. We found the best fit was achieved for all years when c_h = 1.6 m and $C_e b$ = 4.5 m.

Modelled and observed changes to the depth of the lake relative to the ice dam are shown in Figure 3.10. Despite the initial depth of the lake below the ice dam varying by over a factor of two among the different years (from 3.3 m in 2013-2014 to 7.5 m in 2011-2012), the simple drainage model simulated the observed pattern of changes in the depth of the lake each winter well. The model could not account for the abrupt thinning of the lake in January 2012 (elapsed day 140 for 2011-2012) due to the mixing event, so observed and modelled values differ accordingly after this date. Overall, however, the results indicated outflow drainage from the epishelf lake through the basal channel could generally be well simulated by weir outflow hydraulics.

To assess the model we need to determine if the selected values for the parameters are physically realistic. If c_h is 1.6 m then the actual draft of the ice dam z_i varied between 9.4 m and 7.5 m from 2011 to 2014. This is consistent with field measurements of 8 to 11 m thick ice along the re-healed fracture in 2015. Next, for typical weirs C_e varies between 0.55 and 0.8 (ISO, 1980). If we assume this range for C_e is broadly appropriate for the MEL system, then the width of the channel b is between 5.6 and 8.2 m. This value is comparable to the minimum width of the surface expression of the re-healed fracture at its narrowest point (2 – 8 m) from field observations. We conclude that the values chosen for the parameters are physically realistic and appropriate for this system, although

further work is required to validate these parameters.

The model does have some limitations. It does not account for the possibility, and likelihood, of changes in the depth of the ice dam during winter, which could be driven by submarine melting due to outflow of warm epishelf lake water, or alternatively, basal accretion due to freezing of brackish water. These processes are dependent on the actual properties of water in the channel, and the exchange of heat between the outflowing water and the ice, which are dependent on mixing and the character of the boundary layer within the channel, factors which are unknown. Investigation of these processes is ongoing, but beyond the scope of this study. It is also questionable whether the application of a standard weir equation derived for a thin plate weir is appropriate for the epishelf lake system, particularly given the length of the outflow channel (on the order of 20 km). However, the constriction along the channel that is the hydraulic control point may actually be several orders of magnitude shorter (on the order of a few meters). As well, the values of b and h will account for some of the differences between this system and a standard weir, particularly the increased friction likely along the long channel. Further consideration of frictional exchange flow through a long channel is ongoing, and we consider the model presented here as a first step in understanding the hydraulics of the outflow. Acknowledging the model's limitations we attempted to minimize the possibility of over-tuning the model by using the same values for the unknown parameters in all three years. The only variable that changed between years was the initial depth of the lake below the ice dam, and this was determined from mooring observations using a standardized method that was consistent for all years. In summary, despite its simplicity, the model, using apparently physically realistic parameters, simulates the observed depth changes well, indicating drainage of the epishelf lake is hydraulically controlled by the geometry of the outflow channel under the ice shelf.

3.4.7 Implications for MIS

The epishelf lake depth has been considered a proxy for the minimum draft of the MIS. We note that in Milne Fiord interannual depth changes are likely only related to the depth of the ice dam along the outflow channel, not necessarily the overall thinning of the MIS. It is apparent that the ice dam is thinning over time and this is likely due to a combination of surface ablation and basal melting. Mortimer et al. (2012) found a change in thickness along a re-profiled transect that crossed the region of the suspected ice dam of the MIS of 2.63 $\pm$ 2.47 m, or 0.10 $\pm$ 0.09 m a^{-1} between 1981 and 2008/2009. Over roughly the same period (May 1983 to May 2009) the epishelf lake shoaled by 2.8 m, at an average rate of 0.11 m a^{-1}, indicating that changes in epishelf lake depth are valid proxies for changes of ice dam thickness. Extending the time series using our observations suggests the ice dam has thinned a further 5.4 m between 2009 and 2014. This is an average rate of 1.08 m a^{-1}, an order of magnitude faster than the period from 1983 to 2009. However, we know that 4.1 m, or 75%, of the thinning over this period occurred between 2011 and 2012, with at least 1.5 m of thinning, or 27%, related to the mixing event in January 2012. This observation suggests

that 2011-2012 was an anomalous year. The summer of 2011 did record the highest cumulative PDDs on record at Milne Fiord, indicating that the strong melt season may have played a role in the changing dynamics of the ice shelf-epishelf lake system that year.

Observations from July 2014 indicate the ice dam is approximately 8-9 m thick. If the average rate of thinning observed between 2004 and 2014 persists, the MEL will cease to exist as a perennial lake by 2034. However, recent observation of increase fracturing of the Central Unit of the MIS indicate that a sudden fracturing of the MIS could result in the abrupt drainage of the MEL at any time. In addition, enhanced iceberg calving and capsize could result in further mixing of the halocline, quickly eroding the base of the epishelf lake.

3.5 Summary

The MEL has existed since at least 1983, and possibly as early as the 1950's. The lake has grown in extent primarily through melting and breakup of the MIS, likely due in part to submarine melting by the heat retained in the epishelf lake over winter by its salinity stratification. The recent areal expansion has been balanced by losses due to the advance of the terminus of the MGT. Based on estimates of freshwater residence time in the lake, it appears there is sufficient volume of runoff from the fjord catchment to renew the entire volume of the lake at least every 3 years, yet the volume of the lake has decreased since 2004, owing largely to the decrease in depth of the lake.

The summer inflow of meltwater leads to a substantial seasonal increase in depth of the epishelf lake, which has not previously been reported. We found that the magnitude of deepening is directly correlated with the cumulative number of PDDs, a proxy for the volume of surface meltwater inflow. Outflow of the epishelf lake likely follows a basal channel along a re-healed fracture in the MIS. Observations along the hypothesized drainage pathway of the epishelf lake are needed to improve understanding of the hydraulics of the system, and constrain the location of the ice dam.

The seasonality of the epishelf lake suggests that synoptic annual profiles could alias the long-term depth record of the epishelf lake, and thus bias inferred changes in the thickness of the MIS dam. Continuous time series observations are required to place the synoptic profiles in context, however if only annual profiling is feasible in the future we suggest observations collected just prior to the beginning of the melt season (i.e. around June 1st for Milne Fiord) provide the most reliable indicator of steady state epishelf lake depth and ice shelf thickness. The depth of the epishelf lake does appear to have been a reliable indicator of the long-term mass balance of the MIS in the past, however the rapid changes observed in 2011/2012 indicate continual monitoring is required to understand the mechanisms influencing lake depth.

Drainage of an epishelf lake below an ice shelf is hydraulically controlled, dependent on the density between lake water and seawater offshore, the depth of the lake below the draft of the ice, which is determined by the rate and volume of inflow and the mass balance of the ice shelf, and the geometry of the outflow channel. The magnitude of epishelf lake depth variability, and therefore its

utility as an indicator of ice shelf mass balance, will be dependent on the particular epishelf lake-ice shelf system, and will likely change over time, necessitating continual and repeat observations to understand the evolving hydraulics of the system.

The existence of epishelf lakes is highly sensitive to the interactions of the atmosphere, cryosphere and hydrosphere. The warming climate of the Arctic has resulted in an increase freshwater flux to coastal fjords, with the potential to increase the volume of epishelf lakes. However, an overall thinning of the lake has been driven by mass loss of the MIS. At current rates of thinning the Milne Fiord epishelf lake, the last known epishelf lake in the Arctic, will be lost by 2034, however continued breakup of the Milne Ice Shelf suggests a catastrophic drainage could occur at any time.

3.6 Tables

Table 3.1 Milne Fiord epishelf lake depth, area, volume and related observations.

Date(s)	CTD Profile Location	No. of CTD Profiles	Depth mean (range) (m)	Area (km^2)	Volume (km^3)	PDDs to Date (yr total) (°C days)	Image Source for Area Est.	Acquisition Date (yyymmdd)
1959/08/17	-	-	-	13.5	-	-	Aerial photo	19590817
1963/08/29	-	-	-	13.5	-	-	Corona	19630829
1983/05/25	PV	1	17.5[a]	-	-	0 (158)[*]	-	-
1988/08/08	-	-	-	67.3	-	-	SPOT-1	19880808
							SPOT-1	19880808
1992/01/29	-	-	-	60.6	-	-	ERS-1	19920129
							ERS-1	19920316
1998/01/13	-	-	-	61.0	-	-	Radarsat-1	19980113
2003/01/11	-	-	-	59.3	-	-	Radarsat-1	20030111
2004/08/06	NB	1	18.3[b]	-	-	98 (132)[*]	-	-
2006/06/03	NB	1	16.0[b]	65.0	1.04	4 (153)[*]	Radarsat-1	20060114
2007/07/13	NB	1	16.5[b]	-	-	78 (215)[*]	-	-
2009/05/29 - 05/30	PV	18	14.7 (14.5-14.9)	65.2	0.96	0 (274)	Radarsat-2	20090104
2009/07/04	NB	1	14.6	-	-	34 (274)	-	-
2010/07/09	NB	1	15.3	-	-	100 (185)	-	-
2011/05/10	MM	1	13.6	67.6	0.92	0 (278)	Radarsat-2	20110103
							Radarsat-2	20110228
2011/07/05	NB	1	14.4	-	-	94 (278)	-	-
2012/05/05 - 05/14	MM	3	9.5 (9.4-9.6)	64.4	0.61	0 (253)	Radarsat-2	20120203
							Radarsat-2	20120417
2012/06/28 - 07/09	MM, ML	23	10.6 (10.2-11.5)	-	-	50 (253)	-	-
2013/05/11 - 05/18	MM, ML	11	8.0 (7.8-8.1)	67.0	0.54	0 (92)	Radarsat-2	20130427
							Radarsat-2	20130427
2013/07/04 - 07/22	MM, ML	46	8.1 (7.8-8.5)	-	-	10 (92)	-	-
2014/07/12 - 07/24	MM, ML	13	9.3 (9.1-9.4)	71.2	0.66	39 (110)	Radarsat-2	20150327
							Radarsat-2	20150327

PV - Purple Valley Bay

NB - Neige Bay

MM - Milne Fiord mooring

ML - multiple locations inside and outside Milne Fiord

[a]Jeffries, 1985

[b]Veillette et al., 2008

[*]PDDs calculated from air temperatures interpolated from the Eureka weather station where $T_{Milne} = 0.47 * T_{Eureka} + 0.47$ (RMSE = 1.98 °C)

3.7 Figures

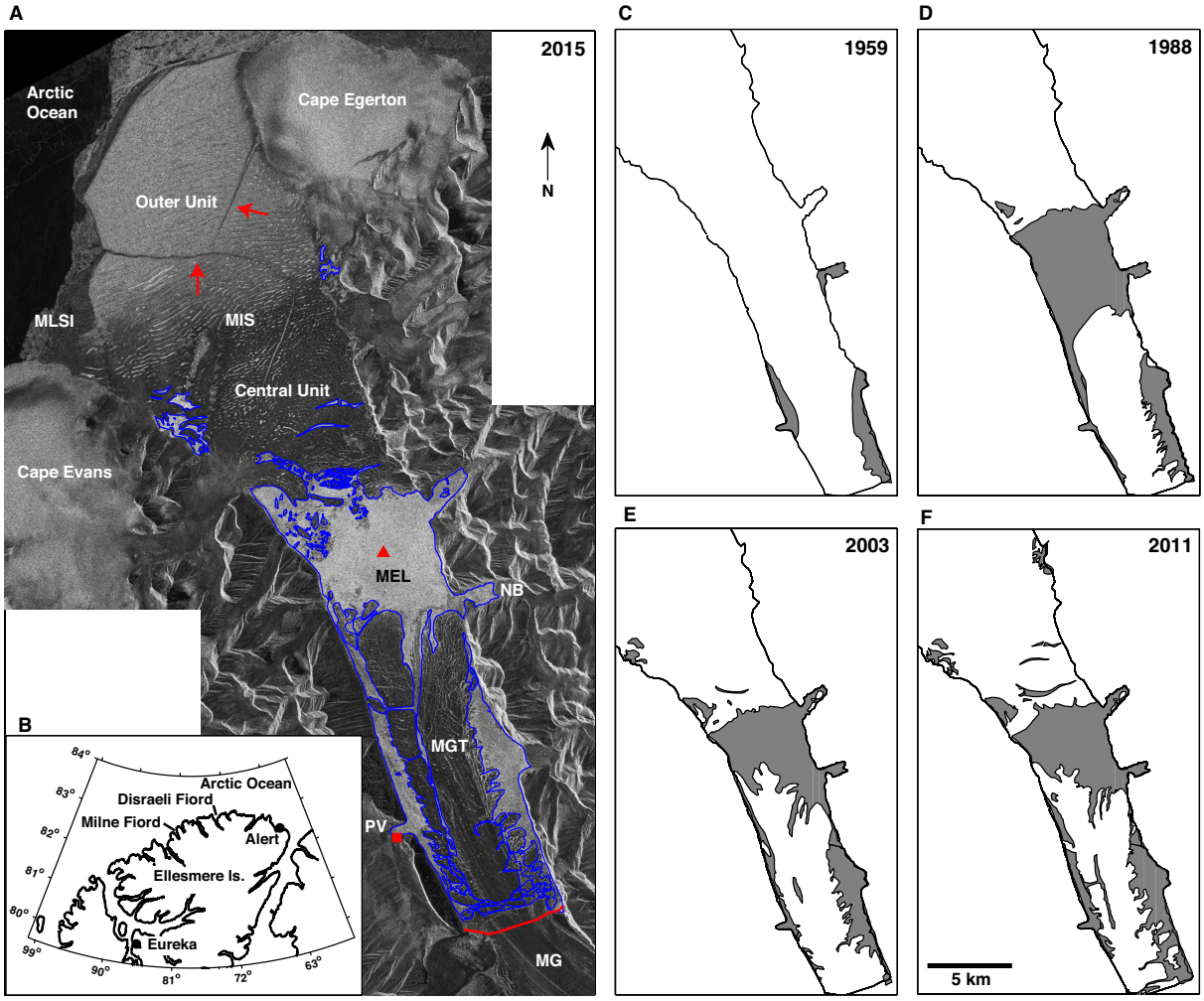

Figure 3.1 Map of Milne Fiord study area. A) RADARSat-2 image of Milne Fiord showing the extent of the Milne Fiord epishelf lake (MEL) in 2015, corresponding to the region of high backscatter (light gray) outlined in blue. The Central and Outer Units of the Milne Ice Shelf (MIS), as well as two re-healed fractures (red arrows), are indicated, as well as the Milne Glacier (MG), grounding line (red line), Milne Glacier tongue (MGT), multiyear landfast sea ice (MLSI), the met station (red square), mooring (red triangle), and two small inlets unoffically named Purple Valley Bay (PV) and Neige Bay (NB). B) Regional map of Ellesmere Island, Canada. The sequence of four panels on right show the increase in area of the MEL (grey) estimated from aerial and satellite imagery from C) 1959, D) 1988, E) 2003, and F) 2011, based on data from Mueller et al. (2016). The coastline of Milne Fiord is outlined in black. White areas inside the coastline are glacier or ice shelf.

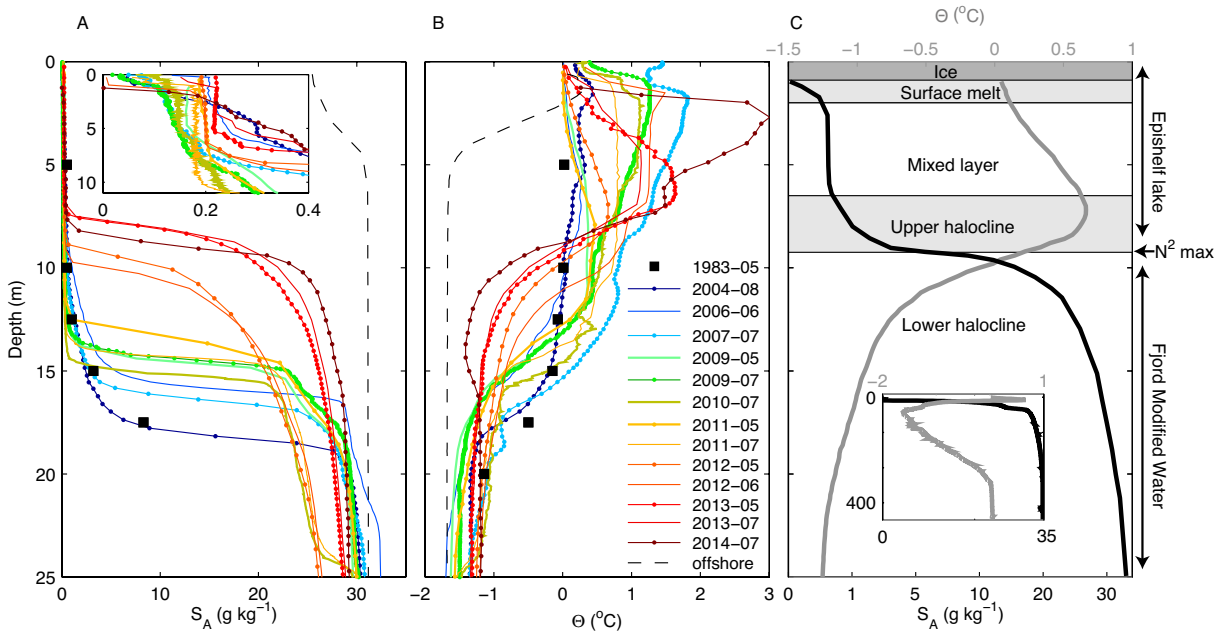

Figure 3.2 Changes in A) salinity and B) temperature properties of the upper 25 m of Milne Fiord from all field campaigns from 1983 to 2014. A single representative profile collected at the mooring site from each field campaign is shown when multiple profiles were collected. Inset in A) shown a zoom in of epishelf lake salinities. Dashed line in A) and B) indicates a representative profile collected offshore of the MIS. C) Idealized salinity (black line) and temperature (grey line) profiles showing the layers of the upper water column. Note the non-linear salinity scale. The epishelf lake is defined as extending from the surface to the buoyancy frequency maximum (N^2 max). The inset shows the full water column properties of the fjord to 440 m depth.

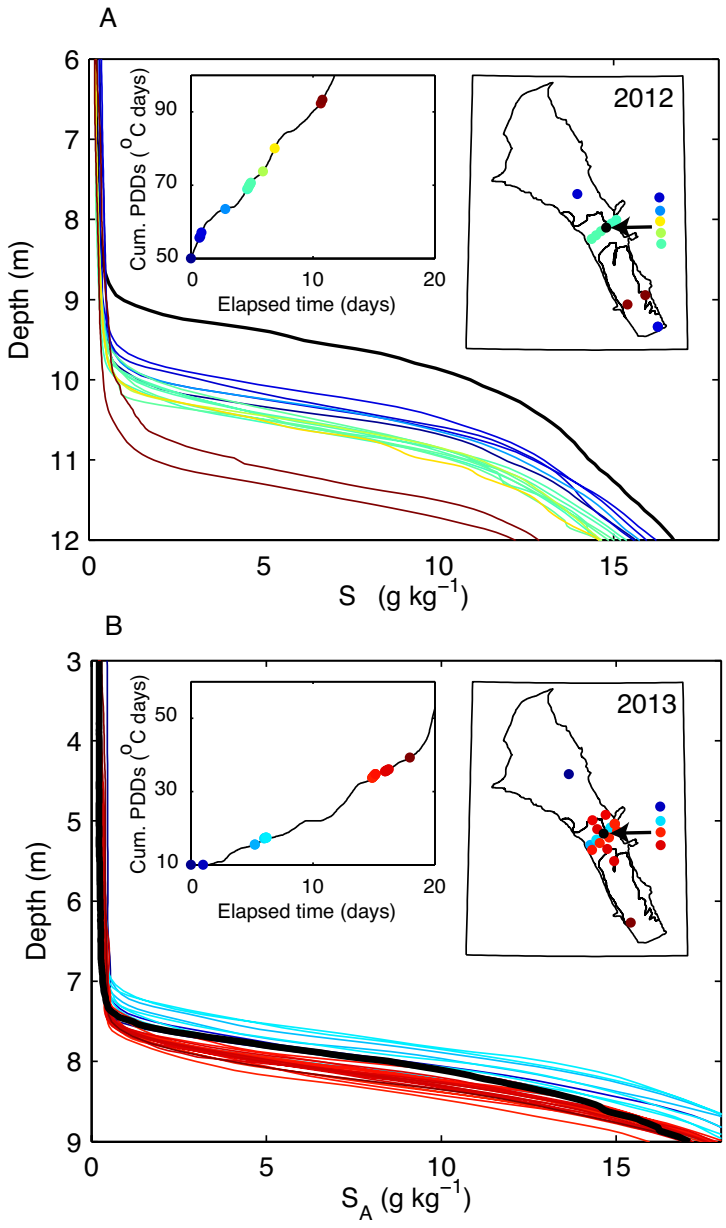

Figure 3.3 Salinity profiles showing seasonal changes in depth of the MEL halocline in a) 2012 and b) 2013. Profiles are coloured by time over the duration of each summer field campaign (10-days in June/July 2012 and 18-days in July 2013). A single profile collected in May of each year, prior to the onset of the melt season, is shown (black line). In each panel the left inset shows the PDD accumulated during each summer field campaign (a proxy for the volume of surface meltwater inflow), with the timing of profiles indicated (coloured circles). Note the different y-axes range between a) and b), although the incremental scales are consistent. The right inset shows the profiling locations on a map of Milne Fiord (the MEL, MIS, and MGT are outlined). Multiple profiles were collected at the mooring site (black circle) during each campaign.

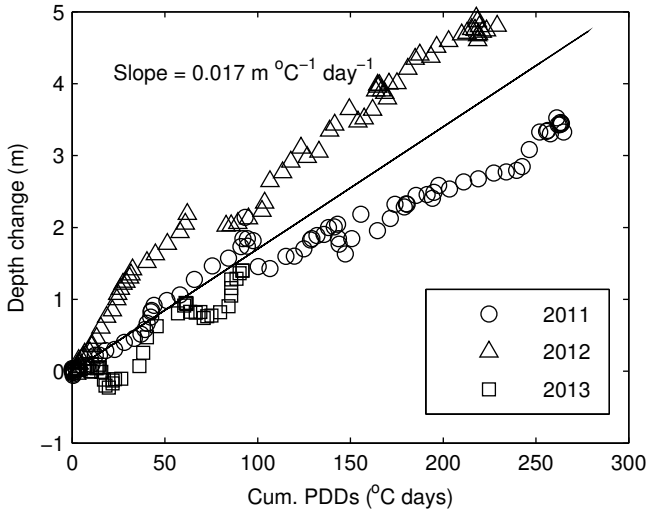

Figure 3.4 Correlation between the cumulative number of PDDs and the change in depth of the epishelf lake. Depth is estimated from the isotherm proxy during the melt season in 2011, 2012, and 2013.

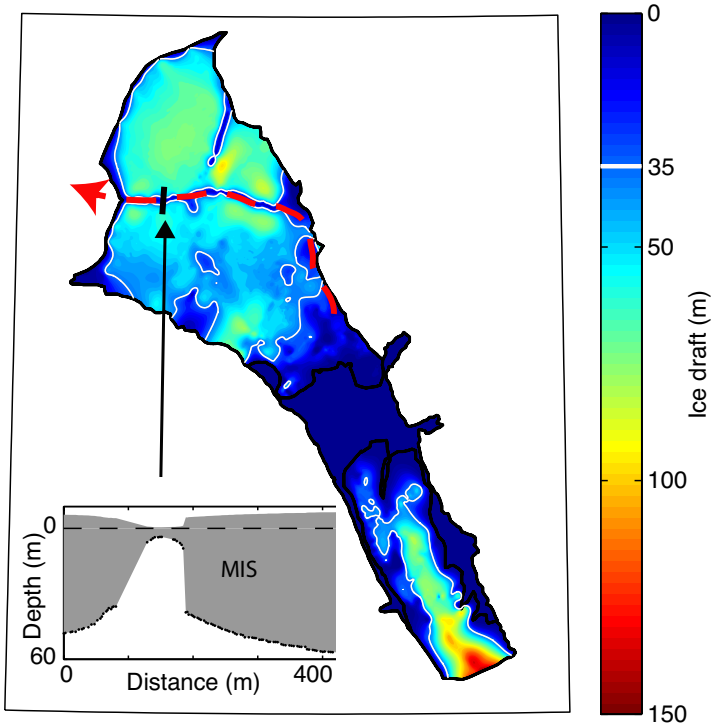

Figure 3.5 Map of ice thickness in Milne Fiord indicating the likely drainage pathway of the MEL along a re-healed fracture in the MIS. The 35 m ice thickness contour is shown to highlight the outflow restriction the MIS imposes across the mouth of the fjord. The inset shows measured ice thickness along a 400 m ice-penetrating radar transect across the re-healed fracture from July 2013.

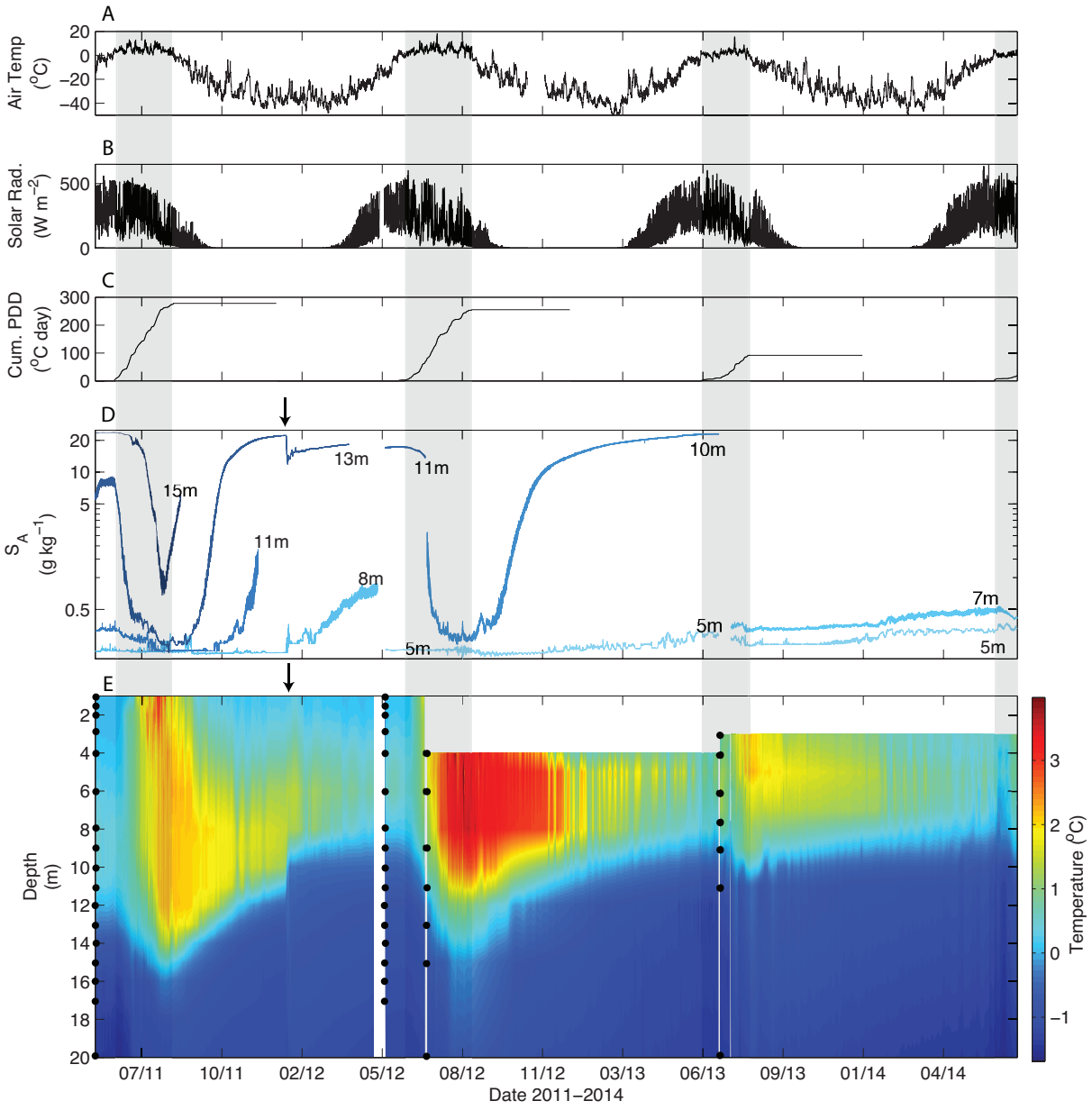

Figure 3.6 Meteorological conditions and epishelf lake properties from May 2011 to July 2014 in Milne Fiord. A) Air temperature. B) Shortwave solar radiation. C) Cumulative positive degree days. D) Absolute salinity from instruments moored at depths between 5 m and 15 m. Note the logarithmic scale. E) Temperature time series from thermistors moored between 1 m and 20 m depth. Black circles indicate thermistor depths at each mooring deployment and white areas in indicate data gaps. Grey regions outline the start and end of the surface melt season each year. Arrows in D) and E) indicate the timing of the mixing event shown in Fig. 3.7.

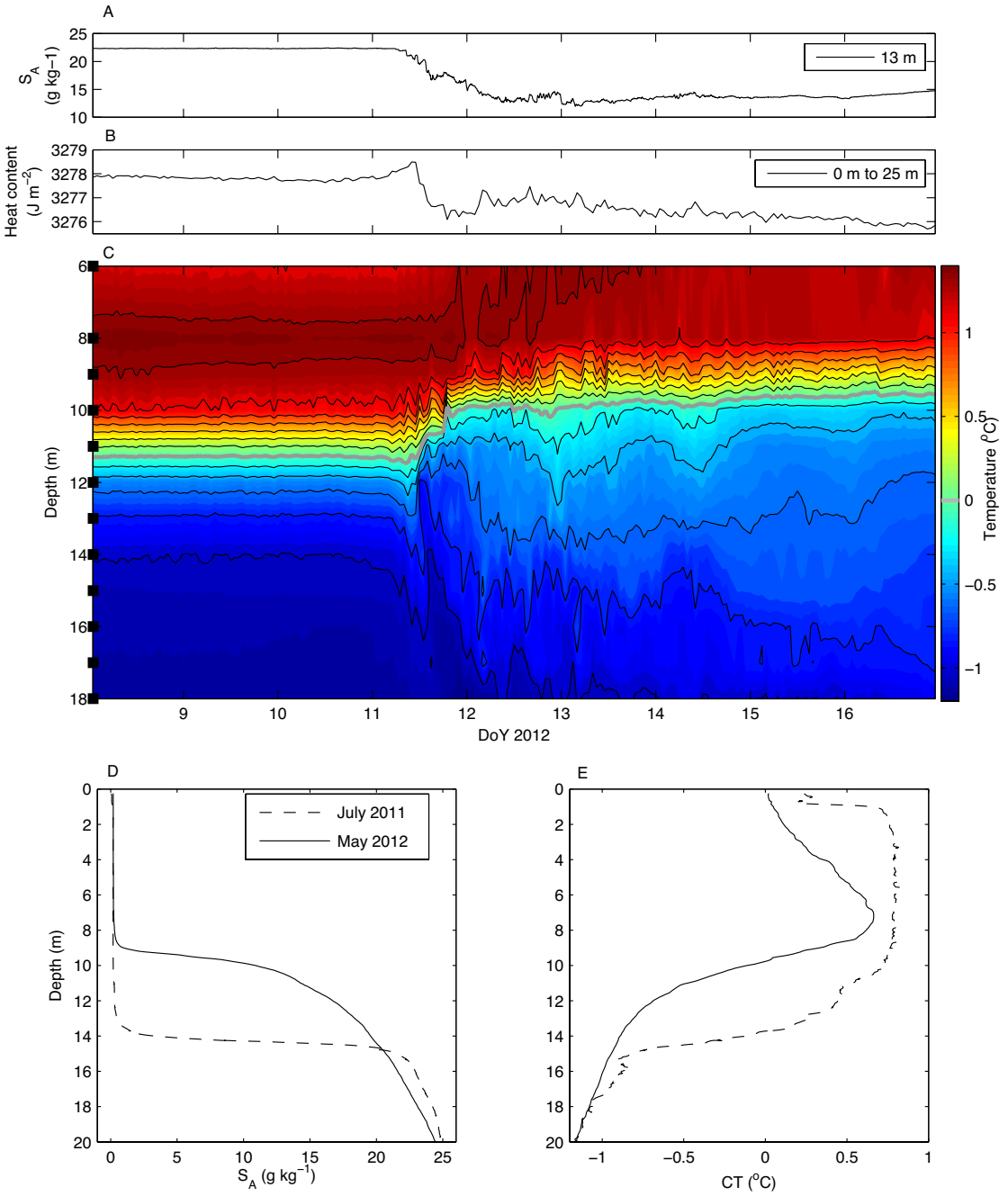

Figure 3.7 January 2012 MEL halocline mixing event. time series of A) salinity at 13 m depth, and B) heat content between 0 m and 25 m, C) temperature between 6 m and 18 m depth, and profiles of D) salinity and E) temperature from field campaigns 6 months before (July 2011) and 4 months after (May 2012) the drainage event. In C) the isotherm increment is 0.2°C and the 0°C isotherm (grey) is highlighted as a proxy for the bottom of the epishelf lake. Black squares on y-axis indicate depth of thermistors.

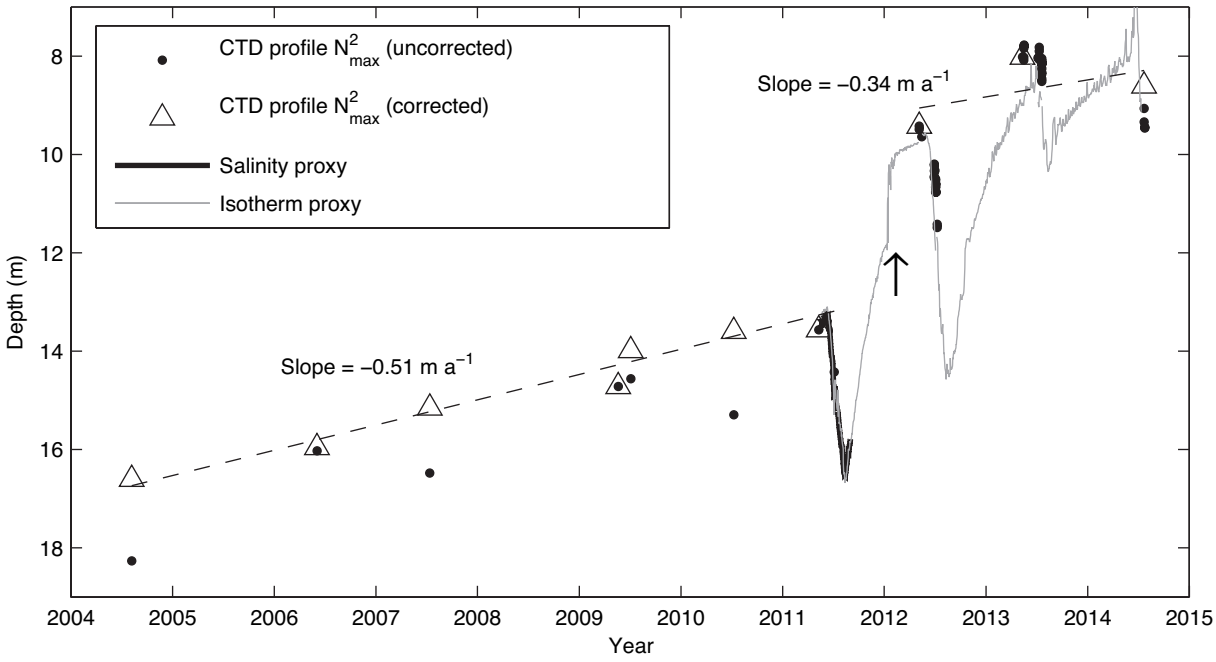

Figure 3.8 Interannual and seasonal changes in the depth of the MEL from 2004 to 2014. Plotted are the uncorrected lakes depths from CTD profiles, and depths corrected for cumulated PDDs (the corrected depth is shown only for the first profile from each field campaign after the continuous mooring records commenced in 2011), as well as depth determined from moored salinity and temperature records from May 2011 to July 2015. The arrow indicates the mixing event in January 2012. Average thinning rates are shown for the periods before and after the mixing event.

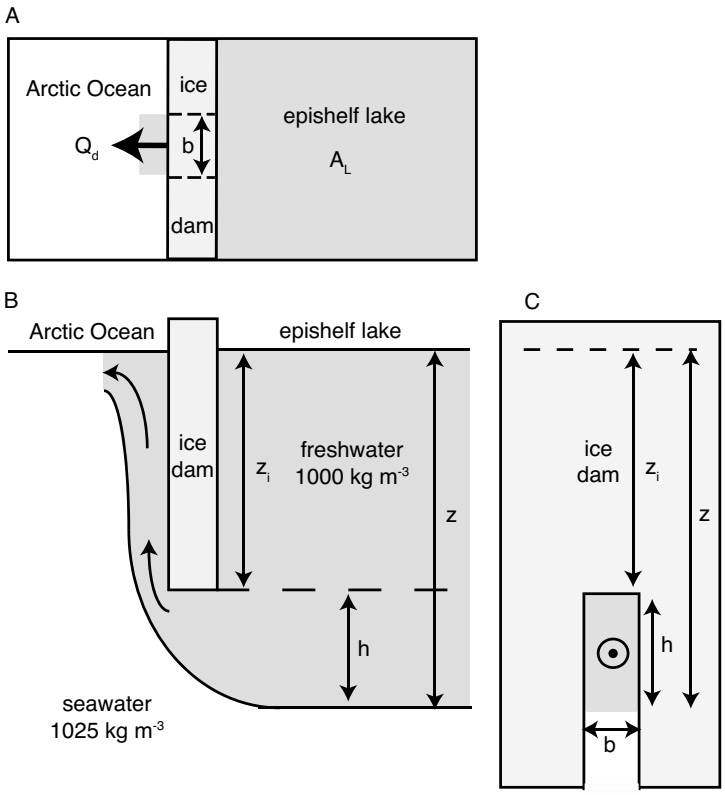

Figure 3.9 Schematic representation of epishelf lake outflow through a basal channel in the ice shelf dam in A) plan, B) elevation, and C) cross-sectional views. The volumetric discharge is modelled using a modified form of the rectangular weir equation.

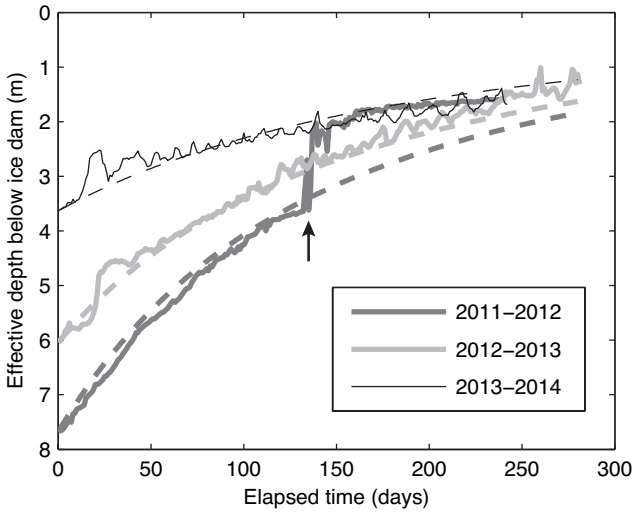

Figure 3.10 Change in the effective depth (h) of the epishelf lake below the ice dam over time during the winter of 2011-2012, 2012-2013, and 2013-2014. Elapsed time is measured from the end of the surface melt season each year. Observed depths (solid lines) are based on the isotherm proxy from the mooring record, while modelled depths (dashed lines) are based on a weir equation. Arrow indicates the mixing event that occurred in January 2012. See Section 3.4.6 for details on methodology.

Chapter 4

Depth-dependent submarine melt rates of a glacier tongue and ice shelf in a High Arctic fjord

4.1 Introduction

The presence of floating glacier tongues and ice shelves at the coast slows the rate of discharge of grounded ice into the ocean. Changes in the thickness or extent of the floating ice buttresses may, if sustained, alter the rate of ice discharge to the ocean and thereby alter the rate of change of sea level. The mass balance of ice shelves is determined by supply from land, calving of icebergs from the ice front, and melting and accumulation at their top and bottom surfaces. Ice shelves are particularly sensitive to change because they are in contact with both the atmosphere and the ocean, and therefore vulnerable to changes in the temperature or circulation pattern of either. Melting at the base of the ice shelf driven by seawater above its in situ freezing temperature is responsible for 80% of total mass loss from the Petermann Gletscher tongue in Greenland (Rignot and Steffen, 2008), and accounts for three quarters of the mass loss via ablation from Antarctic ice shelves (Rignot et al., 2013). These high fractions highlight the importance of ice-ocean interactions to ice-shelf mass balance. The transformation of seawater via ice interaction within the under-ice shelf cavities also affects the ocean, via its impact on ocean stratification and circulation. Understanding basal melt is of interest to oceanographers as well as glaciologists.

Ice shelves and glacier tongues were, until recently, extensive along the northern coast of Ellesmere Island in the Canadian High Arctic. In this region a glacier tongue, which is the floating extension of an outlet glacier at the head of a fjord, needs to be distinguished from an ice shelf, which is a thick platform of ice formed in situ at the mouth of a fjord. Ice shelves here develop via accretion of sea ice on the underside and accumulation on the top side, with additional mass acquired

from tributary glaciers and low-elevation ice caps (Jeffries, 2002). Ice shelves along this coast do not play a large role in directly buttressing grounded ice, however their presence dramatically alters the oceanographic properties of the fjords where they exist (Chapter 2 and 3). The presence of ice shelves at the mouth of fjords can result in perennial freshwater surface layers within the fjord, known as epishelf lakes. The year-round ice cover and stratification associated with the epishelf lake alters surface heat fluxes and eliminates wind mixing, with implications for the properties, and thus melt potential, of the upper water column. The presence of ice shelves at the fjord mouths could also trap icebergs with implications for surface heat fluxes and freshwater content within the fjord. The thinning or loss of ice shelves can impact the mass balance of marine terminating glaciers through changes in ocean forcing.

The recent widespread collapse of ice shelves and glacier tongues on Ellesmere Island has been attributed, in part, to atmospheric warming (Vincent et al., 2001; Mueller et al., 2003; Copland et al., 2007; Mueller et al., 2008; White et al., 2015a). In the Canadian High Arctic atmospheric warming has been twice the global average (IPCC, 2013). Atmospheric warming in this region has resulted in a sharp increase in the rate of surface mass loss from glaciers and ice caps of the Queen Elizabeth Islands (QEI; including Ellesmere, Devon, and Axel Heiberg Islands); values averaged -7 $\pm$ 18 Gt a^{-1} between 2004 and 2006, and -61 $\pm$ 18 Gt a -1 between 2007 and 2009 (Gardner et al., 2011; Gardner et al., 2013). In addition, a widespread acceleration of tidewater glaciers in this region, and increased discharge from a few individual glaciers — Trinity and Wykeham Glaciers accounted for 60% of all dynamic discharge in the QEI during 2011-2014 — and evidence of dynamically induced thinning (Van Wychen et al., 2016) has increased the need to understand the causes. Missing in studies to date in this region have been observations of ocean properties near the termini of tidewater glaciers, estimates of basal melting, and how changes in ocean forcing may influence glacier mass balance.

Milne Fiord on northern Ellesmere Island is a notable exception; ocean properties here have been monitored since 2011. Milne Fiord is also of interest due to its unique geophysical features. The Milne Glacier (MG) terminates at the head of the fjord in the $\sim$16 km long Milne Glacier tongue (MGT), while the separate Milne Ice Shelf (MIS) spans the width of the fjord at its mouth. The presence of the MIS strongly alters the water structure in the fjord because it forms a dam that traps seasonal runoff from land to form a highly stratified upper water column, wherein seawater is capped by a perennial freshwater layer up to 18 m thick; this feature is known as the Milne Fiord epishelf lake (MEL). The vertical distribution of heat in the fjord is likewise affected by the ice shelf; in addition to a temperature maximum below 200 m depth associated with the Atlantic layer of the Arctic Ocean, a near-surface temperature maximum exists at $\sim$10 m depth that is associated with the epishelf lake (Chapter 2). Analytical and numerical modelling studies suggests melt rate has a linear dependence on ocean temperature (Jenkins, 2011; Sciascia et al., 2013) and therefore the thermal stratification of the water column very likely influences the vertical distribution of submarine melt

in Milne Fiord. This study is, to our knowledge, the first to directly estimate basal melt rate and its spatial distribution for an ice shelf or a tidewater glacier in the Canadian Arctic.

Our goal is to estimate submarine melt rates of the MGT and MIS, and understand how melt rates vary with location and time. We use independent oceanographic and glaciological methods to estimate melt rates for the MGT. We then apply the oceanographic method to map the spatial distribution of melt rate across the MGT and MIS.

We first locate the grounding zone of the Milne Glacier from measurements of ice thickness and elevation using the assumption of hydrostatic equilibrium. We then calculate the annual area-averaged submarine melt rate for the floating portion of the MGT from 2011 to 2015 using the law of mass conservation — ice discharge across the grounding line minus terminus advance equals the total of ice loss at the top and bottom surfaces. Next we calculate submarine melt rates each year along the length of the MGT from the divergence of ice flux — from surface ice velocity determined via speckle tracking of satellite imagery — and from a digital elevation model of ice thickness produced from field and remote sensing data. Independently we estimate submarine melt rates along the length of the MGT, over the same period, using measured vertical profiles of ocean temperature, salinity, and current speed. The method is based on the application of a two-equation ice-ocean thermodynamic melt model. We then apply the ice-ocean thermodynamic model to the entire fjord, including the MIS, to investigate spatial and interannual variability of submarine melt. Finally, we discuss the role of submarine melting in recent changes observed in Milne Fiord, and the implications for the future stability of the MIS, MGT, and the dynamics of the Milne Glacier.

4.2 Methods

4.2.1 Site description

Milne Fiord (82°35'N; 80°35'W) lies at the northwest coast of Ellesmere Island on the Arctic Ocean (Fig. 4.1). Milne Fiord is perennially ice-covered, the majority of the fjord covered by the relatively thick ice of the MGT and the MIS, with the thin ($<$1 m thick) freshwater ice of the MEL filling the region between. The Milne Glacier (MG), a 4-5 km wide, 55 km long outlet glacier that drains $\sim$4% by area of the northern Ellesmere Island icefields, flows into the head of Milne Fiord. Van Wychen et al. (2016) estimated the mean ice discharge of the Milne Glacier to be 0.06 ± 0.02 Gt a^{-1} between 2011 and 2015. The MGT varies from approximately 150 m thick near the grounding line to $<$10 m thick at the terminus (Chapter 2). The terminus of the Milne Glacier advanced $>$5 km between 1950 and 2009 (Mortimer, 2011), and it has been identified as a possible surge-type glacier (Jeffries, 1984; Copland et al., 2003).

At the mouth of the fjord, spanning 18 km between Cape Egerton and Cape Evans, and distinct from the MGT, is the MIS, formed through a combination of sea ice accretion, snow accumulation and input from surrounding tributary glaciers and low-lying coastal ice caps (Jeffries, 1986a). The

MIS has an average thickness of 50 m and a maximum thickness of 94 m (Chapter 2). Based on surface morphology and ice characteristics the MIS has been divided into two regions (Jeffries, 1986a), an Outer Unit consisting of uniformly thick ice bisected by two re-healed fractures, and a Central Unit consisting of variable, but generally thinner, ice. By comparing radar measurements of ice thickness from 1981 and and 2009, Mortimer et al. (2012) estimated the ice shelf thinned on average by 8.1±2.8 m over this period, an average rate of 0.26 ± 0.09 m w.e. a^{-1}, although they noted substantial spatial variability. By assuming surface mass balance was equivalent to that measured on the Ward Hunt Ice Shelf, 100 km east of Milne Fiord, over approximately the same period, the authors indirectly inferred that submarine melting may have accounted for ∼73% of the overall thickness change of the MIS, suggesting ocean melting was an important factor in ice shelf mass balance.

Water properties and bathymetry in the fjord have been discussed in detail in Chapter 2 and 3, so are only described here briefly. The near-freshwater MEL lies above a layer of seawater modified by the presence of the MIS to a depth between 35 - 50 m. Below this level, to the approximate depth of the Milne Glacier grounding line, water in the fjord shares similar characteristics to that offshore in the Arctic Ocean, consisting of cool, relatively fresh Polar Water near the freezing point, above warm, saline, modified Atlantic water to the bottom of the fjord at 436 m depth. A ∼260 m deep bathymetric sill lies under the MIS (Chapter 2), however it is substantially deeper than the thickest ice in the fjord, and is not expected to influence submarine melt rates. Limited bathymetric data in the fjord indicate the MIS maybe partially grounded on an seabed ridge near the confluence of the re-healed fractures (Chapter 2) and that the sea bed slopes upward below the MGT toward the head of the fjord.

4.2.2 Bulk mass balance of MGT

We calculate a bulk annual area-averaged annual basal mass balance, a_b (m a^{-1}; positive for melting) under steady state conditions for the MGT from conservation of mass as:

$$a_b = \frac{Q_{gf} - Q_{cf}}{A_{MGT}} - a_{sf}, \tag{4.1}$$

where Q_{gf} is the ice volume flow across the grounding line, Q_{cf} is the change in ice volume over time (m^3 a^{-1}) at the terminus (positive for calving, negative for terminus advance), A_{MGT} is the surface area of the MGT (66 km^2), and a_{sf} (m a^{-1}) is the area-averaged annual surface mass balance (positive for melting).

4.2.3 Ice thickness, motion and terminus position

The digital elevation model (DEM) of ice surface and bed elevation for Milne Fiord produced in Chapter 2 is used to constrain ice thicknesses for melt calculation. Q_{cf} is estimated from changes in

terminus position of the MGT, assuming no change in ice thickness over time. Terminus positions were digitized from Radarsat-2 imagery acquired each winter from 2011 to 2015. Q_{gf} is estimated as the ice flow through a cross section at the grounding line (i.e. a flux gate) from ice surface velocities and ice thickness. Ice surface velocities were calculated by Van Wychen et al. (2016) using a custom speckle-tracking algorithm applied to Radarsat-2 fine beam (8 x 8 m resolution) and ultrafine beam (3 x 3 m resolution) image pairs collected in early spring (November-April) . We assume displacement over the period of image pair acquisition was representative of the entire year, and that there is no vertical velocity shear. Error in velocity measurements are roughly 10 m a^{-1}. Surface velocities of the central ice stream were also measured by the displacement of three ablation stakes, MG01, located 1 km upstream of the grounding line, MG02, located 1 km downstream of the grounding line, and MG03, located 8 km downstream of the grounding line, between July 2012 and July 2013.

Van Wychen et al. (2016) calculated ice discharge through a flux gate near the Milne Glacier grounding line, however we further constrain the position of the grounding line using data from NASA's Operation Icebridge 2014. The grounding line is assumed to correspond to the point of first hydrostatic equilibrium, where the thickness of the ice derived from Airborne Topographic Mapper (ATM) laser altimeter (Krabill, 2010) surface elevation equals that measured by the Multichannel Coherent Radar Depth Sounder (MCoRDS; Leuschen et al., 2010). Upstream of the grounding line the thickness of the glacier, estimated from surface altimetry assuming (incorrectly) that the ice is in hydrostatic equilibrium, is much greater than the actual glacier thickness measured by radar. Downstream of the grounding line, where the ice is floating, the thickness estimated from surface elevation is equal to the actual thickness measured by radar. Therefore, moving from upstream to downstream the first location where the two thickness estimates are equal indicates where the ice goes afloat (i.e. the grounding line; Rignot et al., 2001). Error in the ice depth measurements is $\pm$ 10 m. The cross-sectional bed profile of the fjord at the grounding line was modelled as a U-shaped valley as in Van Wychen et al. (2014), with the maximum cross-fjord ice thickness from the MCoRDS data at the grounding line position.

4.2.4 Surface mass balance

Average annual surface mass balance was estimated from 6 ablation stakes on the MIS between May 2009 and May 2011 and from 3 ablation stakes on the MGT and MG between July 2012 and July 2013. The resulting annual surface melt of 0.78 $\pm$0.64 m a^{-1} is assumed constant in time and spatially uniform over the entire fjord.

4.2.5 Divergence of ice flux along MGT

The depth integrated conservation of mass

$$\frac{\partial H}{\partial t} + \nabla \cdot (\overline{u}H) = -a_{sf} - a_b \tag{4.2}$$

relates the change in ice thickness over time, $\partial h/\partial t$, and the flux divergence ($\nabla \cdot (\overline{u}H)$), where $\overline{u}$ is the depth-averaged along-stream velocity, to the surface mass balance a_{sf} and the basal mass balance a_b. We refer to this model as the divergence of ice flux model throughout this chapter.

Assuming steady state, with no change in ice thickness over time ($\partial h/\partial t = 0$), and constant surface melt, then basal mass balance can be calculated from the divergence in ice flux along the flow line. Seroussi et al. (2011) showed that gridded ice thickness maps based on interpolation of sparse ice thickness source data, produce strong anomalies in ice flux divergence if the interpolation schemes do not conserve mass. Regions of the Milne Fiord DEM produced in Chapter 2 are based on sparse source data (up to 2 km gaps between source data measurements) and did not include any mass conservation scheme, so we refrain from calculating the two-dimensionally resolved ice flux divergence for the entire MGT. Instead, we calculate a one-dimensional width-averaged basal melt rate along the length of the MGT. For free-floating ice we can assume surface velocity is equal to depth-average velocity, i.e. $u_s = \overline{u}$, and calculate the along-stream velocity component. Velocity and ice thickness data were then averaged over the width of the MGT ($\sim$4.2 km) and a distance of 2.5 km along-stream, and ice flux and melt rates were calculated every 500 m from the grounding line to the terminus of the glacier tongue.

4.2.6 Ocean thermodynamic melt model

Thermodynamic models of ice-ocean interaction aim to obtain a realistic prediction of melt rate at the ice shelf base from ocean properties. The models use prescribed interior properties of the ice shelf and the ambient water column to estimate the characteristics exactly at the ice-ocean interface where there are three physical constraints: the interface is at the freezing point, and both heat and salt are conserved during phase changes (Holland and Jenkins, 1999). The transfer of heat and salt through the oceanic boundary layer are parameterized as functions of the bulk differences in velocity, heat, and salt between the ice-ocean interface and the far-field ocean mixed layer.

A hierarchy of models have been formulated to calculate the heat and freshwater fluxes that result from deviations in the far-field ocean properties from freezing point conditions, and these are reviewed in Holland and Jenkins (1999). The three-equation formulation makes no assumption about the conditions at the ice-ocean interface and solves equations for each of the freezing point dependency and the conservation of heat and salt (Chapter 1). This formulation is the most sophisticated, and has been widely used to predict melt rates of ice shelves in ice-ocean thermodynamic models (e.g. Hellmer and Olbers, 1989; Holland and Jenkins, 2001; Losch, 2008; Kimura et al.,

2013). The three-equation model is generally preferred owing to its wider applicability over a range of thermal forcing (the elevation of the mixed layer temperature above freezing). Alternatively, a two-equation model assumes the interface salinity and mixed layer salinity are identical (implying infinite salt diffusivity across the boundary layer) and the model is evaluated using the far-field salinity. In this formulation the rate at which the mixed layer temperature relaxes toward the freezing point is governed by the transport of heat through the oceanic boundary layer. The simpler two-equation model is advantageous in reduced or analytic models, and Jenkins et al. (2010) showed that observations of melting under moderate thermal forcing at the base of the Ronne Ice Shelf could be fitted equally well by either the three-equation or two-equation model. Similarly, McPhee 1992 and McPhee et al. (1999) have shown that beneath sea ice the two-equation formulation produces heat fluxes that agree well with measurements over wide range of basal roughness characteristics.

In any model of ice-ocean interaction, a calculation of the freezing temperature at the ice-ocean interface is required. The freezing point of seawater is a non-linear function of salinity and a linear function of pressure. Solving the fundamental equations requires simultaneously solving three equations with three unknowns, and while the complex polynomial form of the freezing point could be used, a linearized version of the freezing point relation is often invoked to simplify solving the equation analytically and is the standard form used in much of the ice-ocean thermodynamic literature (Hellmer and Olbers, 1989; Holland and Jenkins, 1999; Jenkins et al., 2001; Losch, 2008; Kimura et al., 2013). In this formulation the freezing point T_f equation has the form

$$T_f = \lambda_1 S_w + \lambda_2 + \lambda_3 p_b \tag{4.3}$$

where S_w is the salinity in the mixed layer, p_b is the sea pressure at the interface, and $\lambda_{1,2,3}$ are empirical constants (Millero, 1978). The linearized formulation is only valid over a limited salinity range (e.g. 4-40 psu in Holland and Jenkins (1999)), acceptable for typical seawater salinities under ice shelves. However, the low salinity of the epishelf lake in Milne Fiord lies outside of this range ($<$0.2 g kg^{-1}), and freezing temperatures calculated using the linearized formulation at freshwater salinities could be incorrect by up to 0.1°C, introducing error into the calculated submarine melt rates. To avoid this error we use the International Thermodynamic Equation of Seawater 2010 (TEOS-10) Gibbs Seawater Oceanographic Matlab Toolbox (www.TEOS-10.org) polynomial function to calculate the temperature (ITS-90) at which seawater freezes as a function of Absolute Salinity, S_A (in g kg^{-1}) and sea pressure, p (dbar) (we neglect the influence of dissolved gases on the freezing temperature).

The need for the polynomial form of the T_f equation means solving the three-equation model (**??**) would be non-trivial, so we use the simpler two-equation model of the form

$$\rho_i a_b L_i = \rho_i c_i a_b (T_i - T_f) - \rho_w c_w u_* \Gamma_{(TS)} (T_f - T_w) \tag{4.4}$$

where T_f is calculated using the TEOS-10 function instead of the typical linear form (Eq. 4.3). In the above equations ρ is density, L is latent heat of fusion, c is specific heat capacity, T is temperature, S is salinity; the subscripts i, b, w, and f refer to ice, ice-ocean boundary, water, and the freezing point, respectively. The ablation rate at the ice-ocean boundary, a_b, is expressed as a change in thickness of solid ice per unit time, is positive for ablation, and is determined by the divergence of the sensible heat flux at the phase change interface. The turbulent transfer coefficient for heat and salinity $\Gamma_{(TS)}$ is derived from a single observation beneath the Ronne Ice Shelf in Antarctica (Jenkins et al., 2010). We refer to this model as the ice-ocean model throughout this chapter.

Friction velocity (u_*) is calculated as:

$$u_*^2 = C_d U^2, \tag{4.5}$$

where U is the free-stream velocity beyond the ice-ocean boundary layer and C_d the drag coefficient (Table 4.2). The drag coefficient is based on measurements below sea ice and is not constrained by observations below ice shelves. Its use implies that the turbulent transfer coefficients estimated for sea ice are appropriate for the base of an ice shelf. Temporal variability of the boundary layer and the differing nature of the boundary flow beneath ice shelves, where the forcing comes from buoyancy and tides, and beneath sea ice, where the primary forcing is the wind-driven drift of the ice cover, could violate these assumptions. However, use of the values for C_d and $\Gamma_{(TS)}$ recommended by Jenkins et al. (2010) is required until further observations below ice shelves are available. By applying the two-equation model Jenkins et al. (2010) found these values were able to reproduce observed melt rates at the base of the Ronne Ice Shelf, Antarctica, within observational error.

The model does not explicitly account for circulation induced by buoyant convection of the meltwater plume along the base of a sloping ice shelf. One consequence of this is that the model does not directly account for the so-called 'ice pump', the possibility of ice accretion from the ascending meltwater plume on the base of the ice shelf due to the pressure dependency of the freezing temperature (-7.53 x 10^{-4} °C dbar^{-1}). Therefore the possibility of ice accretion on the shallower portions of the ice shelf or glacier tongue is not accounted for in the model. However, the relatively shallow maximum draft (150 m) of ice in Milne Fiord means this effect will be relatively small (the freezing point changes by $\sim$0.1°C over the water column). This is in contrast to Antarctica where ice shelves are an order of magnitude thicker, and a change in freezing point of $>$1°C over the water column in contact with ice means the ice pump can be the main driver of cavity circulation and basal mass balance.

We also note that the ice-ocean model used here was developed for the near-horizontal slope at the base of an ice shelf and may underestimate the melt rate near vertical ice walls, such as those of the MGT. Using a model based upon one-dimensional buoyant plume theory, Jenkins et al. (2010) showed that changing the slope of the ice-ocean interface from that of a floating ice tongue (basal

slope of ∼4%) to a vertical wall, resulted in a near doubling of the melt rate. This suggests the actual melt rates along the near vertical margins of the MGT could be twice as high as those calculated here.

We use vertical profiles of ocean properties and currents collected each year from 2011 to 2015 in Milne Fiord to derive a depth-dependent melt rate. Then, assuming water properties and currents measured at the mooring site were uniform throughout the fjord, we project the melt rate profile onto the ice draft DEM.

To assess the effect of changing the input values to the calculated melt rates, a sensitivity analysis was performed whereby the model was run adjusting one variable over its likely range while all other variables were held constant. A sensitivity analysis was run for all variables, however the model is only very weakly sensitive to the values of internal ice temperature (a value of - 15°C was used based on 10 m borehole temperature of the Ward Hunt Ice Shelf (Jeffries, 1991)) and the densities of water and ice so we do not include the results of those runs. The range of values for the temperature of the ambient water above the freezing temperature, or thermal driving, $(T_w - T_w^f)$ and U were determined from the variation of observed properties from field measurements. Estimating the appropriate range of possible values for C_d and $\Gamma_{(TS)}$ was more uncertain, given the paucity of observations under ice shelves. We chose to test model sensitivity to these parameters using a range values derived from observations under ice shelves and sea ice, varying C_d from 1 x 10^{-4} to 1 x 10^{-2} and Γ_{TS} from 1 x 10^{-4} to 8 x 10^{-3} (McPhee, 1990; Shirasawa and Ingram, 1991; Holland and Jenkins, 1999). Further investigation will be required to determine the most appropriate values for Milne Fiord.

4.2.7 Ocean properties

To run the ice-ocean model we used conductivity-temperature-depth (CTD) profiles collected May of 2011 and 2012, and July of 2013, 2014, and 2015 at the mooring site in Milne Fiord using a 6Hz RBR XR-620 CTD (except in 2011 when a 4Hz SBE19+ was used). To investigate the influence that the MIS had on melt rates in the fjord, we also run the model using profiles collected a few kilometers off the seaward edge of the MIS (see Fig. 4.1) in the same year. In 2011 and 2012 the offshore profiles were collected as part of the SwitchYard Project (P.I. M. Steele, University of Washington), while in all other years offshore profiles were collected as part of this study. Derived variables were calculated using the TEOS-10 Gibbs Seawater Matlab Toolbox.

4.2.8 Ocean circulation

Water speeds were measured using an ice-anchored, downward-looking 300 kHz RDI acoustic Doppler current profiler (ADCP) at the mooring site in May 2011, July 2012 and July 2013. We calculated the time-averaged water speed over the duration of each deployment: 4, 7, and 10 days, in 2011, 2012, and 2013, respectively. The current profile was consistent between each deployment

so we calculated a time-average current profile over all years. The depth range of the ADCP was limited to <100 m, so we estimate speeds below 100 m by assuming a constant speed with depth equal to the measured average between 75 m and 100 m. Speeds are taken to represent the free-stream current beyond the ice-ocean boundary layer. Finally, the vertical speed profile was assumed to be uniform throughout the fjord and invariant in time, so the same averaged speed profile was used every year.

4.2.9 Temperature timeseries

Theoretical considerations of thermodynamics at the ice-ocean interface suggest submarine melt rate varies in proportion to the thermal driving of the ambient water (Holland and Jenkins, 1999; Jenkins, 2011). To understand the variability of ocean temperature in Milne Fiord over time we deployed an ice-tethered mooring deployed through the epishelf lake from May 2011 toJuly 2014. Thermistors were suspended at 5 m, 25 m, 50 m, and 125 m depths. To calculate T_w^f salinity is also required, however we did not have salinity sensors moored at each depth for the full timeseries. Instead we use the average salinity measured at each depth from all CTD profiles collected at the mooring site between May 2011 and July 2015. The range of salinity then gives an estimate of uncertainty in the calculation of T_w^f. Salinity at 5 m, 25 m, 50 m, and 125 m depths varied by 0.1, 10, 6, and 2 g kg^{-1}, respectively. The saline coefficient of the freezing point in the TEOS-10 equation is approximately -59 mK (g kg^{-1})$^{-1}$, resulting in an error in the calculation of T_w^f due to salinity variation of approximately 0.001, 0.059, 0.035, and 0.012°C at 5, 25, 50, and 125 m, respectively. The largest error in T_w^f, at 25 m depth, was equal to approximately 10% the total variation in thermal driving at this depth over the full timeseries.

4.3 Results

4.3.1 Milne Glacier grounding line

The Milne Glacier is presently grounded on a reverse-sloping bed at about 150 m depth, the bed deepens upstream of the grounding line (Fig. 4.2). The glacier thins rapidly within the first 5 km downstream of the grounding line and then tapers more slowly toward the terminus. We note the aerial survey line flown by the 2014 Icebridge mission crossed over from the central ice stream of the Milne Glacier to the highly fractured north-east and south-west ice streams so surface elevation-derived thicknesses for some sections are highly variable (e.g. from 200 m to 5 km, and 10 km to 12 km). The DEM shown in Fig. 4.1 is better constrained with additional data and shows the cross-fjord variability in the thickness of the MGT. Upstream of the grounding line the bed over-deepens to 200 m below sea level within 2–3 km, and remains below sea level for 26 km inland (not shown).

4.3.2 Glacier surface velocities

Glacier surface velocities showed substantial spatial variability and interannual variation from 2011 to 2015 (Fig. 4.3). From 2011 to 2015, glacier velocities averaged 100 m a^{-1} at the grounding line, with a maximum of 150 m a^{-1} in 2011, and a minimum of 70 m a^{-1} in 2012. These values are broadly consistent with the measured displacement of the ablation stake just upstream of the grounding line (MG01), which showed an average displacement of 95 m just upstream of the grounding line from 2012 to 2015 (Table **??**). Downstream of the grounding line velocities of the MGT generally decreased rapidly in the first 5 km to about 60 m a^{-1} and gradually slowed toward the terminus. However, velocities and flow patterns in 2012 and 2013 were somewhat different, with nearly uniform velocities of 60 m a^{-1} along the full length of the MGT in 2012, while in 2013 velocities were $<$25 m a^{-1} over most of the MGT. Ablation stake displacements on the MGT from 2012-2013 were anomalously high, with both MG02 and MG03 showing 290 m displacement over that interval. Measurements from 2013 to 2015 showed a displacement of 60 m a^{-1}, consistent with the speckle tracking data in those years.

A review of available satellite imagery shows the main transverse fracture at the grounding line, which is first apparent in 2006, grew and extended completely across the width of the central ice stream by 2012, perhaps even 2011. This observation suggests that the MGT became partially detached from the grounded glacier sometime during or prior to 2012. If so, this would help explain the anomalous inter annual velocities for the MGT in 2012 and 2013, and suggest that the melt rates calculated in these years must be viewed in with caution as the MGT was not in steady state.

4.3.3 Ocean properties

Annual CTD profiles revealed the vertical distribution of heat available to drive submarine melting changes annually (Fig. 4.4). The strong salinity stratification in the fjord above 50 m depth, that was not present in offshore profiles, was due to the MIS damming runoff within the fjord. The nearly fresh surface waters ($<$15 m depth) indicated the presence of the epishelf lake. The epishelf lake was associated with a near-surface temperature maximum between 5 m and 15 m depth, that varied between 0.25°C and 2°C above freezing in 2011 and 2015, respectively. Offshore profiles collected in July of 2013-2015 showed a slight surface freshening and warming due to sea ice melt, but temperatures remained at the in situ freezing point from the surface to 30 m depth. Below 50 m depth properties in Milne Fiord were similar to properties offshore that year. The temperature above freezing, or thermal driving, increased steadily with depth below 50 m, the heat supplied by warm waters of Atlantic origin. Deep fjord water near the depth of the Milne Glacier grounding line showed temporal variation in thermal driving of 0.5°C among years, 2013 had the lowest thermal driving (0.9°C) at depth, while 2015 had the highest (1.4°C). Temperature changes above 50 m and below 50 m were not correlated (e.g. in 2013 near-surface waters had the highest thermal driving, while deep waters had the least of all years). The lack of correlation over depth suggests

that surface waters are influenced by local surface conditions (i.e. air temperature, snow cover, solar radiation, surface runoff), while deep waters are influenced by other processes (e.g. offshore variation transmitted into the fjord by intermediary exchange flows). Some of the differences in temperature among years, particularly near the surface, were due seasonal differences in the timing of profiling so interannual trends should not be inferred from the results.

Measured ocean current speeds revealed flow in the fjord was weak and baroclinic, speeds increased from around 1 cm s^{-1} near the surface to a maximum of 3 to 6 cm s^{-1} between 50-60 m, then decreased below this depth to about 2 cm s^{-1} (Fig. 4.5). Tidal oscillations on the order of 2 cm s^{-1} accounted for a substantial portion of the flow speeds in Milne Fiord. However, the MIS formed an obstacle to flow, limiting speeds to $\sim$ 1 cm s^{-1} in the upper 25 m of the water column. We have assumed constant flow below 100 m, however we acknowledge that other processes, such as intermediary exchange below the MIS could lead to variable and potentially higher flow speeds at these depths (Jackson et al., 2014b).

4.3.4 Ocean model sensitivity

The ice-ocean model shows a linear dependence on $T_w - T_w^f$, U, and Γ_{TS}, and a non-linear dependence on C_d (Fig. 4.6). Estimated melt rates are most sensitive to values of $T_w - T_w^f$ and U, which in our model are based on field observations. $T_w - T_w^f$ is known from CTD profiles while U is based on ADCP measurements. We assumed the properties measured at the mooring site were representative of properties throughout the fjord. CTD transects collected at many sites throughout the fjord (Chapter 2) have shown water properties to be relatively homogenous, so our values of $T_w - T_w^f$ are fairly robust. However, we only have current speed measurements from a single location, and only over the top 100 m, so horizontal or vertical differences in current speeds from those used in the model could change the estimated melt rates accordingly. The model is slightly less sensitive to the chosen values of C_d and Γ_{TS}, however the values used here are based on other studies, so further observations are required to validate their use in this system. This study is most concerned with the effect of depth variation of ocean properties on the vertical distribution of melt rates, so although the actual magnitude of the melt rates calculated have some degree of uncertainty, the relative changes with depth are based on field observations and should be fairly robust. We reiterate that the results of the model must be interpreted with proper consideration of above uncertainties.

4.3.5 Submarine melt rates

Width-averaged MGT melt rates

Width-averaged submarine melt rates calculated by the divergence of ice flux and the ocean thermodynamic model along the length of the MGT for 2011 to 2015 are shown in Fig 4.7. The MGT thins rapidly from 150 m depth to $<$75 m depth within the first 2.5 km downstream of the grounding line,

then thins more gradually toward the terminus where the ice is $<$10 m thick. The bottom profile of the MGT is similar to that of other glacier tongues in Greenland (Rignot et al., 2001). Melt rates calculated by both methods showed a similar pattern of high melt rates averaging $\sim$4 m a^{-1} within the first 2.5 km downstream of the grounding line, then decreasing to near zero within 5 km. The ice-ocean model indicated a slight increase in melt rate near the terminus, while the ice flux model did not. There was an $\sim$1 m a^{-1} difference in melt rate between the two methods over the mid-portion if the glacier tongue. Given the assumption inherent in each method it is difficult to quantify the uncertainty in the absolute accuracy of the calculated values, however the offset is likely within error limits. In 2012 and 2013 high variability in ice surface velocities along the MGT suggested the glacier may not have been in steady state, and the values estimated by the ice flux method in those years may not be reliable. Overall, the two method show general agreement in both the magnitude and distribution of melt along the glacier tongue, and relatively little interannual variation (with the noted exception of 2012 and 2013).

4.3.6 Area-averaged melt rates

Annual area-averaged submarine melt rates for the MGT and MIS from 2011 to 2015 calculated using the grounding line flux, divergence of ice flux, and the ice-ocean model are shown in Table 4.3. The average melt rates for the MGT calculated by the grounding line flux method and the divergence of ice flux method each year are comparable, showing $<$1 m a^{-1} melt, and possible net ice accretion in some years (negative melt rates). In contrast, the ice-ocean model results are consistently higher, showing a total average melt rate of 1.6 m a^{-1} for the MGT. Average melt rates calculated by divergence of ice flux and the ice-ocean model over the first 2.5 km downstream of the grounding line are consistently higher, averaging 3.5 m a^{-1}. Annual melt rates for the first 2.5 km calculated by the divergence of ice flux method are quite variable, ranging from a maximum of 6.0$\pm$1.9 m a^{-1} in 2011, to a minimum of 0.9$\pm$0.3 in 2012, owing to the difference in ice surface velocities in those years. Neglecting 2012 and 2013, when velocities of the MGT may have been anomalous due to a partial detachment from the glacier, gives an average melt rate for the first 2.5 km of the MGT of 5 m a^{-1}. Submarine melt rates calculated by the ocean thermodynamic model for the MIS averaged 1.4 m a^{-1} over all years with only 0.2 m a^{-1} variation among years.

4.3.7 Spatial distribution of melt rates

The spatial distribution of submarine melt rates in Milne Fiord from 2011 to 2015, calculated from the ice-ocean model using the CTD profiles acquired at the mooring site are shown in Fig. 4.8). Melt rates are spatially heterogenous in both the magnitude and interannual variability. Thermodynamic melt models predict a linear or quadratic dependence of melt rates with thermal driving (Holland and Jenkins, 1999; Jenkins, 2011), and consequently the vertical distribution of heat in Milne Fiord results in melt rates that vary vertically over the water column. The melt rate is thus

largely dependent on ice draft (see the Discussion for a consideration of other processes that influence melt rate). High melt rates occur where the ice is thick and penetrates deep into warm AW (e.g. the Milne Glacier grounding line and Outer Unit of the MIS), and where the ice is quite thin ($<$15 m deep) and in contact with warm water of the epishelf lake (i.e. along the margins of the epishelf lake). At mid-depths, for ice drafts between approximately 25 m and 60 m, the melt rate is generally lower ($<$1 m a^{-1}), but shows more interannual variability. The Central Unit of the MIS shows a high degree of both spatial and interannual variability. The spatial variability is due to the heterogeneity of ice thickness across the unit, owing to its composite origin of marine ice accretion and input from tributary glaciers. Much of the ice of the Central Unit is between 30 m and 50 m thick and shows much more interannual variability than the $>$80 m thick ice of the Outer Unit. The variability is caused by the high current speeds at 50 m depth (Fig. 4.5) amplifying the effects of small temperature variations at these depths (Fig. 4.4), leading to pronounced differences in calculated melt rate for ice with a draft around 50 m.

The influence of the MIS and the epishelf lake on submarine melting in Milne Fiord is apparent in the results of the ice-ocean model run using profiles acquired outside the fjord (Fig. 4.9). Similar to the model run using the mooring profile, melt rates are consistently high where the ice is thick and in contact with AW. However, where ice is very thin melt rates are low compared to the model run with the mooring CTD profile. A comparison between melt rate calculated from the mooring CTD profile versus the offshore CTD profile are shown in Figure 4.10, revealing the highest melt rate anomalies occur where the ice is thin. This is evidence that the presence of the MIS, and its effect on the water column structure within the fjord results in higher near-surface melt rates than would otherwise be expected if the ice shelf was not present. The Central Unit of the MIS also shows a high melt rate anomaly in 2012. This due to the substantial difference in salinity, temperature, and thermal driving down to 40 m depth between the mooring CTD profile and the offshore CTD profile that year (Fig. 4.4).

We note that the high near-surface ablation rates calculated using the mooring profile are only valid where the water column structure and flow speeds are well represented by measurement taken at the mooring site. CTD profiles acquired throughout the fjord indicate water properties are similar everywhere landward of the Outer Unit, including under the Central Unit (Chapter 2 and 3). No profiles have been acquired through the Outer Unit, the water properties here are unknown. Somewhere below the Outer Unit water properties of the upper water column must transition from having characteristics similar to the mooring site, with a strong stratification and an elevated heat content, to having characteristics similar to offshore, where the near-freezing surface mixed layer extends to 30–50 m depth. It is therefore uncertain whether melt rates estimated for the relatively thin portions of the Outer Unit (i.e. along the re-healed fracture and just to the south of the western extreme of the fracture) are best represented by those calculated using the mooring profile or the offshore profile. In general, melt rates for the Outer Unit are best represented by those calculated using the

offshore profile (Fig. 4.9), while melt rates for the Central Unit and MGT are best represented by those calculated using the mooring profile (Fig. 4.8).

4.3.8 Thermal driving depth-dependence

In Figure 4.11 the variability of thermal driving over 3-years at different depths is shown. The waters of the epishelf lake, at 5 m depth, showed the highest average thermal driving and the greatest magnitude of variation, with seasonal increases $>2^{\circ}$C. This seasonal variation was due to inflow of relatively warm meltwater and solar heating. Waters at 25 m depth showed an abrupt increase of 0.5°C in June 2011, then a long-term gradual decrease over the remaining 3 years of the record, with very little seasonal variation. The flow of water at this depth was largely restricted by the MIS, and was influenced by the accumulation of subglacial runoff within the fjord and its slow drainage under the ice shelf. Water at 50 m depth had the lowest thermal driving and the least interannual variability. At this depth the flow of water under the ice shelf was less restricted and had characteristics of the surface mixed layer of the Arctic Ocean. At 125 m depth there was substantial seasonal and short-term (days to weeks) variation in thermal driving, with annual variation of 0.5°C. Water as this depth was at the interface between Polar Water and Atlantic Water, and the variation was likely representative of offshore depth variation of the main Arctic halocline being transmitted into Milne Fiord under the MIS. Overall, the records indicated a strong depth-dependence on both the magnitude and variability of thermal driving in Milne Fiord, that could substantially alter submarine melt rates over time. The variability of thermal driving at 125 m is of particular interest, as this record is representative of changes in thermal driving of waters in contact with the grounding line of the Milne Glacier.

4.4 Discussion

Submarine melt rates are determined by the heat content and circulation of ocean waters in contact with ice. We have shown that the heat content in Milne Fiord varies with depth, and the spatial distribution of melting in the fjord is therefore largely dependent on ice thickness. The heat content in Milne Fiord has a bimodal distribution, with a near-surface maximum in the epishelf lake, and a gradient toward a deeper maximum in the Atlantic layer, and this has repercussions for the vertical, and thus spatial, distribution of melting in the fjord.

4.4.1 Grounding line melt

Unsurprisingly, melt rates are highest near the Milne Glacier grounding line, a finding consistent with other studies of submarine melting of glacier tongues and ice shelves (Rignot et al., 2001; Rignot and Steffen, 2008). The average melt rates calculated within 2.5 km of the Milne Glacier grounding line are substantially less than those estimated near the grounding lines of other glacier tongues

in Greenland. Rignot et al. (2001) estimated melt rates between 22 m a^{-1} and 26 m a^{-1} within 10 km of the grounding line for six glaciers with ice tongues in northern Greenland. However, the depths of the glacier grounding lines surveyed in Rignot et al. (2001) ranged from 460 to 650 m, so the combined effect of the pressure-induced depression of the freezing point and the increase of temperature of the Atlantic water with depth (to a maximum between 300 m and 800 m; Carmack, 1990) means that thermal driving generally increases with depth in the Arctic, and the higher melt rates for the thicker glaciers in Greenland are expected.

Although Milne Glacier appears to have a substantially lower melt rate than Greenland counterparts, the melt could still cause retreat of the grounding line if basal melt is greater than surface accumulation and dynamic thickening. Retreat of the grounding line into deeper water could increase ice flux, and increase the glacial contribution to sea level. Neglecting other effects, if the average basal melt rate of 5 ± 2 m a^{-1} induces an equivalent thinning of the glacier this could cause the grounding line to retreat approximately 400 ± 200 m a^{-1} given the glacier surface slope (1.5% from 2014 Icebridge ATM data) and bed slope (-3% from MCoRDs data). The appearance in 2013 of new transverse fractures a few hundred meters upstream of the previous hinge fracture suggested the grounding line has retreated. The average rate of basal melt at the grounding line is fives times greater than the estimated surface melt rate for the fjord, suggesting basal melt is a major factor in retreat of the grounding line. The contribution from dynamic thinning, however, remains unclear.

The Milne Glacier is a suspected surge-type glacier (Jeffries, 1984; Copland et al., 2003), and the differences in surface velocities recorded at the grounding line between 2011 and 2012 may indicate the end of a surge cycle, which in the QEI are characterized by quasi-periodic fast flows (7–15 years), followed by periods of slow flow (30–40 years; Van Wychen et al., 2016). Recent evidence also suggests the existence of 'pulse' type tidewater glaciers, which are characterized by brief periods of accelerated motion (2–5 years) (Van Wychen et al., 2016). In addition, the possible detachment of the MGT from the glacier suggest the melt rates calculated by the divergence of ice flux method at the grounding line in 2012 and 2013 are artifacts of unsteady dynamics. The lack of oceanographic data for the fjord before 2011 means it is unclear what role changes in ocean forcing may have had in influencing glacier dynamics prior to this time.

4.4.2 Near-surface melt

The enhanced near-surface melt rates in Milne Fiord due to the strong heat and salt stratification created by the MIS dam are a unique feature of this fjord. Seasonal warming of surface waters from solar radiation and runoff are expected in other glacial fjords, and may lead to seasonally enhanced near-surface melting, however the effect is transient as surface waters return to near-freezing during winter. In contrast, the strong stratification in Milne Fiord is present year-round, and temperatures remain well above above freezing even in mid-winter (e.g. almost 3°C above freezing at 5 m in January 2013; Fig. 4.11), so there is sufficient heat available to drive near-surface melting in Milne

Fiord all year. Melting during winter could account for a significant portion of the total annual near-surface melt in Milne Fiord. It is important to note that the calculated melt rates assume steady state ice thickness. Melting and thinning of ice over time will substantially alter the melt rate over time for ice drafts less than 20 m due to the strong gradients in thermal driving near the surface.

The elevated heat content of the upper water column in Milne Fiord is due to the existence of the MIS. The effect of the MIS was shown by the lower near-surface melt rates calculated when the ice-ocean model was run with the profiles collected offshore. Using the offshore profile was analogous to removing the MIS and its influence on the water properties of the fjord, as free-exchange at the fjord mouth would mean surface properties within the fjord would be very similar to those offshore. Surface temperatures in the Arctic Ocean remain close to the freezing point down to the base of the mixed layer (30-50 m depth) year-round. The year-round enhanced near-surface melt rates in Milne Fiord are then entirely dependent on the presence, and structural integrity, of the MIS dam.

MIS melting

Enhanced near-surface melting in Milne Fiord means the MIS may be contributing to its own demise. Elevated melt rates of the inner margin of the Central Unit of the MIS are owing to its contact with the epishelf lake, whose existence is dependent upon the integrity of the MIS. Analysis of satellite imagery reveals the southern edge of the MIS retreated northward in recent years, and the Central Unit has undergone widespread fracturing and calving (Chapter 3). Our results suggest that weakening and retreat of the southern edge of the Central Unit, is due, in part, to submarine melting (likely in combination with mass loss from surface ablation). This observation also suggests a mechanism for the formation of the epishelf lake, something not explicitly addressed in previous studies (Jeffries, 1984; Mortimer et al., 2012; Chapter 3). The epishelf lake is thought to have expanded as a region of the MIS, known as the Inner Unit, was replaced with freshwater lake ice. We have provided evidence that indicates enhanced submarine melting of the ice shelf, driven by trapped surface runoff behind the ice shelf, was a plausible mechanism for the retreat of the ice shelf margin, and the expansion of the epishelf lake. The melt rate for regions of the MIS with a draft less than 35 m showed a 50% increase when the ice-ocean model was run with the mooring profile compared to the offshore profile, highlighting the impact of the ice dam on melt rates in the fjord. Continued melting induced by the epishelf lake could eventually lead to a compromise of the MIS dam, and a loss of the epishelf lake.

We estimated a surface ablation rate of 0.78 m a^{-1} in Milne Fiord and an areal average basal melt rate for the MIS of 1.4 m a^{-1}, indicating basal melt accounted $\sim$64% of total melt between 2011 and 2015. This is similar to the estimate of Mortimer et al. (2012) who suggested submarine melting may have accounted for $\sim$73% of the overall thickness change of the MIS over the period 1981 - 2009. Longer-term surface mass balance records from the Ward Hunt Ice Shelf show that surface melt increased substantially in recent years, from 0.08 m a^{-1} between 1989-2003, to an average of

0.5 m a^{-1} between 2002-2005 (Braun et al., 2004; Mueller et al., 2006). These observations are consistent with the dramatic regional increases of surface mass loss across the CAA over the period 2003 to 2009 (Gardner et al., 2011; Gardner et al., 2013). The general trend suggests that although submarine melting appeared to have been the dominant factor in thinning of the ice shelves in past decades, surface melt has become an increasingly important factor in the past decade.

The rapid increase in surface melt over the past decade suggests changes in basal melt should also be considered. Our 4-year study is too brief to identify a long-term trend in basal melt rate for the MIS, but we did find interannual variability in the spatial distribution of melting. This was due to both local changes in the water column in Milne Fiord, driven largely by annual variation in runoff, but also changes in the properties of ambient source waters offshore. Jackson et al. (2014a) showed that the water column structure in the Lincoln Sea, north-east of Ellesmere Island, from 1991 to 2012 varied yearly owing to the complex circulation in the region. The region is a bifurcation point, where waters from the Canadian and Eurasian Basins flow toward Nares or Fram Strait, or are advected westward along the continental shelf. Minor shifts in circulation patterns therefore substantially altered the water properties along northern Ellesmere Island. How regional circulation patterns influenced basal melt rate of ice shelves along northern Ellesmere Island in the past, and how future circulation and water column changes may in the future is worthy of further investigation. Although this is beyond the scope of the present study, what is apparent is that ocean-driven melt rates in Milne Fiord are influenced by a variety of factors over a range of spatial and temporal scales.

4.4.3 Circulation in Milne Fiord

One of the key factors in determining melt rates is ocean circulation. The water column in Milne Fiord has sufficient thermal driving to induce melt rates substantially higher than those estimated here, however the transfer of heat to the ice boundary appears to be limited by relatively weak currents. The main factors driving circulation in a typical ice covered fjord are tides, intermediary exchange, and buoyancy-driven flow from freshwater discharge at the head of the fjord. Below an ice shelf or glacier tongue, additional thermohaline processes can also drive circulation. Milne Fiord is somewhat atypical, in that regardless of the forcing, the MIS impedes flow in the upper water column. However, below the draft of the MIS, we expect the main drivers of circulation are the same as a typical fjord. ADCP records showed that tidal flows below 80 m, deeper than the draft of the MIS, were on the order of 2 cm s^{-1}. Lacking observations of current speed below 100 m depth we therefore estimated a constant speed of 2 cm s^{-1}. But what are the potential contributions of intermediary exchange and buoyancy-driven circulation to flow speeds at depth?

We can obtain a rough idea of the significance of buoyancy-driven flow by using a simple model of estuarine circulation. To do so, we assume a simple 2-layer return flow driven by the release of freshwater at the head of the fjord. Although recent studies, including this one, have shown that circulation in glacial fjords is more complex than a simple 2-layer model (Straneo and Cenedese,

2015), the exercise is still useful in providing a conceptual understanding of the magnitude of buoyancy-driven flow as a factor in fjord circulation. We assume freshwater input at the head of the fjord drives an outflowing surface layer with an inflowing bottom layer. From a consideration of the steady state salt and volume continuity of a fjord, and neglecting diffusion, Knudsen's hydrographical theorem provides an estimate of the volume flow in the upper and lower layers

$$Q_1 = \frac{Q_{fw}}{\frac{S_2}{S_1} - 1} \tag{4.6}$$

and

$$Q_2 = \frac{Q_{fw}}{1 - \frac{S_1}{S_2}} \tag{4.7}$$

where Q_1, S_1 and Q_2, S_2 are the volume flows and salinities of the upper and lowers layers, respectively, Q_{fw} is the freshwater (assumed zero salinity) discharged at the head of the fjord. We can therefore estimate volume flow in the two layers from CTD profiles of salinity and an estimate of Q_{fw}. In a glacial fjord $Q_{fw} = Q_{sf} + Q_b$, where Q_{sf} is freshwater runoff from surface melt and Q_b is freshwater input from basal submarine melt. In reality, a portion of surface melt enters the fjord at the surface, and feeds the epishelf lake, while the remainder enters the fjord at depth at the bed of the glacier. However, for the purpose of this estimate we will use the combined total to understand the influence of total runoff on driving estuarine circulation.

We estimate Q_{sf} from regional surface mass loss for the CAA from 2006-2009 (Gardner et al., 2011). Applying an average loss of 310 kg m^{-2} a^{-1} over the 1108 km^2 glaciated area of the MG catchment gives an annual average runoff of 3 x 10^8 m^3 a^{-1}, equivalent to 12 m^3 s^{-1}, or 73 m^3 s^{-1} if only averaged over the 2 month melt season.

The other source of freshwater at the head of the fjord is submarine melting of glacial ice near the grounding line. The average melt rate within 2.5 km of the grounding line was 3.8 m a^{-1} over all years, equating to roughly 4 x 10^7 m^3 a^{-1} of freshwater input from submarine melt. Submarine melt therefore accounts for only 10% of the total freshwater input at the head of the fjord, 90% originates as surface runoff.

Based on salinity and velocity profiles we estimate the upper layer is between 30 and 60 m depth, and the lower layer is between 60 and 260 m depth (the sill depth). The average salinities at these depths give S_1 = 30 g kg^{-1} and S_2 = 33 g kg^{-1}. Inputting the above values into Eq. 4.7 results in upper and lower layer volume flows on the order of 100 m^3 s^{-1}. Assuming a rectangular cross-section equal to the height of each layer, and a fjord width of 5 km, gives estimated current speeds of $<<1$ cm s^{-1}. Even if Q_{fw} is an order of magnitude greater, the estimated current speeds are still <1 cm s^{-1}. It therefore appears unlikely that the small volume of freshwater discharged into Milne Fiord will drive strong fjord-scale currents, and may therefore play only a minor role in determining average melt rates across the fjord. While subglacial discharge could induce high

melt rates at the grounding line, we expect the effect will be localized along subglacial discharge channels and limited to the brief summer melt season. Similarly, outflow along the basal channel in the MIS may enhance local melt rates in the channel, but the effect on fjord-scale circulation is small given the slow export over several months.

Another process that could enhance flows in Milne Fiord is intermediary exchange below the MIS. Jackson et al. (2014b) observed frequent velocity pulses that exceeded 50 cm s^{-1} in the upper 200 m of Sermilik Fjord, Greenland, lasting several days between September and May 2011-2012. The pulses were largely attributed to wind-driven upwelling along the continental shelf setting up baroclinic exchange between the fjord and the continental shelf. The authors suggested that glacier melt rates could vary substantially throughout the year as a result. Similarly, Stigebrandt (1990) found externally forced baroclinic exchange driven by density fluctuations at fjord mouth was an order of magnitude higher than tidal or estuarine flow in a Scandinavian fjord.

Although we lack long-term current measurements at depth that can directly address variability in flow due to offshore exchange, we can obtain a first order estimate of exchange flow in Milne Fiord from changes in isotherm depths from the multiyear temperature timeseries presented in Chapter 2. Those observations showed that isotherms around 125 m depth varied by up to 50 m depth over the course of several days. If the change in height of the isotherm was uniform throughout the inner $\sim$66 km^2 of the fjord, this is equivalent to an inflow volume of 3 x 10^9 m^3. Immediately, we see this is an order of magnitude larger than the total annual freshwater inflow from surface and submarine melting. If we assume the inflow of water occurred over a depth of 200 m across the 5 km width of the fjord, and occurred over 5 days, this would have resulted in an average inflow speed on the order of 1 cm s^{-1}, although peak flows could be substantially higher. This is an admittedly crude calculation, but it does suggest that intermediary exchange flow is of the same order of magnitude as tidal flow, and further investigation is this process is required to accurately estimate basal melt rates in Milne Fiord.

In summary, it appears that tidal and intermediary exchange are important drivers of circulation in Milne Fiord over most of the year. Thermohaline circulation in the ice cavity is a factor that we have not addressed here, but will discuss further in the next section. It is likely that buoyancy-driven flow from subglacial discharge is an important factor in determining localized melt rates in summer, but does not appear to play a large role in fjord-scale circulation and can assumed to be negligible over most of the year. Overall, melt rates are then largely determined by tidal and intermediary exchange flows and the thermal driving of the ambient water column.

4.4.4 Future work

The thermodynamic melt model used here was based on the assumption that water properties and currents speeds were uniform throughout the fjord, and that physical parameterizations of heat transfer through the ice-ocean boundary layer based on observations below a single Antarctic ice shelf

were appropriate for Milne Fiord. Clearly, this is a substantially oversimplified view of the fjord and the results of the melt model presented here must be viewed in this context, as a useful first attempt that can inform future studies.

There are several improvements that could be made to the ocean melt model. First, circulation under the glacier tongue (and ice shelf) can be driven by the thermohaline differences which result from mass and energy exchange at the ice-ocean interface. This process has been modelled using a one-dimensional flow-line model based on buoyant plume theory, where the rising plume along the ice base is treated as a turbulent gravity current initiated at the grounding line, by a flow of subglacial water or in situ melting (Jenkins, 1991; Jenkins, 2011). The subsequent evolution of the plume as it ascends along the ice base has been used to explain the observed distribution of melting and freezing along several ice shelves in Antarctica and glacier tongues and tidewater glacier faces in Greenland and Alaska (Jenkins, 1991; Jenkins, 2011). However, given the complex ice topography and bathymetry of Milne Fiord, circulation may be best derived from 3-dimensional numerical modelling, as has been done for other tidewater glacier fjords in Greenland (Xu et al., 2012; Kimura et al., 2013; Sciascia et al., 2013; ; Xu et al., 2013; Cenedese and Linden, 2014). A numerical modelling approach is likely required for Milne Fiord because melt rates for the MIS are also of interest, and the complex ice topography may defy reduction to a one- or two-dimensional model. Three-dimensional numerical models, however, still rely on turbulent transfer and drag coefficients that have not been validated for these systems, so it is apparent that further observations are needed.

In this study we chose to use the two-equation formulation of ice-ocean thermodynamics rather than the three-equation formulation, due primarily to the error that a linearization of the freezing point equation would introduce across the large salinity range in Milne Fiord. However, in doing so the effects of salinity stratification below the ice, both ambient stratification and that induced by melting at the ice base, have largely been neglected. The value of the combined turbulent transfer coefficient for heat and salt (Γ_{TS}) does in theory account for this, however it was validated below an Antarctic ice shelf, where ambient stratification is much less than that observed in Milne Fiord (Jenkins et al., 2010). Although Jenkins et al. (2010) emphasized that there was no difference in the fit between calculated and observed ablation rates using the two-equation formulation compared to the three-equation formulation for their limited set of measurements, they do state that the three-equation formulation is likely the best parameterization to use over a broader range of oceanographic conditions given its explicit treatment of salt transfer through the boundary layer. A comparison of melt rates calculated between the two- and three-equation formulations for the conditions observed in Milne Fiord would be a useful avenue for future research. Fundamentally, however, improvements to the accuracy of derived melt rates from measured ocean properties can only come with validation against direct observations.

Although the actual magnitude of melt rates calculated using the ice-ocean model must be viewed with caution given the limitations to the model discussed above, the depth-dependence is

likely a robust finding. Thermodynamic melt models predict a linear or quadratic dependence of melt rates with thermal driving (Holland and Jenkins, 1999; Jenkins, 2011), and the vertical distribution of heat in Milne Fiord indicates melting will vary substantially over the water column. Variations in the vertical and horizontal distribution of melt, assuming values of C_d and $\Gamma_{(T,S,TS)}$ are constant throughout the fjord, is therefore dependent on the spatial variation in thermal driving and current speed. Current speeds are the least well constrained of these two measurable variables, and suggests these would be a valuable focus for future field studies. In particular, current speeds at the grounding line of the Milne Glacier could be substantially higher in the vicinity of a subglacial discharge channel, potentially leading to much higher melt rates in localized regions. In addition, current speeds at the base of the MGT, and along the basal outflow channel in the MIS, could be higher and result in higher melt rates at these locations.

4.5 Summary and conclusion

We have estimated submarine melt rates in Milne Fiord using independent methods, including a divergence of ice flux model and an ocean thermodynamic model. Melt rates calculated by both methods were broadly consistent, and revealed a depth-dependence. This was related to the vertical distribution of heat in the fjord and vertical velocity variation. The depth-dependence created spatial heterogeneity of melt rates owing to the variability of ice thickness in Milne Fiord. Melt rates were highest where thick ice penetrated into warm AW, including at the grounding line of the Milne Glacier and below the Outer Unit of the MIS. The ice-ocean model also predicted enhanced near-surface melt rates within the fjord caused by the elevated heat content of the highly stratified waters dammed by the MIS. We found substantial interannual and spatial variability of melt rates around the Central Unit of the MIS, caused by its mean draft being at the depth of maximum current speeds, so minor variations in thermal driving caused large changes in melt rate.

This study provides the first direct estimates of submarine melt rates for an ice shelf or tidewater glacier in the Canadian Arctic Archipelago. The oceanography of glacial fjords in the CAA is in general poorly known. If an effort is made to understand or predict how ocean forcing influences tidewater glaciers in the region, measurements of thermal driving, which are relatively easy to obtain by CTD profiling, must be accompanied by observations of circulation patterns, which require sustained, long-term monitoring. In Milne Fiord, tidal flows and intermediary exchange appear to be the main drivers of circulation, however as surface meltwater production increases, buoyancy-driven circulation may be an increasingly important factor. Although these findings are generally transferable to other fjords in the region, we expect different fjords will respond in different ways owing to variations in bathymetry, ambient stratification, the magnitude and seasonality of meltwater input, ice-cover, and glacier dynamics.

Milne Fiord contains the last intact ice shelf along the northern coast of Ellesmere Island, retains one of only a few floating glacier tongues in the Arctic, and the last known epishelf lake in the

Northern Hemisphere. Our results have revealed that the evolution, and eventual fate, of these features is interlinked. The MIS impounds freshwater within the fjord, which enhances melt rates within the fjord, which in turn is leading to a thinning and erosion of the MIS. The thinning of the MIS could eventually contribute its own demise, and the subsequent loss of the epishelf lake. The loss of the epishelf lake will reduce submarine melting along the margins of the MGT, however, the associated loss of perennial lake ice cover that has been observed with the loss of other epishelf lakes (e.g. in Disraeli Fiord; W. Vincent, pers. comm.), would likely result in increased calving of the Milne Glacier. As the Milne Glacier is currently grounded on a reverse-sloping bed, increased calving could result in further grounding line retreat into deeper water, further enhancing submarine melting, and accelerated glacier flux to the ocean.

4.6 Tables

Table 4.1 Annual horizontal displacement of ablation stakes on the Milne Glacier.

Stake Name	Latitude* (°N)	Longitude* (°W)	Time Interval	Displacement (m)
MG01	82.438880	-80.234604	07/2012 - 07/2013	99
			07/2013 - 07/2014	94
			07/2014 - 07/2015	93
MG02	82.463561	-80.429472	07/2012 - 07/2013	288
			07/2013 - 07/2014	64
			07/2014 - 07/2015	61
MG03	82.528931	-80.673765	07/2012 - 07/2013	295
			07/2013 - 07/2014	63
			07/2014 - 07/2015	na

* Positions are given at the time of ablation stake installation in July 2012.

Table 4.2 Values of physical constants and parameterizations used in ocean thermodynamic ice shelf ablation model.

Symbol	Value	Units	Description
ρ_i	900	kg m^{-3}	Density of ice
L_i	334 000	J kg^{-1}	Latent heat of fusion of ice
ρ_w	1024	kg m^{-3}	Density of seawater
c_w	3974	J °C^{-1} kg^{-1}	Specific heat capacity of seawater
c_i	2009	J °C^{-1} kg^{-1}	Specific heat capacity of ice
T_i	-15	°C	Internal ice shelf temperature
C_d	0.01		Drag coefficient
$\Gamma_{(TS)}$	0.006		Turbulent transfer coefficient

Table 4.3 Submarine melt rates (m a^{-1}) in Milne Fiord from 2011 to 2015.

	Grdln flux	Divergence of ice flux		Ocean therm. model		
Year	MGT	MGT	MGT (2.5 km)	MGT	MGT (2.5 km)	MIS
2011	0.2±0.4	0.6±2.5	6.0±1.9	1.2±1.1	3.0±1.3	1.2±0.8
2012	0.0±0.4	-0.2±0.5	0.9±0.3	1.5±1.1	3.3±1.4	1.6±0.8
2013	-0.2±0.3	-0.1±1.4	3.0±0.9	1.7±1.0	2.6±1.0	1.6±0.7
2014	0.0±0.3	0.3±2.0	4.6±1.4	1.6±1.3	3.3±1.6	1.1±0.8
2015	0.2±0.4	0.2±1.9	4.4±1.7	2.2±1.6	3.7±1.8	1.3±1.0

The three methods used to calculate submarine melt rates are the grounding line flux, the width-averaged divergence of ice flux, and the ocean thermodynamic melt model. Values reported are area-averaged for the entire Milne Glacier tongue (66 km^2), the first 2.5 km downstream of the grounding line where melt rates are highest, and the Milne Ice Shelf (215 km^2). One standard deviation is shown.

4.7 Figures

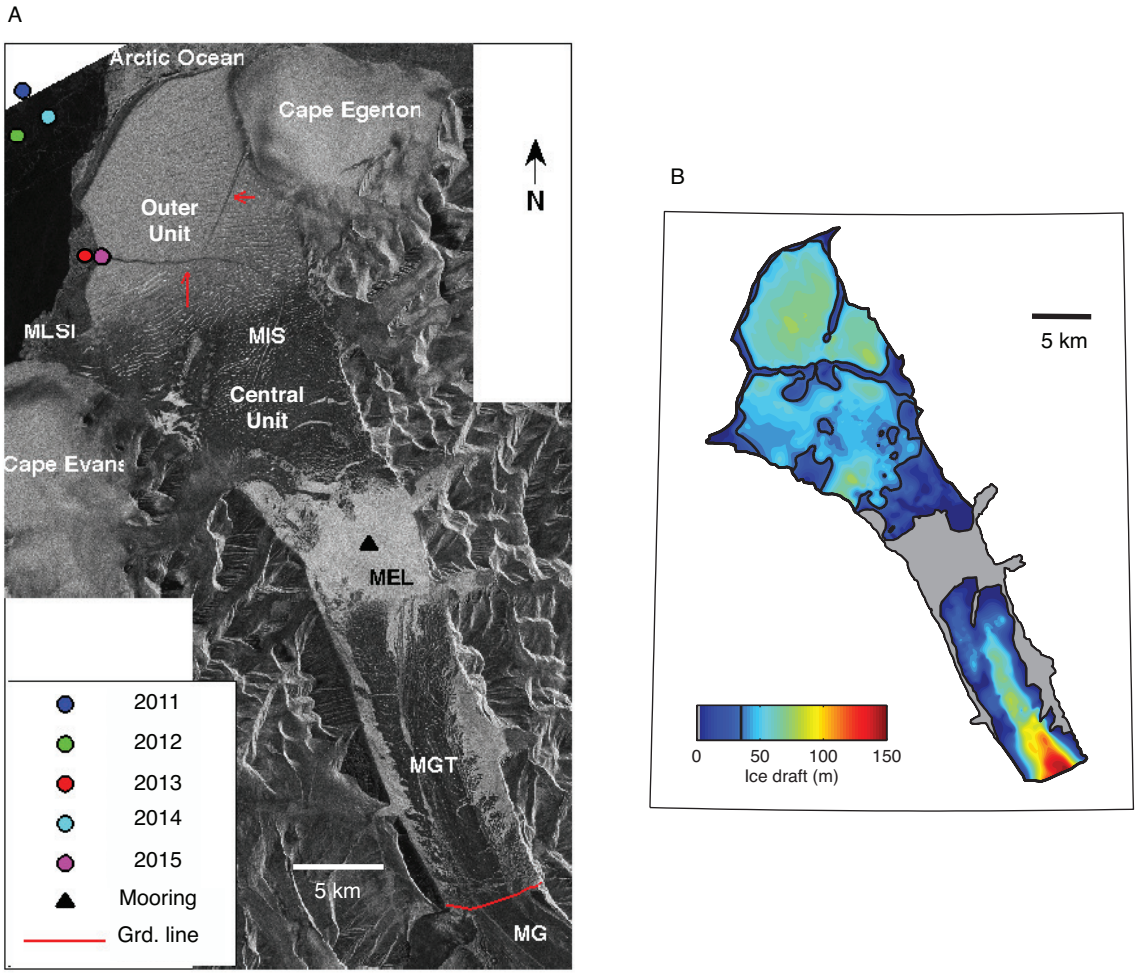

Figure 4.1 Map of Milne Fiord. In A) locations of ocean profiles (coloured circules) collected between 2011 and 2015 are overlain on a RADARSat-2 image acquired in January 2015. Note that profiles were collected at the mooring site (black triangle) in Milne Fiord in all years. Labeled features include the Milne Glacier (MG), the Milne Glacier tongue (MGT), the Milne Fiord epishelf lake (MEL), the Milne Ice Shelf (MIS), and multiyear land-fast sea ice (MLSI). The grounding line of the Milne Glacier is shown in red. B) Digital elevation model of ice draft in Milne Fiord. Grey area indicates thin ($\sim$1 m) epishelf lake ice.

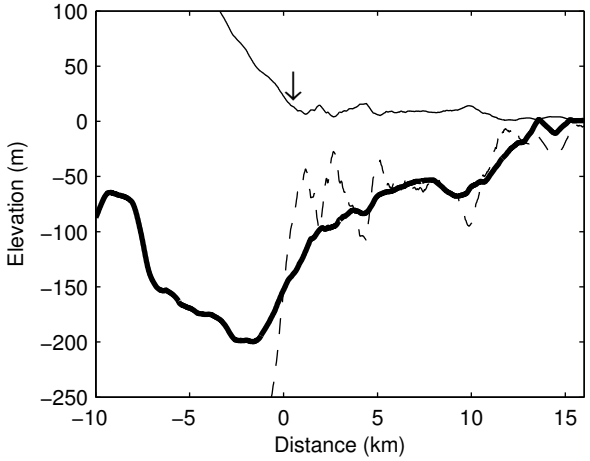

Figure 4.2 Surface and bed elevations along a profile of the MGT. Data are from the NASA IceBridge 2014 aerial survey, with surface elevations (thin solid line) from the airborne topographic mapping (ATM) and bottom elevations (thick solid line) from the Multichannel Coherent Radar Depth Sounder (MCoRDS). The position of the grounding line is the point of first hydrostatic equilibrium of the ice where the thickness calculated from the surface elevation (dashed line) crosses that measured by the MCoRDs. Note the aerial survey line crossed over from the central stream of the Milne Glacier to the highly fractured north-east tributary stream $\sim$100 m downstream of the grounding line for 5 km, so surface elevation-derived thicknesses along this section are variable and are not representative of the central ice stream.

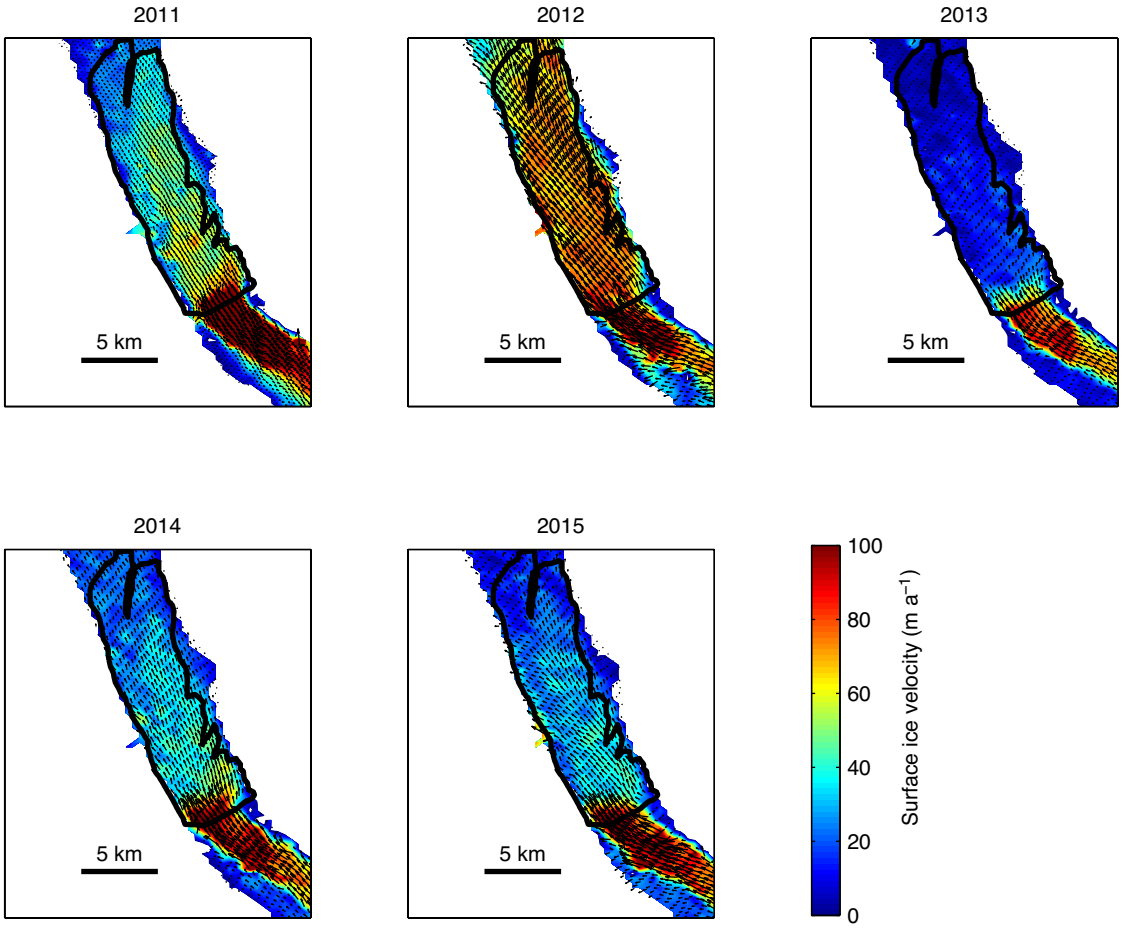

Figure 4.3 Surface ice speed for the Milne Glacier from 2011 to 2015. The model domain used for area-averaged basal melt calculations for the MGT (shown in Fig. 4.7) is marked by the black line. Velocity data is reproduced with permission from Van Wychen et al. (2016).

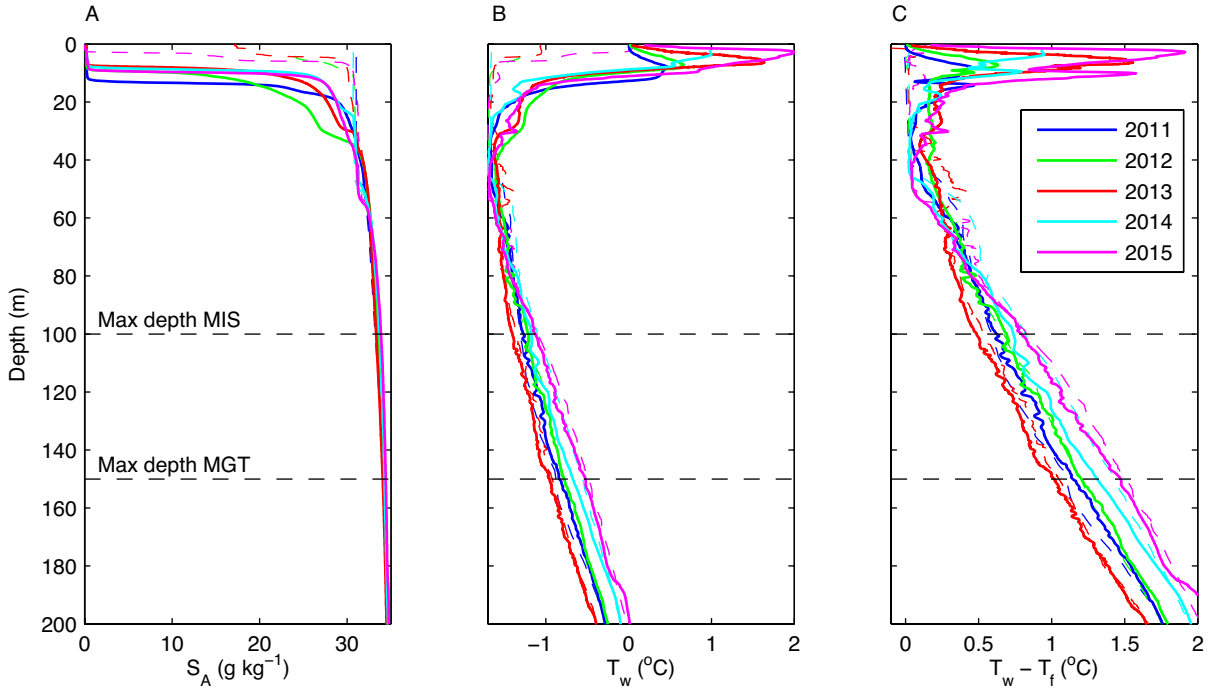

Figure 4.4 Profiles of A) Absolute Salinity (S_A), B) in situ temperature (T_w), and C) temperature above freezing ($T_w - T_f$) in Milne Fiord from 2011 to 2015. Solid lines indicate profiles collected in Milne Fiord at the mooring site, dotted lines are profiles collected offshore (see Fig. 4.1 for locations).

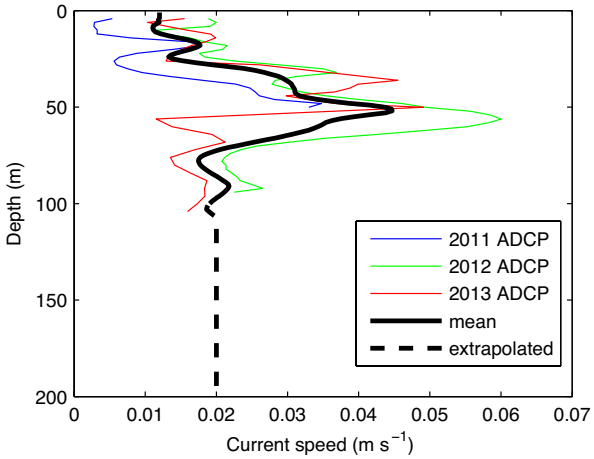

Figure 4.5 Time-averaged current speeds in Milne Fiord. Profiles were collected at the mooring site using an 300 kHz ADCP in May 2011, and July of 2012 and 2013. Input to the ice-ocean model is the average observed velocity from all years from 1 to 100 m depth (solid black line), and an extrapolated velocity below 100 m (dashed black line).

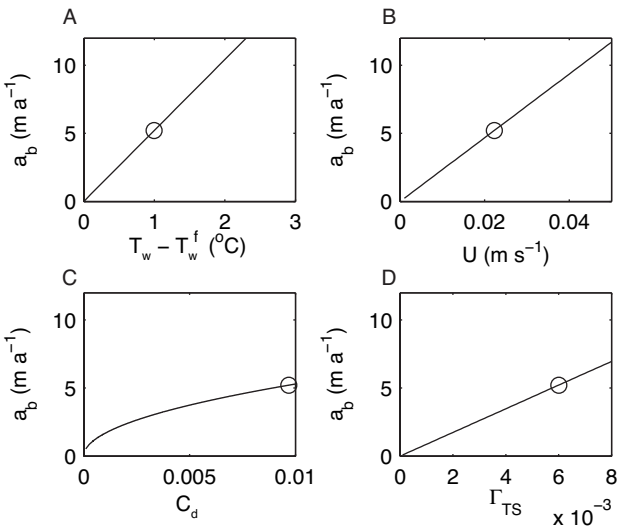

Figure 4.6 Melt rate dependence on the A) thermal driving ($T_w - T_w^f$), B) mixed layer speed (U), C) drag coefficient (C_d), and D) turbulent transfer coefficient (Γ_{TS}). The x-axis limits of each variable are equivalent to the likely range of values in Milne Fiord or in the literature. For each run other variables were fixed at the actual value used in the model (circle), except for $T_w - T_w^f$ which was fixed at 1°C, and U which was fixed at the depth-integrated average of the velocity profile shown in Fig. 4.5.

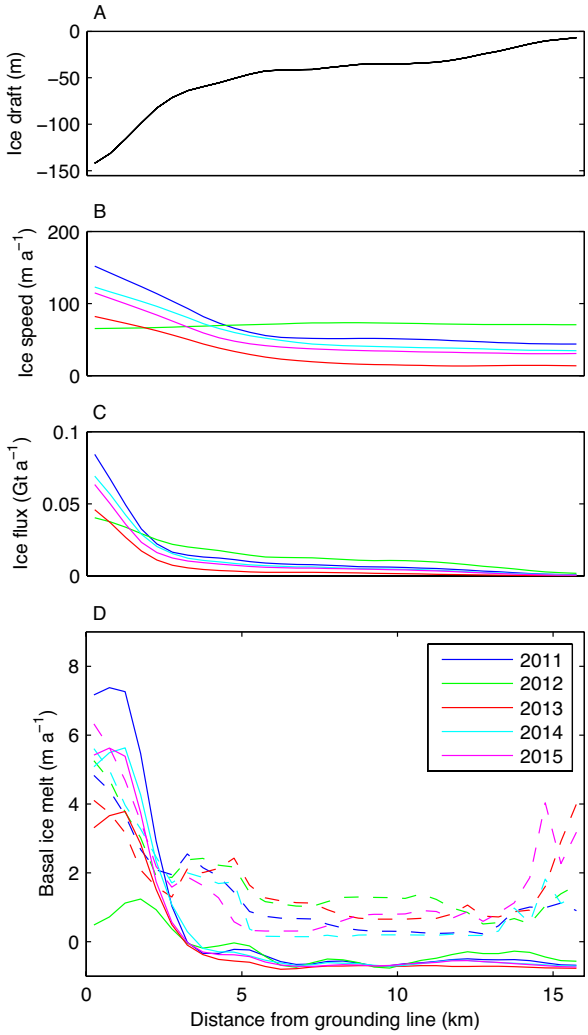

Figure 4.7 Area-averaged submarine melt along the length of the MGT for years 2011 to 2015. Cross-fjord average A) ice draft, B) ice speed, C) ice flux, and D) submarine melt rate vs distance from the Milne Glacier grounding line. The domain used for calculation is shown in Fig. 4.3. Lines in B), C), & D) are coloured by year. Shown in D) are the submarine melt rates calculated by the divergence of ice flux method (solid lines) and the ocean thermodynamic method (dashed lines) for each year.

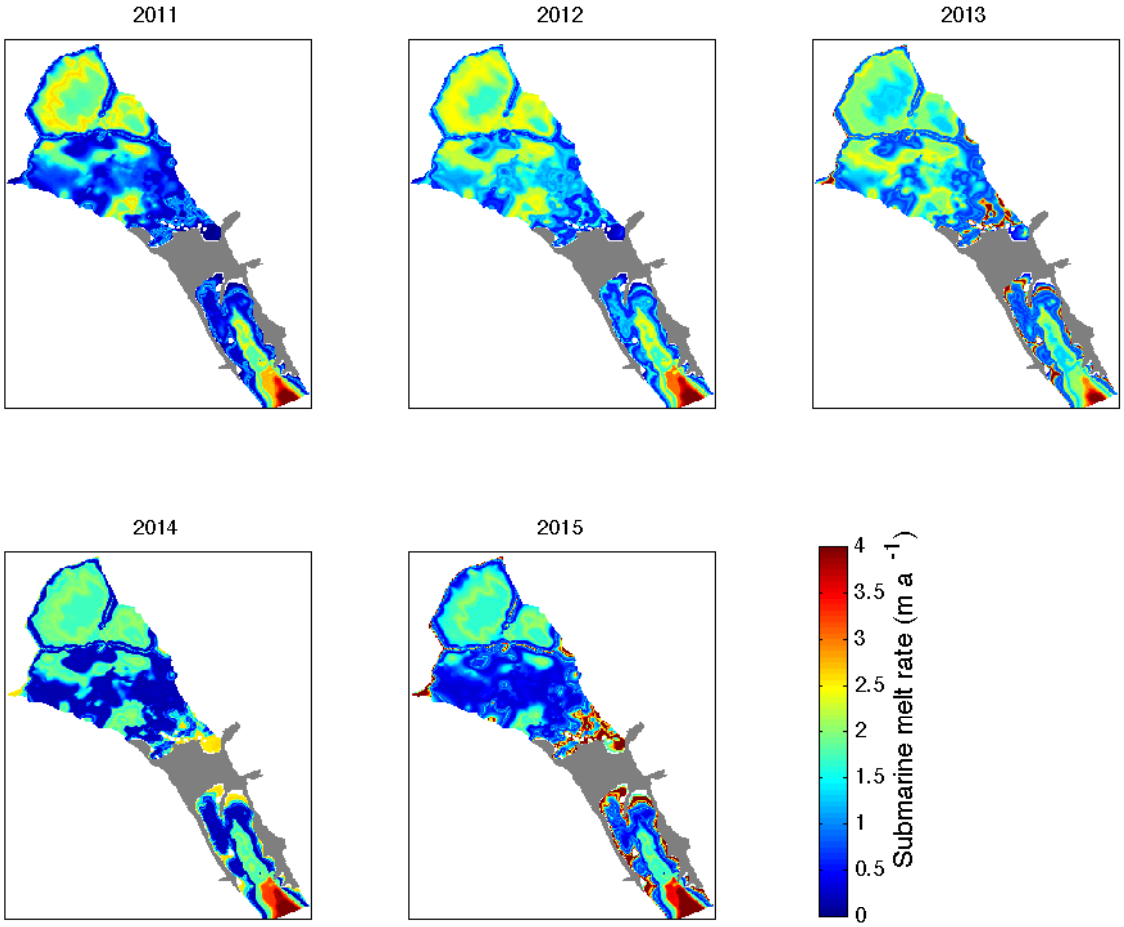

Figure 4.8 Submarine ice melt rates in Milne Fiord from 2011 to 2015 calculated using the ocean thermodynamic model based on ocean profiles collected at the mooring site in the fjord. The grey area indicates the area of the epishelf lake where melt rates were not calculated.

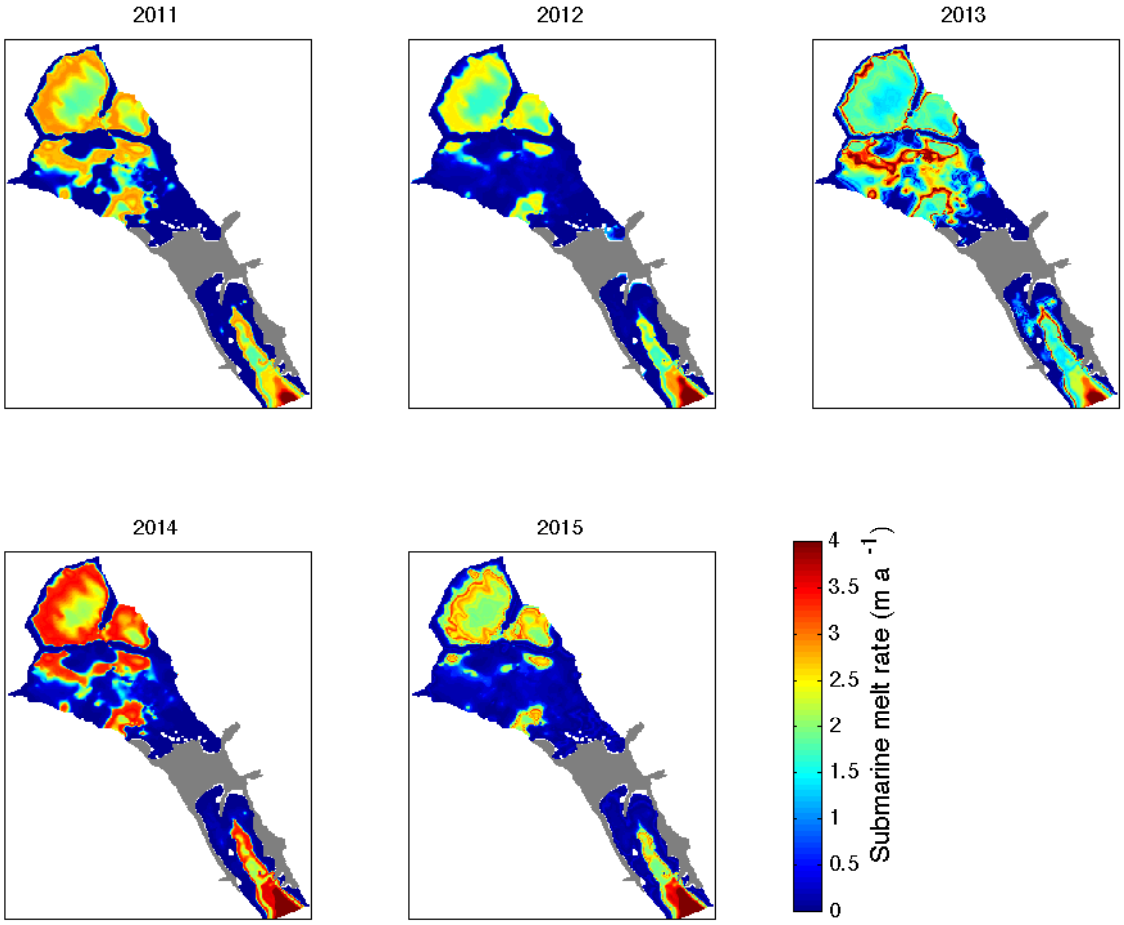

Figure 4.9 Submarine ice melt rates in Milne Fiord from 2011 to 2015 calculated using the ocean thermodynamic model based on profiles collected offshore. The grey area indicates the area of the epishelf lake where melt rates were not calculated.

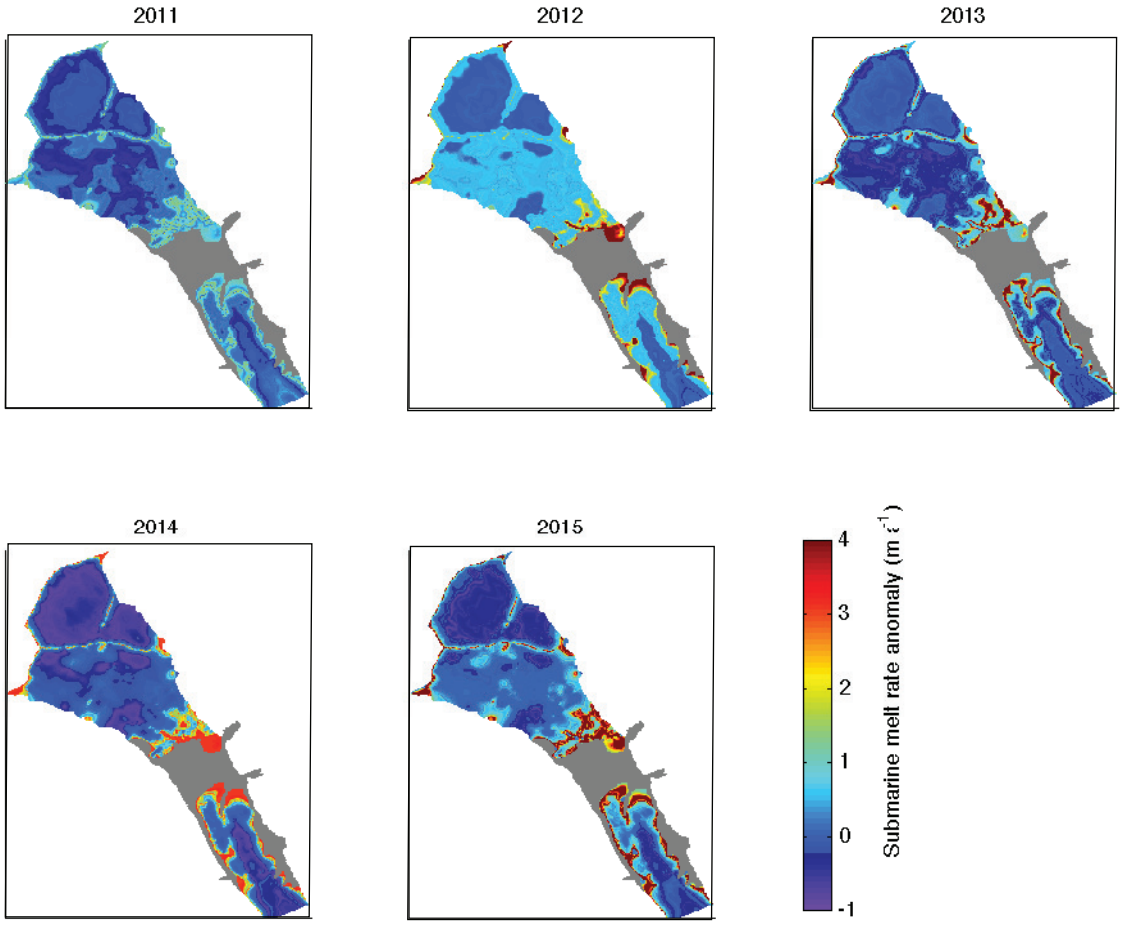

Figure 4.10 Difference in submarine ice melt rates in Milne Fiord from 2011 to 2015 calculated using the ocean thermodynamic model between profiles collected at the mooring site in the fjord versus profiles collected offshore. The grey area indicates the area of the epishelf lake where melt rates were not calculated.

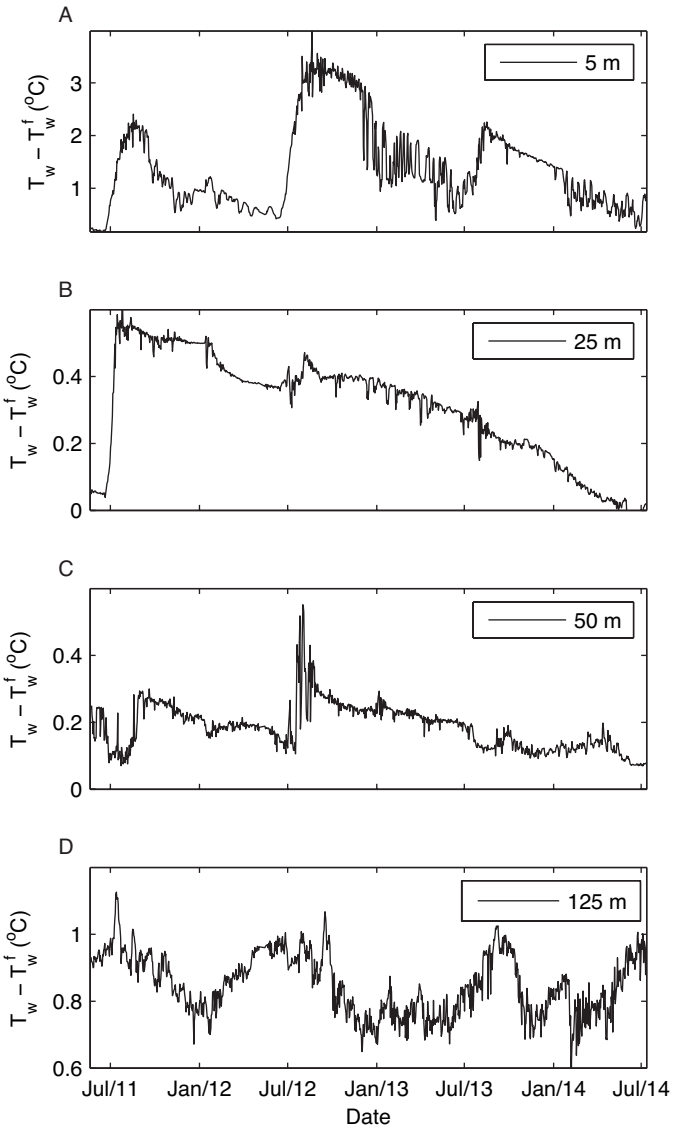

Figure 4.11 Variation in thermal driving ($T_w - T_w^f$) over from May 2011 to July 2014 at A) 5 m, B) 25 m, C) 50 m, and D) 125 m depths. The y-axes scales are equal in B), C) and D), allowing for direct comparison of the magnitude of variability at these depths, although the origins are offset. The y-scale in A) is different given the substantially larger variation.

Chapter 5

Conclusions

5.1 Summary

This thesis has demonstrated the importance of ice-ocean interactions in determining the water properties and circulation in a glacial fjord. Field and analytical methods were used to describe the spatial and temporal variation of water column structure, circulation, and submarine melting in Milne Fiord between 2011 and 2015. The thesis began by setting the geophysical context of the fjord, then provided a general description of the horizontal and temporal variation of water properties and how they were influenced by interaction with ice. Next, factors influencing the seasonal and long-term dynamics of the Milne Fiord epishelf lake, the last remaining epishelf lake in the Arctic, were investigated. Finally, the magnitude and spatial variations of submarine melt rate of an ice shelf and glacier tongue were estimated.

Chapter 2 provided an overall description of the geophysical and oceanographic properties of Milne Fiord. By undertaking an extensive field study I was able to produce the first comprehensive map of both the ice topography and bathymetry over the entire fjord. This provided the critical context in which the oceanographic observations could be interpreted. The vertical distribution of water masses in the fjord reflected the general structure of the adjacent Arctic Ocean, consisting of Polar Water above Atlantic Water. However, I found that the Milne Ice Shelf had a profound impact on both the vertical structure and circulation in the fjord. Inflow of freshwater at the surface was trapped by the ice shelf, creating the epishelf lake, while upwelling of subglacial runoff created an intermediate layer termed fjord-modified water. Export of fjord-modified water was restricted to a narrow basal channel in the ice shelf, resulting in a prolonged (by several months) drainage from the fjord over winter. This effectively de-coupled the timing of freshwater export from the seasonal cycle of meltwater production at the surface. Intermediate water properties varied substantially over broad timescales, from days to months, likely reflecting depth variation of the main Arctic halocline offshore being transmitted into the fjord under the ice shelf. I also inferred the presence of a sill

under the ice shelf from hydrographic data, and presented evidence of a renewal of deep water below sill depth in Milne Fiord.

The work presented in Chapter 2 demonstrated the strong impact that an ice shelf could have on fjord oceanography. The loss of the Milne Ice Shelf will fundamentally alter the water properties and circulation of the fjord, with consequences for the stability and dynamics of the Milne Glacier. The Milne Ice Shelf is the last remaining intact ice shelf along the northern coast of Ellesmere Island, and the observations presented here provide a valuable reference to understand future oceanographic changes in the fjord after the inevitable collapse of the ice shelf.

Chapter 3 related an investigation of the seasonal and long-term dynamics of the last remaining Arctic epishelf lake. Continuous mooring records from the lake revealed that the halocline varied by several meters each year. It was determined this was due to the balance between the volume of meltwater inflow, a function of the intensity of summer surface melt, and hydraulically controlled outflow under the ice shelf, a function of the geometry of the outflow channel. On a long-term basis the depth of the lake was dependent on the thickness of the ice shelf, and the interannual shoaling of the halocline suggested a long-term thinning of the Milne Ice Shelf. However, it was also shown that episodic events that provide sufficient kinetic energy to the system, such as the calving or capsize of an iceberg, could induce mixing of the halocline, thereby altering the depth of the lake.

The findings in Chapter 3 strongly suggest that a full consideration of the hydrology and hydraulics of an epishelf lake must be undertaken where hydrographic profiles are used to infer the thickness of the impounding ice shelf. Epishelf lakes are much more dynamic than previously thought, which also has important implications for the ecology of these rare aquatic ecosystems.

Chapter 4 discussed efforts to estimate submarine melting in Milne Fiord. An average melt rate of $\sim$4 m a^{-1} near the grounding line of the Milne Glacier was found, as was an enhanced near-surface melt rate of $\sim$2 m a^{-1} for ice in contact with the epishelf lake. This finding indicated a depth-dependence of melt rates due, in part, to the vertical distribution of the water temperature above freezing, or thermal driving, in the fjord. The melt rate depth-dependence suggested a complex spatial patterns of basal melting on the Milne Ice Shelf, owing to its variable ice thickness. However, the relationship between melt rate and thermal driving in Milne Fiord was not linear (e.g. the epishelf lake had higher average thermal driving than water near the grounding line, yet the grounding line showed higher melt rates), indicating other factors, notably circulation, were also important in determining melt rates.

The work in Chapter 4 has confirmed that knowledge of current speeds and their variation are fundamental for predicting melt rates and ice-ocean interaction processes in glacial fjords. The results suggest efforts to measure circulation, and its spatial and temporal variation, will be invaluable for more accurate prediction of melt rates. This is particularly important as surface runoff is predicted to continue to increase in the Canadian Arctic Archipelago (CAA; Lenaerts et al., 2013) which is likely to impact buoyancy-driven circulation in tidewater glacial fjords. The submarine

melt rates presented in Chapter 4 are, to the best of my knowledge, the first direct estimates of submarine melt rates for an ice shelf or tidewater glacier in the CAA. The work indicates that processes that alter the vertical distribution of heat in the fjord or circulation patterns, including the collapse of the Milne Ice Shelf, will change the rate and distribution of melting of the Milne Glacier tongue.

The present state of knowledge of Milne Fiord, based on this thesis, is summarized schematically in Figure 5.1. The Milne Ice Shelf is partially grounded on a bathymetric ridge near the mouth of the fjord. There is no freshwater outflow or exchange above the minimum draft of the ice shelf ($\sim$10 m). The epishelf lake, which seasonally deepens by several meters during summers of intense surface melt, drains over several months after the summer melt season along a basal channel in the ice shelf, its rate hydraulically controlled by the dimensions of the channel and the excess depth of the lake below the ice. Warm waters of the epishelf lake are enhancing submarine melting along the landward edge of the ice shelf and around the margins of the glacier tongue. Water exchange across the ice shelf is restricted down to approximately 50 m depth, creating a relatively fresh, warm layer in the fjord that is termed fjord-modified water. Fjord-modified water is also slowly exported along the basal channel in the ice shelf. The source of the fjord-modified water is largely subglacial discharge plume, which enter the fjord at the grounding line of the Milne Glacier, mix with ambient water on their ascent, but do not reach the surface due to the strong stratification imposed by the presence of the epishelf lake, and are consequently exported at depth through the basal channel in the Milne Ice Shelf. Relatively free exchange of water occurs below the ice shelf to the depth of the bathymetric sill, resulting in vertical excursions of water masses, particularly the interface between Polar Water and Atlantic Water, in the fjord that are driven by offshore processes. The warm water of the Atlantic layer drives the highest submarine melt rates at the glacier grounding line, leading to a retreat of the grounding line. Below the sill, deep water of the fjord is relatively homogenous, with evidence of complete deep water renewal events that occur with an as yet unknown frequency.

Milne Fiord presently retains the last intact ice shelf, the last deep epishelf lake, and the last extensive glacier tongue on the northern coast of Ellesmere Island. However, until very recently these features were widespread on this coast: in 2000 there were 6 major ice shelves (Ayles, Markham, Milne, Petersen, Serson, and Ward Hunt), at least two (Milne and Ward Hunt) were known to dam deep ($>$10 m) epishelf lakes, while the others were associated with shallower epishelf or ice-dammed lakes (Veillette et al., 2008; White et al., 2015b), and there were at least two extensive ($>$10 km) glacier tongues (Milne and Yelverton Bay; Copland et al., 2015). Even these features however, are just remnants of what was once a continuous ice shelf that extended at least 500 km along this coast in the late 19$^{\text{th}}$ century (Vincent et al., 2001), that Veillette et al. (2008) suggest may have retained up to 17 epishelf lakes, and a larger number of the 11 major tidewater glaciers along this coast (Copland et al., 2015) may have terminated in glacier tongues. The present-day geophysical setting of Milne Fiord, and the oceanographic processes described in this thesis, may be representative what was once a common system along this coast.

5.2 Future directions

The findings presented in this thesis have answered many of the questions that originally motivated the research. There remain, however, a number of unanswered questions that ongoing and future efforts aim to resolve. The findings have also raised a number of important new questions that could motivate future research directions.

One of the most unexpected findings, presented in Chapter 2, was the discovery that the MIS may be partially grounded on a sea bed ridge. If so, this could explain both the origin of the main re-healed fractures in the ice shelf and provide an explanation for the ice shelf's relative stability compared to others along this coast. Confirmation that the ice shelf is actually grounded, and over what extent, will help constrain the fate of the ice shelf and inform the possible mechanisms of future breakup.

The results of the hydraulic drainage model presented in Chapter 3 strongly suggest that epishelf lake outflow occurs along the basal channel in the MIS, which preliminary field observations appear to support. If confirmed, the geometry of the channel must be further constrained along its length, and measurements of water properties and flow rates will be needed to validate, or refute, the drainage theory. Another important aspect necessitating further study is to investigate how the mechanics and thermodynamics of stratified flow influence melting or freezing along the channel walls and ceiling. A better understanding of this process will provide insight into the variation of the depth of the epishelf lake and preferential melting in basal channels as a mechanism contributing to the breakup of Ellesmere Island ice shelves (Mueller et al., 2003) and leading to highly complex patterns of melt on Antarctic ice shelves (Dutrieux et al., 2013).

Submarine melt rates are strongly influenced by the transport of heat along a fjord and through the boundary layer at the ice-ocean interface. The melt rates estimated using the ocean model in Chapter 4 were based on limited field measurements, requiring broad assumptions about the water properties and circulation under the glacier tongue and ice shelf. The model also required the use of parameterizations that have not been validated for Milne Fiord. Despite these acknowledged limitations the magnitude and distribution of melt predicted for the Milne Glacier tongue generally compared well with those based on the independent divergence of ice flux method, suggesting the assumptions applied were not unrealistic. However, it is clear that improved measurements of circulation, both at the scale of the entire fjord, including intermediary exchange flows and buoyancy-driven circulation, but also proximal to the ice face, including near subglacial outlet channels, are required to more accurately model melt rates. Direct measurements of basal ablation, ocean properties, and currents through the oceanic boundary layer below ice shelves are also required to refine the turbulent transfer and drag coefficients used in the ocean model. These measurements must be acquired in systems appropriate for use in Milne Fiord, that is highly stratified, low energy environments, with similar ice roughness characteristics. If parameterizations are validated, then numerical modelling could provide a valuable tool for understanding the contribution of basal melt to total ice

mass balance in Milne Fiord.

In addition to improved estimates of basal ablation, proper mass balance estimates for the Milne Ice Shelf and Milne Glacier tongue require better resolved, in space and time, measurements of surface ablation. The ablation stake network used in this study was extremely sparse, but the available data indicated there is an along-fjord gradient in surface mass balance with greater accumulation toward the coast on the Outer Unit of the Milne Ice Shelf. Production of repeat, annual high resolution surface elevation models from remote sensing data, calibrated against the existing ablation stake network, would dramatically enhance understanding of surface mass balance, and thus further constrain the contribution of basal melt to total mass balance of the ice shelf and glacier tongue.

Expansion of surface mass balance estimates throughout the Milne Glacier catchment would allow for more precise estimates of surface meltwater into the fjord. This would improve the understanding of both inflow to the epishelf lake, as well as the volume of subglacial discharge. As surface melt is predicted to increase with climate warming, buoyancy-driven circulation and convection-driven melting at the grounding line of the Milne Glacier may be increasingly important, indicating a well-constrained estimate of freshwater input to the fjord is critical to understanding how the dynamics of the fjord will evolve in the future, and how this may effect the stability of ice in the fjord.

Water properties and circulation in Milne Fiord are also strongly dependent on variations of water mass structure and circulation on the continental shelf. How large-scale and long-term changes to ocean properties in the Arctic Ocean are transmitted into Milne Fiord, and what effect this may have on the dynamics of the fjord is unknown. The dynamics of fjords on Ellesmere Island are linked to regional changes in the ocean, atmosphere, and cryosphere, so an interdisciplinary broad-scale view of these processes could help inform the factors driving the observed local changes along this coast.

The eventual collapse of the Milne Ice Shelf, and the loss of the epishelf lake, will have a profound impact on fjord water properties and circulation. These changes are shown schematically in Figure 5.2. Some of the changes predicted to occur include weaker stratification of the upper water column, seasonal export of runoff at the surface, and a transition from perennial to seasonal ice cover. These changes will impact, among other processes, the vertical distribution of heat, buoyancy-driven circulation, wind-mixing of the water column, and wave erosion of the glacier tongue. Ultimately, the loss the Milne Ice Shelf is expected to lead to a collapse of the Milne Glacier tongue with implications for the dynamics of the Milne Glacier. Long-term monitoring of Milne Fiord during its transition from an ice shelf-epishelf lake-glacier tongue system to a seasonally ice covered tidewater glacier system could provide rare insight into the dynamics of glacial fjords.

5.3 Figures

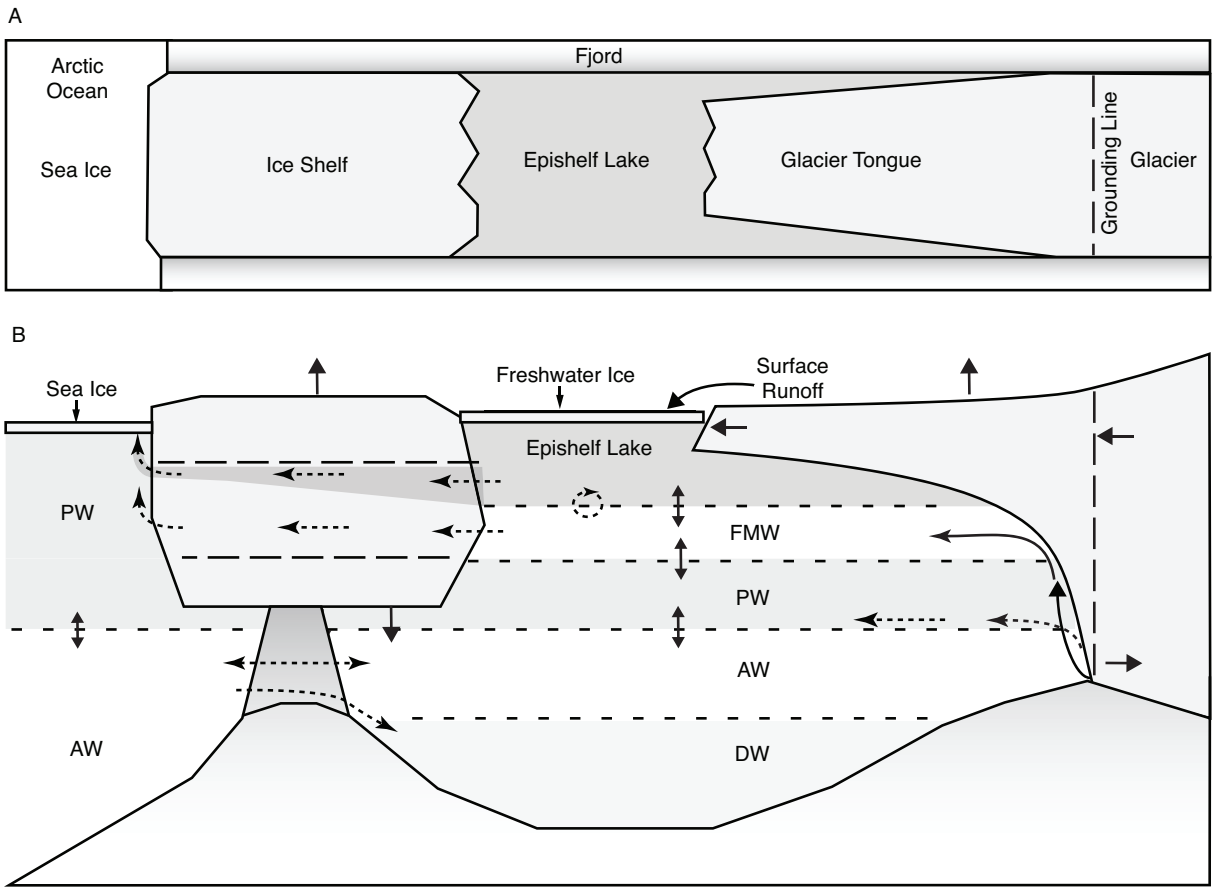

Figure 5.1 Schematic representation of Milne Fiord at present in A) plan and B) elevation view showing known ice features and oceanographic properties based on the work detailed in this thesis. See text for discussion. Water masses are labelled: PW - Polar Water, AW - Atlantic Water, FMW - fjord modified water, DW - deep water.

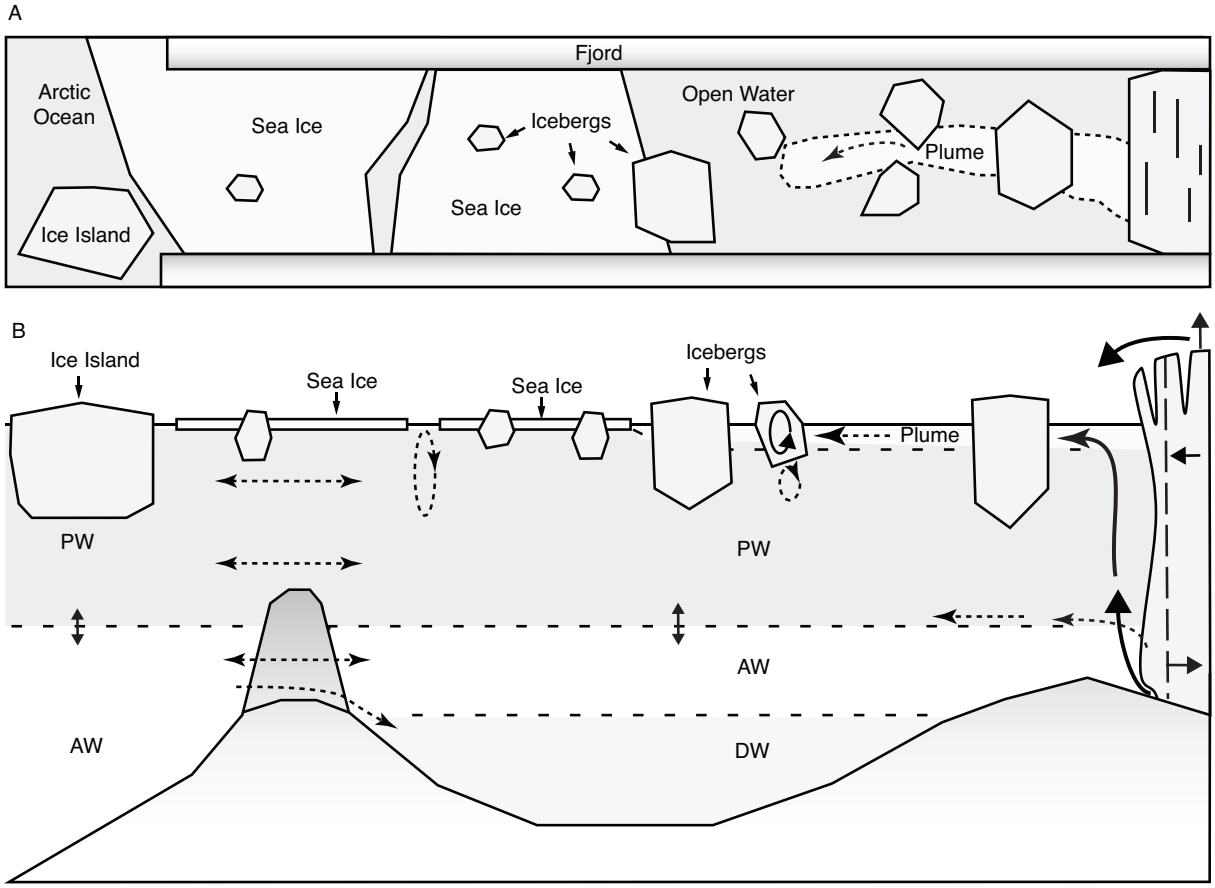

Figure 5.2 Schematic representation of the future of Milne Fiord in A) plan and B) elevation view showing collapse of ice features and associated oceanographic changes. See text for discussion. Water masses are labelled: PW - Polar Water, AW - Atlantic Water, DW - deep water.

Bibliography

Aagaard, K., Coachman, L. K., and Carmack, E. (1981). On the halocline of the Arctic Ocean. *Deep Sea Research Part A. Oceanographic Research Papers*, 28(6):529–545. → pages 5

Aksenov, Y., Bacon, S., Coward, A. C., and Holliday, N. P. (2010). Polar outflow from the Arctic Ocean: A high resolution model study. *Journal of Marine Systems*, 83(1-2):14–37. → pages 5, 24, 25

Alkire, M., Falkner, K., Boyd, T., and Macdonald, R. (2010). Sea ice melt and meteoric water distributions in Nares Strait, Baffin Bay, and the Canadian Arctic Archipelago. *Journal of Marine Research*, 68(6):767–798. → pages 30

Antoniades, D., Francus, P., Pienitz, R., St-Onge, G., and Vincent, W. F. (2011). Holocene dynamics of the Arctic's largest ice shelf. *Proceedings of the National Academy of Sciences of the United States of America*, 108(47):18899–18904. WOS:000297249800016. → pages 6

Braithwaite, R. J. (2005). Mass-balance characteristics of arctic glaciers. *Annals of Glaciology*, 42(1):225–229. → pages 4

Braun, C., Hardy, D. R., Bradley, R. S., and Sahanatien, V. (2004). Surface mass balance of the Ward Hunt Ice Rise and Ward Hunt Ice Shelf, Ellesmere Island, Nunavut, Canada. *Journal of Geophysical Research: Atmospheres*, 109(D22). → pages 7, 24, 114

Burton, J. C., Amundson, J. M., Abbot, D. S., Boghosian, A., Cathles, L. M., Correa-Legisos, S., Darnell, K. N., Guttenberg, N., Holland, D. M., and MacAyeal, D. R. (2012). Laboratory investigations of iceberg capsize dynamics, energy dissipation and tsunamigenesis. *Journal of Geophysical Research: Earth Surface*, 117(F1):n/a–n/a. → pages 80

Carmack, E. C. (1990). Large-Scale Physical Oceanography of Polar Oceans. In Smith, W. O., editor, *Polar Oceanography*, pages 171–222. Academic Press, San Diego. → pages 5, 112

Cenedese, C. and Linden, P. F. (2014). Entrainment in two coalescing axisymmetric turbulent plumes. *Journal of Fluid Mechanics*, 752:R2 (12 pages). → pages 11, 117

Chauch, N., Hubbard, A., Gascard, J.-C., Box, J. E., Bates, R., Koppes, M., Sole, A., Christoffersen, P., and Patton, H. (2014). Iceocean interaction and calving front morphology at two west Greenland tidewater outlet glaciers. *The Cryosphere*, 8(4):1457–1468. → pages 23, 36

Christoffersen, P., Mugford, R. I., Heywood, K. J., Joughin, I., Dowdeswell, J. A., Syvitski, J. P. M., Luckman, A., and Benham, T. J. (2011). Warming of waters in an East Greenland fjord

prior to glacier retreat: mechanisms and connection to large-scale atmospheric conditions. *The Cryosphere*, 5(3):701–714. → pages 9, 23

Copland, L., Dalton, A., White, A., Van Wychen, W., and Dawson, J. (2015). Patterns of glacier disintegration and iceberg production in Yelverton Bay and Inlet, northern Ellesmere Island. In *ArcticNet Annual Scientific Meeting*, Vancouver, Canada. → pages 1, 2, 46, 134

Copland, L., Mueller, D. R., and Weir, L. (2007). Rapid loss of the Ayles Ice Shelf, Ellesmere Island, Canada. *Geophysical Research Letters*, 34(L21501):6. → pages 2, 5, 6, 22, 46, 62, 98

Copland, L., Sharp, M. J., and Dowdeswell, J. A. (2003). The distribution and flow characteristics of surge-type glaciers in the Canadian High Arctic. *Annals of Glaciology*, 36(1):73–81. → pages 25, 99, 112

Cottier, F., Tverberg, V., Inall, M., Svendsen, H., Nilsen, F., and Griffiths, C. (2005). Water mass modification in an Arctic fjord through cross-shelf exchange: The seasonal hydrography of Kongsfjorden, Svalbard. *Journal of Geophysical Research-Oceans*, 110(C12). WOS:000234248800001. → pages 18

Cottier, F. R., Nilsen, F., Skogseth, R., Tverberg, V., Skarhamar, J., and Svendsen, H. (2010). Arctic fjords: a review of the oceanographic environment and dominant physical processes. *Geological Society, London, Special Publications*, 344(1):35–50. → pages 8

Crary, A. (1956). Geophysical studies along northern Ellesmere Island. *Arctic*, 9(3):154–165. → pages 7, 24, 62

Dutrieux, P., Vaughan, D. G., Corr, H. F. J., Jenkins, A., Holland, P. R., Joughin, I., and Fleming, A. H. (2013). Pine Island glacier ice shelf melt distributed at kilometre scales. *The Cryosphere*, 7(5):1543–1555. → pages 135

England, J. H., Lakeman, T. R., Lemmen, D. S., Bednarski, J. M., Stewart, T. G., and Evans, D. J. A. (2008). A millennial-scale record of Arctic Ocean sea ice variability and the demise of the Ellesmere Island ice shelves. *Geophysical Research Letters*, 35(19). WOS:000259803300002. → pages 62

Evans, D. and England, J. (1992). Geomorphological evidence of Holocene climatic change from northwest Ellesmere Island, Canadian high arctic. *The Holocene*, 2(2):148–158. → pages 6

Farmer, D. M. and Freeland, H. J. (1983). The physical oceanography of Fjords. *Progress In Oceanography*, 12(2):147–219. → pages 8, 9, 10, 35

Ford, W. L. and Hattersley-Smith, G. (1965). On the oceanography of the Nansen Sound fiord system. *ARCTIC*, 18(3):158–171. → pages 4, 23, 24

Gade, H. G. (1979). Melting of Ice in Sea Water: A Primitive Model with Application to the Antarctic Ice Shelf and Icebergs. *Journal of Physical Oceanography*, 9:189–198. → pages 29

Galton-Fenzi, B. K., Hunter, J. R., Coleman, R., and Young, N. (2012). A decade of change in the hydraulic connection between an Antarctic epishelf lake and the ocean. *Journal of Glaciology*, 58(208):223–228. → pages 8

Gardner, A., Moholdt, G., Wouters, B., Wolken, G., Burgess, D., Sharp, M., Cogley, J., Braun, C., and Labine, C. (2011). Sharply increased mass loss from glaciers and ice caps in the Canadian Arctic Archipelago. *Nature*, 473(7347):357–360. → pages 2, 4, 23, 46, 98, 114, 115

Gardner, A. S., Moholdt, G., Cogley, J. G., Wouters, B., Arendt, A. A., Wahr, J., Berthier, E., Hock, R., Pfeffer, W. T., Kaser, G., Ligtenberg, S. R. M., Bolch, T., Sharp, M. J., Hagen, J. O., van den Broeke, M. R., and Paul, F. (2013). A Reconciled Estimate of Glacier Contributions to Sea Level Rise: 2003 to 2009. *Science*, 340(6134):852–857. → pages 81, 98, 114

Geyer, W. and Cannon, G. (1982). Sill processes related to deep water renewal in a fjord. *Journal of Geophysical Research*, 87(C10):7985–7996. → pages 35

Gibson, J. and Andersen, D. (2002). Physical structure of epishelf lakes of the southern Bunger Hills, East Antarctica. *Antarctic Science*, 14(3):253–261. → pages 7, 8, 62, 63

GLIMS and NSIDC (2005). GLIMS Glacier Database, Version 1. Technical report, NSIDC: National Snow and Ice Data Center, Boulder, Colorado USA. → pages 25, 64

Hattersley-Smith, G. (1957). The Ellesmere Ice Shelves and the Ice Islands. *Canadian Geographer*, 3(9):65–70. → pages 6

Hattersley-Smith, G. (1969). Results of radio echo sounding in Northern Ellesmere Island, 1966. *Geographical Journal*, 135(4):553–557. → pages 25

Hattersley-Smith, G. (1973). Ice Shelf and Fiord Ice Problems in Disraeli Fiord, Northern Ellesmere Island, NWT. Technical report, Defence Research Board, Department of National Defence Canada, Ottawa, Canada. → pages 7, 63

Hattersley-Smith, G. and Fuzesy, A. (1969). Glacier Depths in Northern Ellesmere Island: Airborne Radio Echo Sounding in 1966. Technical Note, Defence Research Board, Department of National Defence Canada, Ottawa, Canada. → pages 25, 40

Hattersley-Smith, G. and Serson, H. (1966). Reconnaissance oceanography over the ice of the Nansen Sound Fiord System. Technical Report 28, Defense Research Board of Canada, Directorate of Physical Research, Geophysics, Hazen, Ottawa. → pages 4

Hellmer, H. and Olbers, D. (1989). A two-dimensional model for the thermohaline circulation under an ice shelf. *Antarctic Science*, 1(04):325–336. → pages 102, 103

Heywood, R. B. (1977). A Limnological Survey of the Ablation Point Area, Alexander Island, Antarctica. *Philosophical Transactions of the Royal Society of London. B, Biological Sciences*, 279(963):39–54. → pages 6, 7, 62

Hock, R. (2003). Temperature index melt modelling in mountain areas. *Journal of Hydrology*, 282(1-4):104–115. → pages 32, 67

Holland, D. M. (1998). On the parameterization of basal heat flux for sea-ice modelling. *Geophysica*, 34(1-2):1–21. → pages 14

Holland, D. M. and Jenkins, A. (1999). Modeling thermodynamic ice-ocean interactions at the base of an ice shelf. *Journal of Physical Oceanography*, 29(8):1787–1800. → pages 12, 13, 14, 15, 16, 17, 18, 102, 103, 105, 106, 109, 118

Holland, D. M. and Jenkins, A. (2001). Adaptation of an isopycnic coordinate ocean model for the study of circulation beneath ice shelves. *Monthly Weather Review*, 129(8):1905–1927. → pages 17, 102

Holland, D. M., Thomas, R. H., de Young, B., Ribergaard, M. H., and Lyberth, B. (2008a). Acceleration of Jakobshavn Isbrtriggered by warm subsurface ocean waters. *Nature Geoscience*, 1(10):659–664. → pages 12, 23, 45

Holland, P. R., Jenkins, A., and Holland, D. M. (2008b). The Response of Ice Shelf Basal Melting to Variations in Ocean Temperature. *Journal of Climate*, 21(11):2558–2572. → pages 2, 22, 23

Horn, D. A., Imberger, J., and Ivey, G. N. (2001). The degeneration of large-scale interfacial gravity waves in lakes. *Journal of Fluid Mechanics*, 434:181–207. → pages 72

Huppert, H. and Turner, J. (1980). Ice blocks melting into a salinity gradient. *Journal of Fluid Mechanics*, 100(2):367–384. → pages 43

Inall and Gillibrand, P. (2010). The Physics of mid-Latitude Fjords: A Review. *Geological Society Special Publication*, 344(1):17–33. → pages 8, 9

Inall, M. E., Murray, T., Cottier, F. R., Scharrer, K., Boyd, T. J., Heywood, K. J., and Bevan, S. L. (2014). Oceanic heat delivery via Kangerdlugssuaq Fjord to the south-east Greenland ice sheet. *Journal of Geophysical Research: Oceans*, 119(2):631–645. → pages 12, 18

IPCC (2013). *Climate Change 2013: The Physical Science Basis. Contribution of Working Group I to the Fifth Assessment Report of the Intergovernmental Panel on Climate Change*. Cambridge University Press, Cambridge, United Kingdom and New York, NY, USA. → pages 62, 98

ISO (1980). International Organization of Standards. ISO 1438/1-1980(E). Water flow measurement in open channels using weirs and venturi flumes - Part 1: Thin plate weirs. → pages 83

Jackson, J. M., Lique, C., Alkire, M., Steele, M., Lee, C. M., Smethie, W. M., and Schlosser, P. (2014a). On the waters upstream of Nares Strait, Arctic Ocean, from 1991 to 2012. *Continental Shelf Research*, 73:83–96. → pages 5, 25, 30, 44, 114

Jackson, R. H., Straneo, F., and Sutherland, D. A. (2014b). Externally forced fluctuations in ocean temperature at Greenland glaciers in non-summer months. *Nature Geoscience*, 7(7):503–508. → pages 9, 12, 18, 23, 44, 108, 116

Jacobs, S. S., Huppert, H., Holdsworth, G., and Drewry, D. J. (1981). Thermohaline Steps Induced By Melting of the Erebus Glacier Tongue. *Journal of Geophysical Research*, 86(C7):6547–6555. → pages 43

Jakobsson, M., Mayer, L., Coakley, B., Dowdeswell, J. A., Forbes, S., Fridman, B., Hodnesdal, H., Noormets, R., Pedersen, R., Rebesco, M., Schenke, H. W., Zarayskaya, Y., Accettella, D., Armstrong, A., Anderson, R. M., Bienhoff, P., Camerlenghi, A., Church, I., Edwards, M., Gardner, J. V., Hall, J. K., Hell, B., Hestvik, O., Kristoffersen, Y., Marcussen, C., Mohammad, R., Mosher, D., Nghiem, S. V., Pedrosa, M. T., Travaglini, P. G., and Weatherall, P. (2012). The International Bathymetric Chart of the Arctic Ocean (IBCAO) Version 3.0. *Geophysical Research Letters*, 39(L12609):1–6. → pages 4, 25

Jeffries, M. (1991). Massive, ancient sea-ice strata and preserved physical-structural characteristics in the Ward Hunt ice shelf. *Annals of Glaciology*, 15:125–131. → pages 105

Jeffries, M. and Krouse, H. R. (1984). Arctic ice shelf growth, fiord oceanography and climate. *Zeitschrift fur Gletscherkunde und Glazialgeologie*, 20:147–153. → pages 7, 63

Jeffries, M. O. (1984). Milne Glacier, Northern Ellesmere Island, N.W.T., Canada: A Surging Glacier? *Journal of Glaciology*, 30(105):251–253. → pages 25, 99, 112, 113

Jeffries, M. O. (1985). *Physical, Chemical and Isotopic Investigations of Ward Hunt Ice Shelf and Milne Ice Shelf, Ellesmere Island, Nwt*. Ph.D. Thesis, University of Calgary, Calgary. → pages 3, 26, 64, 65, 67, 69, 74, 87

Jeffries, M. O. (1986a). Glaciers and the Morphology and Structure of Milne Ice Shelf, Ellesmere Island, N.W.T., Canada. *Arctic and Alpine Research*, 18(4):397–405. → pages 25, 26, 99, 100

Jeffries, M. O. (1986b). Ice Island Calvings and Ice Shelf Changes, Milne Ice Shelf and Ayles Ice Shelf, Ellesmere Island, N.W.T. *Arctic*, 39(1):15–19. → pages 3

Jeffries, M. O. (2002). Ellesmere Island Ice Shelves and Ice Islands. In *Satellite Image Atlas of Glaciers of the World*, page 147. United States Geological Survey, usgs professional paper 1386 edition. → pages 1, 24, 98

Jenkins, A. (1991). A one-dimensional model of ice shelf-ocean interaction. *Journal of Geophysical Research: Oceans*, 96(C11):20671–20677. → pages 117

Jenkins, A. (1999). The impact of melting ice on ocean waters. *Journal of physical oceanography*, 29(9):2370–2381. → pages 29, 30, 31

Jenkins, A. (2011). Convection-Driven Melting near the Grounding Lines of Ice Shelves and Tidewater Glaciers. *Journal of Physical Oceanography*, 41(12):2279–2294. → pages 10, 11, 98, 106, 109, 117, 118

Jenkins, A. and Bombosch, A. (1995). Modeling the effects of frazil ice crystals on the dynamics and thermodynamics of Ice Shelf Water plumes. *Journal of Geophysical Research: Oceans*, 100(C4):6967–6981. → pages 17

Jenkins, A. and Doake, C. S. M. (1991). Ice-ocean interaction on Ronne Ice Shelf, Antarctica. *Journal of Geophysical Research: Oceans*, 96(C1):791–813. → pages 17

Jenkins, A., Dutrieux, P., Jacobs, S. S., McPhail, S. D., Perrett, J. R., Webb, A. T., and White, D. (2010). Observations beneath Pine Island Glacier in WestAntarctica and implications for its retreat. *Nature Geoscience*, 3(7):468–472. → pages 14, 17, 18, 103, 104, 117

Jenkins, A., Hellmer, H. H., and Holland, D. M. (2001). The Role of Meltwater Advection in the Formulation of Conservative Boundary Conditions at an IceOcean Interface. *Journal of Physical Oceanography*, 31(1):285–296. → pages 103

Johnson, H., Mnchow, A., Falkner, K., and Melling, H. (2011). Ocean circulation and properties in Petermann Fjord, Greenland. *Journal of Geophysical Research*, 116(C01003):1–18. → pages 9, 11, 43

Joughin, I., Alley, R. B., and Holland, D. M. (2012). Ice-sheet response to oceanic forcing. *Science*, 338(6111):1172–1176. → pages 2, 22, 41

Keys, J. E. (1977). *Water regime of ice-covered fjords and lakes*. Ph.D. Thesis, McGill University, Montreal. → pages 4, 8, 18, 23, 24, 72

Keys, J. E. (1978). Water regime of Disraeli Fjord, Ellesmere Island. Technical Report 792, Defense Research Establishment Ottawa, Ottawa. → pages 7, 63

Keys, J. E., Johannssen, O., and Long, A. (1968). On the oceanography of Disraeli Fiord on Northern Ellesmere Island. Technical Report 6, McGill University, Montreal. → pages 4, 7, 63

Keys, J. E. and Seibert, G. H. (1969). Operation Tanquary, Ellesmere Island, N.W.T. 1963-1966. *Canadian Oceanographic Data Centre*, pages 99–100. → pages 4

Kimura, S., Candy, A. S., Holland, P. R., Piggott, M. D., and Jenkins, A. (2013). Adaptation of an unstructured-mesh, finite-element ocean model to the simulation of ocean circulation beneath ice shelves. *Ocean Modelling*, 67:39 – 51. → pages 11, 102, 103, 117

Kindsvater, C. and Carter, R. (1959). Discharge characteristics of rectangular thin-plate weirs. *Transactions of the American Society of Civil Engineers*, 124(1). → pages 82

Krabill, W. B. (2010). IceBridge ATM L1b Elevation and Return Strength, Version 2. Digital Media, NASA DAAC at the National Snow and Ice Data Center, Boulder, Colorado USA. → pages 27, 101

Krishfield, R. A. (2005). Spatial and temporal variability of oceanic heat flux to the Arctic ice pack. *Journal of Geophysical Research*, 110(C7). → pages 24

Lake, R. and Walker, E. (1973). Notes on the Oceanography of d'Iberville Fiord. *Arctic*, 26(3):222–229. → pages 4, 23, 24

Laxon, S. W., Giles, K. A., Ridout, A. L., Wingham, D. J., Willatt, R., Cullen, R., Kwok, R., Schweiger, A., Zhang, J., Haas, C., Hendricks, S., Krishfield, R., Kurtz, N., Farrell, S., and Davidson, M. (2013). CryoSat-2 estimates of Arctic sea ice thickness and volume. *Geophysical Research Letters*, 40(4):732–737. → pages 24

Laybourn-Parry, J., Madan, N. J., Marshall, W. A., Marchant, H. J., and Wright, S. W. (2006). Carbon dynamics in an ultra-oligotrophic epishelf lake (Beaver Lake, Antarctica) in summer. *Freshwater Biology*, 51(6):1116–1130. → pages 7, 62, 63

Laybourn-Parry, J., Quayle, W., Henshaw, T., Ruddell, A., and Marchant, H. (2001). Life on the edge: the plankton and chemistry of Beaver Lake, an ultra-oligotrophic epishelf lake, Antarctica RID D-4634-2011. *Freshwater Biology*, 46(9):1205–1217. WOS:000171284900005. → pages 8

Lenaerts, J., Angelen, J. H., Broeke, M. R., Gardner, A. S., Wouters, B., and Meijgaard, E. (2013). Irreversible mass loss of Canadian Arctic Archipelago glaciers. *Geophysical Research Letters*, 40(5):870–874. → pages 2, 4, 23, 46, 47, 133

Leuschen, C., Gogineni, P., Rodriguez-Morales, F., Paden, J., and Allen., C. (2010). IceBridge MCoRDS L2 Ice Thickness, Version 1. Digital Media, NASA National Snow and Ice Data Center Distributed Active Archive Center, Boulder, Colorado USA. → pages 26, 27, 101

Lewis, E. L. and Perkin, R. G. (1986). Ice pumps and their rates. *Journal of Geophysical Research: Oceans*, 91(C10):11756–11762. → pages 11

Losch, M. (2008). Modeling ice shelf cavities in a z coordinate ocean general circulation model. *Journal of Geophysical Research: Oceans*, 113(C8). C08043. → pages 102, 103

Ludlam, S. (1996). Stratification patterns in Taconite Inlet, Ellesmere Island, NWT. *Journal of Paleolimnology*, 16(2):205–215. → pages 4, 23, 24

Manning, C. C., Hamme, R. C., and Bourbonnais, A. (2010). Impact of deep-water renewal events on fixed nitrogen loss from seasonally-anoxic Saanich Inlet. *Marine Chemistry*, 122(1-4):1–10. → pages 35

Maslanik, J., Stroeve, J., Fowler, C., and Emery, W. (2011). Distribution and trends in Arctic sea ice age through spring 2011. *Geophysical Research Letters*, 38(L13502):1–6. → pages 24

Masson, D. (2002). Deep Water Renewal in the Strait of Georgia. *Estuarine, Coastal and Shelf Science*, 54(1):115–126. → pages 35

McPhee, M. G. (1990). 6 - Small-Scale Processes A2 - Smith, Walker O. In *Polar Oceanography*, pages 287–334. Academic Press, San Diego. → pages 105

McPhee, M. G. (1992). Turbulent heat flux in the upper ocean under sea ice. *Journal of Geophysical Research: Oceans*, 97(C4):5365–5379. → pages 16, 103

McPhee, M. G., Kottmeier, C., and Morison, J. H. (1999). Ocean Heat Flux in the Central Weddell Sea during Winter. *Journal of Physical Oceanography*, 29(6):1166–1179. → pages 16, 18, 103

McPhee, M. G., Maykut, G. A., and Morison, J. H. (1987). Dynamics and thermodynamics of the ice/upper ocean system in the marginal ice zone of the Greenland Sea. *Journal of Geophysical Research: Oceans*, 92(C7):7017–7031. → pages 14, 17, 18

McPhee, M. G., Morison, J. H., and Nilsen, F. (2008). Revisiting heat and salt exchange at the ice-ocean interface: Ocean flux and modeling considerations. *Journal of Geophysical Research*, 113(C6). → pages 13

Melling, H., Haas, C., and Brossier, E. (2015). Invisible polynyas: Modulation of fast ice thickness by ocean heat flux on the Canadian polar shelf. *Journal of Geophysical Research: Oceans*, 120(2):777–795. → pages 18

Mellor, G. L., McPhee, M. G., and Steele, M. (1986). Ice-Seawater Turbulent Boundary Layer Interaction with Melting or Freezing. *Journal of Physical Oceanography*, 16(11):1829–1846. → pages 17

Millero, F. J. (1978). Annex 6: Freezing point of seawater. Eighth report of the Joint Panel of Oceanographic Tables and Standards. Technical Report 28, UNESCO. → pages 13, 103

Mingo, L. and Flowers, G. E. (2010). Instruments and Methods: An integrated lightweight ice-penetrating radar system. *Journal of Glaciology*, 56(198):709–714. → pages 27

Mortensen, J., Bendtsen, J., Lennert, K., and Rysgaard, S. (2014). Seasonal variability of the circulation system in a west Greenland tidewater outlet glacier fjord, Godthbsfjord (64N): Godthbsfjord. *Journal of Geophysical Research: Earth Surface*, 119(12):2591–2603. → pages 18

Mortensen, J., Bendtsen, J., Motyka, R. J., Lennert, K., Truffer, M., Fahnestock, M., and Rysgaard, S. (2013). On the seasonal freshwater stratification in the proximity of fast-flowing tidewater outlet glaciers in a sub-Arctic sill fjord. *Journal of Geophysical Research: Oceans*, 118(3):1382–1395. → pages 9, 23, 30

Mortensen, J., Lennert, K., Bendtsen, J., and Rysgaard, S. (2011). Heat sources for glacial melt in a sub-Arctic fjord (Godthbsfjord) in contact with the Greenland Ice Sheet. *Journal of Geophysical Research*, 116(C01013):1–13. → pages 11, 23

Mortimer, C. A. (2011). *Quantification of Changes for the Milne Ice Shelf, Nunavut, Canada, 1950 - 2009*. M.Sc. thesis, University of Ottawa, Ottawa. → pages 3, 26, 64, 99

Mortimer, C. A., Copland, L., and Mueller, D. R. (2012). Volume and area changes of the Milne Ice Shelf, Ellesmere Island, Nunavut, Canada, since 1950. *Journal of Geophysical Research*, 117(F04011):1–12. → pages 3, 25, 26, 33, 40, 46, 64, 73, 77, 84, 100, 113

Morton, B. R., Taylor, G., and Turner, J. S. (1956). Turbulent Gravitational Convection from Maintained and Instantaneous Sources. *Proceedings of the Royal Society of London A: Mathematical, Physical and Engineering Sciences*, 234(1196):1–23. → pages 10

Motyka, R. J., Truffer, M., Fahnestock, M., Mortensen, J., Rysgaard, S., and Howat, I. (2011). Submarine melting of the 1985 Jakobshavn Isbr floating tongue and the triggering of the current retreat. *Journal of Geophysical Research*, 116(F01007):1–17. → pages 2, 12, 22, 23, 41

Mueller, D., Vincent, W., and Jeffries, M. (2006). Environmental gradients, fragmented habitats, and microbiota of a northern ice shelf cryoecosystem, Ellesmere Island, Canada. *Arctic, Antarctic, and Alpine Research*, 38(4):593–607. → pages 6, 114

Mueller, D. R., Copland, L., Hamilton, A., and Stern, D. (2008). Examining Arctic Ice Shelves Prior to the 2008 Breakup. *Eos, Transactions American Geophysical Union*, 89(49):502–503. → pages 1, 6, 22, 40, 46, 98

Mueller, D. R., Copland, L., and Jeffries, M. (2016). Changes in Canadian Arctic ice shelf extent since 1906. In *Arctic Ice Shelves and Ice Islands. ed. L. Copland and D.R. Mueller.* Dordrecht: Springer SBM. → pages 88

Mueller, D. R., Vincent, W. F., and Jeffries, M. O. (2003). Break-up of the largest Arctic ice shelf and associated loss of an epishelf lake. *Geophysical Research Letters*, 30(20):1–4. → pages 1, 2, 7, 22, 46, 62, 63, 66, 80, 98, 135

Nares, G. (1878). *Narrative of a voyage to the polar sea during 1875-6 in HM ships 'Alert' and 'Discovery'*. Sampson Low, Marston, Searle & Rivington, London. → pages 6

Narod, B., Clarke, G., and Prager, B. (1988). Airborne UHF radar sounding of glaciers and ice shelves, northern Ellesmere Island, Arctic Canada. *Canadian Journal of Earth Sciences*, 25(1):95–105. → pages 3, 25, 40, 64

Newton, J. L. and Sotirin, B. J. (1997). Boundary undercurrent and water mass changes in the Lincoln Sea. *Journal of Geophysical Research*, 102(C2):3393–3403. → pages 5, 25, 44

Nst, O. A. and Foldvik, A. (1994). A model of ice shelf-ocean interaction with application to the Filcher-Ronne and Ross Ice Shelves. *Journal of Geophysical Research: Oceans*, 99(C7):14243–14254. → pages 15

Padman, L. and Erofeeva, S. (2004). A barotropic inverse tidal model for the Arctic Ocean. *Geophysical Research Letters*, 31(L02303):1–4. → pages 31

Pawlowicz, R. (2008). Calculating the conductivity of natural waters. *Limnology and Oceanography: Methods*, 6(9):489–501. → pages 66

Pawlowicz, R., Beardsley, B., and Lentz, S. (2002). Classical tidal harmonic analysis including error estimates in MATLAB using T_tide. *Computers & Geosciences*, 28(8):929–937. → pages 31, 67

Peary, R. E. (1907). *Nearest the Pole*. Hutchinson, London. → pages 6

Polyakov, I. V., Alekseev, G. V., Timokhov, L. A., Bhatt, U. S., Colony, R. L., Simmons, H. L., Walsh, D., Walsh, J. E., and Zakharov, V. F. (2004). Variability of the Intermediate Atlantic Water of the Arctic Ocean over the Last 100 Years. *Journal of Climate*, 17(23):4485–4497. → pages 45

Pope, S., Copland, L., and Mueller, D. (2012). Loss of multiyear landfast sea ice from Yelverton Bay, Ellesmere Island, Nunavut, Canada. *Arctic, Antarctic, and Alpine Research*, 44(2):210–221. → pages 1, 5, 22

Rignot, E. (1998). Hinge-line migration of Petermann Gletscher, north Greenland, detected using satellite radar interferometry. *Journal of Glaciology*, 44(148):469–476. → pages 2

Rignot, E., Gogineni, S., Joughin, I., and Krabill, W. (2001). Contribution to the glaciology of northern Greenland from satellite radar interferometry. *Journal of Geophysical Research: Atmospheres*, 106(D24):34007–34019. → pages 101, 109, 111, 112

Rignot, E., Jacobs, S., Mouginot, J., and Scheuchl, B. (2013). Ice-Shelf Melting Around Antarctica. *Science*, 341(6143):266–270. → pages 2, 97

Rignot, E., Koppes, M., and Velicogna, I. (2010). Rapid submarine melting of the calving faces of West Greenland glaciers. *Nature Geoscience*, 3(3):187–191. → pages 12

Rignot, E. and Steffen, K. (2008). Channelized bottom melting and stability of floating ice shelves. *Geophysical Research Letters*, 35(L02503):1–5. → pages 2, 11, 23, 97, 111

Rudels, B. (2013). Arctic Ocean circulation, processes and water masses: A description of observations and ideas with focus on the period prior to the International Polar Year 20072009. *Progress in Oceanography*. → pages 30

Rudels, B., Friedrich, H. J., and Quadfasel, D. (1999). The Arctic circumpolar boundary current. *Deep Sea Research Part II: Topical Studies in Oceanography*, 46(6):1023–1062. → pages 5, 25

Salcedo-Castro, J., Bourgault, D., Bentley, S. J., and deYoung, B. (2013). Non-hydrostatic modeling of cohesive sediment transport associated with a subglacial buoyant jet in glacial fjords: A process-oriented approach. *Ocean Modelling*, 63:30–39. → pages 10

Sciascia, R., Straneo, F., Cenedese, C., and Heimbach, P. (2013). Seasonal variability of submarine melt rate and circulation in an East Greenland fjord. *Journal of Geophysical Research: Oceans*, 118(5):2492–2506. → pages 11, 23, 98, 117

Seroussi, H., Morlighem, M., Rignot, E., Larour, E., Aubry, D., Ben Dhia, H., and Kristensen, S. S. (2011). Ice flux divergence anomalies on 79north Glacier, Greenland: THE 79north GLACIER. *Geophysical Research Letters*, 38(9). → pages 102

Sharp, M., Burgess, D. O., Cogley, J. G., Ecclestone, M., Labine, C., and Wolken, G. J. (2011). Extreme melt on Canada's Arctic ice caps in the 21st century. *Geophysical Research Letters*, 38(11):n/a–n/a. L11501. → pages 2, 4

Shirasawa, K. and Ingram, R. G. (1991). Characteristics of the turbulent oceanic boundary layer under sea ice. Part 1: A review of the ice-ocean boundary layer. *Journal of Marine Systems*, 2(1):153–160. → pages 105

Smith, J. A., Hodgson, D. A., Bentley, M. J., Verleyen, E., Leng, M. J., and Roberts, S. J. (2006). Limnology of Two Antarctic Epishelf Lakes and their Potential to Record Periods of Ice Shelf Loss. *Journal of Paleolimnology*, 35(2):373–394. → pages 7, 8, 18, 62, 63

Steele, M. and Boyd, T. (1998). Retreat of the cold halocline layer in the Arctic Ocean. *Journal of Geophysical Research: Oceans*, 103(C5):10419–10435. → pages 5, 30, 45

Steele, M., Mellor, G. L., and Mcphee, M. G. (1989). Role of the Molecular Sublayer in the Melting or Freezing of Sea Ice. *Journal of Physical Oceanography*, 19(1):139–147. → pages 17, 18

Steele, M., Morison, J., Ermold, W., Rigor, I., Ortmeyer, M., and Shimada, K. (2004). Circulation of summer Pacific halocline water in the Arctic Ocean. *Journal of Geophysical Research*, 109(C02027):1–18. → pages 5, 25

Steur, L., Steele, M., Hansen, E., Morison, J., Polyakov, I., Olsen, S. M., Melling, H., McLaughlin, F. A., Kwok, R., and Smethie, W. M. (2013). Hydrographic changes in the Lincoln Sea in the Arctic Ocean with focus on an upper ocean freshwater anomaly between 2007 and 2010. *Journal of Geophysical Research: Oceans*, 118(9):4699–4715. → pages 5, 25

Stevens, L. A., Straneo, F., Das, S. B., Plueddemann, A. J., Kukulya, A. L., and Morlighem, M. (2015). Linking catchment-scale subglacial discharge to subsurface glacially modified waters near the front of a marine terminating outlet glacier using an autonomous underwater vehicle. *The Cryosphere Discussions*, 9(5):4583–4624. → pages 43

Stigebrandt, A. (1990). On the response of the horizontal mean vertical density distribution in a fjord to low-frequency density fluctuations in the coastal water. *Tellus A*, 42(5):605–614. → pages 116

Stigebrandt, A. (2012). Hydrodynamics and Circulation of Fjords. In Bengtsson, L., Herschy, R. W., and Fairbridge, R. W., editors, *Encyclopedia of Lakes and Reservoirs*, pages 327–344. Springer Netherlands, Dordrecht. → pages 8, 9

Straneo, F. and Cenedese, C. (2015). The Dynamics of Greenland's Glacial Fjords and Their Role in Climate. *Annual Review of Marine Science*, 7(1):89–112. → pages 2, 4, 9, 10, 12, 22, 43, 114

Straneo, F., Curry, R. G., Sutherland, D. A., Hamilton, G. S., Cenedese, C., Vge, K., and Stearns, L. A. (2011). Impact of fjord dynamics and glacial runoff on the circulation near Helheim Glacier. *Nature Geoscience*, 4(5):322–327. → pages 11, 23, 36

Straneo, F., Hamilton, G. S., Sutherland, D. A., Stearns, L. A., Davidson, F., Hammill, M. O., Stenson, G. B., and Rosing-Asvid, A. (2010). Rapid circulation of warm subtropical waters in a major glacial fjord in East Greenland. *Nature Geoscience*, 3(3):182–186. → pages 9, 18, 23

Straneo, F., Sutherland, D. A., Holland, D., Gladish, C., Hamilton, G., Johnson, H., Rignot, E., Xu, Y., and Koppes, M. (2012). Characteristics of ocean waters reaching Greenlands glaciers. *Annals of Glaciology*, 53(60):202–210. → pages 2, 22, 45

Sutherland, D. A. and Straneo, F. (2012). Estimating ocean heat transports and submarine melt rates in Sermilik Fjord, Greenland, using lowered acoustic Doppler current profiler (LADCP) velocity profiles. *Annals of Glaciology*, 53(60):50–58. → pages 9, 12, 23

Sutherland, D. A., Straneo, F., and Pickart, R. S. (2014). Characteristics and dynamics of two major Greenland glacial fjords. *Journal of Geophysical Research: Oceans*, 119(6):3767–3791. → pages 9, 11

Thomson, R. E. (1981). *Oceanography of the British Columbia Coast*. Number 56 in Canadian Special Publication of Fisheries and Aquatic Sciences. Ottawa, Canada. → pages 37

Turner, J. S. (1973). *Buoyancy Effects in Fluids*. Cambridge University Press. Cambridge Books Online. → pages 10

Van-Hove, P., Swadling, K., Gibson, J., Belzile, C., and Vincent, W. (2001). Farthest north lake and fjord populations of calanoid copepods Limnocalanus macrurus and Drepanopus bungei in the Canadian high Arctic. *Polar Biology*, 24(5):303–307. → pages 7

Van Wychen, W., Burgess, D. O., Gray, L., Copland, L., Sharp, M., Dowdeswell, J. A., and Benham, T. J. (2014). Glacier velocities and dynamic ice discharge from the Queen Elizabeth Islands, Nunavut, Canada. *Geophysical Research Letters*, 41(2):484–490. → pages 4, 26, 32, 47, 101

Van Wychen, W., Davis, J., Burgess, D. O., Copland, L., Gray, L., Sharp, M., and Mortimer, C. (2016). Characterizing interannual variability of glacier dynamics and dynamic discharge (1999-2015) for the ice masses of Ellesmere and Axel Heiberg Islands, Nunavut, Canada. *Journal of Geophysical Research: Earth Surface*, 121(1):39–63. → pages 4, 25, 98, 99, 101, 112, 124

Veillette, J., Lovejoy, C., Potvin, M., Harding, T., Jungblut, A. D., Antoniades, D., Chenard, C., Suttle, C. A., and Vincent, W. F. (2011a). Milne Fiord epishelf lake: A coastal Arctic ecosystem vulnerable to climate change. *Ecoscience*, 18(3):304–316. → pages 3, 7, 26, 40, 63

Veillette, J., Martineau, M., Antoniades, D., Sarrazin, D., and Vincent, W. (2011b). Effects of loss of perennial lake ice on mixing and phytoplankton dynamics: insights from High Arctic Canada. *Annals of Glaciology*, 51(56):56–70. → pages 26, 64, 65, 66, 78

Veillette, J., Mueller, D. R., Antoniades, D., and Vincent, W. F. (2008). Arctic epishelf lakes as sentinel ecosystems: Past, present and future. *Journal of Geophysical Research*, 113(G04014):1–11. → pages 2, 3, 7, 8, 22, 26, 62, 63, 65, 66, 87, 134

Vincent, W., Gibson, J., and Jeffries, M. (2001). Ice-shelf collapse, climate change, and habitat loss in the Canadian high Arctic. *Polar Record*, 37(201):133–142. → pages 2, 6, 7, 18, 22, 62, 63, 98, 134

Vincent, W. F. and Laybourn-Parry, J. (2008). *Polar Lakes and Rivers: Limnology of Arctic and Antarctic Aquatic Ecosystems*. Oxford University Press, Oxford. → pages 7

Vincent, W. F., Whyte, L. G., Lovejoy, C., Greer, C. W., Laurion, I., Suttle, C. A., Corbeil, J., and Mueller, D. R. (2009). Arctic microbial ecosystems and impacts of extreme warming during the International Polar Year. *Polar Science*, 3(3):171–180. → pages 62

Wand, U., Hermichen, W.-D., Brggemann, E., Zierath, R., and Klokov, V. D. (2011). Stable isotope and hydrogeochemical studies of Beaver Lake and Radok Lake, MacRobertson Land, East Antarctica. *Isotopes in Environmental and Health Studies*, 47(4):407–414. → pages 7, 62

White, A., Copland, L., Mueller, D., and Van Wychen, W. (2015a). Assessment of historical changes (19592012) and the causes of recent break-ups of the Petersen ice shelf, Nunavut, Canada. *Annals of Glaciology*, 56(69):65–76. → pages 1, 6, 22, 46, 62, 65, 98

White, A., Mueller, D., and Copland, L. (2015b). Reconstructing hydrographic change in Petersen Bay, Ellesmere Island, Canada, inferred from SAR imagery. *Remote Sensing of Environment*, 165:1–13. → pages 8, 134

Wilson, N. J., Flowers, G. E., and Mingo, L. (2013). Comparison of thermal structure and evolution between neighboring subarctic glaciers. *Journal of Geophysical Research: Earth Surface*, 118(3):1443–1459. → pages 27

Wilson, N. J. and Straneo, F. (2015). Water exchange between the continental shelf and the cavity beneath Nioghalvfjerdsbrae (79 North Glacier). *Geophysical Research Letters*, 42(18):7648–7654. → pages 11

Xu, Y., Rignot, E., Fenty, I., Menemenlis, D., and Flexas, M. M. (2013). Subaqueous melting of Store Glacier, west Greenland from three-dimensional, high-resolution numerical modeling and ocean observations. *Geophysical Research Letters*, 40(17):4648–4653. → pages 11, 12, 117

Xu, Y., Rignot, E., Menemenlis, D., and Koppes, M. (2012). Numerical experiments on subaqueous melting of Greenland tidewater glaciers in response to ocean warming and enhanced subglacial discharge. *Annals of Glaciology*, 53(60):229–234. → pages 11, 23, 117

Zwally, H., Schutz, R., Bentley, C., Bufton, J., Herring, T., Minster, J., Spinhirne, J., and Thomas, R. (2011). GLAS/ICESat L2 Antarctic and Greenland ice sheet altimetry data V031. Digital Media, NASA Distributed Active Archive Center at the National Snow and Ice Data Center, Boulder, Colorado USA. → pages 27